MTA DOCTORAL THESIS

BONE MARROW DERIVED STEM CELLS IN HEALTH AND DISEASE

Éva Mezey

Budapest, 2011

Szüleim Emlékére

FREQUENTLY USED ABBREVIATIONS:

BM	bone marrow
HSC	hematopoietic stem cell
MSC/BMSC	mesenchymal stem cell (used as a synonym for bone marrow derived stem cell or bone marrow derived stromal cell)
GFP	green fluorescent protein
GCSF	granulocyte colony stimulatory factor
SCF	Stem cell factor
GPCR	G protein coupled receptor

Table of Contents

I.) Introduction

This thesis summarizes my work of the last 15 years on the role of bone marrow derived cells in the maintainance of the healthy environment in the body. My interest in these cells stemmed from the observation that they are able to move from the blood into the brain. This observation stood against a longstanding dogma that all the cells that constitute the CNS we are either born with or they derive from neural stem cells that seed the brain during embryonal development. The significance of the observation was that - if held true for humans - it would constitute new means to get pharmaceutical agents into or replace missing natural agents in the central nervous system. My first experiments showed that stem cells in the blood could indeed give rise to microglia and astrocytes in the rat brain. Subsequently, we showed that cells from gender-mismatched transplanted bone marrow make their way into the brain and differentiate into all neural linages in the mouse. These results were confirmed independently by other groups before we also demonstrated the same phenomenon in humans. In human transplant recipients, we found that bone marrow derived cells also colonize the oral mucosa and salivary glands.
In addition to their regenerative capacity, in the last years new evidence emerged that non-hematopoietic cells in the bone marrow might modulate the function of the immune system and these data prompted us to study this new phenomenon as well. Our published data indicate that administration of bone marrow stromal cells to animals corrects imbalances in the immune system. Based on our work and studies by other groups, a number of clinical trials are underway to determine whether these immunomodulatory effects of BMSCs can be exploited to treat diseases.

I have separated the description of my work into two parts: First I have described our studies demonstrating the role of circulating BM cells in tissue regeneration. Then I have summarized our work on the immuno-regulatory properties of bone marrow derived stromal cells.

II.) Contribution of circulating cells to tissue regeneration

The first attempt in medical history to use BM for tissue regeneration was to renew the BM itself. Around the middle of the 20th century scientists realized that certain organs might be transplanted from one person into another - but problems associated with transplantation quickly surfaced. Sir Peter Brian Medawar's work shed light on graft rejection and this eventually allowed clinicians to use matched donated organs to recipients and/or use immune-suppression to prevent rejection. However, there were way too few organs to meet the demand, and the need to manufacture organs in vitro arose. To imagine making organs we need to understand how they develop in the embryo and how tissues are maintained throughout life physiologically. A logical choice of cells that contribute to tissue regeneration is those that circulate and thus can easily access all organs of the body, such as blood cells. These cells arise in the BM known to have two populations of stem cells: the hematopoietic (HSC) and the stromal (BMSC) stem cells. HSCs are generally accepted to give rise to the different classes of blood cells (myeloid, erythroid, lymphoid, platelets, and mast cells), while BMSCs give rise to the structural elements of the skeleton, such as bone, cartilage, and marrow fat.

1.) CNS

1a)Rodents

a(1) Uninjured brain

Our first sets of experiments was aimed at determining whether circulating blood cells can enter the CNS and differentiate into cells of the neural lineage, e.g., microglia, microglia, neurons, or vascular endothelial cells. We worked out a technique to detect the Y chromosome in cells and to colocalize it with a variety of protein markers that confirm the identity of differentiated cells. Once the technique was working reliably, we irradiated female rats to destroy their BM and then injected them with genetically identical male bone marrow.

Subsequently, we examined the rats' brains for the presence of Y chromosome positive (i.e., male donor) cells. We found both macroglia and microglia that contained the Y chromosome, suggesting that these cells derived from the donor BM and entered the brain through the general circulation. After we published these results in 1997 (1), we wondered whether bone marrow cells could contribute to the neuronal population of the brain as well as the glial populations. Since radiation might injure the blood-brain barrier and make it leaky, we designed a new experiment that circumvented this problem. To achieve this, we collaborated with a group of scientists who developed a special transgenic mouse that lacks a gene (PU1) vital for the development of the white cell lineage. PU1-/- mice have to be given BM transplants at birth in order to survive, and we transplanted them with gender mismatched BM within 48 hours of their births (2). At different time points following these transplantations we perfused the mice and used Y chromosome in situ hybridization histochemistry (ISHH) to colocalize the Y chromosome and NeuN, a specific marker of neurons (Fig.1). We found that 0.3-2.3% of all neurons were positive for both markers. The shortest survival time following BM transplant was 1 month, the longest was 4 months. We did not find a correlation between the elapsed time post-transplant and the number of double-positive cells. We also did not find any specific regional localization; the double-positive cells could be found in all brain regions examined in a seemingly random distribution.

Fig.1.
Y chromosome staining in the CNS. Coronal sections from 4-month-old nontrans- planted (A) female and (B) male brains were mounted and processed together. The panels show the over- lay of the NeuN (red) immunostaining, Y chromosome nonradioactive ISH [visualized with tyramide-FITC conjugate (green)], and DAPI stain- ing of cell nuclei (blue). The Y chromosome was restricted to the male brain, demonstrating hybridization specifici- ty. (C) Confocal image of coronal sections from a 4-month-old recipient female striatum that was double-immunostained for the neuron-specific antigens NeuN and NSE (neuron specific enolase). All NeuN-expressing cells (red) were also immunoreactive for NSE (green). (D) Sagittal section from a 1-month-old female PU.1 knockout mouse brain transplanted at birth with male bone marrow. The Y chromosome was visualized with BCIP/NBT (dark purple dots) to identify anatomical landmarks. cc, corpus callosum; cx, cerebral cortex; CPu, caudate putamen; fi, fimbria hippocampi; hi, hippocampus; LV, lateral ventricle. (E to G) Identical fields showing NeuN, Y chromosome, and DAPI nuclear triple staining in the hypothalamic dorsomedial nucleus of a 3-month-old female recipient. Colocalization of the Y chromosome [visualized with tyramide-

FITC conjugate (green)] to a NeuN immunopositive (red) nucleus is shown in (E). In (F), DAPI staining identifies all cell nuclei (blue). Overlays of the NeuN, Y chromosome, and DAPI fluorescence are shown in (G). The arrow identifies a cell nucleus that contained both the Y chromosome (indicating the bone marrow origin) and NeuN. Scale bar in (G) represents the following sizes: 30 µm, (A) and (B); 10 µm, (C); 250 µm (D); and 12 µm, (E) to (G).

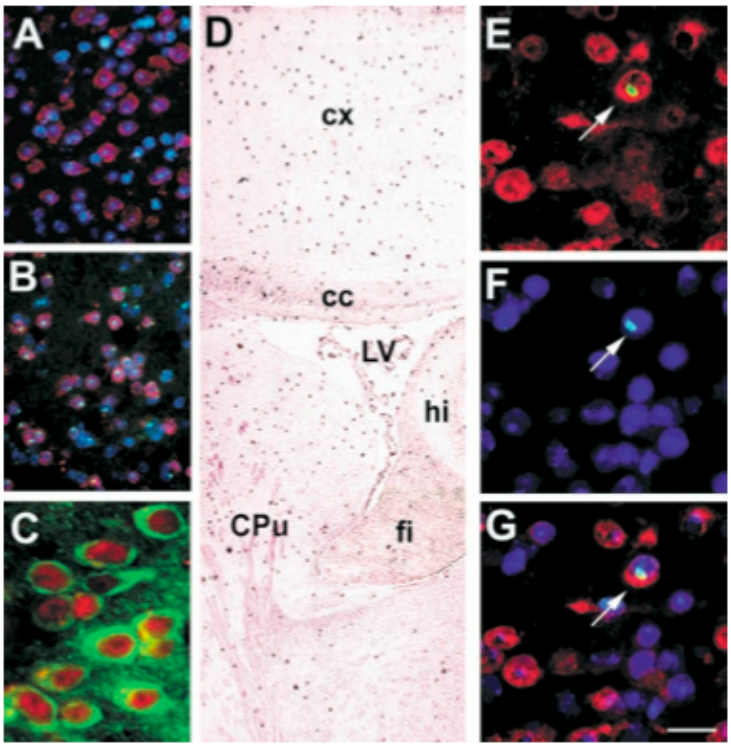

a(2) Injured brain

After we established that circulating cells can enter the CNS and differentiate into neural cells, we asked whether this process might be used physiologically for repair following brain injury. A month after transplanting PU1-/- mice with GFP expressing, gender mismatched bone marrow, we induced hypoxic brain injury using a permanent ligation of the middle cerebral artery (MCAO) and examined the brains 1-6 months later (3). We used both the GFP and the Y chromosome as markers of donor cells. We observed that few neurons, but numerous astrocytes and many new vessels were derived from cells of the transplanted BM.

Mobilizing BM cells with a combination of GCSF/SCF induced the formation of many new vessels and significantly decreased the infarct volume (Fig.2) in the mice. These results suggested that mobilized circulating cells might contribute to brain healing

Fig.2.

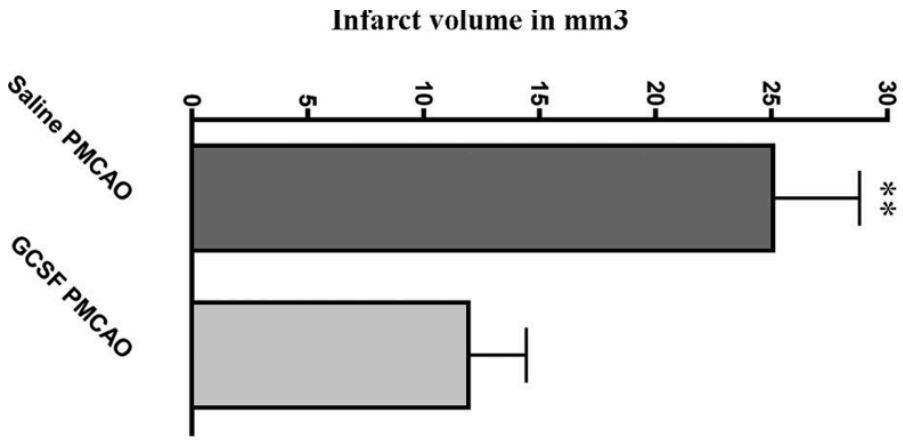

in a variety of ways, e.g., by stimulating neovascularization and also generating new cells.

1b) Human Brains

Following our rodent studies we wanted to know whether BM cells could colonize the brains of humans. In a collaboration with scientists at the Johns Hopkins School of Medicine, we collected samples from brains of four female patients who died after receiving bone marrow transplants from male donor relatives (4). The brains were immersion fixed in formaldehyde and paraffin embedded, which made it difficult to use the staining methods that we had employed earlier. However, once again, we worked out a suitable method to colocalize the human Y chromosome with specific nuclear (NeuN) and cytoplasmic (Kv2.1) neuronal markers. Using the new techniques we found that, indeed, cells that derived from the transplanted male donor blood entered the brains and did bear neuronal markers in all four patients. We found the greatest number of donor-derived neurons (7 in 10,000) in the youngest patient, a 2 year old child, who also lived the longest time after transplantation. The distribution of the labeled cells in the brains was not homogeneous. There were clusters of Y-positive cells, suggesting that single progenitor cells underwent clonal expansion and differentiation.

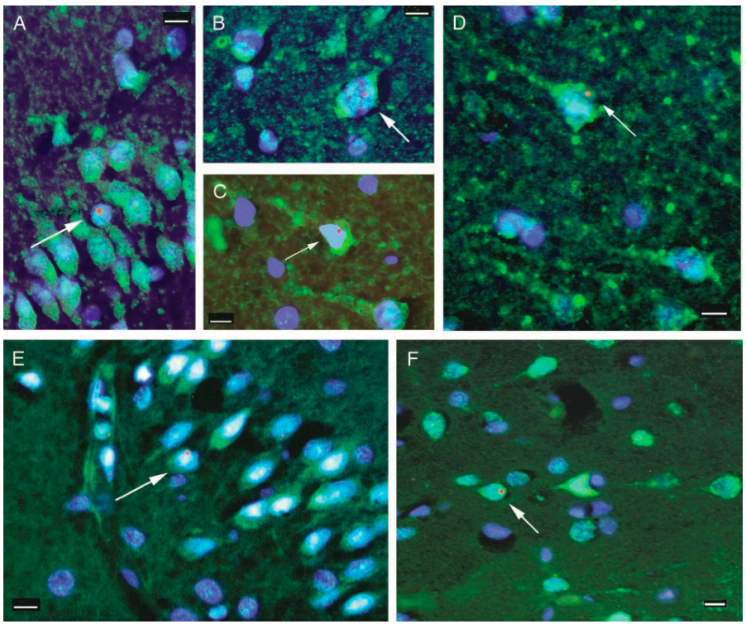

Fig.3. Neuronal markers colocalized with the Y chromosome in human postmortem brain samples. Fluorescent microscopic images of neocortex from patients 2 (A–C) and 1 (E) and hippocampus from patients 1 (D) and 3 (F) are shown. The green color represents the immunostaining for neuronal markers Kv2.1 (A–D) and NeuN (E and F), and the Y chromosome is represented by the red fluorescent dots. All cell nuclei are stained with 4 ,6-diamidino-2-phenylindole, a chromosomal marker that shows up as blue fluorescence. All images are overlays of the images seen through the three separate filters to show all colors. Arrows point to cells that are labeled with neuronal markers and are also Y chromosome-positive. In the Kv2.1 immunostaining the initial axons of some neurons can also be visualized. (Scale bars, 10 µm.)

2) Epithelial tissues

2a) Mouse uterus

Since the uterine epithelium needs to regenerate after every cycle (in the mouse every 4 days), we decided that this tissue would be ideal to look for contribution of BM derived cells to epithelial regeneration (5). Out of the two major populations of the BM stem cells only the hematopoietic cells have an accepted marker, CD45, also called common leukocyte antigen. We created a novel transgenic mouse where we introduced Cre recombinase cDNA into a

bacterial artificial chromosome (BAC) containing the complete mouse *CD45* gene (Fig.4).

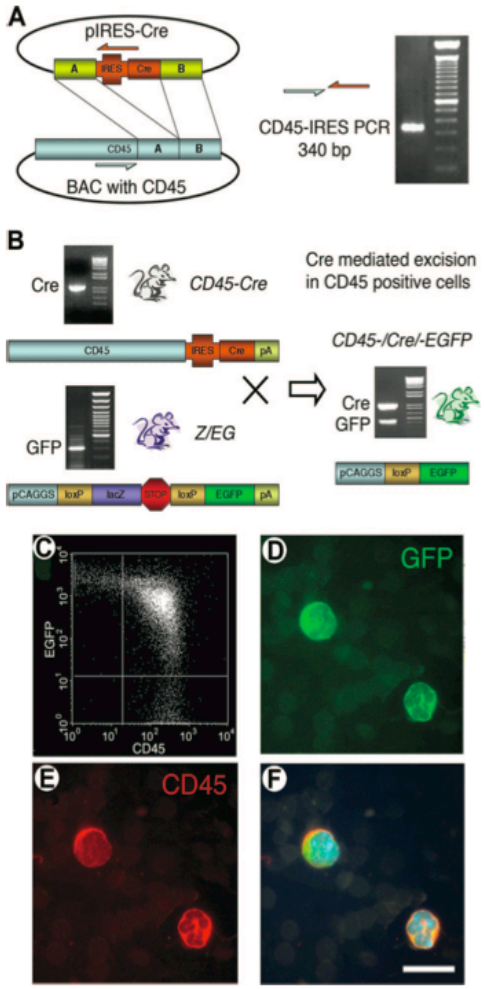

Fig. 4. The recombinase cDNA was inserted downstream of an internal ribosomal entry site (IRES), which in turn was placed downstream of the last coding exon of CD45. The resulting BAC was used to make transgenic mice (*CD45/Cre*) where Cre recombinase is made in any cell that expresses CD45. GFP is expressed in CD45+ cells of the double-transgenic (*CD45/Cre-Z/EG*) mice. **(A):** Upon homologous recombination, the IRES-Cre recombination cassette flanked by two homologous fragments (A and B) was inserted into exon 33 of the *CD45* gene in a BAC containing the entire coding region. The recombinant construct was confirmed to be correct by restriction mapping, PCR with primers flanking the recombination fragments, and sequencing. **(B):** To track the fate of CD45+ cells, we created a double-transgenic strain by breeding *CD45/Cre* mice with the double-reporter *Z/EG* mice. In the crossbred mice, every CD45+ cell expresses the Cre recombinase that will excise the floxed lacZ cassette, thus enabling the activation of GFP. Regardless of the future fate of CD45+ cells, GFP will be expressed continuously throughout their life spans. **(C):**

Fluorescence-activated cell sorting of peripheral blood of a double-transgenic animal demonstrating a high percentage (85%) of double-positive blood cells using green fluorescence for GFP and red for CD45. **(D–F):** White blood cells immunostained with GFP (green) **(D)**, CD45 (red) **(E)**, and an overlay of **(D)** and **(E)** with added 4,6-diamidino-2-phenylindole (nuclear-blue) staining **(F)**. Scale bar = 15 µm. Abbreviations: BAC, bacterial artificial chromosome; bp, base pairs; EGFP, enhanced green fluorescent protein; GFP, green fluorescent protein; IRES, internal ribosomal entry site; PCR, polymerase chain reaction.

Once we crossed this novel transgenic mouse with the double reporter mice we looked at the uterine epithelium and found that the more cycles the mice had the more GFP+ epithelial cells we found. These green cells were always in patches suggesting a clonal origin, i.e. that a circulating cell becomes a uterine stem cell and continues to repopulate the mucosa. The most striking finding in this study was that following pregnancy - at which event the surface area of the uterus has to enlarge by a factor of 20X, about 80% of the uterine epithelium became GFP+.

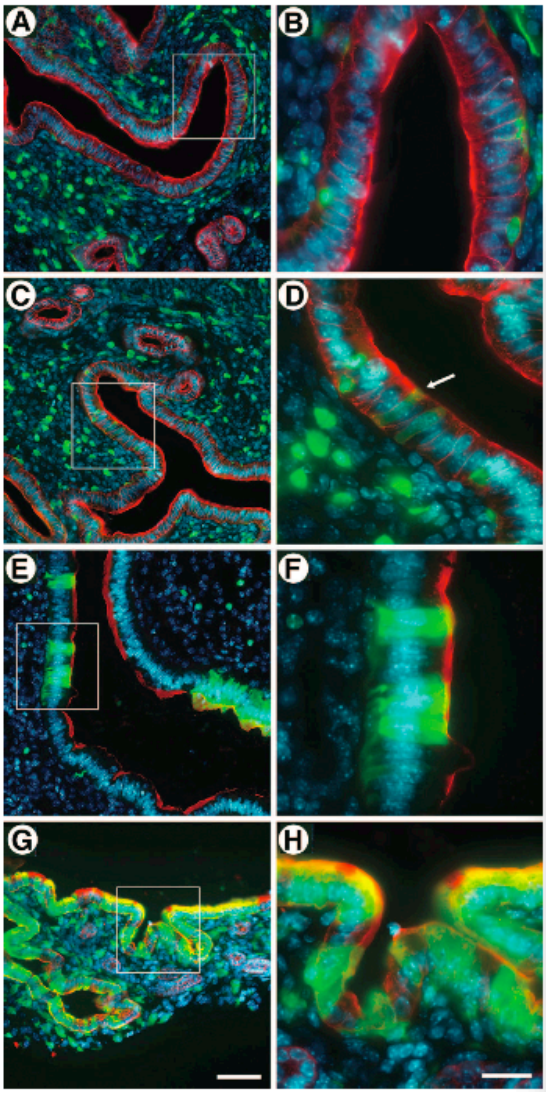

Fig.5.GFP-expressing uterine epithelial cells from double transgenic mice of different ages and pregnant mice. All nuclei were stained in blue with DAPI. **(A, B):** No GFP-positive (green) uterine epithelial (red staining represents *L. tetragonolobus*, the epitheli-al marker) cells were detect-ed in 6-week-old animals. **(C, D):** Sporadic GFP-positive uterine epitheli-al cells were present at 12 weeks of age. Arrow indicates a GFP uterine epithelial cell. **(E, F):** At 20 weeks of age, 6% of uterine epithelial cells expressed GFP. **(G, H):** In 12-week-old pregnant mice, there was a robust increase in the number of GFP-expressing cells: 82% of the uterine epithelial cells were GFP . Scale bars : 60 µm (left column) and 20 µm (right column)

Since our work was published, other groups confirmed that human uterine epithelium behaves very similarly and that circulating BM cells contribute to its regeneration physiologically. Our findings also suggest a new possible explanation of endometriosis, a painful, difficult to treat human disease, when ectopic uterine epithelium is present in the abdominal cavity and responds to hormonal changes.

2b) Human cheek cells and salivary glands

The oral mucosa is constantly exposed to a variety of insults, such as extreme heat and cold, spices, mechanical injuries. All of these cause cell death and the dead cells need continuous replacement throughout life. Fortunately, the oral cavity is also easily accessible and sampling the mucosa is quick and painless. For all of the above reasons we decided to use the buccal mucosa to test whether BM derived cells contribute to the regeneration of this epithelial tissue. We took cheek scrapings from five females who had received either a bone-marrow transplant or an allogeneic mobilized peripheral-blood progenitor-cell transplant (enriched in CD34+ cells) from male donors years before (6).

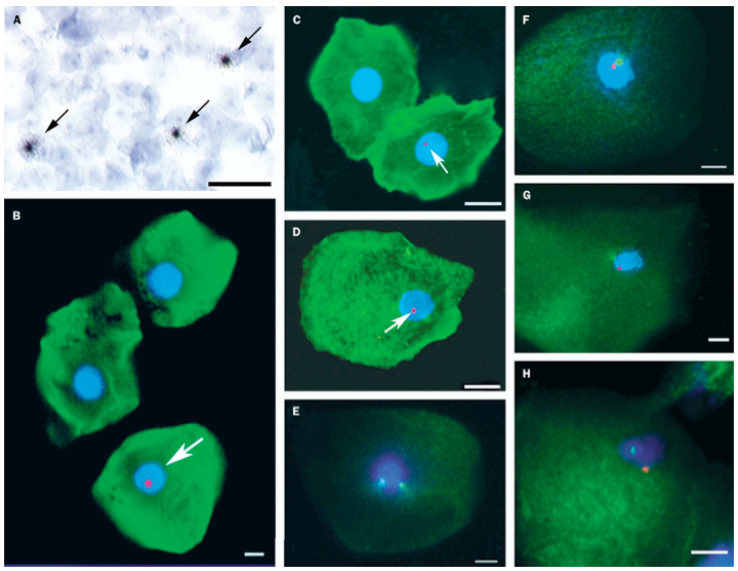

Fig.6. In-situ hybridization and immunohistochemistry in human buccal cells (A) Y-chromosome autoradiography on a smear of buccal cells. The arrows point to the autoradiographic grains (black dots) above the nuclei of Y-chromosome containing cells. (B, C, D) The cells were first immunostained for cytokeratin 13 (green), then hybridized with a human Y-chromosome riboprobe (red fluorescent dots shown by the arrows). The nuclei of the cells are stained blue with DAPI. (E, F, G, H) FISH with X-chromosome and Y-chromosome probes. Individual buccal cells are shown. The green fluorescent dot in the nucleus represents the X probe and the red dot the Y probe. The nuclei of the cells are stained blue with DAPI. The scale bar represents 10 µm in all panels, except 100 µm for panel A.

We then performed in-situ hybridization on the cheek cells with Y and X chromosome probes. In separate experiments we combined fluorescent ISH for the Y chromosome in the buccal epithelial cells with immunohistochemistry to label cytokeratin 13, an accepted specific epithelial marker. When examined 4-6 years after male-to-female marrow-cell transplantation, all female recipients had Y-chromosome-positive buccal cells between 0.8-12.7%. In more than 9700 cells studied, we detected only one XXXY-positive cell (0·01%) and one XXY cell (0·01%), both of which could have arisen when an XY cell fused with an XX cell. These results suggested that BMD cells migrate into the cheek and differentiate into epithelial cells, an occurrence that does not depend on fusion of BMD cells to recipient cells. This finding might be an example of transdifferentiation of haematopoietic or stromal progenitor cells. The HSCs seem more likely to be the cells responsible for this effect because:

1. There is no solid proof yet that the BMSCs from the bone marrow circulate;
2. Even if they do circulate, their numbers in the BM is orders of magnitude lower than their hematopoietic counterparts; and
3. Three out of the five patients received stem cell enriched peripheral blood instead of BM transplant, and the former are enriched in CD34+, CD38- hematopoietic stem cells and progenitors. These patients showed as high a percentage of chimerism (11%), as the ones receiving full BM (including the stromal stem cells)

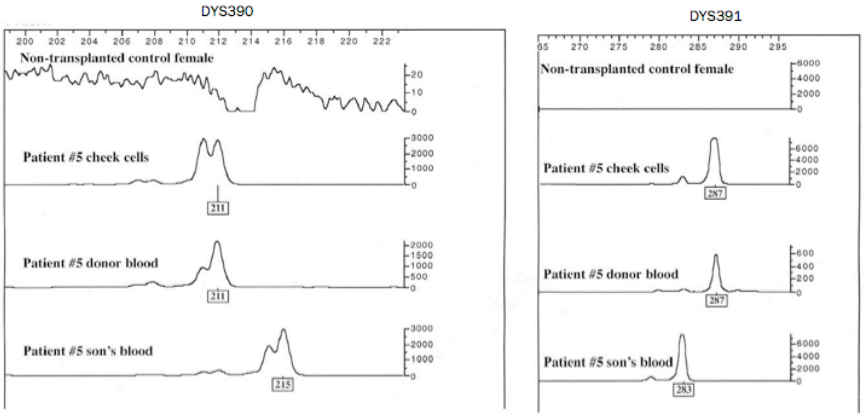

Fig.7. Blood from a non-transplanted female control, buccal cells from recipient 5, her donor's blood, and her son's blood, were analyzed with four sets of Y-chromosome markers. X axis shows product length in bases, and Y axis shows signal strength.

Finally, we wanted to test the hypothesis that the Y chromosome positive cells did not derive from the transplanted tissues (BM or PB), but from a previous pregnancy with a male fetus. We succeeded in collecting samples from the donor and the son of one of the patients and used microsatellite markers to identify the Y chromosome that we found in the cheek cells. The DNA analysis proved that the buccal cell Y chromosome was identical to that of the male donor versus the son of the patient. We also tested several normal volunteers, who did not receive BM transplants, but were pregnant and gave birth to male children. None of the samples from these women had Y chromosome positive buccal cells. As a follow-up to this study we investigated the presence of Y chromosome-positive cells in salivary gland biopsies of 5 females who had received a marrow or blood stem cell transplant from male donors (7). One to 16 years after transplantation all scattered Y chromosome-positive cells were found in the acini, ducts, and stroma of their salivary glands (mean of 1.01%). Potentially, if their numbers can be boosted, these cells could be used for treatment of Sjögren's syndrome and salivary glands damaged by therapeutic irradiation for cancers of the head and neck.

c. References

1. Eglitis MA and E **Mezey**. (1997). Hematopoietic cells differentiate into both microglia and macroglia in the brains of adult mice. Proc Natl Acad Sci U S A 94:4080-5
IF: 9.040 9108108 Cited: 631

2. **Mezey** E, KJ Chandross, G Harta, RA Maki and SR McKercher. (2000). Turning blood into brain: cells bearing neuronal antigens generated in vivo from bone marrow. Science 290:1779-82.
IF: 23.872 11099419 Cited: 1091

3. **Mezey** E, S Key, G Vogelsang, I Szalayova, GD Lange and B Crain. (2003). Transplanted bone marrow generates new neurons in human brains. Proc Natl Acad Sci U S A 100:1364-9
IF: 10.272 Cited: 307

4. Toth ZE, Leker RR, Shahar T, Pastorino S, Szalayova I, Asemenew B, Key S, Parmelee A, Mayer B, Nemeth K, Bratincsák A, Mezey E
The combination of granulocyte colony-stimulating factor and stem cell factor significantly increases the number of bone marrow-derived endothelial cells in brains of mice following cerebral ischemia.
Blood 111:(12) pp. 5544-5552. (2008)
IF: 10.432 Cited: 23

5. Bratincsak A, MJ Brownstein, R Cassiani-Ingoni, S Pastorino, I Szalayova, ZE Toth, S Key, K Nemeth, J Pickel and E **Mezey**. (2007). CD45-positive blood cells give rise to uterine epithelial cells in mice. Stem Cells 25:2820-6
IF: 7.531 Cited:14

6. Tran SD, SR Pillemer, A Dutra, AJ Barrett, MJ Brownstein, S Key, E Pak, RA Leakan, A Kingman, KM Yamada, BJ Baum and E **Mezey**. (2003). Differentiation of human bone marrow-derived cells into buccal epithelial cells in vivo: a molecular analytical study. Lancet 361:1084-8.
IF: 18.316 Cited: 91

7. Tran SD, Redman RS, Barrett AJ, Pavletic SZ, Key S, Liu Y, Carpenter A, Nguyen HM, Sumita Y, Baum BJ, Pillemer SR, **Mezey E** (2011) Micro-chimerism in salivary glands after blood- and marrow-derived stem cell transplantation. Biology Of Blood And Marrow Transplantation 17:(3) pp. 429-433.
IF: 3.149

III. Immune-regulatory effects of bone marrow stromal cells

A group from the Karolinska Institute headed by Dr. Katarina LeBlanc had a young patient who developed graft vs. host disease (GVHD) as a complication of a BM transplantation. After all known treatment strategies failed, they decided to request permission for a new therapeutic intervention. It was known that BM derived stromal cells (BMSCs or also called mesenchymal stem cells-MSCs) suppress T cell proliferation. Thus, they infused isolated and cultured BMSCs from the patient's mother and saw a dramatic improvement in the GVHD. They published their results in Lancet and started a whole new chapter in the clinical use of BMSCs.

1) *Septic conditions*

After reading LeBlanc's Lancet paper, we became interested in the biology of BMSCs and the mechanisms by which they regulate immune responses. One of the most complicated of these occurs in sepsis, when the response to microbial invasion frequently overshoots and ends up killing the host as well. We wondered if a live cellular therapy could be beneficial in a septic environment that changes very quickly

and the appropriate immune response at any given timepoint could make the difference between life and death. We used a mouse model of human peritonitis, called cecal ligation and puncture (CLP) and either injected the mice with BMSCs of different sources or vehicle intravenously at the time of septic injury (8). We found that the injected cells significantly improved the survival of the mice due to an improvement in organ functions. We then studied the mechanism of this action using a wide variety of techniques and using BMSCs from many transgenic mice that lacked certain factors. With this approach we determined that the injected BMSCs induce pro-inflammatory macrophages to become anti-inflammatory and produce large amounts of IL-10. The BMSCs were stuck in the capillaries of the lung where they were surrounded by monocytes/macrophages. Monocytes and/or macrophages from septic lungs made more IL-10 when prepared from mice treated with BMSCs versus untreated mice. In vitro, lipopolysaccharide (LPS)-stimulated macrophages produced more IL-10 when cultured with BMSCs, but this effect was eliminated if the BMSCs lacked the genes encoding Toll-like receptor 4 (TLR4), myeloid differentiation primary response gene-88 (MyD88), tumor necrosis factor (TNF) receptor-1a or cyclooxygenase-2 (COX2). Thus we concluded that BMSCs (activated by LPS or TNF-a) can reprogram macrophages by releasing prostaglandin E2 that acts through the prostaglandin EP2 and EP4 receptors.

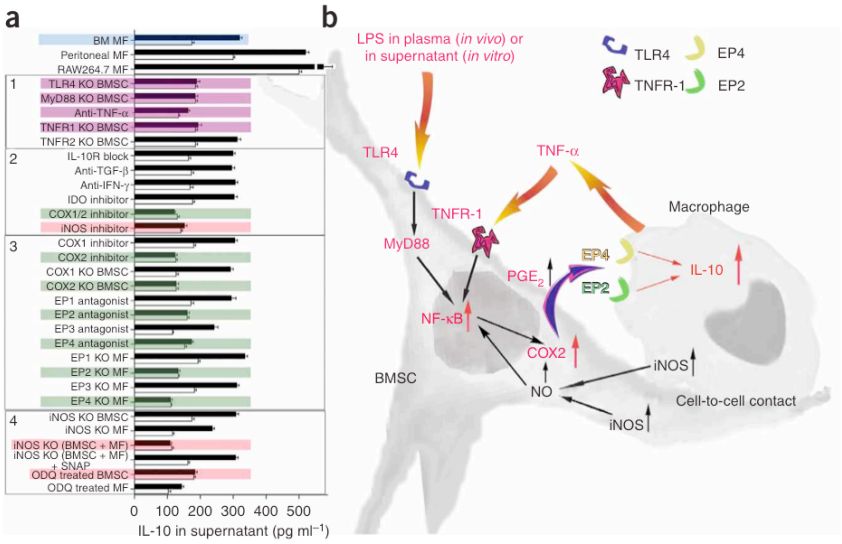

Fig.8. Summary of studies of the molecular pathways involved in the interaction between BMSC and macrophages. (a) IL-10 concentration changes in supernatants of

cocultures in a variety of treatment conditions after LPS stimulation. Colored graphs (except for the blue color that labels the bone marrow macro-phages as the source of all consecutive experiments) show treatments that eliminate the effect of BMSCs on macrophages. Black graphs show IL-10 levels after LPS stimulation, whereas open graphs show the control (nonstimulated) values. The experiments where the conditions eliminated the effect are colored. Purple color shows the effect of septic environment, green color shows agents and cellular compartments related to the PGE2 pathway and pink color shows agents related to the nitric oxide pathway. Three separate kinds of macrophages (bone marrow macrophages; peritoneal macrophages and the RAW264.7 cell line) were examined initially. Because they behaved identically in the assay, we used bone marrow derived macrophages (BM MF) for the rest of the experiments. In the box labeled 1, the effect of septic environment on the BMSCs is studied in BMSCs from TLR4-, MyD88-, TNFR1- and TNFR2- deficient mice, or antibody to TNF-α was used to neutralize the effect of TNF. The box labeled with 2 shows the cytokines and agents that have been implicated in the literature in immunomodulation of T cells by BMSCs, including COX1/2 and iNOS inhibitors. The box labeled 3 shows studies of the COX2 pathway, including the prostaglandin receptors EP1–EP4. Finally, in the box labeled with 4, we show studies related to nitric oxide. (b) A summary of our current hypothesis about the mechanisms that underlie the interactions between BMSCs and macrophages in the CLP sepsis model. Bacterial toxins (for example, LPS) and circulating TNF-α act on the TLR4 and TNFR-1 receptors of the BMSCs, respectively. This results in the translocation of NFkB into the nucleus. This activation process seems to be nitric oxide dependent. Activated NFkB induces the production of COX2, resulting in increased production and release of PGE2. PGE binds to EP2 and EP4 receptors on the macrophage, increasing its IL-10 secretion and reducing inflammation.

2) Th2 dominant (allergic) environment

We learned from the sepsis study that BMSCs are able to correctly respond to environmental clues and regulate the immune system according the needs of the body. Proliferating helper T cells differentiate into two major subtypes of cells known as Th1

and Th2 lymphocytes. Our study of sepsis and others as well had shown that BMSC-driven immunomodulation is mediated by the suppression of proinflammatory Th1 responses, rebalancing the Th1/Th2 ratio toward Th2. We wondered whether BMSCs could act in a Th2-dominant environment—e.g., the one that prevails in the ragweed induced mouse asthma model. Intravenous injection of BMSCs at the time of the antigen challenge protected the animals from the majority of asthma-specific pathological changes (9), including inhibition of eosinophil infiltration and excess mucus production in the lung, decreased levels of Th2 cytokines (IL-4, IL-5, and IL-13) in the bronchial lavage (BAL), and lowered serum levels of Th2 immunoglobulins (IgG1 and IgE). We used BMSCs derived from a variety of transgenic mice; performed in vivo blocking of cytokines; studied how asthmatic serum and BAL from ragweed challenged animals effect the BMSCs of in vitro to find the mechanism of the effect. Our results suggest that IL-4 and/or IL-13 activate the STAT6 pathway in the BMSCs that in turn causes an increase of their TGF-b production, which seems to mediate the beneficial effect, either alone, or in concert with regulatory T cells, that might also be recruited by the BMSCs.

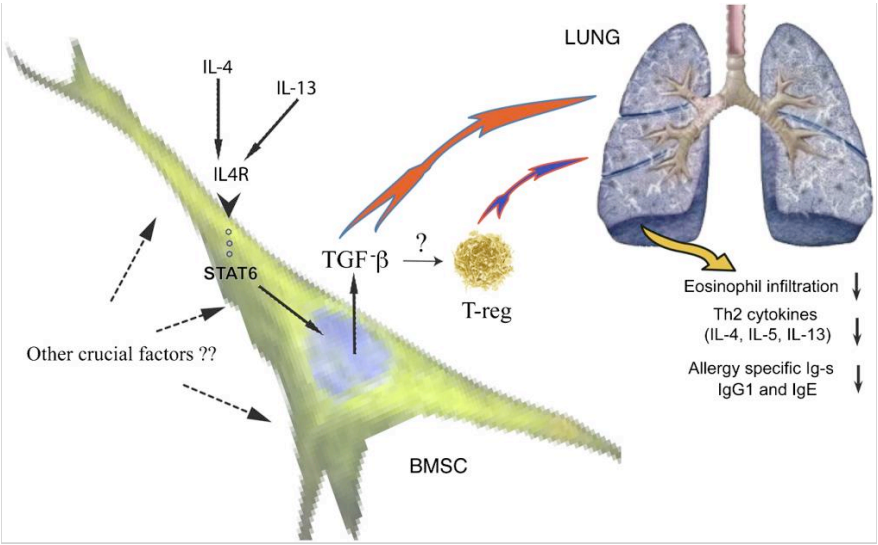

Fig. 9. Schematic drawing shows the mechanism of effect based on data of the present study. BMSCs “sense” the allergic environment, and as a result of the increased levels of IL-4/IL-13, they respond by producing higher amounts of TGF-β that, either alone or by recruiting regulatory T cells, will ultimately lead to a decrease of lung eosinophil infiltration, as well as allergy-specific cytokine and Ig production.

3) Histamine rich environment

In humans mast cells (MCs) play a major role in the reaction to allergens. Thus we examined the effect of MC degranulation and histamine on the function of BMSCs. Mast cells (MCs) have a central role in allergic responses, including certain types of asthma and in the development of autoimmune disease. These cells represent an important link between innate and acquired immunity. We studied the interaction between mouse bone marrow-derived stromal cells and mouse bone marrow derived MCs (10) and found that BMSCs can efficiently suppress several MC functions in vitro as well as in vivo. When MCs are cocultured with BMSCs directly (allowing cell to cell contact), the BMSCs suppress MC degranulation, proinflammatory cytokine production, chemokinesis, and chemotaxis.

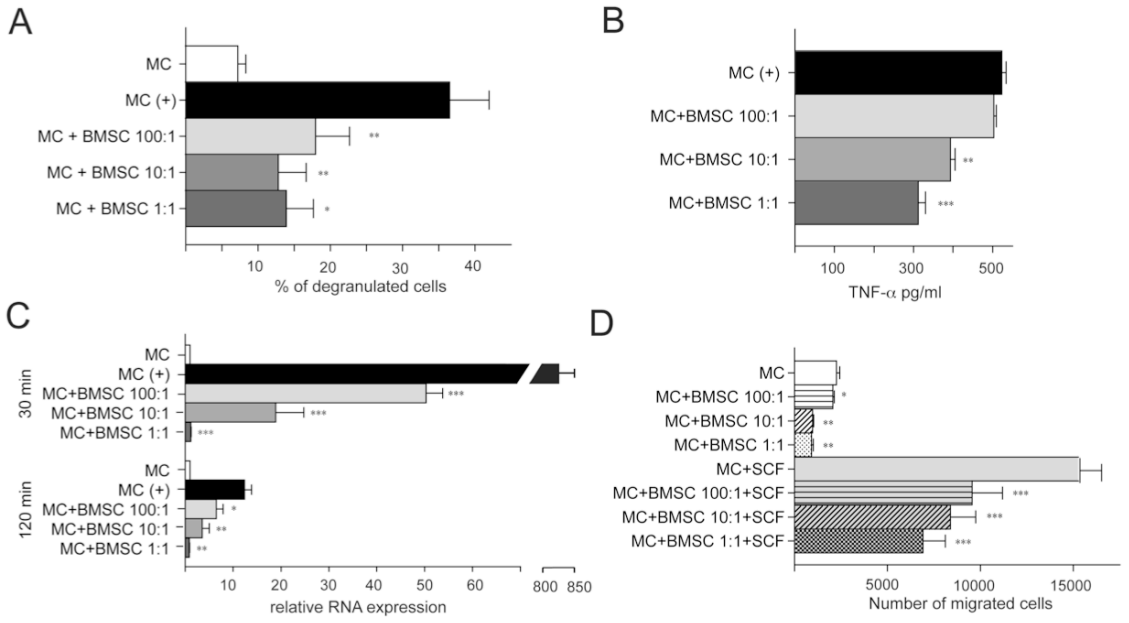

Fig. 10. In vitro studies of the interactions between MCs and BMSCs
A: Different ratios (1:1; 1:10 and 1:100) of IgE sensitized MCs and BMSCs were cultured together for 24 hours prior to IgE specific antigen challenge. ®-hex release was used as a marker of MC degranulation. BMSCs attenuate MC degranulation in all ratios tested. B: Different ratios (1:1; 1:10 and 1:100) of IgE sensitized MCs and BMSCs were cultured together for 24 hours prior to IgE specific antigen challenge for 12 hours. The BMSCs decreased the amount of released TNF-α in a ratio dependent manner as measured by ELISA. C: The experiment in B was repeated to measure TNF-α mRNA levels at two time-points (30 and 120 min) following antigen challenge. Similar to the

levels of TNF-α protein, mRNA synthesis also decreased in response to the presence of BMSCs at both time- points in a ratio dependent manner. D: The migration of MCs was affected by the presence of BMSCs in the culture – with increasing numbers of BMSCs within the co-culture, the spontaneous (upper four columns) as well as SCF induced migration (chemokinesis and chemotaxis, respectively) of MCs were significantly reduced. In all Figures:*=p<0.05; **=p<0.01 and ***=p,0.001

Similarly, MC degranulation within mouse skin or the peritoneal cavity was suppressed following *in vivo* administration of BMSCs. Further, we demonstrate that these inhibitory effects were dependent on upregulation of COX2 in BMSCs and facilitated through the activation of EP4 receptors on MCs.

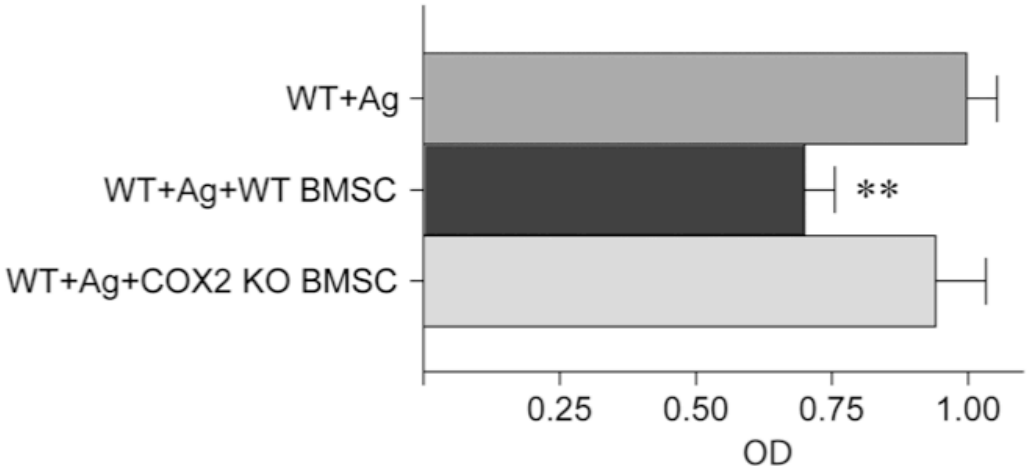

Fig.11. In vivo confirmation of COX2 mediated mechanism. The peritoneal assay was repeated using COX2 KO BMSCs followed by challenging the sensitized resident MCs with antigen (Ag). In contrast to wild-type (WT) BMSCs, COX2 deficient BMSCs failed to suppress hexosaminidase release by peritoneal MCs.

Based on these data we suggest that BMSCs might represent a novel cell based therapeutic approach in the treatment of MC driven allergic diseases.

d. References

8. Nemeth K, A Leelahavanichkul, PS Yuen, B Mayer, A Parmelee, K Doi, PG Robey, K Leelahavanichkul, BH Koller, JM Brown, X Hu, I Jelinek, RA Star and E **Mezey**. (2009). Bone marrow stromal cells attenuate sepsis via prostaglandin E(2)-dependent reprogramming of host macrophages to increase their interleukin-10 production. Nat Med 15:42-9.
IF:27.146 Cited: 107

9. Nemeth K, A Keane-Myers, JM Brown, DD Metcalfe, JD Gorham, VG Bundoc, MG Hodges, I Jelinek, S Madala, S Karpati and E **Mezey**. (2010). Bone marrow stromal cells use TGF-beta to suppress allergic responses in a mouse model of ragweed-induced asthma. Proc Natl Acad Sci U S A 107:5652-7.
IF: 9.432 Cited: 14

10. Brown JM, Nemeth K, Kushnir-Sukhov NM, Metcalfe DD, **Mezey E** (2011) Bone marrow stromal cells inhibit mast cell function via a COX2-dependent mechanism Clin.Exp. Allergy 41:526-534
IF: 4.084

IV. Conclusions

I. Contribution of circulating cells to tissue regeneration

1) CNS

1a) Rodents

Cells that circulate in the bloodstream can gain access to the brain in rodents. In animals without brain injury these cells are evenly distributed and can become neural cells including microglia, macroglia, endothelial cells and neurons.

When a brain injury (stroke) occurs, the number of circulating cells entering the brain seems to increase. Many of these cells become vascular endothelial cells and form new vessels. The neovascularization facilitates healing, decreasing the necrotized volume and increasing the number of surviving cells.

1b) Humans

In samples of postmortem human brains we determined the presence of donor derived cells in the CNS following gender mismatched bone marrow transplants. As in rodents, we found that cells from the donor bone marrow entered the brains and differentiated into neural cells there. We found the greatest numbers of these cells in the youngest patient (2 years old) who also survived the longest following BM transplantation. Although we can not do functional tests in postmortem human samples, based on morphology and multiple neuronal markers, the donor derived cells were undistinguishable from the host neurons. Another important observation is that statistical analysis of the donor derived cells suggest that they are clonal, i.e. a cell from the circulation seeds the brain and multiplies and differentiates there.

Significance of the above findings: ***the demonstration that circulating cells cross the blood-brain suggests that these cells might be used as vehicles to introduce growth factors/differentiation factors or enzymes into the CNS. The enzymes might correct or slow the progression of genetic neurological diseases. The finding that GCSF/SCF treatment significantly enhances neovascularization indicates that this treatment may be beneficial in patients with stroke***

2) Epithelial tissues

2a) Mouse uterus

Based on the human cheek cell data we used a genetic tool to see if hematopoetic progenitors can indeed seed epithelial tissues. Using genetic marking of hematopoetic progenitors we have demonstrated that these cells get into the endometrium and participate in replenishing lost cells during the cycle. In some mice 70% of the epithelium was of hematopoetic origin following a pregnancy, which is known to inclrease the uterine surface area by 20 fold.

2b) Human cheek cells and salivary glands

Using a similar approach to the brain studies, we found that donor derived blood cells contribute to the population of cheek epithelium. Due to the unique patient population we were also able to establish the fact that in two patients the new cheek cells derived from hematological progenitors, since these patients did not receive BM, but isolated hematological progenitors from peripheral blood. We also examined the possibility that Y chromosome containing cheek cells might derive from an earlier pregnancy with a male fetus. DNA analysis conclusively showed that the Y chromosome in the cheek cells was from the donor vs the male offspring of the recipient.

Significance of the above findings: ***the demonstration that circulating BM derived cells can contribute to epithelial tissues supplies a. an alternative explanation to the pathomechanism of endometriosis, a rather common disease in the female population and b. raises the possibility that if this process can be boosted, than oral mucosa and salivary gland function could be restored in people who lose them due to autoimmune disease (Sjogren's Syndrome) or head- and neck irradiation.***

III. Immunoregulatory effect of BMSCs

1) Septic environment

We analyzed the role that BMSCs play in regulating immune function in sepsis. Our results demonstrated that iv injected BMSCs are entrapped in the lungs where they communicate with monocytes/macro-phages that surround them. In the septic environment, these monocytes/macrophages are proinflammatory and make TNF-α. When they come in contact with BMSCs they change character and becomy anti-inflammatory. This tunes down the immune attack on body organs and allows animals to survive the septic process.

The crosstalk between BMSCs and the monocytes/macrophages involves the production and release of PDG2 by the BMSCs and a resulting increase of the monocytes/macrophages IL-10 production. The final outcome is a decreased number of neutrophils in body organs and less oxidative damage. On the other hand, there are more circulating neutrophils, and consequently more efficient clearence of bacteria.

2) Th2 dominant (allergic) environment

Using a ragweed induced allergy mouse model we determined that BMSCs are able to "sense" the allergic environment (increased levels of IL-4 /IL-13) and respond by producing large amounts of TGF-β that (either alone or by recruiting regulatory T cells) will ultimately lead to a decrease of lung eosinophil infiltration, and the allergy-specific cytokine and Ig production.

3) Histamine rich environment

As a continuation of the above studies, since mast cells (MCs) play a significant role in humans in allergic settings, we examined how BMSCs interact with MCs and how they respond to histamine, which is the major MC mediator. We demonstrated that BMSCs have the ability to affect the biology of MCs by limiting their activation and migration. Our data additionally show that these effects are mediated through the EP4 receptor on MCs.

<u>Significance of the above findings:</u>

Our results in the sepsis model indicate that BMSCs might be a very effective therapeutic intervention in human sepsis – when no other treatment option is available. Live cells may be superior to drugs, because the cells respond to their environment while drugs can only play the role that they were designed for. Since a large number of people die of sepsis every year (over 250000 in the US alone), a new therapy is badly needed.

The second set of studies indicate that in steroid resistant asthmatic conditions the use of BMSCs should be considered, since they are able to mitigate the allergic response and to counter the effects of MC degranulation.

V. ACKNOWLEDGEMENTS

Looking back at my scientific carreer makes me realize that one needs a village (in my case a city and two continents..) to raise a scientist just as one does to raise a child. I have to start with my family, who supported all my adventures from childhood. My parents were always there to encourage me and help me find my way. My Mom planted the seeds of scientific curiosity in me at a very young age and my Dad helped me develop independent (and sometimes unusual) patterns of thinking. My brother, András, kept me in line and taught me many life skills, and both he and his wife, Lasy, gave me tremendous support after my parents were gone. My husband, Michael Brownstein, was an incredible force, whose scientific advice and input shaped my career in numerous ways. Without him I would not be writing this thesis. And as far as family goes, I also have to thank my daughter, Anna, who gave me a reason to go on even when things were bad, and whose unconditional love and support was always there for me. Last but not least I want to thank Dr. Judit Futo, my best friend since childhood, for all the times we spent discussing life and death, fun and misfortunes. She made me feel that if I fell, she would always be there to pick me up.

Trying to think of all of my mentors (many of whom also became close friends) I have to start with Janos Szentagothai, whose lectures during my years in medical school attracted me to his Department at the beginning of my student research carreer. Later on he was always supportive and encouraging, and never had a problem with untraditional ways of thinking. He permanently engraved in me he love of the miracle of the nervous system. In the Anatomy Department I had the fortune of having Miklos Palkovits as my immediate supervisor. There is not enough space in this thesis to list all the ways he shaped my life: my approach to problems, the numerous pitfalls of experimental designs and analysis of the results and the lessons about how to avoid them (after he let me fall first..). He knew when to keep close control, when to point out my mistakes, and also when to let me go and succeed or fail, and take the consequences. I want to mention Endre Csanda, the Chair of Neurology, and a very close personal friend, who was always willing to

answer my sometimes silly and unusual questions about the brain and life and acted as a surrogate father after I lost mine. My first foreign mentor, Prof. David DeWied helped me grow scientifically and remaind supportive long after I left his Institute in Utrecht. After I moved to the US, once again, I met many wonderful people of the older and younger generation (including my fellows). In the interest of saving space, I will list their names without giving a detailed description of our interactions, but I want to emphasize that each and every one of them helped me in many ways to be what I am today as a scientist and as a person. I want to thank Tomas Hokfelt, Ronald DeKloet, Irvin Kopin, Julie Axelrod, Bruce Baum, Hal Gainer, Lana Skirboll, Pam Robey, Stefan Hansson, Andreas Zimmer, Janet Clark, Ruth Siegel, Joe Martin, Harry Webster, William Paul, Martin Eglitis, Karen Chandross, Gyongyi Harta, Bela Hunyady, Nancy Buckley, Tal Shahar, Andras Bratincsak, Zsuzsanna Toth, Krisztian Nemeth, Sarolta Karpati, Balazs Mayer, Miklos Krepuska, Sharon Key, Ildiko Szalayova. Many additional colleagues helped me along the way and I apologize to everyone I could not mention here. In addition, I have not listed the many personal friends who stood by me and helped me through hard times. These include my beloved dog P.H. who served as both a psychiatrist and exercise therapist for more than eleven years and is sorely missed.

Proc. Natl. Acad. Sci. USA
Vol. 94, pp. 4080–4085, April 1997
Neurobiology

dc_219_11

Hematopoietic cells differentiate into both microglia and macroglia in the brains of adult mice

(gene transfer/bone marrow transplantation/stem cells/lineage analysis)

MARTIN A. EGLITIS*† AND ÉVA MEZEY‡

*Laboratory of Cell Biology, National Institute of Mental Health, and ‡Clinical Neuroscience Branch, National Institute of Neurological Disorders and Stroke, Bethesda, MD 20892

Communicated by Richard L. Sidman, Harvard Medical School, Southborough, MA, January 28, 1997 (received for review October 9, 1996)

ABSTRACT **Glial cells are thought to derive embryologically from either myeloid cells of the hematopoietic system (microglia) or neuroepithelial progenitor cells (astroglia and oligodendrocytes). However, it is unclear whether the glia in adult brains free of disease or injury originate solely from cells present in the brain since the fetal stage of development, or if there is further input into such adult brains from cells originating outside the central nervous system. To test the ability of hematopoietic cells to contribute to the central nervous system, we have transplanted adult female mice with donor bone marrow cells genetically marked either with a retroviral tag or by using male donor cells. Using *in situ* hybridization histochemistry, a continuing influx of hematopoietic cells into the brain was detected. Marrow-derived cells were already detected in the brains of mice 3 days after transplant, and their numbers increased over the next several weeks, exceeding 14,000 cells per brain in several animals. Marrow-derived cells were widely distributed throughout the brain, including the cortex, hippocampus, thalamus, brain stem, and cerebellum. When *in situ* hybridization histochemistry was combined with immunohistochemical staining using lineage-specific markers, some bone marrow-derived cells were positive for the microglial antigenic marker F4/80. Other marrow-derived cells surprisingly expressed the astroglial marker glial fibrillary acidic protein. These results indicate that some microglia and astroglia arise from a precursor that is a normal constituent of adult bone marrow.**

Besides the cells of the vasculature, the brain comprises two general cell types: neurons and glial cells. Glial cells provide physiological support to neurons and repair neuronal damage due to injury or disease. Macroglia (astroglia and oligodendroglia) are generally considered to be derived from neuroectoderm and are believed to be developmentally distinct from microglia (1). However, the developmental origin of microglia remains debatable (2, 3), the two major views being that they derive either from neuroepithelial cells (4–6) or from hematopoietic cells (i.e. monocytes) (7, 8). The extent to which cells outside the central nervous system (CNS) contribute to the maintenance of microglia in adults remains debatable (compare refs. 9 and 10), and no such contribution to adult neurons or macroglia has been previously described.

To learn if cells of the hematopoietic system are a source of progenitor cells for the CNS, we have used genetically tagged bone marrow cells and monitored their appearance in the brain by *in situ* hybridization histochemistry (ISHH). We combined ISHH and immunohistochemistry, and performed double-ISHH with digoxigenin and radioactively labeled probes to analyze which cell types might be derived from bone marrow stem cells.

MATERIALS AND METHODS

Gene Transfer and Bone Marrow Transplantation. Gene transfer into hematopoietic precursors was done as previously described (11, 12), with the addition of stem cell factor to optimize transduction of reconstituting hematopoietic stem cells (13). C57BL/6J mice (The Jackson Laboratory), 6–8 weeks old, were used as donors. Forty-eight hours before marrow harvest, the mice were injected with 5-fluorouracil at a dose of 150 mg/kg to ablate mature blood cells and thereby induce progenitor cells into cycle. Upon harvest, marrow was placed into liquid culture in suspension dishes and grown in DMEM containing 15% fetal bovine serum (BioWhittaker) and supplemented with interleukin 3 (50 ng/ml), interleukin 6 (100 ng/ml), and stem cell factor (100 ng/ml). Growth factors were used to maintain early hematopoietic cells in cycle (13). All were obtained from R & D Systems. After 48 h in culture with growth factors, marrow cells were collected and added to tissue culture dishes containing the F5B producer cell line at subconfluent density. F5B cells shed the N2 retroviral vector, packaged with the ecotropic envelope and carrying the bacterial gene for neomycin resistance (neo^R) (14). After 48 h coculture with F5B cells, bone marrow cells were collected by gentle aspiration, suspended to 1×10^7 cells per ml in PBS (in all cases 0.1 M phosphate/140 mM NaCl, pH 7.6) and injected intravenously ($2–3 \times 10^6$ cells per mouse) via the tail vein into sublethally irradiated (4.5 Gy) female WBB6F1/J-Kit^W/Kit^{W-v} mice. WBB6F1/J-Kit^W/Kit^{W-v} mice are particularly good recipients for bone marrow transplantation because they have genetically defective stem cells (15). This gives normal C57BL/6J donor stem cells a strong repopulating advantage.

In transplants of male donor marrow into female recipients, some marrow was marked with retroviral vector as described. In other cases, marrow was harvested, washed with PBS, and transplanted directly into recipient mice without culturing in growth factor-containing medium or irradiation of recipient animals.

A total of 46 mice were transplanted, 38 with vector-tagged marrow and 8 with male marrow. Five of the transplants with vector-tagged marrow used male donor cells. Mice were sacrificed at various times after transplantation. At least 2 animals were analyzed at each time point, although more were used at the 14-day ($n = 10$), 35-day ($n = 14$), and 70-day ($n = 6$) time points. Tissues were collected and immediately frozen

The publication costs of this article were defrayed in part by page charge payment. This article must therefore be hereby marked "*advertisement*" in accordance with 18 U.S.C. §1734 solely to indicate this fact.

0027-8424/97/944080-6$0.00/0
PNAS is available online at **http://www.pnas.org**.

Abbreviations: ISHH, *in situ* hybridization histochemistry; neo^R, neomycin resistance; GFAP, glial fibrillary acidic protein; CNS, central nervous system; FITC, fluorescein isothiocyanate; DAPI, 4′,6-diamidino-2-phenylindole.

†To whom reprint requests should be sent to the present address: Experimental Therapeutics Branch, National Institute of Neurological Disorders and Stroke, Building 10, Room 5C211, 10 Center Drive, MSC 1406, Bethesda, MD 20892-1406.

on dry ice for subsequent sectioning. Some animals underwent cardiac perfusion with PBS before tissue harvest. Animals for perfusion were anesthetized with carbon dioxide, then their chests were opened, and PBS was introduced through a cannula placed in the left ventricle. The right atrium was incised to allow release of blood. Animals were perfused with 50 ml of ice-cold PBS over a period of 5 min.

***In Situ* Hybridization Histochemistry.** Tissues were evaluated with both oligonucleotide and RNA probes. To detect neo^R transcripts, two oligonucleotide probes were prepared, complementary to the sequence of the neo^R gene either from nucleotides 222–269 or nucleotides 447–494 (numbering with the A of the initiation codon as 1). The oligonucleotides were labeled using terminal transferase (Boehringer Mannheim) and [^{35}S]thio-dATP (New England Nuclear) as described previously (16). An RNA probe, complementary to the entire neo^R coding region, was labeled with [^{35}S]thio-UTP using SP6 polymerase (17). Labeling with radioactive probes was detected by dipping hybridized sections in photographic emulsion. Emulsion was exposed for 14 days, then developed and sections were stained, air dried, and coverslipped for microscopic examination. To detect male bone marrow cells transplanted into female recipients, sequences specific to the donor mouse Y chromosome were detected using a complementary RNA probe derived from the plasmid pY353/b (18). Glial fibrillary acidic protein (GFAP) gene expression was detected using an RNA probe complementary to the entire GFAP coding region. The Y chromosome and GFAP probes were labeled using digoxigenin-UTP (19), and digoxigenin labeling was developed for GFAP using alkaline phosphatase as described (19). For detection of the donor Y chromosome, before overnight hybridization with digoxigenin-labeled probes at 55°C, the slides were heated at 90°C for 10 min in hybridization buffer containing the probes to improve access to nuclear DNA. The digoxigenin-labeled Y chromosome was visualized using a modification (20) of an immunostaining amplification method (21), which results in green fluorescein isothiocyanate (FITC) fluorescence.

Twelve-micrometer thick frozen sections were cut in a cryostat, and ISHH was performed as described previously (16, 17). The sections were fixed, dehydrated, and delipidated in ethanol and chloroform, and then hybridization buffer containing the probe(s) was put on the sections. Slides were incubated overnight in a humidified chamber at 37°C (for oligonucleotide probes) or 55°C (for riboprobes).

Nuclear Staining. To confirm that Y chromosome ISHH coincided with cell nuclei, sections were counterstained with ethidium bromide or 4′,6-diamidino-2-phenylindole (DAPI). Staining was detected by illumination with a mercury lamp using a microscope equipped for fluorescence micrography.

Immunohistochemical Analysis. For combined ISHH/immunohistochemical analysis, sections were fixed as described previously (22). They then were incubated for 30 min at room temperature in 3% normal goat serum diluted in PBS (containing 0.6% Triton-X 100) to block nonspecific binding. Then, the sections were exposed for 1 h at room temperature to either (*i*) a polyclonal rabbit antibody that detects the mouse F4/80 monocyte/macrophage marker (23) or (*ii*) a polyclonal CY-3-labeled rabbit antibody against the astroglial marker GFAP (Sigma) used at a dilution of 1:2,000. Binding of nonlabeled primary antisera was detected with a biotinylated goat anti-rabbit IgG (Jackson ImmunoResearch) diluted 1:500. To detect biotinylated secondary antibody, the sections were incubated for 1 h in an avidin-biotin-peroxidase complex diluted 1:250 in PBS with 0.6% Triton-X 100 (24). The slides then were transferred into 0.1 M Tris·HCl (pH 7.6) and were developed using diaminobenzidine as a substrate. After a thorough wash, the sections were processed for ISHH. Colabeling of cells was determined using a combination of bright-field, polarized, fluorescent, and epi-illumination microscopy. Controls for the immunostaining included leaving out the primary antibodies and using several secondary antibodies (from different species) to confirm that there was no nonspecific binding.

RESULTS

Detection of Donor Cells in the Brain After Bone Marrow Transplantation. To evaluate the appearance and distribution of donor cells in the brains of recipient mice, animals were sacrificed 3, 5, 7, 14, 28, 35, 42, and 70 days after transplantation with bone marrow cells. At least two animals transplanted with retrovirally tagged marrow were studied at each time point. Mice transplanted with male marrow were analyzed at 35 days ($n = 9$) and 70 days ($n = 4$) after transplantation. Using probes specific to the vector neo^R transcripts, donor cells were detected beginning with day 3, the earliest time of analysis. Many cells were easily detected throughout the brain by day 7, and cells continued to be detected at all subsequent times. To estimate total number of neo^R-positive cells in a brain, every 25th section was collected, and all labeled cells in the sections were counted. The number of labeled cells was multiplied by 25 to arrive at the approximate total number of marked cells in a brain. These calculations showed that the overall number of marrow-derived cells per brain gradually increased with increasing time after transplantation. Three days after transplant, 500 cells were detected per brain. Two to four weeks after transplant the number of cells present had increased to at least 2,000 per brain. In several animals more than 10,000 cells per brain were seen, and in one animal the number of cells was over 30,000.

At 1 week, and occasionally at later times, concentrations of neo^R-marked cells were observed in the basal subarachnoid space. Cells marked by the retroviral vector were detected in the hippocampus (Fig. 1*A* and *B*), septum (Fig. 1*C*), and hypothalamus (Fig. 1*D*). Cells were also detected, among other regions, in the cortex, habenula, pons, and cerebellum (data not shown). Labeled cells were detected after PBS perfusion,

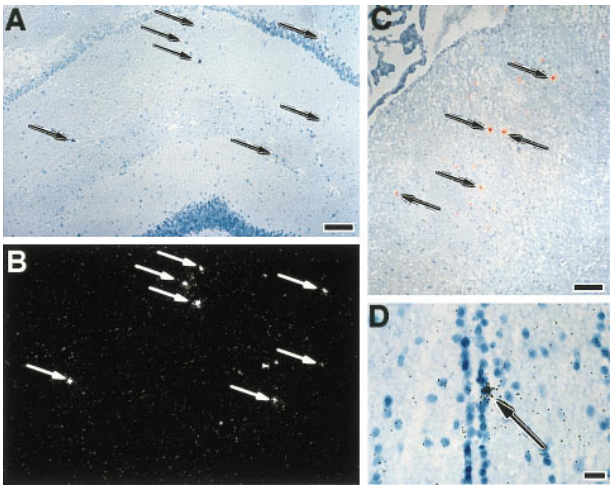

FIG. 1. Detection of donor cells in the brain after bone marrow transplantation with retrovirally tagged bone marrow cells. Arrows indicate representative cells positive by ISHH with ^{35}S-labeled oligonucleotide (*A–C*) or riboprobe (*D*). (*A* and *B*) Bright (*A*) and dark (*B*) field photographs of the same section. ISHH-positive cells (arrows) detected in the hippocampus of an animal 14 days postbone marrow transplantation. (*C*) Positive cells in the region of the septum of an animal sacrificed 14 days after bone marrow transplantation. The photograph is a double exposure of a bright field image with a dark field image of the same area. The dark field image was photographed using a red filter so that the autoradiographic grains would appear red. (*D*) A cell (arrow) within the ependyma of the third ventricle. [Bars = 10 μm (*A–C*) and 40 μm (*D*).]

indicating that bone marrow-derived cells were an integral part of the brain parenchyma.

Similar regional distribution of donor marrow cells was seen using the Y chromosome probe to detect male donor cells (Fig. 2). Ethidium bromide counter-staining to highlight the nucleus confirmed the nuclear localization of the Y chromosome probe. Many male donor-derived cells were easily detected throughout the brain 35 days after transplantation, and cells continued to be detected at all subsequent times. Cells positive for the Y chromosome marker were detected in the mesencephalon (Fig. 2 *A–C*), septum (Fig. 2*D*), striatum (Fig. 2*E*), and habenula (Fig. 2*F*). Cells also were detected in the cortex, pons, and cerebellum, among other regions (data not shown). *Ex vivo* manipulation of the bone marrow cells was not necessary, because male cells were detected in female recipients' brains even when the transplant was done immediately after marrow harvest.

Several parameters were used to verify that the labeling observed after ISHH was specific. First, no labeling was detected in any tissues of animals transplanted with nonmarked bone marrow cells. That is, without retroviral tagging, probes for the neo^R gene exhibited no background labeling, and the Y chromosome probe did not label female tissues. With the Y chromosome riboprobe, we also confirmed that both sense and antisense probes exhibited the same distribution, as expected when hybridizing to chromosomal DNA. The pattern of retrovirally labeled cells was identical in all tissues analyzed, both qualitatively and quantitatively, regardless of which probe was used. Finally, we found donor cells in hematologic organs such as bone marrow and spleen at all time points analyzed (data not shown). The pattern of engraftment was qualitatively similar between retrovirally tagged and male donor cells. However, when female mice were transplanted with retrovirally tagged male marrow, more donor cells were detected with the Y chromosome probe than with the neo^R probe. This suggests that not all of the cells migrating from the bone marrow into the brain expressed the retrovirally introduced neo^R gene at a level high enough to be detected by ISHH.

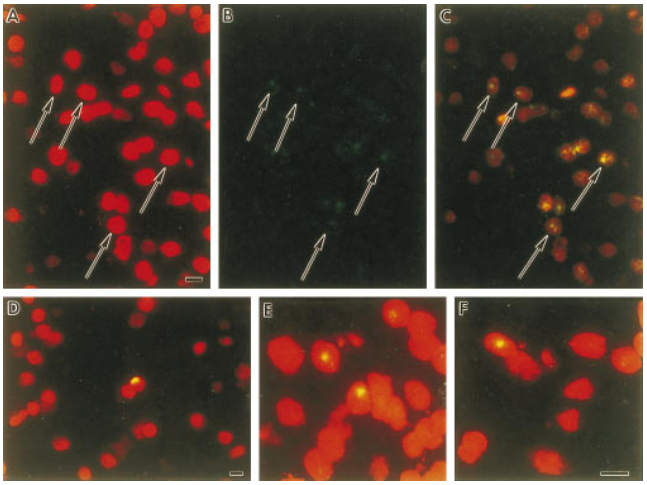

FIG. 2. Detection of donor cells in several brain regions of a female recipient 6 weeks after transplantation with male bone marrow cells. Arrows indicate representative cells positive for the Y chromosome by ISHH. (*A–C*) Photomicrographs of a section through the ventral mesencephalon. *A* is photographed using a rhodamine filter to excite ethidium bromide staining of the nucleus; *B* is photographed using a FITC filter to excite Y chromosome-specific FITC staining; and *C* is photographed with a double-pass filter to show overlap of Y chromosome labeling and nucleus-specific ethidium bromide staining. Arrows indicate some of the double-labeled cells. (*D–F*) Photomicrographs demonstrating Y chromosome positive cells in other brain regions. (*D*) Septum. (*E*) Striatum. (*F*) Habenula. (Bars = 10 μm.)

Labeling of Brain Sections after ISHH with the Microglial Marker F4/80. The F4/80 antibody detects the plasma membrane protein F4/80 expressed exclusively on macrophages and microglia (23). Colocalization in brain sections revealed cells labeled by the N2 retroviral vector that also expressed the F4/80 antigen (Fig. 3), confirming that bone marrow-derived cells do contribute to the microglial population in the adult brain. However, only a small percentage of ISHH-positive cells were labeled by immunostaining. Similarly, the minority of antigen-positive cells was doubly labeled by ISHH. The distribution of doubly labeled cells reflected the distribution of cells labeled only by ISHH or by immunoshistochemistry, i.e., they were widely distributed throughout the brain.

Labeling of Brain Sections for Both the Astroglial Marker GFAP and the neo^R Retroviral or Y Chromosome Donor Cell Tag. The ISHH-positive, F4/80 negative cells could be cells of the myeloid lineage that had not differentiated to express the F4/80 antigen. Or, they could represent a contribution of bone marrow-derived cells to other than myeloid cell lineages. To distinguish between these alternative possibilities, ISHH-positive cells were examined for the expression of another lineage marker, GFAP, specific for astroglia. Surprisingly, we found occasional cells (Fig. 4*A*) which were labeled both by ISHH (for the donor marrow neo^R marker) and by indirect immunohistochemistry (for GFAP). Counting all of the donor cells present in every 25th section obtained from recipient mice 4 weeks after transplantation (n = 3), we calculated that as many as 3×10^4 neo^R-marked donor cells were present per brain. Of that total donor cell number, we estimated between 0.5% and 2% exhibited GFAP expression.

To confirm that GFAP mRNA was present in some neo^R-positive cells, we also did double-ISHH analysis. Cells coexpressing GFAP and neo^R mRNAs were identified using a digoxigenin-labeled riboprobe against GFAP mRNA together with a ^{35}S-labeled probe for the neo^R gene marking the donor marrow. As illustrated in Fig. 4 *B* and *C*, we found cells labeled with both probes. Their frequency was approximately equal to the frequency of the ISHH/GFAP immunostained double cells.

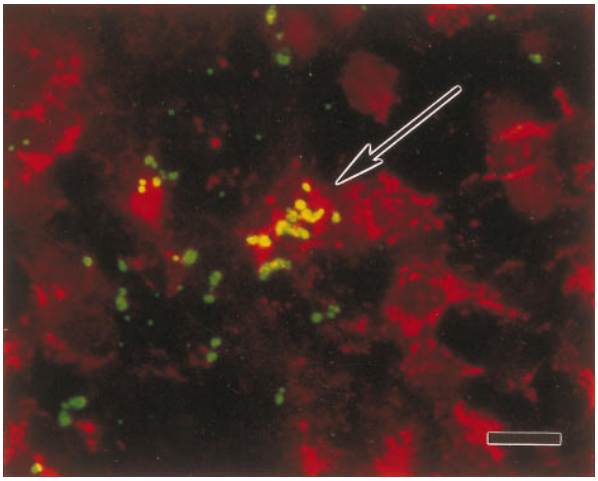

FIG. 3. Double-labeling of brain sections detects cells coexpressing the microglial marker F4/80 and the neo^R retroviral tag. The F4/80 monocyte/macrophage antigen was detected by indirect immunofluorescent antibody labeling; ^{35}S-radiolabeled probes were used to hybridize to neo^R mRNA. The photomicrograph is of a representative field from an animal sacrificed 35 days after bone marrow transplantation. A cell in the center stains positive for the F4/80 antigen (red) and exhibits labeling with radioactive probe to neo^R transcripts. The dark field image was photographed using a green filter so that autoradiographic grains would appear green (yellow where they overlap red immunostaining). (Bar = 10 μm.)

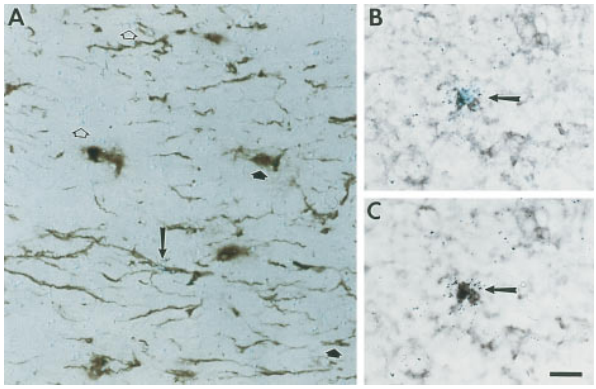

FIG. 4. Double-labeling of brain sections detects cells coexpressing the astroglial marker GFAP and the neo^R retroviral tag. (*A*) Detection of cells within the optic tract expressing GFAP protein using peroxidase-based immunohistochemical staining combined with ISHH to detect expression of neo^R transcripts. The arrow indicates a double-labeled cell. Open arrowheads indicate clusters of grains indicative of a neo^R-marked cell that is not expressing GFAP. Filled arrowheads indicate GFAP-positive positive cells that are not marked with the retroviral tag. (*B* and *C*) Detection of GFAP transcripts by ISHH using digoxigenin-labeled probes combined with detection of neo^R transcripts by ISHH using ^{35}S-labeled probes. The photograph is of a section through the cerebral cortex. (*B*) Polarized epifluorescent illumination to emphasize grains indicative of hybridization with ^{35}S-labeled probe for neo^R. (*C*) Bright field illumination emphasizing digoxigenin staining of GFAP transcripts. The cell indicated by the arrow is double-labeled. (All photomicrographs are at the same magnification. Bar = 20 μm.)

We also found doubly labeled cells in multiple animals when ISHH to detect male cells with the Y chromosome marker was combined with immunohistochemistry to detect GFAP protein (Fig. 5). Using DAPI staining to highlight the nucleus and three-channel photomicrography, we confirmed that the Y-chromosome ISHH was associated with the nuclei of GFAP-positive cells (Fig. 5 *C–H*).

DISCUSSION

The results reported here confirm that cells derived from the bone marrow can migrate into the brains of adult mice. Furthermore, we have found that this migration is rapid, with numerous cells present by the third day after transplant. These new cells are distributed throughout the brain, and appear to reside within the parenchyma, because perfusion with PBS does not remove them. Occasional donor marrow-derived cells were found in association with vascular structures. Moreover, densities of donor cells in the parenchyma paralleled the capillary density of a given region. For instance, cortex, with fewer capillaries, had a lower cell density than the more vascularized choroid plexus. Regions with a higher capillary density, such as the area postrema, also had the highest density of marrow-derived cells within the parenchyma.

Double-labeling analyses show that at least some bone marrow-derived cells acquire microglial antigenic markers. However, we also observed many cells positively labeled by ISHH that did not express the F4/80 antigen. This may be due simply to a level of antigen below the limits of detection in our assay. Alternatively, it is possible that the F4/80 marker is expressed on marrow-derived cells only after they fully differentiate into microglia, while less mature microglial precursors are not recognized by the antibody to F4/80. Nonetheless, our results strongly support the view that hematopoietic cells outside the CNS contribute to the maintenance of microglia in healthy adults. While a partial CNS origin of adult microglia cannot be excluded, our data is inconsistent with an exclusively CNS origin. Moreover, although our experiments did not examine fetal origins of microglia, the finding of hematopoietically derived microglia in healthy adults is also consistent with a hematopoietic origin of microglia in development.

Surprisingly, we found that some hematopoietic cells (tagged either with a retroviral vector or by transplant of male cells into a female recipient) give rise to cells other than microglia, specifically to cells that exhibit astroglial markers. Although this observation is unexpected, it is based on identical results in multiple animals using two independent means of cell tagging with both cytoplasmic and nuclear markers.

The appearance of marrow-derived astroglia seems a normal process in these animals. Because marrow-derived cell numbers detected in the brain increased over time, their appearance does not appear to be a consequence of the transplantation procedure itself. If appearance in the brain was a byproduct of transplantation, one might expect tagged cell numbers in the brain to peak and then decline, which was not observed. Rather, the data is consistent with existence of cells, among the populations of marrow-engrafting cells, capable of continuous generation of progenitors that migrated to the brain. Interestingly, cells with marrow markers were seen in the ventricular ependyma (Fig. 1*D*). In fact, in many animals, marrow-derived cells could be found concentrated subependymally (unpublished data). The subependymal zone is an important source of neuronal and glial progenitors during development (25–27) and in adults (28, 29). Finding bone-marrow derived cells in this location opens the possibility that such cells receive cues guiding their differentiation once they enter the brain. Studies evaluating this possibility are ongoing.

No obvious pathology such as gliosis was detected in the brain of any transplant recipient (n = 46). Some recipient animals were irradiated before receiving bone marrow transplants to see if marrow purging enhanced engraftment and seeding of implanted cells. However, radiation dosages were at least one order of magnitude below those known to induce pathological changes in the CNS (30). Indeed, we found preconditioning of recipients was not necessary. Male donor cells engrafted and persisted for at least 10 weeks even without irradiation (Fig. 5 *C–H*). Furthermore, as many Y chromosome/GFAP double-positive cells were seen with as without irradiation. The wide distribution of GFAP-positive cells in both gray and white matter suggests that bone marrow-derived progenitors are not restricted to differentiate into a particular subclass of astroglia. That is, marrow-marked cells contributed to both fibrous astrocytes in the white matter (Figs. 4*A* and 5 *C–E*) and protoplasmic astrocytes in the gray matter (Figs. 4 *B* and *C* and 5*A*).

One alternative explanation for our observing GFAP staining of cells bearing marrow markers is that processes from endogenous astroglia surround the in-migrating cells from the donor marrow. However, some of our data argue against this possibility. First, cytoplasmic neo^R ISHH labeling coincided with cytoplasmic GFAP immunostaining (Fig. 4*A*). Furthermore, upon evaluation of 50 to 100 male nuclei associated with GFAP staining, no nuclei were seen that could be considered part of an engulfing astroglial cell. If endogenous astroglia were the source of the GFAP staining associated with donor male nuclei, one might expect the geometry in 12 μm sections to reveal the cell body and nucleus corresponding to the putative engulfing processes in at least a few cases. After analyzing dozens of sections, no such cases were observed. Culturing astroglia obtained from brains of transplant recipients may help to resolve this issue in the future.

Because only about 10% of marrow-derived cells in the brain exhibit expression of either the microglial F4/80 antigen or the astroglial marker GFAP, the identity of the majority of bone marrow-derived cells remains an open question. Nonetheless, there is clearly a measurable contribution by cells of hematopoietic origin to the glial cell population of the brain in adult mice, which suggests that some glial progenitors reside outside

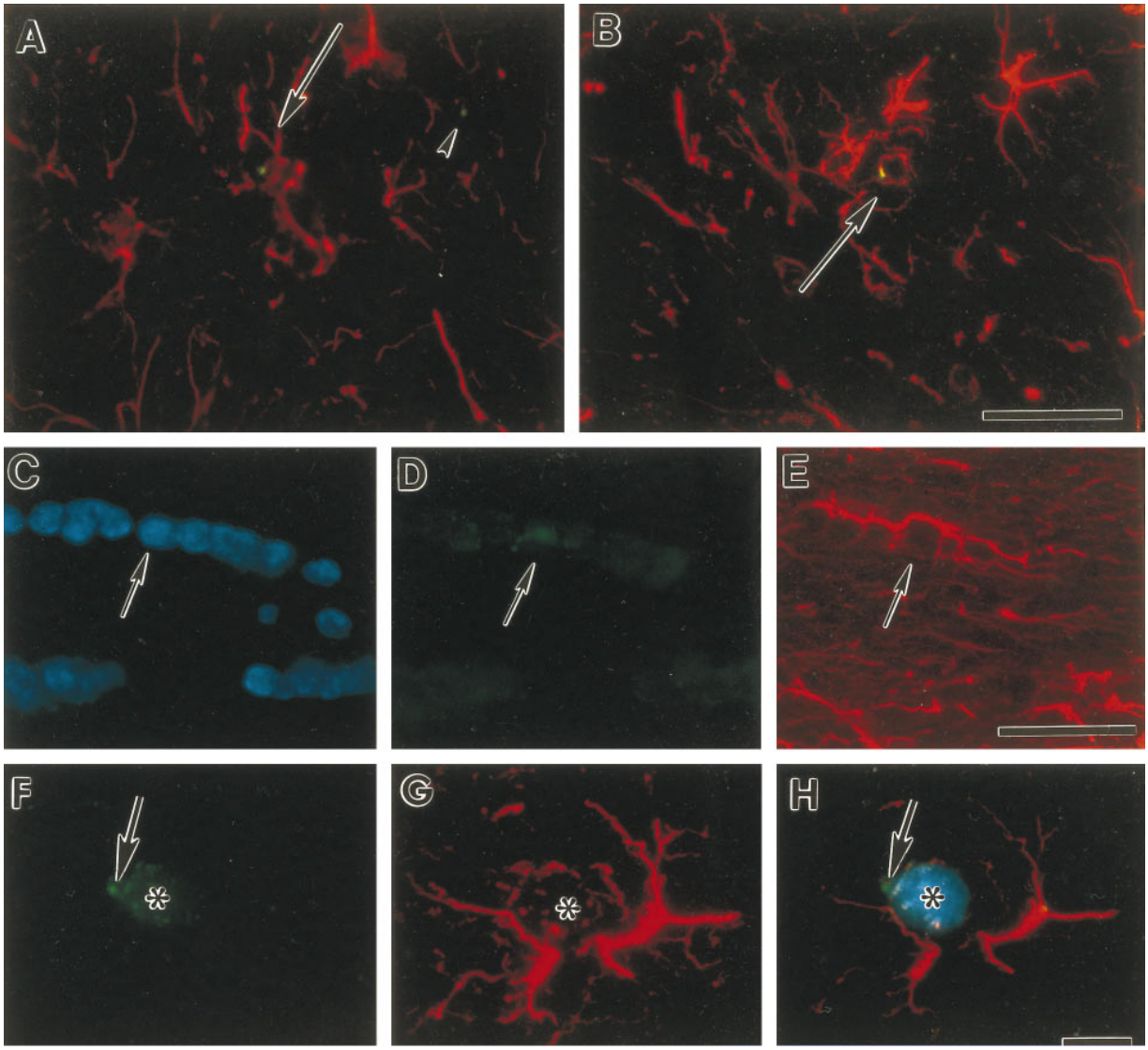

FIG. 5. Male bone marrow derivative cells express GFAP. Photomicrographs are of double-labeled cells found in the brains of two different female recipient mice 10 weeks after bone marrow transplantation. Male donor cells were detected with a Y chromosome-specific riboprobe as described in Fig. 1. Astroglia were identified using a CY3-labeled polyclonal antibody against the astroglial marker GFAP. (*A* and *B*) Double-labeled cells are indicated by arrows. The arrowhead in *A* points to a Y chromosome-positive cell derived from the male donor marrow that is not GFAP immunopositive. *A* is a section through the cortex. *B* is a section through the septum. (Bar in *B* applies to *A* and *B* and equals 20 μm.) (*C*, *D*, and *E*) Photomicrographs of a section through the corpus callosum. In *C*, the section is illuminated with ultraviolet light to excite DAPI fluorescent staining of the nucleus. Nuclei from all cells are stained. *D* is illuminated to excite FITC staining of the Y chromosome. *E* is illuminated to excite CY3-immunostaining of GFAP. A Y chromosome/GFAP double labeled cell is indicated by the arrow. (Bar in *E* applies to *C–E* and equals 20 μm.) (*F*, *G*, and *H*) Photomicrographs of a single field from a section through the amygdala. *F* illustrates the green FITC staining associated with the Y chromosome. *G* shows the red GFAP immunostaining, and *H* is a double-exposure of the same field, first with a double band pass filter to excite FITC and CY3 fluorescence, then with ultraviolet illumination to excite the blue DAPI fluorescent staining of the nucleus (*). The green Y chromosome fluorescence is indicated by the arrow (*F* and *H*). (Bar in *H* applies to *F–H* and equals 4 μm.) Sections in *A* and *C–E* were obtained from one mouse, while those in *B* and *F–H* were obtained from another.

the CNS. The observation of marrow-derived astroglia in the optic tract (Fig. 4*A*) suggests that some of these marrow-derived progenitors may be similar to the previously recognized astroglial precursor (31). Alternatively, two classes of astroglia may exist, one arising from the previously recognized neuroepithelial astroglial precursor present in the brain from birth, and another from a different precursor that is a normal constituent of adult bone marrow. It would be interesting to determine if astroglia arising from the different sources of progenitors also exhibit different functional characteristics.

Microglia and astroglia respond differently to brain injury. In fact, astrogliosis often appears to be a response to primary microgliosis (32, 33). There is also evidence that different brain lesions elicit different microglial and astroglial responses (34). Our results suggest that gene transfer into hematopoietic progenitors can be used to introduce genes into microglia and astroglia that then might participate in the gliosis associated with a CNS pathology. The detection of marrow-derived cells in brains within days of transplantation implies that genetically altered hematopoietic cells could be used to treat acute diseases of the brain.

Although many neurotrophic factors show promise in the treatment of CNS disorders, their use has been hindered by their inability to cross the blood-brain barrier and by their limited diffusion into CNS tissues (35). In addition, adverse effects have been reported after systemic administration of some neurotrophins (36). Using marrow-derived cells to deliver therapeutic proteins directly to the site of CNS pathology

may be more benign than systemic administration of toxic molecules. In addition, using vectors with cell type-specific promoters could restrict gene expression specifically to reactive astroglia or microglia, thereby providing greater therapeutic precision for gene therapy of CNS disease.

We are grateful to Gyöngyi Harta for her skillful technical assistance, and to Ricardo Dreyfuss for his expert help with the photomicrography. We also thank Drs. Miklos Palkovits, Henry D. F. Webster and Beth J. Hoffman for their comments on the manuscript. We also appreciate the generosity of Dr. Siamon Gordon in providing the rabbit polyclonal antiserum against F4/80.

1. Skoff, R. P. & Knapp, P. E. (1995) in *Neuroglia*, eds. Kettenmann, H. & Ransom, B. R. (Oxford Univ. Press, New York), pp. 135–148.
2. Theele, D. P. & Streit, W. J. (1993) *Glia* **7,** 5–8.
3. Altman, J. (1994) *Trends Neurosci.* **17,** 47–49.
4. Lewis, P. D. (1968) *Brain* **91,** 721–738.
5. Kitamura, T., Miyake, T. & Fujita, S. (1984) *J. Comp. Neurol.* **226,** 421–433.
6. Neuhaus, J. & Fedoroff, S. (1994) *Glia* **11,** 11–17.
7. Perry, V. H. & Gordon, S. (1988) *Trends Neurosci.* **11,** 273–278.
8. Ling, E.-A. & Wong, W.-C. (1993) *Glia* **7,** 9–18.
9. Perry, V. H. (1994) *Macrophages and the Nervous System* (Landes, Austin, TX).
10. Fedoroff, S. (1995) in *Neuroglia*, eds. Kettenmann, H. & Ransom, B. R. (Oxford Univ. Press, New York), pp. 162–181.
11. Eglitis, M. A., Kantoff, P., Gilboa, E. & Anderson, W. F. (1985) *Science* **230,** 1395–1398.
12. Bodine, D. M., Seidel, N., Karlsson, S. & Nienhuis, A. W. (1990) *Prog. Clin. Biol. Res.* **352,** 287–299.
13. Luskey, B. D., Rosenblatt, M., Zsebo, K. & Williams, D. A. (1992) *Blood* **80,** 396–402.
14. Armentano, D., Yu, S.-F., Kantoff, P. W., von Ruden, T., Anderson, W. F. & Gilboa, E. (1987) *J. Virol.* **61,** 1647–1650.
15. Russell, E. S. (1979) *Adv. Genet.* **20,** 357–459.
16. Young, W. S., Mezey, E. & Siegel, R. E. (1986) *Brain Res.* **387,** 231–241.
17. Bradley, D. J., Towle, H. C. & Young, W. S. (1992) *J. Neurosci.* **12,** 2288–2302.
18. Bishop, C. E., Boursot, P., Baron, B., Bonhomme, F. & Hatat, D. (1985) *Nature (London)* **315,** 70–72.
19. LeMoine, C. & Young, W. S. (1992) *Proc. Natl. Acad. Sci. USA* **89,** 3285–3289.
20. Hunyady, B., Krempels, K., Harta, G. & Mezey, E. (1996) *J. Histochem. Cytochem*. **44,** 1353–1362.
21. Berghorn, K. A., Bonnett, J. H. & Hoffman, G. E. (1994) *J. Histochem. Cytochem.* **42,** 1635–1642.
22. Lawson, L. J., Perry, V. H., Dri, P. & Gordon, S. (1990) *Neuroscience* **39,** 151–170.
23. Austyn, J. M. & Gordon, S. (1981) *Eur. J. Immunol.* **11,** 805–815.
24. Hsu, S. M., Raine, L. & Fanger, H. (1981) *J. Histochem. Cytochem.* **29,** 577–580.
25. Smart, I. (1961) *J. Comp. Neurol.* **116,** 325–347.
26. Altman, J. (1969) *J. Comp. Neurol.* **137,** 433–458.
27. Sturrock, R. R. & Smart, I. H. M. (1980) *J. Anat.* **130,** 391–415.
28. Alvarez-Buylla, A. & Lois, C. (1995) *Stem Cells (Dayton)* **13,** 263–272.
29. Weiss, S., Reynolds, B. A., Vescovi, A. L., Morshead, C., Craig, C. G & van der Kooy, D. (1996) *Trends Neurosci.* **19,** 387–393.
30. Chiang, C. S., McBride, W. H. & Withers, H. R. (1993) *Radiother. Oncol.* **29,** 60–68.
31. Lillien, L. E. & Raff, M. C. (1990) *Neuron* **5,** 111–119.
32. Giulian, D. (1988) in *The Biochemical Pathology of Astrocytes*, eds. Norenberg, M. D., Hertz, L. & Schoustoe, A. (Liss, New York), pp. 91–105.
33. Giulian, D., Chen, J., Ingeman, J. E., George, J. K. & Noponen, M. (1989) *J. Neurosci.* **9,** 4416–4429.
34. Wilson, M. A. & Molliver, M. E. (1994) *Glia* **11,** 18–34.
35. Lindsay, R. M., Wiegand, S. J., Altar, C. A. & DiStefano, P. S. (1994) *Trends Neurosci.* **17,** 182–190.
36. Verrall, M. (1994) *Nature (London)* **370,** 6.

neuronal markers in tissue culture (*32*); however, their ability to yield neuronal phenotypes in response to physiological signals in vivo has not previously been shown. Thus, our findings are not only of fundamental interest but also, once more robust, could have application as a cell-mediated therapy. Not only could neurons be contributed to the adult brain, but, if genetically engineered, they could be a potentially useful tool for treating disorders characterized by defective neuronal function or a loss of neurons such as Parkinson's disease, lysosomal storage disorders, psychiatric disorders, trauma, and other types of CNS injury.

References and Notes

1. B. T. Spear, S. M. Tilghman, *Mol. Cell. Biol.* **10**, 5047 (1990).
2. W. E. Wright, *Exp. Cell Res.* **151**, 55 (1984).
3. H. M. Blau, C. P. Chiu, C. Webster, *Cell* **32**, 1171 (1983).
4. H. M. Blau, D. Baltimore, *J. Cell Biol.* **112**, 781 (1991).
5. J. B. Gurdon, *J. Embryol. Exp. Morphol.* **10**, 622 (1962).
6. I. Wilmut, A. E. Schnieke, J. McWhir, A. J. Kind, K. H. Campbell, *Nature* **385**, 810 (1997).
7. A. L. Vescovi, E. Y. Snyder, *Brain Pathol.* **9**, 569 (1999).
8. F. H. Gage, G. Kempermann, T. D. Palmer, D. A. Peterson, J. Ray, *J. Neurobiol.* **36**, 249 (1998).
9. B. E. Petersen *et al.*, *Science* **284**, 1168 (1999).
10. G. Ferrari *et al.*, *Science* **279**, 1528 (1998).
11. E. Gussoni *et al.*, *Nature* **401**, 390 (1999).
12. C. R. Bjornson, R. L. Rietze, B. A. Reynolds, M. C. Magli, A. L. Vescovi, *Science* **283**, 534 (1999).
13. M. Okabe, M. Ikawa, K. Kominami, T. Nakanishi, Y. Nishimune, *FEBS Lett.* **407**, 313 (1997).
14. Marrow was isolated in a sterile environment from 8- to 10-week-old, male transgenic mice that ubiquitously expressed enhanced green fluorescent protein (GFP) and non-GFP control mice. After lethal irradiation, 8- to 10-week-old C57BL/6 mice (Stanford) received 6×10^6 cells by tail vein injection.
15. Isolated brains were minced with a razor blade, dissociated with proteases, washed, stained with TriChrome (TC)–conjugated rat antibody to mouse CD11b and allophycocyanin (APC)–conjugated rat antibodies to mouse CD45, and analyzed by flow cytometry.
16. F. H. Gage *et al.*, *Proc. Natl. Acad. Sci. U.S.A.* **92**, 11879 (1995).
17. J. A. Ledbetter, L. A. Herzenberg, *Immunol. Rev.* **47**, 63 (1979).
18. T. Springer, G. Galfre, D. S. Secher, C. Milstein, *Eur. J. Immunol.* **8**, 539 (1978).
19. H. Akiyama, P. L. McGeer, *J. Neuroimmunol.* **30**, 81 (1990).
20. Each GFP^+ cell was analyzed for antibody staining by three-dimensional confocal laser scanning microscopy. Data was collected with sequential laser excitation to eliminate bleedthrough and with confocal parameters (e.g., pinhole sizes) selected to minimize the thickness of the calculated optical section.
21. J. W. Hinds, *J. Comp. Neurol.* **134**, 287 (1968).
22. M. B. Luskin, *Neuron* **11**, 173 (1993).
23. C. Lois, A. Alvarez-Buylla, *Science* **264**, 1145 (1994).
24. Eight or 12 weeks after bone marrow transplant, experimental mice and age-matched control mice were perfused and fixed with 1.5% paraformaladehyde (PF)/0.1% glutaraldehyde, snap frozen in TISSUE-TEK O.C.T. compound, cryosectioned, and stained as floating sections with antibodies against NeuN, 200-kD neurofilament, class III β-tubulin, GFAP, F4/80, and CD45. All sections were blocked with 25% normal goat serum, 0.25% Triton-X 100, and antibody to CD16/32. Goat antibodies to mouse and to rabbit conjugated to Texas Red or Cy5 were used as secondary antibodies.
25. R. J. Mullen, C. R. Buck, A. M. Smith, *Development* **116**, 201 (1992).
26. M. A. Eglitis, E. Mezey, *Proc. Natl. Acad. Sci. U.S.A.* **94**, 4080 (1997).
27. Mice were anesthetized with Methoxyflurane and surgically decapitated, and the OBs were rapidly isolated and incubated in Tyrode solution. OBs were fixed in 1.5% paraformaldehyde/4 mM EGTA and were sliced to yield coronal sections. The samples were blocked and permeabilized in 0.3% Triton-X 100, 3% bovine serum albumin (BSA), monoclonal antibody to mouse CD16/CD32, and 100 mM glycine. Staining was performed with polyclonal antibody to pCREB and monoclonal antibody to NeuN, washed, and stained with secondary antibodies (Texas Red, goat antibody to rabbit; Cy5, goat antibody to mouse).
28. K. Deisseroth, H. Bito, R. W. Tsien, *Neuron* **16**, 89 (1996).
29. A. J. Shaywitz, M. E. Greenberg, *Annu. Rev. Biochem.* **68**, 821 (1999).
30. N. Liu *et al.*, *J. Biol. Chem.* **274**, 3042 (1999).
31. G. M. Shepherd, *Physiol. Rev.* **52**, 864 (1972).
32. D. Woodbury, E. J. Schwarz, D. J. Prockop, I. B. Black, *J. Neurosci. Res.* **61**, 364 (2000).
33. P. S. Eriksson *et al.*, *Nature Med.* **4**, 1313 (1998).
34. Web video and supplemental text are available at *Science* Online at www.sciencemag.org/cgi/content/full/290/5497/1775/DC1.
35. We wish to thank neurobiologists S. McConnell, K. Deisseroth, and J. Weimann for their expertise and ongoing guidance; U. Wang and S. Heck for technical expertise; B. Blakely for insightful comments; M. Okabe for transgenic GFP mice; and M. Greenberg for antibody to pCREB. This research was supported by the Life and Health Insurance Medical Research Fund and a NIH predoctoral training grant (T.R.B.), a fellowship from Human Frontiers in Science Program (F.M.V.R.), a postdoctoral fellowship (G.I.K.), and NIH research grants CA59717, AG09521, and HD18179 (H.M.B).

8 September 2000; accepted 31 October 2000

Turning Blood into Brain: Cells Bearing Neuronal Antigens Generated in Vivo from Bone Marrow

Éva Mezey,[1]* Karen J. Chandross,[2] Gyöngyi Harta,[1] Richard A. Maki,[3,4] Scott R. McKercher[3]

Bone marrow stem cells give rise to a variety of hematopoietic lineages and repopulate the blood throughout adult life. We show that, in a strain of mice incapable of developing cells of the myeloid and lymphoid lineages, transplanted adult bone marrow cells migrated into the brain and differentiated into cells that expressed neuron-specific antigens. These findings raise the possibility that bone marrow–derived cells may provide an alternative source of neurons in patients with neurodegenerative diseases or central nervous system injury.

Neural stem cells, the self-renewing precursors of neurons and glia, are the focus of intensive research aimed at developing transplantation strategies to promote neural recovery in the diseased or injured nervous system (*1, 2*). Recently, Bjornson *et al.* (*3*) demonstrated that neural stem cells could also differentiate into a variety of hematopoietic cells, including the myeloid and the lymphoid cell lineages, as well as more immature blood cells. Circulating T cells, B cells, and macrophages enter the brain (*4–7*). Rodent bone marrow cells migrate into the brain and differentiate into microglia and astrocytes when transplanted into previously irradiated recipients (*8, 9*). Recent evidence suggests that, under experimental culture conditions, human and rodent bone marrow stromal cells can differentiate into cells bearing neuronal markers (*10, 11*). When transplanted into the lateral ventricle or striatum of mice, cultured marrow stromal cells migrate into the brain and differentiate into astrocytes (*12, 13*). There is evidence that other types of mesodermal-derived cells can also differentiate within the mammalian nervous system. For example, luteinizing hormone-releasing hormone (LHRH)–producing neurons originate from outside the central nervous system (CNS) and migrate into the hypothalamus (*14*). In the present study, we show that bone marrow–derived cells enter the brain and differentiate into cells that express neuronal markers, supporting the idea that mesodermal-derived cells can adopt neural cell fates.

Mice homozygous for a mutation in the *PU.1* gene were used as bone marrow transplant recipients. PU.1 is a member of the ETS (DNA binding domain) family of transcription factors and is expressed exclusively in cells of the hematopoietic lineage. In the

[1]Basic Neuroscience Program, [2]Laboratory of Developmental Neurogenetics, National Institute of Neurological Disorders and Stroke, National Institutes of Health, Bethesda, MD 20892, USA. [3]The Burnham Institute, 10901 North Torrey Pines Road, La Jolla, CA 92037, USA. [4]Neurocrine Biosciences, 10555 Science Center Drive, San Diego, CA 92121, USA.

*To whom correspondence should be addressed. E-mail: mezey@codon.nih.gov

absence of donor bone marrow cells, PU.1 knockout mice lack macrophages, neutrophils, mast cells, osteoclasts, and B and T cells at birth (*15, 16*). These animals are born alive but require a bone marrow transplant within 48 hours after birth to survive and develop normally. There are no gross morphological differences in the brain cytoarchitecture of these mice versus wild-type mice. In the present study, PU.1 null mice were used as bone marrow recipients to optimize the number of cells derived from the donor and to permit an accurate estimation of the numbers of bone marrow cells that migrate into the nervous system.

NeuN, a nuclear protein that is found exclusively in neurons (*17–19*), was used as a neuronal marker. Specific NeuN immunoreactivity was not present in acutely isolated (*20*) bone marrow cells. Acutely isolated bone marrow cells were also examined for neural antigens in our transgenic mouse line in which oligodendrocytes and Schwann cells express LacZ (*21*). No LacZ-expressing or β-galactosidase–immunopositive cells were present, and there was no specific immunostaining for NG2 chondroitin sulfate proteoglycan or O4, antigens that are present in Schwann cells and oligodendrocytes (*22–24*). These results strongly suggest that the bone marrow cell preparations were devoid of neurons and glia at the time of transplantation. When adult bone marrow cells were grown in culture for several weeks, the neural stem cell antigen, nestin, was present in 18% of the population [see Web fig. 1 (*25*)], indicating that bone marrow can give rise to neural stem cells.

Within 24 hours after birth, PU.1 homozygous recipients were given intraperitoneal injections of bone marrow cells from wild-type mice (*20*). Seven transplant recipient mice and nontransplanted control littermates were examined between 1 and 4 months of age. To determine the efficiency of the transplantation, we analyzed different organ tissues for the presence of donor-derived cells. Y chromosome–positive male cells were identified in hematopoietic organs of female recipients by fluorescent in situ hybridization histochemistry. Greater than 90% of spleen cells, in both white and red pulp, and ~10 to 15% of liver cells were Y chromosome–positive. All brains were examined by using a combination of in situ hybridization (ISH) to detect the Y chromosome and immunohistochemistry to visualize the neuronal nuclear marker, NeuN. Brains from a 4-month-old nontransplanted female [Fig. 1A and Web fig. 2, A to E (*25*)] and a nontransplanted male [Fig. 1B and Web fig. 2, F to J (*25*)] were processed together and served as controls for the Y chromosome hybridization specificity and efficiency (*26*). There was no specific Y chromosome staining in the female brain. The Y chromosome was frequently localized at the periphery of the nucleus, which is characteristic of heterochromatin (*27, 28*). The NeuN immunostaining was predominantly localized to the nucleus, although some neurons [as reported by others (*19*)] also exhibited perinuclear staining [Figs. 1 and 2 and Web figs. 2 to 5 (*25*)].

Marrow-derived cells (i.e., Y chromosome–positive) were present in the CNS of all of the transplanted mice examined. Between 2.3 and 4.6% of all cells (i.e., all identifiable nuclei, including vasculature) were Y chromosome–positive (Table 1). The

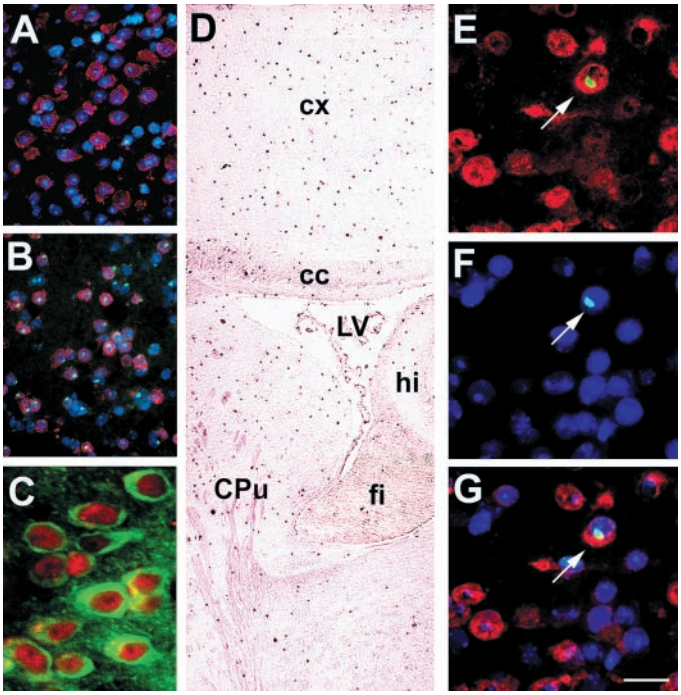

Fig. 1. Y chromosome staining in the CNS. Coronal sections from 4-month-old nontransplanted (**A**) female and (**B**) male brains were mounted and processed together. The panels show the overlay of the NeuN (red) immunostaining, Y chromosome nonradioactive ISH [visualized with tyramide-FITC conjugate (green)], and DAPI staining of cell nuclei (blue). The Y chromosome was restricted to the male brain, demonstrating hybridization specificity. (**C**) Confocal image of coronal sections from a 4-month-old recipient female striatum that was double-immunostained for the neuron-specific antigens NeuN and NSE. All NeuN-expressing cells (red) were also immunoreactive for NSE (green). (**D**) Sagittal section from a 1-month-old female PU.1 knockout mouse brain transplanted at birth with male bone marrow. The Y chromosome was visualized with BCIP/NBT (dark purple dots) to identify anatomical landmarks. cc, corpus callosum; cx, cerebral cortex; CPu, caudate putamen; fi, fimbria hippocampi; hi, hippocampus; LV, lateral ventricle. (**E** to **G**) Identical fields showing NeuN, Y chromosome, and DAPI nuclear triple staining in the hypothalamic dorsomedial nucleus of a 3-month-old female recipient. Colocalization of the Y chromosome [visualized with tyramide-FITC conjugate (green)] to a NeuN immunopositive (red) nucleus is shown in (E). In (F), DAPI staining identifies all cell nuclei (blue). Overlays of the NeuN, Y chromosome, and DAPI fluorescence are shown in (G). The arrow identifies a cell nucleus that contained both the Y chromosome (indicating the bone marrow origin) and NeuN. Scale bar in (G) represents the following sizes: 30 μm, (A) and (B); 10 μm, (C); 250 μm (D); and 12 μm, (E) to (G). Similar results were observed with three different animals for each experimental condition.

Table 1. Quantitation of the number of donor cells in the forebrains of transplanted mice. A total of 21,682 cells was counted from seven animals. Ten to 20 random fields were photographed, and all DAPI-, NeuN-, or Y chromosome–positive nuclei were counted. Counts of cells represent an average from three independent investigators. The ratio of total cells to neurons was in good agreement with previous reports (*45, 46*).

Age (months)	DAPI-positive nuclei counted	NEU-positive nuclei counted	Y chromosome–positive cells	Y chromosome/NEU (double-labeled)	Neu-positive nuclei in all cells (%)	Y chromosomes in all cells (%)	Y of Neu-positive cells (%)
4	4831	1908	120	6	39	2.5	0.3
4	1322	221	60	5	17	4.5	2.3
3	3675	1483	130	16	40	3.5	1.1
3	4550	1825	105	15	40	2.3	0.8
2	3731	1039	162	16	28	4.3	1.5
1	1913	464	86	8	24	4.5	1.7
1	1660	380	76	7	23	4.6	1.8

Y chromosome–bearing cells were evenly distributed throughout the different brain regions [Fig. 1D and Web fig. 2, K and L (*25*)], in both white and gray matter. The Y chromosome was present in 0.3 to 2.3% of the NeuN-immunoreactive nuclei (Table 1). Confocal microscopy confirmed the presence of the Y chromosome in NeuN-immunopositive nuclei [Fig. 2 and Web figs. 4 and 5 (*25*)]. Y chromosome staining was localized to NeuN immunopositive cells and was not associated with any other neighboring nuclei in the *x*, *y*, or *z* planes. In the CNS of transplanted female mice, all NeuN-immunopositive nuclei were found in neuron-specific enolase (NSE)–containing cells (Fig. 1C). In the brain, NSE is expressed exclusively in neurons (*29*), demonstrating that Y chromosome–bearing cells can express two neuronal antigens. Most of these cells were found in the cerebral cortex [Web fig. 3, A to F (*25*)]; however, they were also present in the hypothalamus (Fig. 1, E to G), hippocampus, amygdala [Web fig. 3, G to I (*25*)], periaqueductal gray, and striatum. We did not detect Y chromosome–positive large motor neurons in the spinal cord or brainstem. A substantial number of Y chromosome–positive cell nuclei were present in cells within the choroid plexus of the lateral ventricle, in the ependyma of the ventricular system, and in the subarachnoid space, suggesting the cerebrospinal fluid as a primary route of entry [Web fig. 6 (*25*)]. We did not observe an overall increased density of Y chromosome–positive cell nuclei in neurogenic regions, including the subventricular zone, olfactory migratory region, or hippocampus. Because mesodermal stem cells can differentiate into microglia (*8*) and all microglia in these recipient animals arise from the donor bone marrow and are also Y chromosome–positive, we could not determine regional differences in the distribution of Y chromosome–positive nuclei.

These studies demonstrate that bone marrow cells migrate into the brain and differentiate into cells that express neuron-specific antigens. In combination with previous in vivo studies (*9, 12*, *13*), the present work suggests that the bone marrow can supply the brain with an alternative source of neural cells. Neurons and macroglia (oligodendrocytes and astrocytes) are thought to arise from pluripotent neural stem cells that are present both in the developing (*30*) and adult mammalian CNS (*31–35*). It has been estimated that, for every 2000 existing neurons, one new neuron is produced each day (*35, 36*). In the rodent brain, there are two well-characterized neurogenic regions: one in the subgranular zone of the dentate gyrus and one in the forebrain subventricular zone (*37–41*). Two populations of neural stem cells have been identified in adult mammals: one in the ependymal cell layer lining the ventricles (*33*) and one in the subventricular zone [glial fibrillary acidic protein–immunoreactive cells (*34*), each of which gives rise to glial cells and neurons]. We suggest that, in addition to these sources of neural stem cells, there may be a continuous influx of bone marrow stem cells into the ependymal and subependymal zones that give rise to a variety of CNS neural cell types. An interesting possibility is that these entry routes might also serve as portals into the CNS for diseases that primarily originate in and affect the hematopoietic system (i.e., leukemia and AIDS).

Bone marrow is far more accessible than neural stem cells and has the added advantage of having inherent host compatibility, thereby obviating the need to screen for viral and foreign antigens. Although our study showed that only a small number of transplanted cells expressed neuronal antigens in the adult brain, there may be factors that promote the differentiation of bone marrow cells into distinct neural cell types. Once these factors are identified, bone marrow cells might be expanded in vitro and provide an unlimited source of cells for the treatment of CNS disease and injury. Because at least two different types of stem cells have been isolated from bone marrow (hematopoietic and stromal), characterizing the potential for each population will be an important step toward optimizing regenerative therapies.

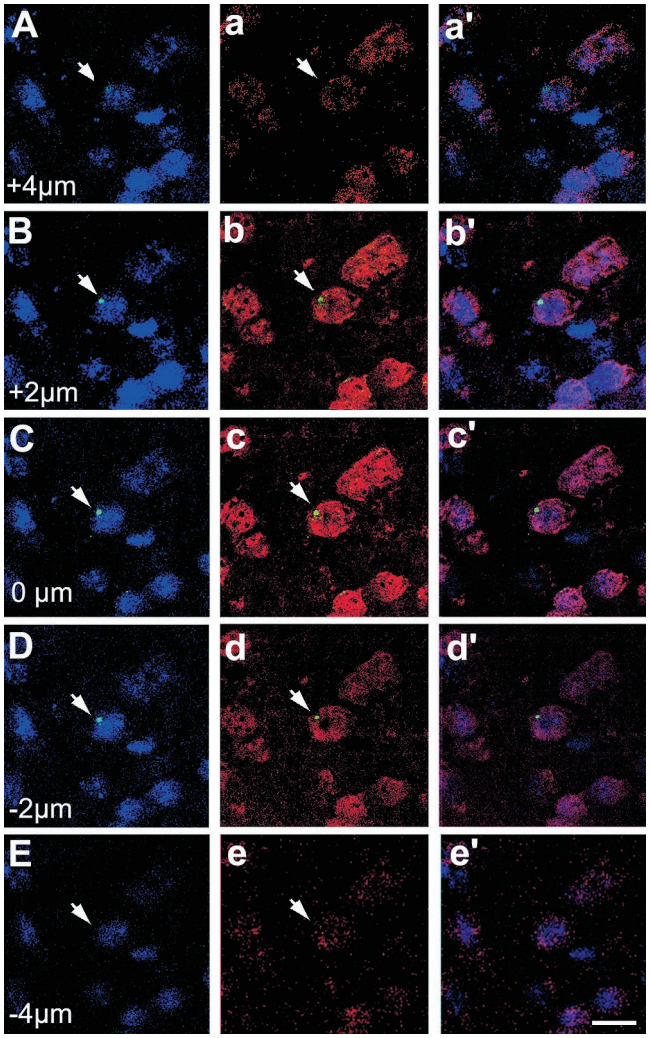

Fig. 2. A NeuN- and Y chromosome–positive cell in the cingulate cortex (1.2 mm behind the bregma) of a 3-month-old homozygous female PU.1 knockout transplanted at birth with male bone marrow. The images were obtained with a Zeiss confocal microscope. (**A** to **E**) Five different levels through the section (1 μm thick each), overlaying the Y chromosome [visualized with tyramide-FITC (green) and DAPI (blue) staining]. (**a** to **e**) Overlays of the corresponding NeuN (red) and Y chromosome staining. (**a′** to **e′**) Overlays of the corresponding NeuN, Y chromosome, and DAPI fluorescence. The Y chromosome hybridization was localized to a NeuN-immunopositive cell (arrow) and was not associated with any neighboring nuclei in the *x*, *y*, or *z* planes. Scale bar, 10 μm. These results were observed with five independent Z series from three different animals.

References and Notes

1. A. Bjorklund, C. Svendsen, *Nature* **397**, 569 (1999).
2. R. McKay, *Science* **276**, 66 (1997).
3. C. R. R. Bjornson, R. L. Rietze, B. A. Reynolds, M. C. Magli, A. L. Vescovi, *Science* **283**, 534 (1999).
4. P. M. Knopf *et al.*, *J. Immunol.* **161**, 692 (1998).
5. K. C. Williams, W. F. Hickey, *Curr. Top. Microbiol. Immunol.* **202**, 221 (1995).
6. W. F. Hickey, B. L. Hsu, H. Kimura, *J. Neurosci. Res.* **28**, 254 (1991).
7. W. F. Hickey, *Semin. Immunol.* **11**, 125 (1999).
8. D. P. Theele, W. J. Streit, *Glia* **7**, 5 (1993).
9. M. A. Eglitis, E. Mezey, *Proc. Natl. Acad. Sci. U.S.A.* **94**, 4080 (1997).
10. J. Sanchez-Ramos *et al.*, *Exp. Neurol.* **164**, 247 (2000).
11. D. Woodbury, E. J. Schwarz, D. J. Prockop, I. B. Black, *J. Neurosci. Res.* **61**, 364 (2000).
12. S. A. Azizi, D. Stokes, B. J. Augelli, C. DiGirolamo, D. J. Prockop, *Proc. Natl. Acad. Sci. U.S.A.* **95**, 3908 (1998).
13. G. C. Kopen, D. J. Prockop, D. G. Phinney, *Proc. Natl. Acad. Sci. U.S.A.* **96**, 10711 (1999).

14. M. Schwanzel-Fukuda, *Microsc. Res. Tech.* **44**, 2 (1999).
15. S. R. McKercher *et al.*, *EMBO J.* **15**, 5647 (1996).
16. M. M. Tondravi *et al.*, *Nature* **386**, 81 (1997).
17. H. B. Sarnat, D. Nochlin, D. E. Born, *Brain Dev.* **20**, 88 (1998).
18. H. K. Wolf *et al.*, *J. Histochem. Cytochem.* **44**, 1167 (1996).
19. R. J. Mullen, C. R. Buck, A. M. Smith, *Development* **116**, 201 (1992).
20. PU.1 null mice were reconstituted as follows. Adult male mice (8 to 24 weeks old) were killed, and both femurs were removed under sterile conditions. The muscle was removed, and the ends of the bones were cut off with a scalpel. The remaining central portion of the femur was placed into Dulbecco's modified Eagle's medium (DMEM) (Gibco, Gaithersburg, MD) containing 10% fetal bovine serum (Gibco). Marrow cells from each femur were flushed out with medium. A suspension of the bone marrow cells was prepared by pushing the marrow and medium through 18-gauge, 21-gauge, and 25-gauge needles, consecutively. The cell suspension was centrifuged at 300*g* for 8 min, and the supernatant was discarded. The cells were washed in DMEM without serum, and an aliquot was removed for NeuN immunostaining. For the transplantation experiments, the remainder of live cells was centrifuged and resuspended in DMEM without serum. For immunostaining of acutely isolated bone marrow cells, see supplemental methods (*25*). Bone marrow transplants were performed as follows. At birth, each female neonate was given an intraperitoneal injection of a 0.05-ml suspension that contained 1×10^7 male bone marrow cells (equivalent to one adult mouse). Approximately 0.05 to 0.5% of the total number of the marrow cellularity are hematopoietic stem cells and ~0.125% are stromal cells (*42–44*). All pups were given subcutaneous injections of enrofloxacin for 2 weeks, as previously reported (*15*), to help reduce the incidence of infection.
21. K. J. Chandross *et al.*, *J. Neurosci.* **19**, 759 (1999).
22. S. C. Barnett, A. M. Hutchins, M. Noble, *Dev. Biol.* **155**, 337 (1993).
23. K. R. Jessen, R. Mirsky, *Glia* **4**, 185 (1991).
24. R. Reynolds, R. Hardy, *J. Neurosci. Res.* **47**, 455 (1997).
25. Supplemental Web material is available at www.sciencemag.org/cgi/content/full/290/5497/1779/DC1.
26. Tissues were collected as follows. Reconstituted and normal mice were killed at the appropriate age with carbon dioxide gas. Tissues were collected and immediately stored at −80°C until used. ISH, histochemistry, and immunohistochemistry were performed as follows. Fresh frozen brain sections (12 μm thick) or acutely isolated bone marrow cells were fixed with 2 to 4% paraformaldehyde and immunostained with the neuronal nuclear marker NeuN [monoclonal immunoglobulin G1, 1:1000 dilution (Chemicon, Temecula, CA)]. The antibody was detected by using the Mouse on Mouse kit (Innogenex, San Ramon, CA) and subsequent deposition of biotinylated tyramide preceding the ISH. After the ISH, streptavidin-546 Alexa dye conjugate (Molecular Probes, Eugene, OR) was added to bind the biotin. Immediately following the deposition of the tyramide, nonradioactive ISH was performed on the same sections to detect the Y chromosome by using a 1.5-kb RNA probe, pY3531B, that was generated against a repeat sequence of the mouse Y chromosome (*17*) and labeled with digoxigenin–uridine 5′-triphosphate (for technical details, see http://intramural.nimh.nih.gov/lcmr/snge/Protocol.html). After several washes, the digoxigenin was developed using an antibody to digoxigenin conjugated to either alkaline phosphatase (1:1500 dilution) or peroxidase (1:400 dilution) (Roche Pharmaceuticals, Indianapolis, IN). The antibody to digoxigenin was then visualized with either 5-bromo-4-chloro-3-indolyl phosphate/nitroblue tetrazolium (BCIP/NBT) as substrate (purple precipitate with light microscopy) or tyramide–fluorescein isothiocyanate (FITC) (NEN, Boston, MA) (green fluorescence). Subsequently, cell nuclei were stained with 4′,6-diamidino-2-phenylindole (DAPI) (blue fluorescence). Representative sections from transplanted mice were double-labeled with NeuN and NSE [polyclonal, 1:10,000 dilution (Polysciences, Warrington, PA)] antibodies. Primary antibodies were visualized with an Alexa 594 antibody to mouse (NeuN, 1:1000 dilution, Molecular Probes) or Alexa 488 secondary antibodies to rabbit (NSE, 1:500 dilution, Molecular Probes).
27. B. Alberts *et al.*, *Molecular Biology of the Cell* (Garland, New York, ed. 2, 1989).
28. J. D. Watson, *Molecular Biology of the Gene* (Benjamin, Menlo Park, CA, ed. 3, 1976).
29. S. A. Vinores, M. M. Herman, L. J. Rubinstein, P. J. Marangos, *J. Histochem. Cytochem.* **32**, 1295 (1984).
30. T. Mujtaba, M. Mayer-Proschel, M. S. Rao, *Dev. Biol.* **200**, 1 (1998).
31. S. Weiss *et al.*, *Trends Neurosci.* **19**, 387 (1996).
32. S. Weiss, D. van der Kooy, *J. Neurobiol.* **36**, 307 (1998).
33. C. B. Johansson *et al.*, *Cell* **96**, 25 (1999).
34. F. Doetsch, I. Caille, D. A. Lim, J. M. Garcia-Verdugo, A. Alvarez-Buylla, *Cell* **97**, 703 (1999).
35. F. H. Gage, *Science* **287**, 1433 (2000).
36. G. Kempermann, H. G. Kuhn, F. H. Gage, *Proc. Natl. Acad. Sci. U.S.A.* **94**, 10409 (1997).
37. S. Weiss *et al.*, *J. Neurosci.* **16**, 7599 (1996).
38. B. A. Reynolds, S. Weiss, *Science* **255**, 1707 (1992).
39. C. M. Morshead *et al.*, *Neuron* **13**, 1071 (1994).
40. C. Lois, A. Alvarez-Buylla, *Proc. Natl. Acad. Sci. U.S.A.* **90**, 2074 (1993).
41. M. B. Luskin, *J. Neurobiol.* **36**, 221 (1998).
42. S. J. Morrison, N. Uchida, I. L. Weissman, *Annu. Rev. Cell Dev. Biol.* **11**, 35 (1995).
43. S. J. Morrison, I. L. Weissman, *Proc. Assoc. Am. Physicians* **107**, 187 (1995).
44. N. B. Nardi, Z. Z. Alfonso, *Braz. J. Med. Biol. Res.* **32**, 601 (1999).
45. D. Heumann, G. Leuba, T. Rabinowicz, *J. Hirnforsch.* **18**, 483 (1977).
46. E. A. Ling, C. P. Leblond, *J. Comp. Neurol.* **149**, 73 (1973).
47. E.M. dedicates this report to the memory of János Szentágothai (1912–94), anatomist, statesman, romantic, artist, and mentor, who helped me understand the difference between looking at tissue sections and seeing the secrets they hold. The authors would like to express their sincere thanks to R. Dreyfus for his help with the conventional microscopy and C. L. Smith and R. Cohen for their help with the confocal microscopy. We are also grateful to M. Brownstein, R. Cohen, H. Gainer, L. Hudson, and M. Palkovits for their helpful suggestions and support throughout the work. These studies were supported by NIH grant AI30656 to R.A.M.

7 September 2000; accepted 31 October 2000

Coding the Location of the Arm by Sight

Michael S. A. Graziano,* Dylan F. Cooke, Charlotte S. R. Taylor

Area 5 in the parietal lobe of the primate brain is thought to be involved in monitoring the posture and movement of the body. In this study, neurons in monkey area 5 were found to encode the position of the monkey's arm while it was covered from view. The same neurons also responded to the position of a visible, realistic false arm. The neurons were not sensitive to the sight of unrealistic substitutes for the arm and were able to distinguish a right from a left arm. These neurons appear to combine visual and somatosensory signals in order to monitor the configuration of the limbs. They could form the basis of the complex body schema that we constantly use to adjust posture and guide movement.

Without an accurate sense of the position of the limbs, head, and torso, we would be unable to guide movement, process the spatial location of nearby objects, or distinguish our own body parts from external objects. People with damage to their parietal lobes can have difficulty in all of these dimensions (*1, 2*). Studies in normal humans show that the body schema is not simply a representation of joint angles, but a complex integration of vision, proprioception, touch, and motor feedback (*3–6*). Although a great deal is known about the processing of joint angle and muscle stretch in the somatosensory system (*7*), little is known about how different sensory modalities are combined by neurons in the parietal lobe or elsewhere to construct the body schema (*8, 9*).

The present set of studies focused on the coding of static arm position. The sense of arm position depends on many sources of information, including proprioception and vision (*3–6, 10–12*). Here we show that neurons in parietal area 5 of the monkey brain, but not in the primary somatosensory cortex, respond in relation to the seen position of a false arm. They are also sensitive to somatosensory signals, responding in relation to the felt position of the monkey's actual arm. These somatosensory and visual signals are combined in individual neurons to provide a possible code for static limb position.

Responses of single neurons in area 5 were studied in two monkeys (*13*). The recording site in monkey 1 is shown in Fig. 1A, and the apparatus is shown in Fig. 1B. The arm contralateral to the recording electrode was outstretched, and the ipsilateral arm was held close to the body (not shown). The arms were covered with a black plastic plate. On top of the plate, a realistic false arm was placed in the monkey's view. This false arm was from a monkey of the same species and had been prepared by a taxidermist. The cut end was covered from view by a portion of

Department of Psychology, Princeton University, Princeton, NJ 08544, USA.

*To whom correspondence should be addressed. E-mail: graziano@princeton.edu

Transplanted bone marrow generates new neurons in human brains

Éva Mezey*†, Sharon Key*, Georgia Vogelsang‡, Ildiko Szalayova§, G. David Lange¶, and Barbara Crain‡

*National Institutes of Health (NIH)/National Institute of Neurological Disorders and Stroke (NINDS)/*In situ* Hybridization Facility (ISHF) and §NIH/National Institute of Mental Health/Laboratory of Genetics (LOG), Building 36, 3D06, Bethesda, MD 20892; ‡Johns Hopkins University, School of Medicine, Baltimore, MD 21287; and ¶NIH/NINDS/Instrument and Computer Section, Building 36, 2A03, Bethesda, MD 20892

Edited by Tomas Hökfelt, Karolinska Institute, Stockholm, Sweden, and approved December 18, 2002 (received for review October 24, 2002)

Adult bone marrow stem cells seem to differentiate into muscle, skin, liver, lung, and neuronal cells in rodents and have been shown to regenerate myocardium, hepatocytes, and skin and gastrointestinal epithelium in humans. Because we have demonstrated previously that transplanted bone marrow cells can enter the brain of mice and differentiate into neurons there, we decided to examine postmortem brain samples from females who had received bone marrow transplants from male donors. The underlying diseases of the patients were lymphocytic leukemia and genetic deficiency of the immune system, and they survived between 1 and 9 months after transplant. We used a combination of immunocytochemistry (utilizing neuron-specific antibodies) and fluorescent *in situ* hybridization histochemistry to search for Y chromosome-positive cells. In all four patients studied we found cells containing Y chromosomes in several brain regions. Most of them were nonneuronal (endothelial cells and cells in the white matter), but neurons were certainly labeled, especially in the hippocampus and cerebral cortex. The youngest patient (2 years old), who also lived the longest time after transplantation, had the greatest number of donor-derived neurons (7 in 10,000). The distribution of the labeled cells was not homogeneous. There were clusters of Y-positive cells, suggesting that single progenitor cells underwent clonal expansion and differentiation. We conclude that adult human bone marrow cells can enter the brain and generate neurons just as rodent cells do. Perhaps this phenomenon could be exploited to prevent the development or progression of neurodegenerative diseases or to repair tissue damaged by infarction or trauma.

Neurogenesis used to be thought to be completed during embryonic life in rodents as well as humans. During the last decade, however, numerous studies have suggested that neurogenesis continues in adult animals and humans, at least to a certain extent in a few privileged areas of the brain (1–4). Most of these studies have focused on endogenous neural progenitor cells (neural stem cells) localized in the subventricular zone of the lateral ventricle and in the dentate gyrus in the hippocampus in rodents (4). In the monkeys these cells are present in the hippocampus and neocortex (5, 6). Likewise, Eriksson *et al.* (7) found that new neurons are generated continuously in the human dentate gyrus throughout life.

It is also conceivable that stem cells from other sources might enter the brain and form neurons there. Uchida *et al.* (8) isolated CNS stem cells from human fetal tissue and transplanted them into the brains of mice, where they subsequently proliferated and differentiated into neuronal cells. One source of such cells in the brain could be the bone marrow. Adult bone marrow stem cells seem able to differentiate into muscle, skin, liver, lung, and neural cells in rodents (9–18). Furthermore, transplanted bone marrow cells in humans have also been shown to form myocardial cells (19, 20), hepatocytes (21, 22), and epithelium of the skin and gastrointestinal tract (20). Because we have demonstrated previously that transplanted bone marrow cells migrate into the brains of mice and give rise to neurons there (15), we hypothesized that the same thing might occur in the human CNS after bone marrow transplantation. We tested this hypothesis by looking for Y chromosome-positive neuron-like cells in postmortem brain samples from females who had received bone marrow transplants from male donors.

Methods

Four female patients who had had bone marrow transplants from male donors were selected from the autopsy files of The Johns Hopkins Hospital. Patient 1 had Omenn's syndrome, was transplanted at 9 months of age, and died 10 months later. Patient 2 had Hodgkin's disease and was transplanted at 34 years of age. Patient 3 had acute lymphocytic leukemia and was transplanted at 10 years of age. Patient 4 had acute lymphocytic leukemia and was transplanted at 20 years of age. Patients 2–4 died within ≈2 months of receiving their transplants.

Formalin-fixed, paraffin-embedded sections (6 μm) from the following brain areas were examined in each case: neocortex, striatum including the lateral ventricular wall, hippocampus with adjacent mesial temporal lobe structures, and cerebellum. Sections from three nontransplanted female patients were used as negative controls for Y-chromosomal staining. Sections from four male patients were used as positive controls. One tissue sample each from a male and a control female brain were reembedded together into one paraffin block and serially sectioned at a thickness of 6 μm; sections from this block were used as controls in all experimental series.

After deparaffinization in Citrisolv (Fisher Scientific) the sections were rehydrated, and heat-induced antigen retrieval was performed in a histology microwave oven by using a citrate buffer (Citra-plus, Innogenex, San Ramon, CA) for 5 min at 600 W. Next, immunostaining was performed by using primary antibodies that were detected by the Sternberger peroxidase antiperoxidase (PAP) method (23) followed by either biotinylated tyramide (for Kv2.1) or FITC-tyramide plus [(for neuronal nuclear antigen (NeuN)] (Perkin–Elmer). The primary antibodies used were directed against two neuronal proteins: NeuN (24), a neuron-specific nuclear protein, and Kv2.1, a neuron-specific voltage-gated potassium channel antibody (25, 26). Kv2.1 was recognized as a neuron-specific potassium channel that was first described in the principal neurons of the hippocampus and cortex and later shown to be present in the vast majority of interneurons as well (26). The NeuN antibody was a mouse monoclonal (used at 1:1,000) (Chemicon), and the Kv2.1 antibody was a rabbit polyclonal (used at 1:500, Alomone, Jerusalem). After immunostaining, the *in situ* hybridization was carried out as described (15) by using a digoxigenin-labeled riboprobe complementary to the satellite region of the human Y chromosome. We prepared the template from which we made probe from human genomic DNA by using primers that amplified a 1.3-kb-long DNA of the human Y chromosome. The probe was visualized by using peroxidase-conjugated antidigoxigenin antibody (Roche, Indianapolis) followed by a tyramide-CY3 fluo-

This paper was submitted directly (Track II) to the PNAS office.

Abbreviations: NeuN, neuronal nuclear antigen; Kv2.1, neuron-specific potassium channel.

†To whom correspondence should be addressed. E-mail: mezey@codon.nih.gov.

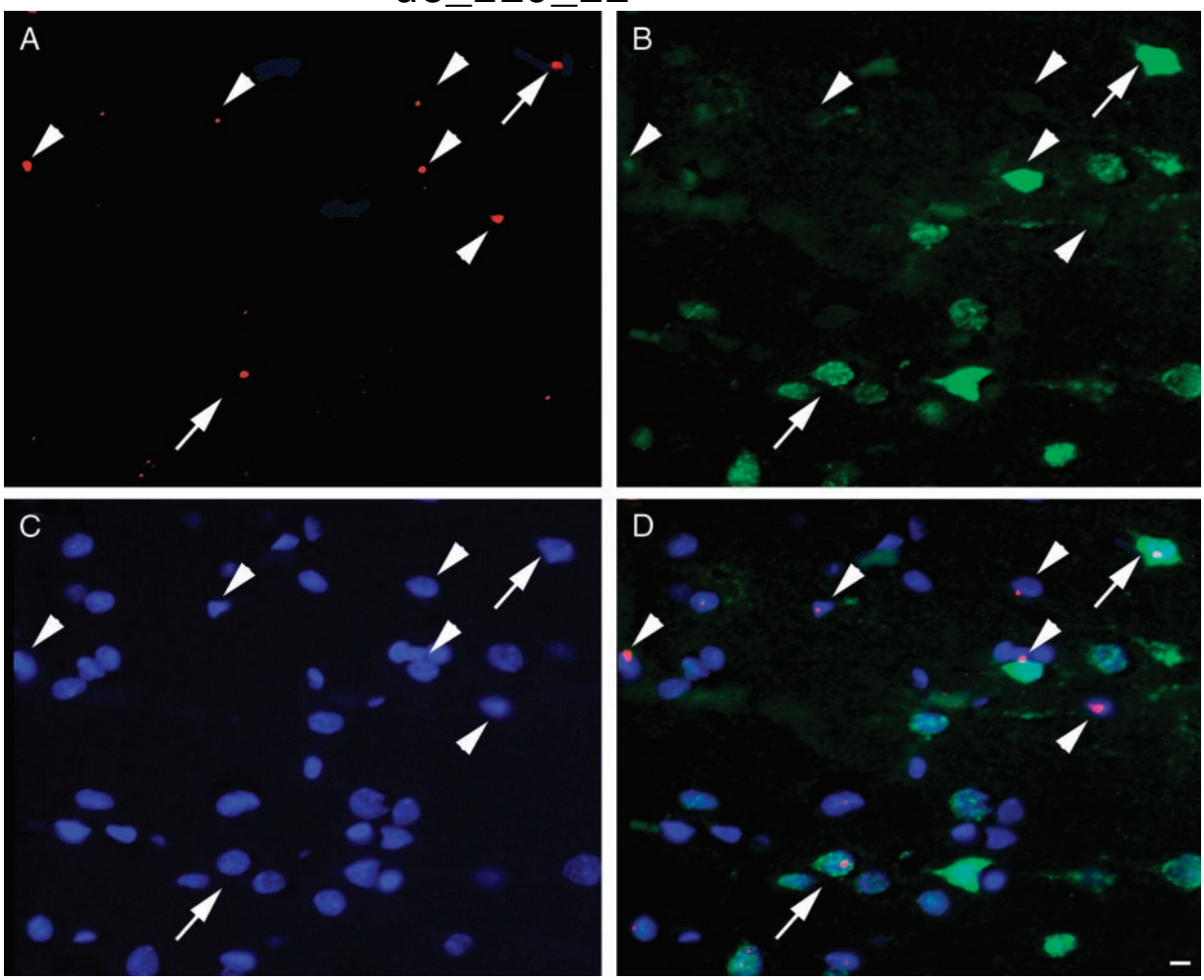

Fig. 1. (*A*) A 6-μm-thin section from somatosensory cortex of patient 2 demonstrates the presence of the Y chromosome depicted as red dots and viewed through a rhodamine filter. The same field as in *A* is shown when viewed through the FITC filter to demonstrate the immunostaining for the neuronal marker NeuN in green (*B*), and the UV filter shows all cell nuclei in blue after staining with 4′,6-diamidino-2-phenylindole, a chromosomal stain (*C*). (*D*) The overlay of the three filters, where arrows point to cells that carry all markers, indicating that they derived from the donor bone marrow (Y chromosome-positive) and bear the specific neuronal marker NeuN. Arrowheads point at nonneuronal donor-derived cells. (Scale bars, 10 μm.)

rochrome plus (Perkin–Elmer) amplification. At the end, all sections were stained with a 1% Sudan-black solution to mask lipofuscin-induced autofluorescence, which is a common problem when working with human brain tissue (27). All sections were stained with 4′,6-diamidino-2-phenylindole (DAPI, Sigma), a chromosomal stain to label nuclei, and mounted with 80% glycerol/20% Tris. A separate series of sections was hybridized by using a radiolabeled Y chromosome probe, which is easily visualized at low magnification. This enabled us to count Y-positive cells and examine their overall distribution. All sections were viewed with conventional Leitz and confocal Zeiss microscopes.

In addition to the nontransplanted male and female brains, to make sure of the specificity of the techniques we ran as controls immunostaining with amplification without primary and/or without the secondary antibodies.

Analysis of the distribution of Y chromosome-positive cells was done as follows. The Y chromosome probe was radiolabeled with [^{35}S]UTP and hybridized to brain sections. After emulsion coating and autoradiographic development of the sections, the Y-positive nuclei were counted at low magnification ($\times$10). The counts in individual 1.2-mm^2 microsquares (visual field) of a grid that covered the entire section were determined. The mean and variance of the counts and the variance-to-mean ratio were calculated. In a random (Poisson) distribution, the variance-to-mean ratio is 1. Therefore, the nearness to 1 of this ratio is a measure of the randomness of the distribution (28).

Results

In the control male brain sections we detected the Y chromosome with both the fluorescent and autoradiographic techniques in >90% of the nuclei, whereas no labeling was observed in the brain sections of female patients who have not received transplants. In each of the transplanted patients examined we readily detected Y-positive cells by means of autoradiography. In all patients using conventional fluorescent microscopy we observed double-labeled cells that were positive for both the Y chromosome and one of the neuronal markers as shown in an example in Fig. 1. Most of the cells that were double-labeled with the Y chromosome and the neuronal markers were detected in the hippocampus and the neocortex of patients (Fig. 2). The antibody that binds to Kv2.1 gave a very convincing staining of neuronal somata and dendrites in all cortical areas and in the hippocampus (as described in the literature; see ref. 26), and also a few axons seemed to show a patchy immunostaining after signal amplification.

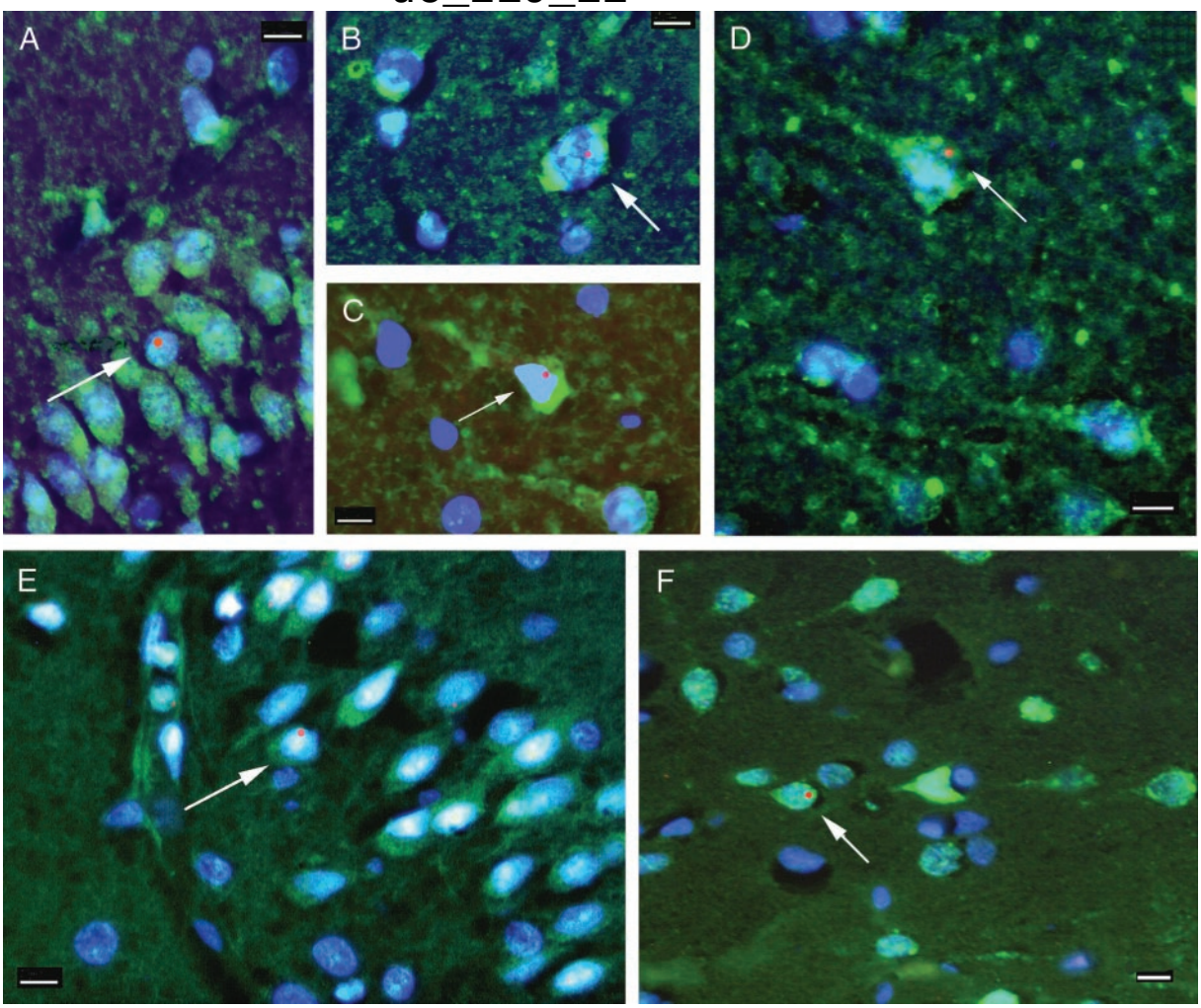

Fig. 2. Neuronal markers colocalized with the Y chromosome. Fluorescent microscopic images of neocortex from patients 2 (*A–C*) and 1 (*E*) and hippocampus from patients 1 (*D*) and 3 (*F*) are shown. The green color represents the immunostaining for neuronal markers Kv2.1 (*A–D*) and NeuN (*E* and *F*), and the Y chromosome is represented by the red fluorescent dots. All cell nuclei are stained with 4′,6-diamidino-2-phenylindole, a chromosomal marker that shows up as blue fluorescence. All images are overlays of the images seen through the three separate filters to show all colors. Arrows point to cells that are labeled with neuronal markers and are also Y chromosome-positive. In the Kv2.1 immunostaining the initial axons of some neurons can also be visualized. (Scale bars, 10 μm.)

Confocal z series confirmed the presence of Y chromosomes in the nuclei of the same cells that were immunopositive for the neuronal markers. Examples from two patients are shown in Fig. 3. In the patient with the greatest number of double-labeled cells (patient 1), the distribution of the Y-positive cells suggested that clonal expansion had occurred: We detected no labeled cells in many visual fields but typically saw clusters of positive cells when such cells were detected. This pattern was easier to recognize in the autoradiographic sections, which could be examined at low magnification. In several clusters, the Y-positive cells were both neuronal and nonneuronal. In the cortex, based on morphology and location, the Y-positive neurons were small pyramidal cells, whereas in the hippocampus the Y-positive cells seemed to be granule cells. We also saw Y-positive cells in the white matter, some of which looked like oligodendrocytes based on the shape, size, and arrangement of their nuclei. We saw many Y-positive cells inside vessels (in cross section) and also some Y-positive endothelial cells in the vascular wall.

We counted all the Y chromosome-positive cells in two entire sections of striatum/cortex and hippocampus/cortex blocks from two patients, analyzing 281 and 247 microscopic fields from patients 1 and 3, respectively (Table 1). In patient 1 we found 519 Y-positive cell nuclei among 182,000 nuclei (stained with ethidium bromide), and in patient 3 we found 1,842 Y-positive nuclei among 196,700. In the same sections we found 19 and 5 Y chromosome-containing nuclei, respectively, that also colocalized with neuronal antigens. Based on these observations and conservatively assuming that 25% of all nuclei in the human brain are neurons [this number in the cortex of primates varies between 27% and 60% (29, 30)], one in every 2,000–4,000 neurons might derive from the bone marrow.

When we evaluated the distribution of Y chromosome-positive cells in patients 1 and 3 we found that it was not random. The variance-to-mean ratios of all counts in microsquares overlaying the sections studied were calculated to be 10.2 (patient 1) and 4.7 (patient 3).

Discussion

Several studies have shown that there is neurogenesis in the adult brain, even though it may be limited. Cells with neuron-specific markers can be formed by neural stem cells *in vivo* (1, 3, 31) as well as by bone marrow cells *in vitro* (32, 33) and *in vivo* (9, 15). Recently, Priller *et al.* (34) published a picture of a well differentiated, enhanced GFP-positive Purkinje cell in the cerebellum of a mouse transplanted with enhanced GFP-tagged bone marrow from a second animal. Along with earlier studies, this finding

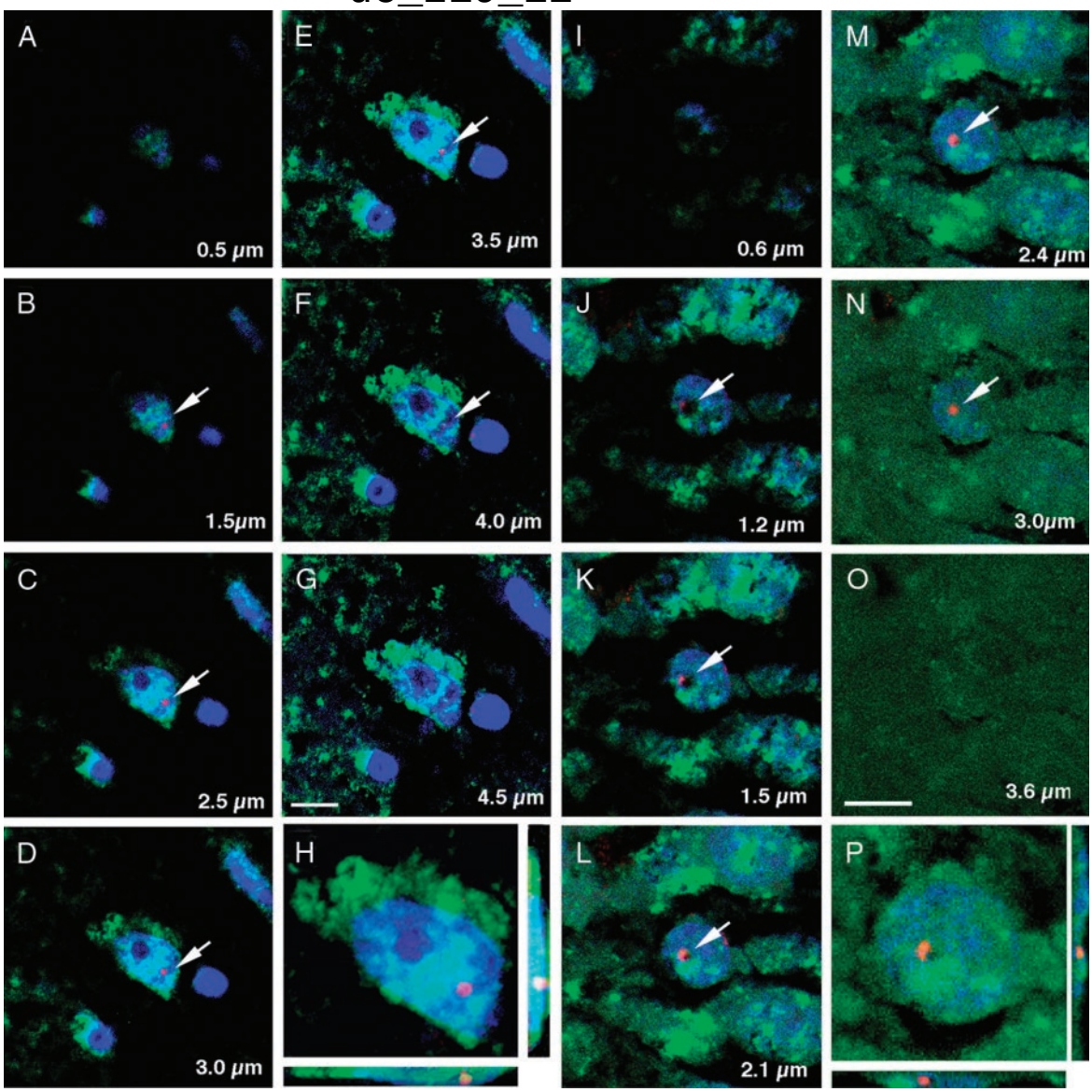

Fig. 3. Two confocal z series are shown. (*A–D*) Optical sections (1-μm-thin) of a neocortical neuron from patient 2. (*E–F*) Optical 1-μm-thin slices of a hippocampal granule cell from patient 1. Both cells are immunostained with the neuronal marker Kv2.1 (green); the Y chromosome is red (CY3-plus), and the nucleus is blue (4′,6-diamidino-2-phenylindole). The arrowheads point to the double-labeled cells. Note that the cell nucleus and the Y chromosome are consistently in the same plane.

was a significant step toward showing that fully functional neurons can be generated from bone marrow cells. Based on our present study, we have no way of knowing which population of bone marrow cells entered the CNS and differentiated into cells expressing neuronal morphology and neuronal markers. Mesenchymal stem cells have been shown to differentiate into many different cell lineages (35). All of our patients received total bone marrow transplants containing both hematopoietic and mesenchymal stem cells.

Recently, two studies (36, 37) suggested the possibility that Y-positive cells of bone marrow origin might simply fuse with embryonic stem cells instead of transdifferentiating into cells characteristic of various tissues. Although this idea is interesting, no data support its relevance *in vivo* (see ref. 38). In fact, the fusion process is very inefficient *in vitro*: 1 in a million, which is a figure much lower than the number of double-labeled cells that we see in the brain. Recently, Castro *et al.* (39) failed to detect blue cells in the brains of lethally

Table 1. Number of Y chromosome-positive (Y^+) cells in two patient samples

Patient	No. of visual fields (1 field = 0.94 mm^2)	No. of Y^+ nuclei	No. of all nuclei	No. of Y^+ nuclei in cells with neuronal markers
1	281	519	182,000	19
3	247	1,842	196,700	5

irradiated mice that received bone marrow from Rosa26 mice with a β-galactosidase-containing transgene. The use of protein products of transgenes as markers to follow graft fate is plagued with problems, but to date these may not have been emphasized enough. It is practically impossible to achieve ubiquitous transgene expression. Transgenes, including those driven by the Rosa26 promoter, suffer from instability in several tissues. Furthermore, to detect low levels of lacZ is difficult, and the detection is sensitive to fixation and staining conditions (40). Because one would have expected to see at least labeled microglia in the brain, one must assume that the results reported were due to technical problems.

In the present cases it is difficult to make general statements about the extent of CNS colonization or to conclude whether cells enter the brain continuously or just at the time of the transplant. All of our patients received irradiation to eliminate the underlying disease. We do not know how much effect the irradiation might have on the migration of circulating cells into the brain by either injuring the blood–brain barrier and/or releasing possible recruiting factors due to the injury caused by the radiation. It is known, however, that circulating blood cells are able to enter the brain parenchyma freely in healthy subjects (41). We studied a limited number of patients with different diseases, ages, survival times after transplant, and treatments of postmortem tissue. Because of the technical difficulties of double-labeling cells in paraffin-embedded postmortem tissue and the fact that we had to reduce the sensitivity of the method to eliminate background, we believe that our numbers are in fact lower that the real number of differentiating cells *in vivo*. Although we found donor (i.e., Y chromosome-positive) cells exhibiting two specific neuronal markers (NeuN and Kv2.1) in the hippocampus and neocortex in all three of the patients with technically satisfactory samples, the numbers of double-labeled cells were much lower than those reported in rodents (9, 15). We found 2–5 Y-positive neurons per 10,000 human neurons vs. 50 per 10,000 rodent neurons. Whether this is a species difference is unclear. The sections with the highest number of newly formed neurons (7 per 10,000 neurons) were from patient 1, the youngest studied, who had her transplant in infancy and also had the longest posttransplant survival time. All the other patients lived only weeks after the transplant, and there was no significant difference in the number of donor-positive cells in their brains.

It should also be noted that among the Y-positive cells, neurons were consistently in the minority. Based on their nuclear morphology, size, and location, we feel that the nonneuronal cells bearing the Y chromosome were a mixture of oligodendrocytes, astrocytes, and possibly microglia. We also detected endothelial, meningeal, and ependymal cells that were Y-positive. Finally, many circulating white blood cells within the vascular lumen were also Y-positive, as one would expect.

Our analysis showed that the distribution of Y-positive cells within the brain is not random. Instead, the cells appeared in clusters, a spatial distribution that suggests nondifferentiated cells may enter an area and then further propagate there. In these areas we see different kinds of Y-positive cells (neuronal and nonneuronal). One possibility is that one undifferentiated cell migrates into an "area of need" and then goes through asymmetrical divisions to produce different lineages of cells. Another possibility is that many progenitor cells are "called in," and they differentiate into different lineages of cells. Whichever is the case, we speculate that areas in need of new cells (because of physiological turnover or pathological loss of cells) may be able to signal to potential stem cells to coax them into the region, and then clonal expansion occurs to help restore the number of cells to normal. Therefore, it will be very important to try to find the factors responsible for inducing stem cells to migrate into lesioned or sick areas of the brain. Discovering these factors could aid the attempt to use bone marrow cells to repair the brain.

We thank Ted Usdin for help in preparing the human Y chromosome probe; Carolyn Smith for help in confocal microscopy; and Michael Brownstein and Harold Gainer for helpful suggestions and for editing the manuscript.

1. Gage, F. H. (2000) *Science* **287,** 1433–1438.
2. Gage, F. H., Kempermann, G., Palmer, T. D., Peterson, D. A. & Ray, J. (1998) *J. Neurobiol.* **36,** 249–266.
3. McKay, R. (1997) *Science* **276,** 66–71.
4. Weissman, I. L., Anderson, D. J. & Gage, F. (2001) *Annu. Rev. Cell Dev. Biol.* **17,** 387–403.
5. Gould, E., Vail, N., Wagers, M. & Gross, C. G. (2001) *Proc. Natl. Acad. Sci. USA* **98,** 10910–10917.
6. Gould, E. & Gross, C. G. (2002) *J. Neurosci.* **22,** 619–623.
7. Eriksson, P. S., Perfilieva, E., Bjork-Eriksson, T., Alborn, A. M., Nordborg, C., Peterson, D. A. & Gage, F. H. (1998) *Nat. Med.* **4,** 1313–1317.
8. Uchida, N., Buck, D. W., He, D., Reitsma, M. J., Masek, M., Phan, T. V., Tsukamoto, A. S., Gage, F. H. & Weissman, I. L. (2000) *Proc. Natl. Acad. Sci. USA* **97,** 14720–14725.
9. Brazelton, T. R., Rossi, F. M., Keshet, G. I. & Blau, H. M. (2000) *Science* **290,** 1775–1779.
10. Bittner, R. E., Schofer, C., Weipoltshammer, K., Ivanova, S., Streubel, B., Hauser, E., Freilinger, M., Hoger, H., Elbe-Burger, A. & Wachtler, F. (1999) *Anat. Embryol.* **199,** 391–396.
11. Eglitis, M. A. & Mezey, E. (1997) *Proc. Natl. Acad. Sci. USA* **94,** 4080–4085.
12. Ferrari, G., Cusella-De Angelis, G., Coletta, M., Paolucci, E., Stornaiuolo, A., Cossu, G. & Mavilio, F. (1998) *Science* **279,** 1528–1530.
13. Gussoni, E., Soneoka, Y., Strickland, C. D., Buzney, E. A., Khan, M. K., Flint, A. F., Kunkel, L. M. & Mulligan, R. C. (1999) *Nature* **401,** 390–394.
14. Mahmood, A., Lu, D., Wang, L., Li, Y., Lu, M. & Chopp, M. (2001) *Neurosurgery* **49,** 1196–1203.
15. Mezey, E., Chandross, K. J., Harta, G., Maki, R. A. & McKercher, S. R. (2000) *Science* **290,** 1779–1782.
16. Orlic, D., Kajstura, J., Chimenti, S., Jakoniuk, I., Anderson, S. M., Li, B. S., Pickel, J., McKay, R., Nadal-Ginard, B., Bodine, D. M., *et al.* (2001) *Nature* **410,** 701–705.
17. Theise, N. D., Badve, S., Saxena, R., Henegariu, O., Sell, S., Crawford, J. M. & Krause, D. S. (2000) *Hepatology* **31,** 235–240.
18. Theise, N. D., Nimmakayalu, M., Gardner, R., Illei, P. B., Morgan, G., Teperman, L., Henegariu, O. & Krause, D. S. (2000) *Hepatology* **32,** 11–16.
19. Quaini, F., Urbanek, K., Beltrami, A. P., Finato, N., Beltrami, C. A., Nadal-Ginard, B., Kajstura, J., Leri, A. & Anversa, P. (2002) *N. Engl. J. Med.* **346,** 5–15.
20. Korbling, M., Katz, R. L., Khanna, A., Ruifrok, A. C., Rondon, G., Albitar, M., Champlin, R. E. & Estrov, Z. (2002) *N. Engl. J. Med.* **346,** 738–746.
21. Lagasse, E., Connors, H., Al-Dhalimy, M., Reitsma, M., Dohse, M., Osborne, L., Wang, X., Finegold, M., Weissman, I. L. & Grompe, M. (2000) *Nat. Med.* **6,** 1229–1234.
22. Alison, M. R., Poulsom, R., Jeffery, R., Dhillon, A. P., Quaglia, A., Jacob, J., Novelli, M., Prentice, G., Williamson, J. & Wright, N. A. (2000) *Nature* **406,** 257.
23. Sternberger, L. A. & Petrali, J. P. (1977) *J. Histochem. Cytochem.* **25,** 1036–1042.
24. Mullen, R. J., Buck, C. R. & Smith, A. M. (1992) *Development (Cambridge, U.K.)* **116,** 201–211.
25. Betancourt, L. & Colom, L. V. (2000) *J. Neurosci. Res.* **61,** 646–651.
26. Du, J., Tao-Cheng, J. H., Zerfas, P. & McBain, C. J. (1998) *Neuroscience* **84,** 37–48.
27. Schnell, S. A., Staines, W. A. & Wessendorf, M. W. (1999) *J. Histochem. Cytochem.* **47,** 719–730.
28. Pielou, E. C. (1976) *Mathematical Ecology* (Wiley Interscience, New York).
29. Leuba, G. & Garey, L. J. (1989) *Exp. Brain Res.* **77,** 31–38.
30. O'Kusky, J. & Colonnier, M. (1982) *J. Comp. Neurol.* **210,** 278–290.
31. Gage, F. H. (1998) *Curr. Opin. Neurobiol.* **8,** 671–676.
32. Woodbury, D., Schwarz, E. J., Prockop, D. J. & Black, I. B. (2000) *J. Neurosci. Res.* **61,** 364–370.
33. Sanchez-Ramos, J., Song, S., Cardozo-Pelaez, F., Hazzi, C., Stedeford, T., Willing, A., Freeman, T. B., Saporta, S., Janssen, W., Patel, N., *et al.* (2000) *Exp. Neurol.* **164,** 247–256.

34. Priller, J., Persons, D. A., Klett, F. F., Kempermann, G., Kreutzberg, G. W. & Dirnagl, U. (2001) *J. Cell Biol.* **155,** 733–738.
35. Jiang, Y., Jahagirdar, B. N., Reinhardt, R. L., Schwartz, R. E., Keene, C. D., Ortiz-Gonzalez, X. R., Reyes, M., Lenvik, T., Lund, T., Blackstad, M., *et al.* (2002) *Nature* **418,** 41–49.
36. Ying, Q. L., Nichols, J., Evans, E. P. & Smith, A. G. (2002) *Nature* **416,** 545–548.
37. Terada, N., Hamazaki, T., Oka, M., Hoki, M., Mastalerz, D. M., Nakano, Y., Meyer, E. M., Morel, L., Petersen, B. E. & Scott, E. W. (2002) *Nature* **416,** 542–545.
38. McKay, R. (2002) *Nat. Biotechnol.* **20,** 426–427.
39. Castro, R. F., Jackson, K. A., Goodell, M. A., Robertson, C. S., Liu, H. & Shine, H. D. (2002) *Science* **297,** 1299.
40. Trainor, P. A., Zhou, S. X., Parameswaran, M., Quinlan, G. A., Gordon, M. A., Sturm, K. & Tam, P. P. L. (1999) in *Molecular Embryology: Methods and Protocols* (Humana, Totowa, NJ), Vol. 97, pp. 183–200.
41. Hickey, W. F. (1991) *Brain Pathol.* **1,** 97–105.

Corrections

MEDICAL SCIENCES. For the article "Linkage disequilibrium in human populations," by Christine Lonjou, Weihua Zhang, Andrew Collins, William J. Tapper, Eiram Elahi, Nikolas Maniatis, and Newton E. Morton, which appeared in issue 10, May 13, 2003, of *Proc. Natl. Acad. Sci. USA* (**100,** 6069–6074; First Published April 29, 2003; 10.1073/pnas.1031521100), due to a printer's error, the last three column headings in Table 5 incorrectly contained dashes in "European-Asian," "African-American-Yoruban," and "African-Eurasian" instead of the necessary minus signs. The corrected table appears below.

Table 5. Weighted difference estimates ± standard errors: Samples with cosmopolitan maps

Estimated	Parameter	European − Asian	African-American − Yoruban	African − Eurasian
ε estimated	ε	0.001 ± 0.043	0.162 ± 0.053	0.638 ± 0.046
ε, M estimated	ε	0.005 ± 0.048	0.110 ± 0.052	0.418 ± 0.052
ε, M estimated	$-\ln M$	−0.002 ± 0.006	0.026 ± 0.011	0.130 ± 0.013

www.pnas.org/cgi/doi/10.1073/pnas.1432848100

MEDICAL SCIENCES. For the article "Normal viability and altered pharmacokinetics in mice lacking mdr1-type (drug-transporting) P-glycoproteins," by Alfred H. Schinkel, Ulrich Mayer, Els Wagenaar, Carla A. A. M. Mol, Liesbeth van Deemter, Jaap J. M. Smit, Martin A. van der Valk, Arie C. Voordouw, Hergen Spits, Olaf van Tellingen, J. Mark J. M. Zijlmans, Willem E. Fibbe, and Piet Borst, which appeared in issue 8, April 15, 1997, of *Proc. Natl. Acad. Sci. USA* (**94,** 4028–4033), the authors note the following correction. Fig. 1, and the first few lines of the *Materials and Methods* and *Results* sections, indicate that during gene disruption, exons 3 and 4 of the *Mdr1b* gene were deleted. However, there is an error in the map of the *Mdr1b* gene: exon 3 is positioned upstream (not downstream) of the first indicated *Nco*I site. As a consequence, only exon 4 of *Mdr1b* was deleted, and not exons 3 and 4. For the validity of the *Mdr1b* and *Mdr1a/1b* knockout mouse strains, this error has no consequences: deletion of exon 4 alone still results in a frameshift and still removes the first transmembrane segment plus some flanking sequences in Mdr1b. The absence of Mdr1b at the protein and functional level in the knockout mice also remains well documented. This correction, therefore, does not affect the conclusions of the paper.

www.pnas.org/cgi/doi/10.1073/pnas.1332736100

NEUROSCIENCE. For the article "Transplanted bone marrow generates new neurons in human brains," by Éva Mezey, Sharon Key, Georgia Vogelsang, Ildiko Szalayova, G. David Lange, and Barbara Crain, which appeared in issue 3, February 4, 2003, of *Proc. Natl. Acad. Sci. USA* (**100,** 1364–1369; First Published January 21, 2003; 10.1073/pnas.0336479100), the lettering in the Fig. 2 legend is incorrect. The corrected legend should read: "**Fig. 2.** Neuronal markers colocalize with the Y chromosome. Fluorescent microscopic images of neocortex from patients 2 (*B*, *D*, and *F*) and 3 (*C*) and hippocampus from patients 1 (*A*) and 3 (*E*). The green color represents the immunostaining for neuronal markers Kv2.1 (*A–D*) and NeuN (*E* and *F*), and the red color represents the Y chromosome. All cell nuclei are stained with 4′,6-diamidino-2-phenylindole, a blue fluorescent chromosomal marker. All images are overlays of the images seen through the three separate filters. Arrows point to cells that are labeled with neuronal markers and are also Y chromosome-positive. In the Kv2.1 immunostaining, the initial axons of some neurons can also be visualized. (Scale bars = 10 μm.)"

www.pnas.org/cgi/doi/10.1073/pnas.1332662100

BIOCHEMISTRY. For the article "Crystal structure of a photoactive yellow protein from a sensor histidine kinase: Conformational variability and signal transduction," by Sudarshan Rajagopal and Keith Moffat, which appeared in issue 4, February 18, 2003, of *Proc. Natl. Acad. Sci. USA* (**100,** 1649–1654; First Published January 31, 2003; 10.1073/pnas.0336353100), the authors note that part of Fig. 1*B* was incorrectly labeled as a π helix. It should have been labeled as a 3–10 helix. This correction does not affect the conclusions of the article. The corrected figure and its legend appear below.

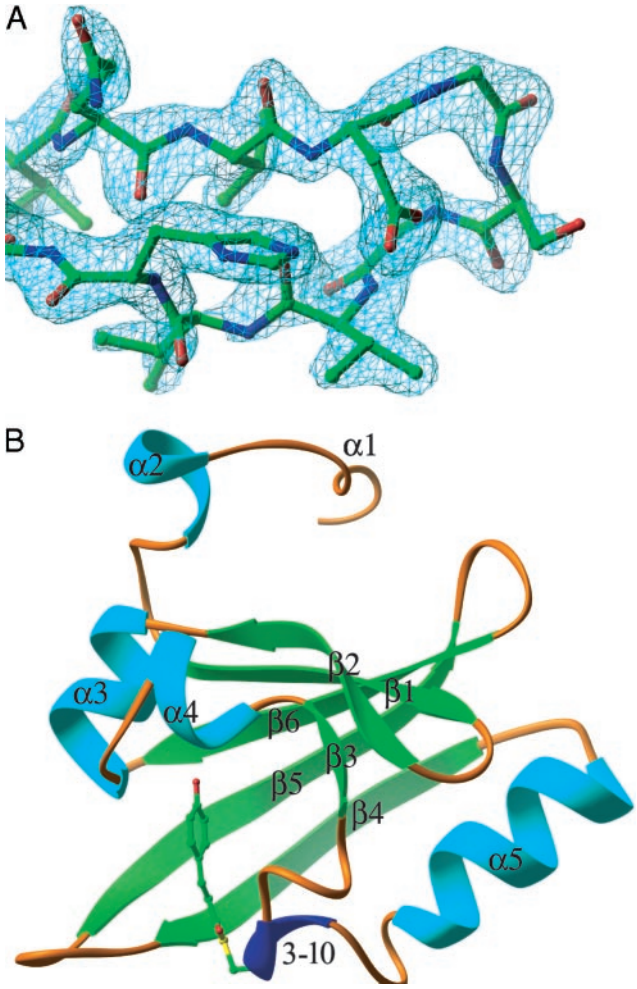

Fig. 1. Crystal structure of Ppr-PYP. (*A*) A simulated annealing composite omit map at 2.0σ level of the β1–β2 turn of chain B. (*B*) Chain B of Ppr-PYP with secondary structure labeled according to ref. 20.

www.pnas.org/cgi/doi/10.1073/pnas.1432896100

dc_219_11

blood

2008 111: 5544-5552
Prepublished online February 11, 2008;
doi:10.1182/blood-2007-10-119073

The combination of granulocyte colony-stimulating factor and stem cell factor significantly increases the number of bone marrow –derived endothelial cells in brains of mice following cerebral ischemia

Zsuzsanna E. Toth, Ronen R. Leker, Tal Shahar, Sandra Pastorino, Ildiko Szalayova, Brook Asemenew, Sharon Key, Alissa Parmelee, Balazs Mayer, Krisztian Nemeth, Andras Bratincsák and Éva Mezey

Blood (print ISSN 0006-4971, online ISSN 1528-0020), is published weekly by the American Society of Hematology, 2021 L St, NW, Suite 900, Washington DC 20036.

The combination of granulocyte colony-stimulating factor and stem cell factor significantly increases the number of bone marrow–derived endothelial cells in brains of mice following cerebral ischemia

*Zsuzsanna E. Toth,[1] *Ronen R. Leker,[2] *Tal Shahar,[2] Sandra Pastorino,[3] Ildiko Szalayova,[1] Brook Asemenew,[1] Sharon Key,[1] Alissa Parmelee,[1] Balazs Mayer,[1] Krisztian Nemeth,[1] Andras Bratincsák,[4] and Éva Mezey[1]

[1]National Institute of Dental and Craniofacial Research, Bethesda, MD; [2]National Institute of Neurological Disorders and Stroke, Bethesda, MD; [3]National Cancer Institute, Bethesda, MD; and [4]National Institute of Mental Health, National Insitutes of Health, Bethesda, MD

Granulocyte colony-stimulating factor (G-CSF) induces proliferation of bone marrow–derived cells. G-CSF is neuroprotective after experimental brain injury, but the mechanisms involved remain unclear. Stem cell factor (SCF) is a cytokine important for the survival and differentiation of hematopoietic stem cells. Its receptor (c-kit or CD117) is present in some endothelial cells. We aimed to determine whether the combination of G-CSF/SCF induces angiogenesis in the central nervous system by promoting entry of endothelial precursors into the injured brain and causing them to proliferate there. We induced permanent middle cerebral artery occlusion in female mice that previously underwent sex-mismatched bone marrow transplantation from enhanced green fluorescent protein (EGFP)–expressing mice. G-CSF/SCF treatment reduced infarct volumes by more than 50% and resulted in a 1.5-fold increase in vessel formation in mice with stroke, a large percentage of which contain endothelial cells of bone marrow origin. Most cells entering the brain maintained their bone marrow identity and did not transdifferentiate into neural cells. G-CSF/SCF treatment also led to a 2-fold increase in the number of newborn cells in the ischemic hemisphere. These findings suggest that G-CSF/SCF treatment might help recovery through induction of bone marrow–derived angiogenesis, thus improving neuronal survival and functional outcome. (Blood. 2008;111:5544-5552)

Introduction

Granulocyte colony-stimulating factor (G-CSF) was identified more than 2 decades ago,[1] and was found to mobilize hematopoietic bone marrow cells to the systemic circulation. Although G-CSF has been used in many patients to counter the side effects of chemotherapy as well as to prepare donors for peripheral cell harvesting, some concerns regarding its long-term safety still remain.[2-4] G-CSF may have several beneficial effects in animals with stroke.[5,6] Thus, it was reported that rats treated with G-CSF following middle cerebral artery occlusion (MCAO) have smaller infarcts and better functional outcome compared with controls.[5,7-9] The molecular basis of these neuroprotective effects has not yet been fully determined, but signaling through the JAK-STAT and PI3K-Akt pathways leading to a reduction in proapoptotic factors, and an increase in antiapoptotic factors was suggested to play an important role.[10] Furthermore, it was shown that rats that received transplants of G-CSF–mobilized peripheral blood precursor cells (PBPCs) demonstrated a significant improvement in functional recovery following permanent MCAO (PMCAO).[11] Moreover, G-CSF reportedly has an important role in inducing neurogenesis in the brain.[12] Combinations of G-CSF and stem cell factor (SCF) may further increase the positive effects of G-CSF by augmenting tyrosine kinase–related downstream effects and increasing prosurvival signals.[10]

Lee and colleagues[13] found that G-CSF treatment increased angiogenesis after focal cerebral ischemia. However, the origin of these newly formed blood vessels remains unclear. Thus, they may arise from in situ proliferation of existing endothelial cells in the central nervous system (CNS), or they might originate from bone marrow–derived endothelial precursor cells (BMDECs) that home to the brain. Because G-CSF in combination with SCF mobilizes BMDECs from bone marrow, we used enhanced green fluorescent protein (EGFP) chimeric animals that underwent PMCAO to see if G-CSF/SCF treatment might induce angiogenesis from BMDECs and whether this combination would have beneficial effects on functional outcome.

Methods

Preparation of the mice and surgery

All experiments were approved by the institutional animal care and use committee and were conducted according to National Institutes of Health (NIH) guidelines. Female 4- to 6-week-old C57B mice were subjected to irradiation (2 × 4.5 Gy [450 rad] 6 hours apart) to deplete their own bone marrow (BM), and then were given transplants of BM[14] generated from male mice that ubiquitously express GFP (with the exception of erythrocytes) and kept in a sterile environment for 10 days. After recovery, they were subjected to PMCAO as described before.[15] This model results in cortical injury limited to the frontal and parietal cortex and spares the subcortical structures. Mice received vehicle or a combination of 200 μg/kg

Submitted October 18, 2007; accepted February 5, 2008. Prepublished online as *Blood* First Edition paper, February 11, 2008; DOI 10.1182/blood-2007-10-119073.

An Inside *Blood* analysis of this article appears at the front of this issue.

*Z.E.T., R.R.L., and T.S. contributed equally to this work.

The online version of this article contains a data supplement.

The publication costs of this article were defrayed in part by page charge payment. Therefore, and solely to indicate this fact, this article is hereby marked "advertisement" in accordance with 18 USC section 1734.

Table 1. List of antibodies used

Antigen	Source (catalog no.)	Host	Dilution	Pretreatment	Incubation	Detection
GFP	Molecular Probes/Invitrogen (11122)	Rabbit	1:40000	—	1 h at RT	anti–rabbit HRP, FITC-Tyr
GFP	Chemicon/Millipore, Billerica, MA (AB16901)	Chicken	1:5000	—	1 h at RT	anti–chicken biotin, ABC, FITC-Tyr
GFP	Abcam, Cambridge, MA (Ab290)	Rabbit	1:10000	—	1 h at RT	anti–rabbit HRP, FITC-Tyr
VWF	Novocastra, Newcastle Upon Tyne, United Kingdom (NCL-VWFp)	Rabbit	1:500	Microwave	Overnight at 4°C	anti–rabbit HRP, A594-Tyr
CD31	PharMingen, San Diego, CA, (550274)	Rat	1:200	—	Overnight at 4°C	anti–rat A594, α-rat A647
VE-cadherin	Santa Cruz Biotechnology, Santa Cruz, CA (Sc-6458)	Goat	1:100	—	Overnight at 4°C	anti–goat biotin, SA-A594
Iba1	WAKO, Richmond, VA (019-19741)	Rabbit	1:1000	—	1 h at RT	anti–rabbit HRP, A594-Tyr
BrdU	Accurate, Westbury, NY (OBT0030)	Rat	1:200	Microwave	Overnight at 4°C	anti–rat HRP, A350-Tyr

A350, A594, A647 indicate AlexaFluor dyes; ABC, avidin-biotin complex (Vector Laboratories, Burlingame, CA); TYR, tyramide conjugate; VWF, von Willebrand factor; and —, none.

G-CSF and 50 μg/kg SCF per day intraperitoneally, respectively (Peprotech, Rocky Hill, NJ), to increase the number of circulating bone marrow stem cells (BMSCs) for 5 days following the surgery. All mice were given BrdU (50 mg/kg twice daily intraperitoneally; Roche Applied Sciences, Indianapolis, IN) to follow cell proliferation on days 1 to 5 after PMCAO.

Infarct size determination

At 60 days after stroke, serial sections of the forebrains of the mice studied (n = 7 per group) were cut at 200-μm intervals. The sections were stained with toluidine blue and photographed using a DM16000 Leica inverted fluorescence microscope (Wetzlar, Germany), and the hemispheres were traced using Image J software (NIH, Bethesda, MD). Because the cortical stroke tissue had already liquefied and disappeared by the time of death, the infarct volume was calculated as the difference between the sizes of the 2 hemispheres multiplied by the distance between the sections.

Immunohistochemistry

Mice were perfused at different time points (2 to 6 months after surgery) using 4% paraformaldehyde through the ascending aorta. Following perfusion, the brains were taken out and processed using cryoprotection achieved by increasing concentration of sucrose. The brains were then frozen on dry ice, and serial sections were cut at a 10-μm thickness and mounted on positively charged microscope slides. The slides were kept at −80°C until used. Immunohistochemistry was performed to visualize GFP as well as other markers. For photography, all sections were freshly mounted with 0.01 M Tris-HCI buffer (pH 7.8).

The perfused sections were washed in phosphate-buffered saline (PBS) 3 times for 3 minutes, microwaved for antigen retrieval when needed in 10 mM citric acid buffer (pH 6.1) for 5 minutes after the liquid started to boil, and then cooled at room temperature (RT) for 30 minutes. Following pretreatment, the sections were blocked with Universal Blocking Reagent (Biogenex, San Ramon, CA) for 10 minutes. The primary antibody was applied according to Table 1, diluted in 1% bovine serum albumin (BSA) containing 0.25% Triton-X 100 and followed by blocking endogenous peroxidase activity using 3% H_2O_2 for 15 minutes. In case of a double staining with a second tyramide amplification step, we added 0.5% sodium-azide to the H_2O_2 solution in order to block the horseradish peroxidase (HRP) still present from the first staining. The secondary antibodies were anti-rabbit HRP polymer conjugate (Zymed-Invitrogen, Carlsbad, CA) applied for 30 minutes, biotinylated donkey anti–chicken IgY or goat Ig-G (Jackson ImmunoResearch, West Grove, PA) at 1:1000 for 1 hour, and HRP-conjugated anti–rat IgG (Jackson ImmunoResearch) at 1:500 overnight. The AlexaFluor or FITC-conjugated tyramides were homemade and used in ratios of 1:2000 or 1:20 000, respectively. When antibodies were derived from the same host, we used a microwave treatment step to eliminate any nonspecific cross reaction.[16] Controls were performed with no primary antibodies.

Y chromosome hybridization

To further confirm the origin of the GFP in a few animals, we colocalized Y chromosome in the same cells as GFP as follows: sections were washed in PBS (pH: 7.4) 3 times for 3 minutes, rinsed in distilled water, and incubated in universal blocking reagent for 10 minutes. The sections were then incubated in rabbit anti-GFP antibody (Molecular Probes-Invitrogen, Carlsbad, CA) for 1 hour at room temperature. The endogenous peroxidase activity was blocked with a 3% hydrogen peroxide, and following PBS washes, the secondary antibody—an anti-rabbit HRP polymer conjugate—was applied undiluted for 30 minutes. The staining was then visualized using FITC-conjugated tyramide at 1:10 000 for 10 minutes at RT. To perform Y chromosomal fluorescence in situ hybridization (FISH), the same sections were immersed in 10 mM citric acid (pH 6.1) and microwaved in a kitchen microwave (700 W; GE, Louisville, KY) for 2 × 5 minutes at 50% power after the liquid started to boil. The water that evaporated was replaced with distilled water between and after the microwaving sessions, and the sections were left in the solution to cool for 2 hours at RT. Microwave treatment inactivates any HRP activity that is present in the tissue (ie, endogenous HRP and/or HRP incorporated in reagents used in previous steps).[16] The Y chromosomal hybridization was performed as described earlier[14] using a 1.5-kb RNA probe (pY3531B) generated against a repeat sequence of the mouse Y chromosome that was labeled with digoxigenin using a labeling kit (Roche Applied Sciences). After the hybridization step and several washes in salt sodium citrate (for details, see http://intramural.nimh.nih.gov/lcmr/snge/), the digoxigenin was detected with an antidigoxigenin antibody that was conjugated to HRP (1:600; Roche Applied Sciences) and visualized using the TSA-Plus CY3 System (1:600; Invitrogen, Carlsbad, CA). Determination of colocalization of the Y chromosome with GFP was performed by counting the cells manually on 3 different sections per animal, 5 animals per group, and by 2 independent people using a DMI6000 Leica inverted fluorescence microscope.

Vascular density analysis

To determine the percentage of area surface of vessels, an alkaline phosphatase reaction was performed using BCIP/NBT substrates (Roche Applied Sciences). The stained sections were scanned and photographed using the motorized stage and brightfield illumination. For colocalization studies between GFP, CD31, the Y chromosome, and BRDU, the immunostained sections were evaluated with a DMI6000 Leica inverted fluorescence microscope or a Leica TCS SP2 with AOBS and 2-Photon on an upright Leica DM RE-7 confocal microscope. Conventional fluorescent images were captured using the Volocity 4.01 software (Improvision; PerkinElmer, Waltham, MA). Z-stacks were collected at 0.5-μm intervals using a motorized stage. After image capturing, iterative restoration was performed at a 95% confidence level. The images were evaluated using the NIH Image J software. The data were analyzed using analysis of variance (ANOVA) and the Prism software (GraphPad, San Diego, CA).

In vitro endothelial cell proliferation assay

Mouse brain endothelial cells were acquired from ATCC (Manassas, VA) and maintained in Dulbecco modified Eagle medium (DMEM) containing 10% fetal bovine serum (FBS) at 37°C, 5% CO_2.[17] Cells were plated in 96-well cell-culture plates, 3000 cells/well, in 150 μL medium without FBS

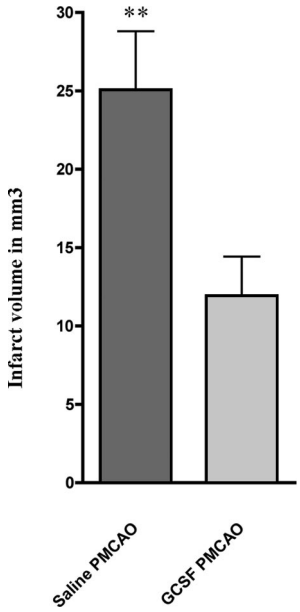

Figure 1. Infarct volumes in vehicle and G-CSF/SCF–treated mice. Columnar graph showing the infarct volume in millimeters cubed in the brains of the saline-treated versus GSCF-treated mice. Values are means plus SEM. $^{**}P < .01$.

or growth factors. After 24 hours, different concentrations of G-CSF and SCF were added to the medium together with BrdU (1:1000 dilution of BrdU; final dilution, 1:4000). The plates were then placed into a normal (37°C, 5% CO_2) or hypoxic (37°C, 5% CO_2, 1% O_2) incubator for 24 hours. The cell proliferation assay was performed according to the manufacturer's instructions (catalog no. 11647229001; Roche Applied Sciences). Control experiments included cells cultured without the growth factors. The experiment was done twice with triplicate samples.

Results

Infarct volumes

Injury size was measured 60 days after PMCAO. Lesion size was significantly smaller ($P = .012$) in animals treated with G-CSF/SCF ($11.3 + 2.5$ mm^3) as compared with controls ($25.1 + 3.7$ mm^3; Figure 1).

G-CSF/SCF increases influx of GFP$^+$ cells into the injured brain

In animals that underwent PMCAO but did not receive G-CSF/SCF that were killed at 2 months, we observed a 2.4 fold increase in the number of GFP$^+$ cells (Figure 2A,C,E) in the ischemic hemisphere compared with the nonischemic hemisphere (343 ± 24.7 vs 140 ± 31; $P < .05$, n = 4). Most of these cells expressed the microglial marker Iba1 (data not shown). Stimulation of peripheral stem cells using a combination of G-CSF and SCF after PMCAO resulted in a significant, 3.75-fold increase in the number of GFP$^+$ cells in the ischemic hemisphere as compared with the controls (Figure 2B,D,E). In the G-CSF/SCF–stimulated mice, the number of GFP$^+$ cells in the ischemic side were 1288 plus or minus 272 versus 229.8 plus or minus 54.2 in the nonischemic side ($P < .01$, n = 4; Figure 2E). To ensure that cells expressing GFP originate from donor BM, we used FISH to determine the presence of a Y chromosome in the GFP$^+$ cells (Figure 3 and Figure S1, available on the *Blood* website; see the Supplemental Materials link at the top of the online article).[18] The present findings confirmed our previously published results[18] that about 10% of cells expressing the Y chromosome were not positive for GFP (even when signal amplification was used), suggesting that when using only GFP as a marker we significantly underestimate the percentage of brain cells originating from the donor BM. This may be due to silencing of the GFP expression during neural differentiation. At 2 months after the injury, many of the GFP$^+$ cells coexpressed Iba1, suggesting that the early influx of BM-derived cells consists of mainly inflammatory cells. At this time point we could identify occasional GFP cells that colocalized with neuronal markers such as NeuN and rare cells that coexpressed GFP and the glial marker GFAP (not shown).

G-CSF/SCF increases cell proliferation in the ischemic brain

Cell proliferation was studied with BrdU immunostaining at 60 days after PMCAO (n = 4 in each group). Following PMCAO, BrdU$^+$ cells were significantly more abundant in the ischemic hemisphere (140 ± 27 vs 30 ± 5; $P < .002$; Figure 2F). The number of proliferating cells significantly increased following G-CSF/SCF treatment in both hemispheres, but a much larger increase was noted on the ischemic side (358 ± 64 vs 68 ± 15.5; $P < .001$). Overall, G-CSF/SCF treatment resulted in a 2.5-fold increase in the absolute number of BrdU$^+$ cells in the ischemic side. When we tried to colocalize GFP with BrdU, we found less than 1% of GFP$^+$ cells that were double labeled; most of these were endothelial cells based on their location, nuclear morphology, and their elongated endothelial-like shape. Specifically, at this time point we could not identify any cells that coexpressed GFP, BrdU, and neuronal markers, and only very rare cells that coexpressed GFP, BrdU, and GFAP. Most of the BRDU$^+$ cells were astrocytes or microglial or endothelial cells. These results suggest that most BM-derived cells failed to proliferate in the brain for long periods of time and that most of those that did proliferate maintained a BM fate. However, because G-CSF/SCF treatment did increase the number of BrdU-expressing cells, it presumably did increase endogenous neurogenesis in the brain.

G-CSF/SCF increases angiogenesis in the injured brain

Alkaline phosphatase staining of vascular endothelium was performed on all brains at the level of the bregma plus 0.5 mm (n = 4 in the G-CSF/SCF and n = 3 in the control groups, respectively). Blood vessel density was also counted in naive mice and in mice that did not undergo PMCAO but received G-CSF/SCF. Ischemic and nonischemic hemispheres were compared in PMCAO mice that received G-CSF/SCF or vehicle. As shown in Figure 4A-C, we found that vessels occupy 3% plus 0.1% of the surface area in naive mice. In control animals that did not suffer from stroke, but received G-CSF/SCF, the surface area occupied by vascular endothelium increases slightly ($3.9\% \pm 0.2\%$). In ischemic animals in the ischemic hemisphere, the area occupied by blood vessels increased significantly ($4.8\% \pm 0.3\%$) and there was a further, statistically significant ($P < .001$) increase in PMCAO mice that also received G-CSF/SCF ($6.7\% \pm 0.45\%$; Figure 4). Overall, we observed a 2.23-fold increase in the number of blood vessels in ischemic animals treated with G-CSF/SCF compared with naive animals. Interestingly, G-CSF/SCF also significantly increased blood vessel density in the nonischemic hemisphere.

dc_219_11

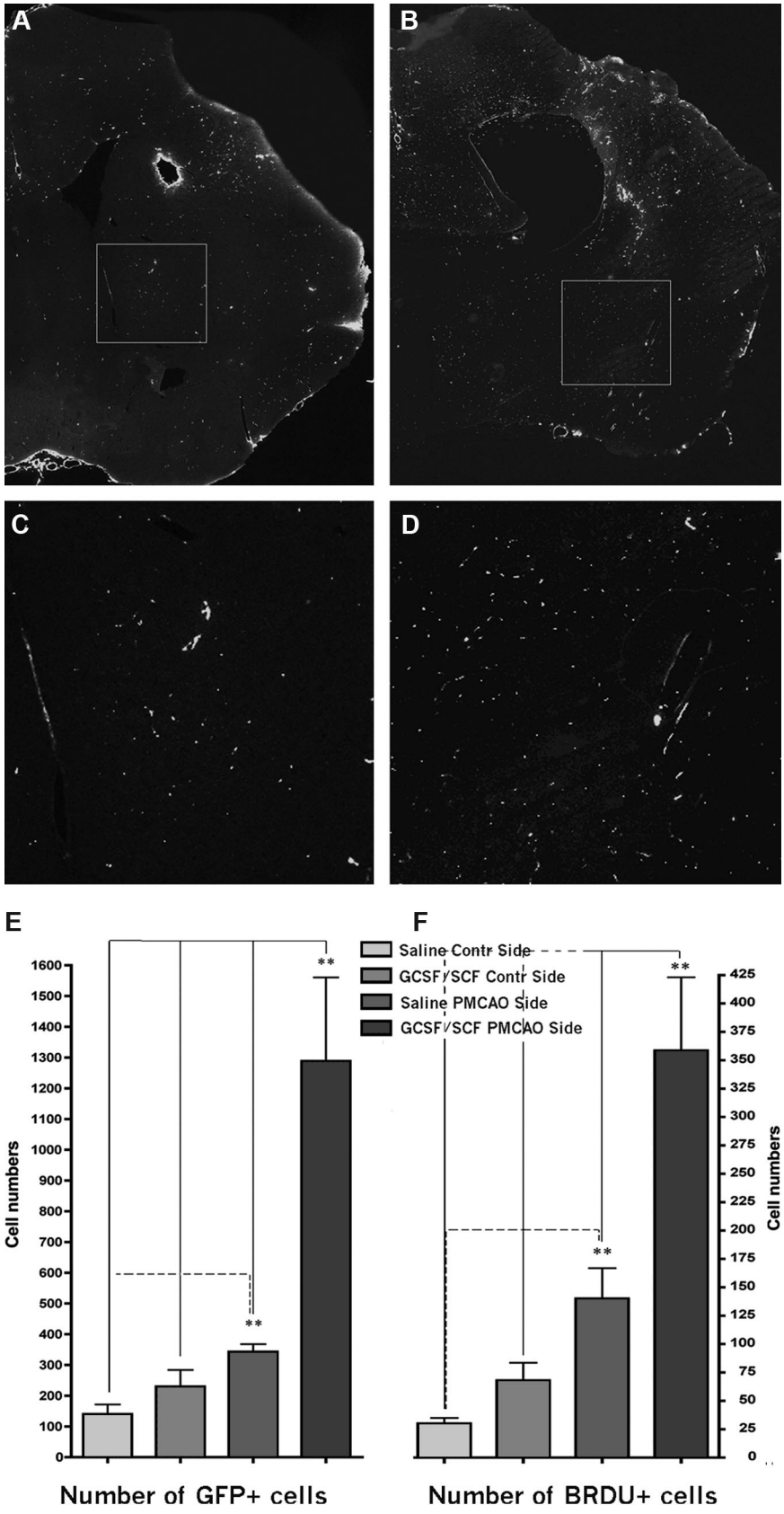

Figure 2. GFP expression and proliferation at 2 months following PMCAO. (A) Coronal section of a vehicle-treated brain at 2 months after PMCAO at the level of the lesion. GFP-immunopositive cells were visualized using amplified immunostaining. (B) Similar level in the brain like in panel A from a mouse that received daily injection of G-CSF/SCF for 5 consecutive days following the stroke. (C,D) Magnifications of the boxed areas in panels A and B, respectively. Note the significantly higher number of green fluorescent cells in the G-CSF/SCF–treated animal's brain. Horizontal side of box equals 500 μm (A,B) and 125 μm (C,D). Panels A,B: objective, 10×; numeric aperture, 0.3, Plan Fluo. (E) Columnar graph showing the mean number of GFP- and (F) BRDU-immunopositive cells in the sections of the saline-treated versus G-CSF–treated mice in both hemispheres.

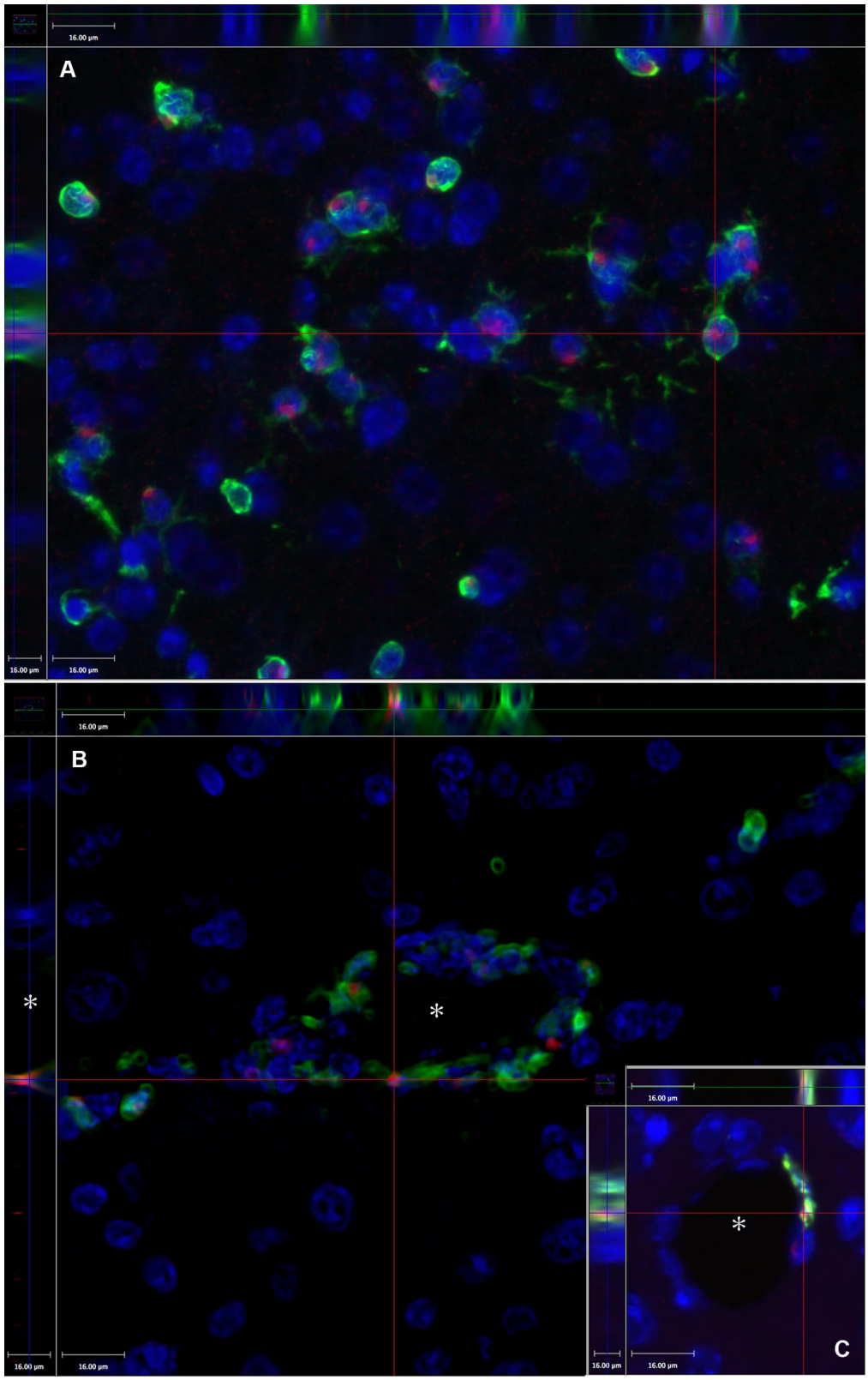

Figure 3. Demonstration of the technique of colocalization of the GFP and the Y chromosome in a female brain at 2 months after PMCAO. Y chromosome hybridization was performed in sex-mismatched GFP BM-transplanted mice brains. (A) Presence of the Y chromosomes in red (Alexa-594); green fluorescence indicates the presence of the GFP, and blue fluorescence labels cell nuclei based on DAPI, a chromosomal stain. The section is one level of a Z-series demonstrating that the Y chromosome is localized in the same cells that are also GFP$^+$ (side panels). (B) Cross-section of a capillary (*) of a Z-series depicting several luminally localized GFP cells that are also positive for the Y chromosome (red dots). The inset (C) shows another example, where the side panel of the confocal image illustrates that the Y chromosome and the GFP colocalize in a cell that borders the vascular lumen (*). Objective, 40×; numeric aperture, 0.6 (A); and objective, 20×; numeric aperture, 0.7 (B). Scale bar equals 16 µm.

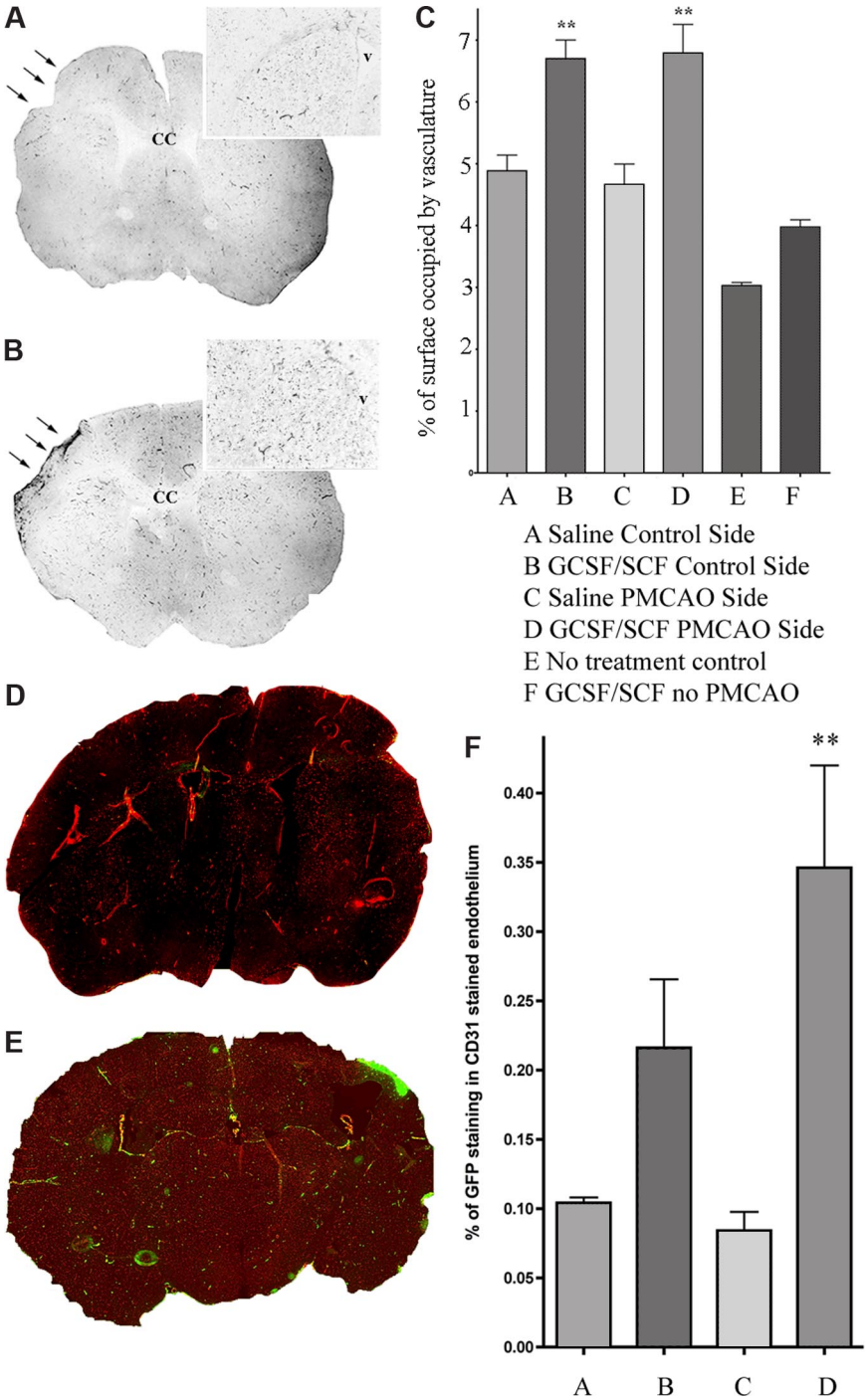

Figure 4. G-CSF/SCF treatment increases angiogenesis and many of the new endothelial cells are of donor BM origin. Vascular density is demonstrated in untreated (A) and G-CSF/SCF–treated (B) mice after stroke (→). The insets are high-magnification representative images of coronal sections from similar rostrocaudal levels of the brains. (C) Columnar graph showing the percentage of the surface area occupied by vessels based on alkaline phosphatase staining in the sections of the saline-treated versus G-CSF/SCF–treated mice in both hemispheres. Vascular density is demonstrated in untreated (D) and G-CSF/SCF–treated (E) mice after stroke. The vascular endothelial cells are immunostained for CD31 (red fluorescence due to Alexa-594), and the GFP cells are immunostained in green following signal amplification using FITC-tyramide. For panels A,B,D,E: objective, 10×; numeric aperture, 0.3, Plan Fluo. Note the increased density of vessels as well as more green vascular structures in the G-CSF/SCF–treated brain. (F) The columnar graph demonstrates the percentage of GFP$^+$ (ie, BM-derived; green) cell surfaces compared with all (red) endothelial (CD31-stained) surfaces in the saline-treated versus G-CS/SCF–treated mice brains in both hemispheres (n = 4). Values are means plus SEM. $^{**}P < .01$. CC indicates corpus callosum; v, lateral ventricle.

Newly formed blood vessels at the infarct border originate from BM endothelial precursors

We used GFP- and endothelium-specific immunostaining in the same sections to see if endothelial cells and precursors in newly formed blood vessels derive from BM. We chose 3 markers that are generally accepted to be specific for vascular endothelium: von Willebrand factor, CD31 (PECAM1), and VE-cadherin. GFP immunostaining was amplified to ensure visualization of cells that express the marker protein at very low levels. We found that many endothelial cells in the immediate infarct vicinity expressed GFP. In the untreated ischemic animals GFP$^+$ endothelial cells were identified in both hemispheres with a frequency of 0.1% and 0.08% of all endothelial surface for the nonischemic versus ischemic hemisphere, respectively. In G-CSF/SCF–treated mice there was a robust increase of new GFP$^+$ endothelial cells compared with the saline-treated cells that was more significant on the side of the stroke than in the control side (0.35% ± 0.07% vs 0.22% ± 0.05%; $P = .008$; Figures 4D-F; S3). The colocalization of CD31 (Figures 5A-C; S2), von Willebrand factor (Figure 5D,E), and VE-cadherin (Figure 5F) and BRDU (Figures S4; 5G) with GFP was demonstrated using confocal Z-stacks (at 0.5-μm intervals) and iterative restoration. Except for occasional rare cells, we could not detect GFP$^+$ endothelial cells in control chimeric animals that did not experience stroke with or without G-CSF/SCF treatment.

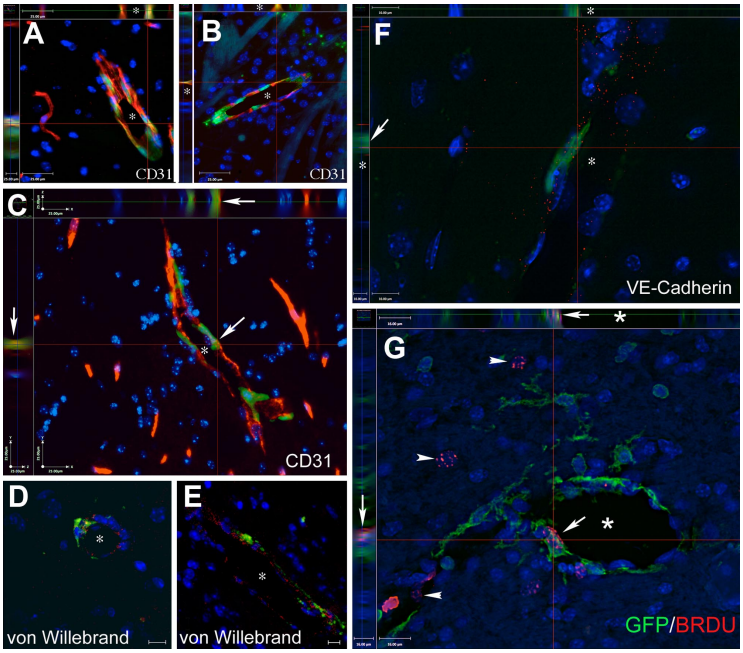

Figure 5. Cells of BM origin populate the vascular endothelium in mice with PMCAO treated with G-CSF/SCF. (A-C) Images from Z-stacks, where sections from G-CSF/SCF–treated PMCAO mice were immunostained with CD31, a specific marker of vascular endothelium, and GFP to track the bone marrow origin. The side panels demonstrate the colocalization of the 2 markers (endothelial marker and GFP) in several cells of the vascular wall. (D,E) demonstrates colocalization of GFP with the von Willebrand factor in vascular endothelium shown in red. (F) One level of a Z-series with side panels demonstrating that a GFP$^+$ cell lining the lumen of a capillary (*) is also labeled with red dots representing the antibody staining for VE-cadherin, another specific endothelial cell marker. (G) Colocalization of BRDU (red dots over labeled nuclei) with GFP in a luminal cell lining a capillary (*). Arrow points to the colocalization of the red and green in the main panel as well as in the side panels. Arrows point to BRDU$^+$ nuclei that do not belong to GFP$^+$ cells. The images are a single level taken out of a Z-series, where the section was optically sliced into 0.5-μm–thin sections and iterative restoration was perfomed using Volocity 4.0 software. Objective, 40×; numeric aperture, 0.6 (A-E); and objective, 63×; numeric aperture, 0.7 (F). Scale bar equals 25 μm (A-C), 10 μm (D-F), and 16 μm (G).

SCF induces proliferation of cerebral vascular endothelium in vitro

Our in vitro data show that SCF induces endothelial proliferation at concentrations between 5 and 100 ng/mL, while G-CSF seems to have no direct effect on proliferation (Figure 6). When the cells are grown in a hypoxic environment, the proliferative effect of SCF is significantly enhanced. The combination of SCF/G-CSF has the same effect as SCF alone.

Discussion

The current study identifies BM-derived cells as a major source of poststroke angiogenesis in the brain. The number of newly formed blood vessels increased 2.2-fold when we applied G-CSF/SCF after PMCAO. To ensure that newly formed blood vessels did originate from BMDECs, we used BM from GFP-expressing male donors that engrafted into the BM of recipient female mice prior to PMCAO. We then identified donor marrow cells as expressing GFP and the Y chromosome. Using this system, we could isolate newly formed blood vessels originating from BMDECs from those derived from the brain's resident endothelial cell population. Our results show that most newly formed blood vessels in the infarct vicinity were composed of GFP$^+$/Y$^+$ cells, indicating their BM origin. Given the fact that not all Y$^+$ cells expressed GFP—probably due to silencing of the transgene related with progressive differentiation—it is highly likely that our results based on GFP expression in newly formed blood vessels are an

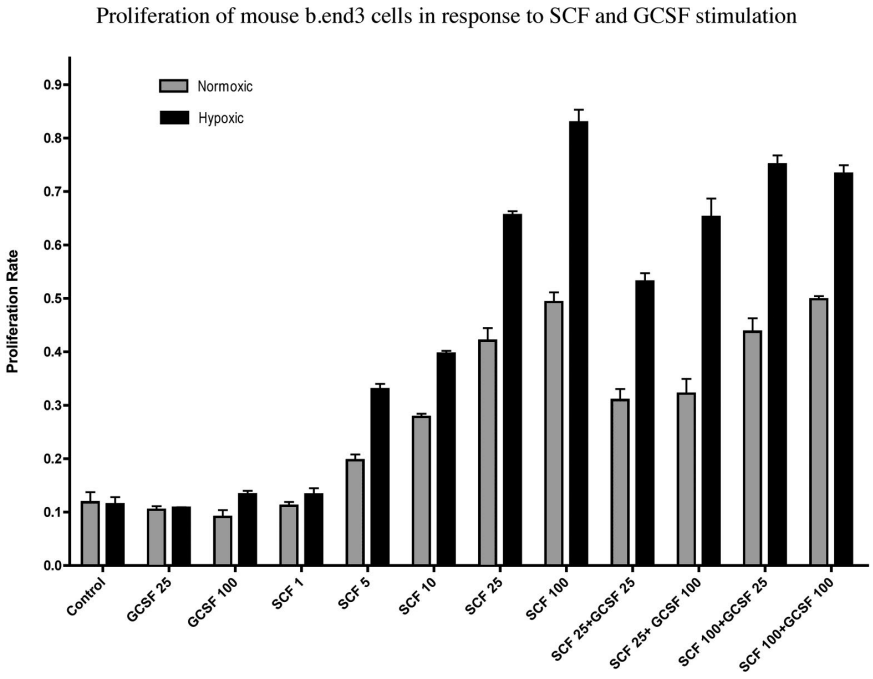

Figure 6. Proliferative effect of G-CSF, SCF, and its combination on murine cerebral endothelial cells in vitro. A mouse brain endothelial cell line (b.end3) was used in the experiment. Following a 24-hour incubation of the cells with the factors at different concentrations (values are mean nanograms per milliliter media) and BRDU, the proliferation rate was calculated based on optical density (OD) measurements. ▒ represents proliferation at normoxic conditions; ■ shows proliferation rate in hypoxic conditions. Controls received no factors but BRDU. G-CSF seems to be ineffective in the concentrations used, while SCF has a dose-dependent, significant proliferative effect, starting at 5 ng/mL. Combining the 2 factors results in proliferation rates similar to that of SCF alone. Hypoxic conditions seem to further increase the effectiveness of SCF. Values are means plus SD.

underestimate of the true contribution of BMDECs to angiogenesis in the injured brain.

Our results corroborate previous reports that found increased recruitment of BM-derived cells to the brain following injury and those that found G-CSF to augment this process.[19,20] However, while others focused on the short-term effects of this recruitment we waited for 2 months prior to analysis of the effects. This allowed us to avoid the early phase in which most recruited cells represent inflammatory cells and focus on angiogenesis, which takes a longer time to accomplish. In contrast to work reported earlier, in our studies we treated animals with a combination of G-CSF/SCF. This results in a 2-fold increase in circulating $CD34^+$cells[21] versus treatment with G-CSF alone. Both G-CSF and SCF are known to stimulate the survival, proliferation, and differentiation of BM cells, including endothelial cells.[21-27] Our results suggest that while G-CSF is important in recruiting cells from the BM into the circulation, SCF might be responsible for the proliferation of vascular endothelial cells, many of which are derived from the donor BM. The in vitro data also suggest that hypoxia, which is found in ischemic tissue, significantly enhances the proliferative effect exhibited by SCF. This may be due to an increased expression of endothelial c-kit receptors under hypoxic conditions. The finding of BRDU and GFP double-positive cells (ie, proliferating endothelial cells of BM origin) among the lining of cerebral vasculature in ischemic areas suggest that our in vitro observations may indeed be important in vivo as well.

Our current set of results argues against transdifferentiation of BM-derived cells into neurons as an important mechanism to functional improvement in stroke.[28,29] Thus, despite a major increase in the influx of GFP^+ BM-derived cells into the injured brain with G-CSF/SCF, we could only identify isolated astrocytes in the brain that coexpressed GFP and almost no GFP^+ neurons. In contrast, most BM-derived GFP^+ cells in the brain retained their BM fate and represented either microglia, which were most prevalent in the early poststroke period, or endothelial cells, which were the prevalent GFP^+ cell type at 2 months after stroke. However, we cannot rule out a more significant contribution of BM-derived neurogenesis in other circumstances.[14,30,31]

Importantly, G-CSF reduces infarct volumes in injury models by activation of antiapoptotic and anti-inflammatory mechanisms.[19,32] A neuroprotective effect for G-CSF/SCF was also identified in the current experiment, lending further validity to our results. G-CSF treatment in stroke animals also results in greater improvements in neurologic deficits. Our data suggest that G-CSF/SCF–driven angiogenesis is likely another mechanism that could contribute to functional gains after stroke by improving metabolism and function of surviving cells in the peri-infarct area. Furthermore, given the increase in BrdU cells that were not of BM origin following G-CSF/SCF therapy, it is also likely that stimulation of endogenous neurogenesis is another mechanism that could improve functional outcome after stroke.

In conclusion, the combination of G-CSF/SCF may have synergistic beneficial effects both on lesion size and on angiogenesis. G-CSF/SCF–driven angiogenesis results from G-CSF–induced recruitment of BM-derived cells into the ischemic brain, and SCF might facilitate the proliferation and survival of endothelial cells. Most of the BM-derived cells maintain their BM identity and do not appear to significantly transdifferentiate into neural cells. These angiogenic and neuroprotective effects translate into better functional outcome after stroke and should promote future clinical studies in humans to study the efficacy of this therapeutic avenue in stroke victims.

Acknowledgments

The authors would like to acknowledge Dr David A. Davis (National Cancer Institute, NIH) for use of the hypoxia chamber.

This research was supported by the Division of Intramural Research, National Institute of Dental and Craniofacial Research, NIH. Z.E.T. is supported by OTKA (Hungarian Scientific Research Fund) T-043169.

Authorship

Contribution: Z.E.T. performed histology, analyzed data, and wrote portions of the paper; R.L.L. performed surgeries and helped write the paper; T.S. designed the experiment, performed surgeries, and analyzed data; A.B. and S.P. participated in surgeries and analyzed data; I.S. and S.K. contributed reagents and helped analyze data; A.P. performed sectioning and immunostaining for VE-cadherin; B.M. and K.N. performed the endothelial cell proliferation studies; and E.M. designed the experiment, performed histochemistry, analyzed data, and wrote the paper.

Conflict-of-interest disclosure: The authors declare no competing financial interests.

Correspondence: Éva Mezey, NIH, NIDCR, CSDB, Bldg 49, Rm 5A-76, 49 Convent Dr, Bethesda, MD 20892, e-mail: mezeye@mail.nih.gov.

References

1. Nagata S, Tsuchiya M, Asano S, et al. Molecular cloning and expression of cDNA for human granulocyte colony-stimulating factor. Nature. 1986;319:415-418.
2. Morstyn G, Lieschke GJ, Sheridan W, Layton J, Cebon J, Fox RM. Clinical experience with recombinant human granulocyte colony-stimulating factor and granulocyte macrophage colony-stimulating factor. Semin Hematol. 1989;26:9-13.
3. Neidhart J, Mangalik A, Kohler W, et al. Granulocyte colony-stimulating factor stimulates recovery of granulocytes in patients receiving dose-intensive chemotherapy without bone marrow transplantation. J Clin Oncol. 1989;7:1685-1692.
4. Sheridan WP, Morstyn G, Wolf M, et al. Granulocyte colony-stimulating factor and neutrophil recovery after high-dose chemotherapy and autologous bone marrow transplantation. Lancet. 1989; 2:891-895.
5. Beck H, Voswinckel R, Wagner S, et al. Participation of bone marrow-derived cells in long-term repair processes after experimental stroke. J Cereb Blood Flow Metab. 2003;23:709-717.
6. Six I, Gasan G, Mura E, Bordet R. Beneficial effect of pharmacological mobilization of bone marrow in experimental cerebral ischemia. Eur J Pharmacol. 2003;458:327-328.
7. Shyu WC, Lin SZ, Lee CC, Liu DD, Li H. Granulocyte colony-stimulating factor for acute ischemic stroke: a randomized controlled trial. CMAJ. 2006;174:927-933.
8. Shyu WC, Lin SZ, Yang HI, et al. Functional recovery of stroke rats induced by granulocyte colony-stimulating factor-stimulated stem cells. Circulation. 2004;110:1847-1854.
9. Yanqing Z, Yu-Min L, Jian Q, Bao-Guo X, Chuan-Zhen L. Fibronectin and neuroprotective effect of granulocyte colony-stimulating factor in focal cerebral ischemia. Brain Res. 2006;1098:161-169.
10. Duarte RF, Frank DA. SCF and G-CSF lead to the synergistic induction of proliferation and gene expression through complementary signaling pathways. Blood. 2000;96:3422-3430.
11. Willing AE, Vendrame M, Mallery J, et al. Mobilized peripheral blood cells administered intravenously produce functional recovery in stroke. Cell Transplant. 2003;12:449-454.
12. Schneider A, Kruger C, Steigleder T, et al. The hematopoietic factor G-CSF is a neuronal ligand that counteracts programmed cell death and drives neurogenesis. J Clin Invest. 2005;115: 2083-2098.
13. Lee ST, Chu K, Jung KH, et al. Granulocyte colony-stimulating factor enhances angiogenesis after focal cerebral ischemia. Brain Res. 2005; 1058:120-128.

14. Mezey E, Chandross KJ, Harta G, Maki RA, McKercher SR. Turning blood into brain: cells bearing neuronal antigens generated in vivo from bone marrow. Science. 2000;290:1779-1782.
15. Leker RR, Teichner A, Grigoriadis N, et al. NAP, a femtomolar-acting peptide, protects the brain against ischemic injury by reducing apoptotic death. Stroke. 2002;33:1085-1092.
16. Toth ZE, Mezey E. Simultaneous visualization of multiple antigens with tyramide signal amplification using antibodies from the same species. J Histochem Cytochem. 2007;55:545-554.
17. Song L, Pachter JS. Culture of murine brain microvascular endothelial cells that maintain expression and cytoskeletal association of tight junction-associated proteins. In Vitro Cell Dev Biol Anim. 2003;39:313-320.
18. Toth ZE, Shahar T, Leker R, et al. Sensitive detection of GFP utilizing tyramide signal amplification to overcome gene silencing. Exp Cell Res. 2007;313:1943-1950.
19. Schneider A, Kuhn HG, Schabitz WR. A role for G-CSF (granulocyte-colony stimulating factor) in the central nervous system. Cell Cycle. 2005;4:1753-1757.
20. Kawada H, Takizawa S, Takanashi T, et al. Administration of hematopoietic cytokines in the subacute phase after cerebral infarction is effective for functional recovery facilitating proliferation of intrinsic neural stem/progenitor cells and transition of bone marrow-derived neuronal cells. Circulation. 2006;113:701-710.
21. Hess DA, Levac KD, Karanu FN, et al. Functional analysis of human hematopoietic repopulating cells mobilized with granulocyte colony-stimulating factor alone versus granulocyte colony-stimulating factor in combination with stem cell factor. Blood. 2002;100:869-878.
22. Broudy VC, Kovach NL, Bennett LG, Lin N, Jacobsen FW, Kidd PG. Human umbilical vein endothelial cells display high-affinity c-kit receptors and produce a soluble form of the c-kit receptor. Blood. 1994;83:2145-2152.
23. Hess DC, Abe T, Hill WD, et al. Hematopoietic origin of microglial and perivascular cells in brain. Exp Neurol. 2004;186:134-144.
24. Kocher AA, Schuster MD, Szabolcs MJ, et al. Neovascularization of ischemic myocardium by human bone-marrow-derived angioblasts prevents cardiomyocyte apoptosis, reduces remodeling and improves cardiac function. Nat Med. 2001;7:430-436.
25. Powell TM, Paul JD, Hill JM, et al. Granulocyte colony-stimulating factor mobilizes functional endothelial progenitor cells in patients with coronary artery disease. Arterioscler Thromb Vasc Biol. 2005;25:296-301.
26. Takamiya M, Okigaki M, Jin D, et al. Granulocyte colony-stimulating factor-mobilized circulating c-Kit+/Flk-1+ progenitor cells regenerate endothelium and inhibit neointimal hyperplasia after vascular injury. Arterioscler Thromb Vasc Biol. 2006;26:751-757.
27. Yamaguchi H, Ishii E, Saito S, et al. Umbilical vein endothelial cells are an important source of c-kit and stem cell factor which regulate the proliferation of haemopoietic progenitor cells. Br J Haematol. 1996;94:606-611.
28. Ono K, Yoshihara K, Suzuki H, et al. Preservation of hematopoietic properties in transplanted bone marrow cells in the brain. J Neurosci Res. 2003;72:503-507.
29. Roybon L, Ma Z, Asztely F, et al. Failure of transdifferentiation of adult hematopoietic stem cells into neurons. Stem Cells. 2006;24:1594-1604.
30. Crain BJ, Tran SD, Mezey E. Transplanted human bone marrow cells generate new brain cells. J Neurol Sci. 2005;233:121-123.
31. Mezey E, Key S, Vogelsang G, Szalayova I, Lange GD, Crain B. Transplanted bone marrow generates new neurons in human brains. Proc Natl Acad Sci U S A. 2003;100:1364-1369.
32. Komine-Kobayashi M, Zhang N, Liu M, et al. Neuroprotective effect of recombinant human granulocyte colony-stimulating factor in transient focal ischemia of mice. J Cereb Blood Flow Metab. 2005;26:402-413.

STEM CELLS®

dc_219_11

TISSUE-SPECIFIC STEM CELLS

CD45-Positive Blood Cells Give Rise to Uterine Epithelial Cells in Mice

ANDRÁS BRATINCSÁK,[a] MICHAEL J. BROWNSTEIN,[a,b] RICCARDO CASSIANI-INGONI,[c] SANDRA PASTORINO,[d] ILDIKÓ SZALAYOVA,[e] ZSUZSANNA E. TÓTH,[e] SHARON KEY,[e] KRISZTIÁN NÉMETH,[e,f] JAMES PICKEL,[a] ÉVA MEZEY[e]

[a]National Institute of Mental Health, Bethesda, Maryland, USA; [b]The J. Craig Venter Institute, Gaithersburg, Maryland, USA; [c]National Institute of Neurological Disorders and Stroke, Bethesda, Maryland, USA; [d]National Cancer Institute, Bethesda, Maryland, USA; [e]National Institute of Dental and Craniofacial Research, Bethesda, Maryland, USA; [f]Department of Dermato-Venereology and Oncology, Semmelweis University, Budapest, Hungary

Key Words. Adult stem cell • Hematopoietic stem cell • Endometrium • Regeneration

ABSTRACT

The uterine endometrium is composed of epithelial and stromal cells, which undergo extensive degeneration and regeneration in every estrous cycle, and dramatic changes occur during pregnancy. The high turnover of cells requires a correspondingly high level of cell division by progenitor cells in the uterus, but the character and source of these cells remain obscure. In the present study, using a novel transgenic mouse, we showed that CD45-positive hematopoietic progenitor cells colonize the uterine epithelium and that in pregnancy more than 80% of the epithelium can derive from these cells. Since we also found green fluorescent protein (GFP)-positive uterine endothelial cells in long-term GFP bone marrow-transplanted mice, we conclude that circulating CD45+ cells play an important role in regenerating the uterine epithelium. STEM CELLS *2007;25:2820–2826*

Disclosure of potential conflicts of interest is found at the end of this article.

INTRODUCTION

The lining of the uterus goes through extensive regeneration during the cycle and in pregnancy [1, 2]. Tanaka et al. studied the clonality of endometrium and demonstrated that individual uterine endometrial glands consist of monoclonal populations of epithelial cells [3]. Their findings indicated that single or multiple as yet unidentified stem cells with uniform clonality exist on the bottom of each endometrial gland [3]. Several investigators have used bone marrow (BM) transplants to show that bone marrow-derived stem cells can repopulate a variety of organs in irradiated hosts [4–7]. The existence of a uterine endometrial stem cell has been proposed, but its character, origin, and exact anatomical location have proven elusive [8]. Recently, Taylor showed that transplanted bone marrow cells give rise to uterine epithelial cells in humans [9]. Taylor's patients were exposed to full body irradiation and chemotherapy before they received BM transplants [9]; thus, the physiological significance of his finding, as well as the nature of the BM-derived cells that entered the uterus and differentiated there, could not be determined. Recently, Du and Taylor demonstrated in lethally irradiated mice that transplanted full bone marrow gives rise to endometrial tissue, including epithelium, and suggested that BM mesenchymal cells might be responsible for the phenomenon [10]. On the basis of these data and a recent article demonstrating the presence of hematopoietic stem cells and lymphoid progenitors in endometrial biopsies in women [11], we asked the following questions: Do BM cells contribute to the uterine epithelium in healthy animals? If they do, what kind of BM cells populate the tissue? How extensive is their contribution? To answer these questions, we first injected green fluorescent protein (GFP)-tagged BM cells [12] into lethally irradiated female *C57BL/6J* mice and confirmed the fact that uterine epithelial cells can indeed arise from BM. We then created a transgenic mouse model to determine whether CD45+ cells might contribute to the epithelium.

MATERIALS AND METHODS

Bone Marrow Transplantation Studies

Allogenic bone marrow transplantation was used to detect progeny of GFP+ BM-derived cells. Briefly, *C57BL/6J* mice ($n = 6$) received whole-body irradiation (900 rad) and were transplanted intravenously 2 hours after irradiation with 10^6 bone marrow cells harvested from a GFP+ mouse (C57BL/6-Tg [ACTB-EGFP] 1Osb/J, 003291; Jackson Laboratory, Bar Harbor, ME, http://www.jax.org). At later time points, transplanted animals were sacrificed and tissues harvested as described above.

Transgenic Mouse Studies

To determine whether CD45 cell progeny contribute to the repopulation of the uterine epithelium under physiological conditions, we generated a novel transgenic mouse. First, we introduced Cre recombinase cDNA into a bacterial artificial chromosome (BAC) containing the complete mouse *CD45* gene (Fig. 1A). The recombinase cDNA was inserted downstream of an internal ribosomal

Correspondence: Éva Mezey, M.D., Ph.D., 49 Convent Drive, Building 49, Room 5A76, Bethesda, Maryland 20892, USA. Telephone: 301-435-5635; Fax: 301-496-1339; e-mail: mezeye@mail.nih.gov Received April 24, 2007; accepted for publication July 20, 2007; first published online in STEM CELLS *EXPRESS* July 26, 2007; available online without subscription through the open access option. 1066-5099/2007/$30.00/0 doi: 10.1634/stemcells.2007-0301

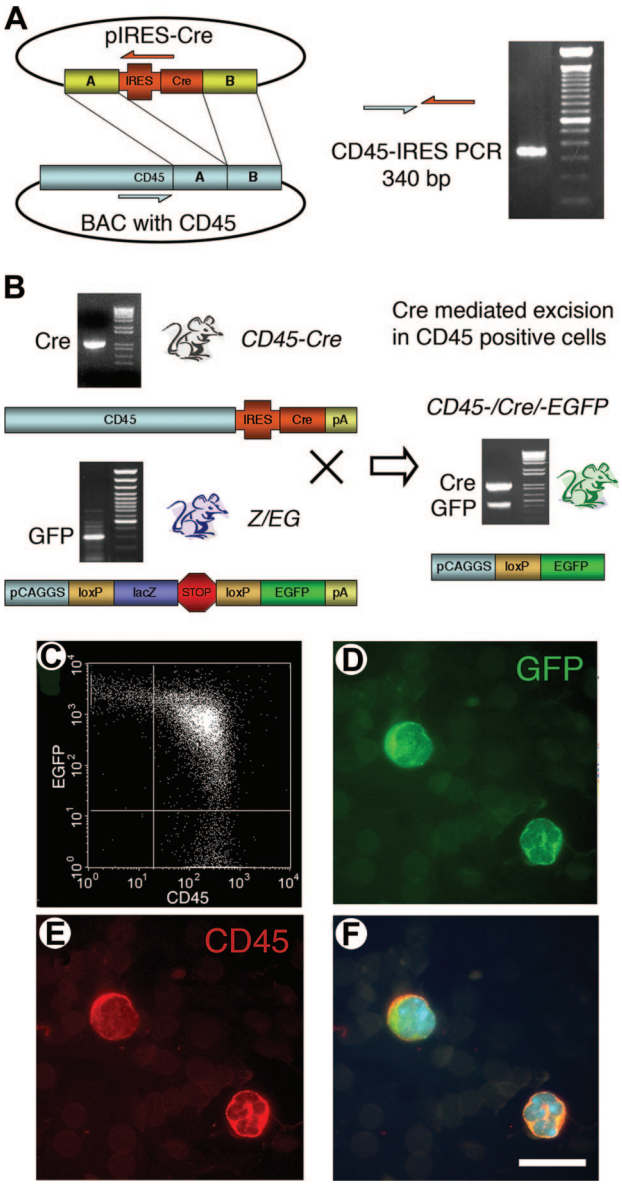

Figure 1. GFP is expressed in CD45+ cells of the double-transgenic (*CD45/Cre-Z/EG*) mice. **(A):** Upon homologous recombination, the IRES-Cre recombination cassette flanked by two homologous fragments (A and B) was inserted into exon 33 of the *CD45* gene in a BAC containing the entire coding region. The recombinant construct was confirmed to be correct by restriction mapping, PCR with primers flanking the recombination fragments, and sequencing. **(B):** To track the fate of CD45+ cells, we created a double-transgenic strain by breeding *CD45/Cre* mice with the double-reporter *Z/EG* mice. In the crossbred mice, every CD45+ cell expresses the Cre recombinase that will excise the floxed lacZ cassette, thus enabling the activation of GFP. Regardless of the future fate of CD45+ cells, GFP will be expressed continuously throughout their life spans. **(C):** Fluorescence-activated cell sorting of peripheral blood of a double-transgenic animal demonstrating a high percentage (85%) of double-positive blood cells using green fluorescence for GFP and red for CD45. **(D–F):** White blood cells immunostained with GFP (green) **(D)**, CD45 (red) **(E)**, and an overlay of **(D)** and **(E)** with added 4,6-diamidino-2-phenylindole (nuclear-blue) staining **(F)**. Scale bar = 15 μm. Abbreviations: BAC, bacterial artificial chromosome; bp, base pairs; EGFP, enhanced green fluorescent protein; GFP, green fluorescent protein; IRES, internal ribosomal entry site; PCR, polymerase chain reaction.

entry site (IRES), which in turn was placed downstream of the last coding exon of CD45. The resulting BAC was used to make transgenic mice (*CD45/Cre*). In such mice, Cre recombinase is produced in any cell that expresses CD45. First-generation heterozygous mice carrying the *Cre* transgene were bred. These *CD45/Cre* animals were then bred with *Z/EG* double reporter mice [13]. The latter express lacZ ubiquitously during embryonic development and adulthood. In the presence of Cre recombinase, the *lacZ* gene and the transcriptional stop following it are excised (Fig. 1B), activating the expression of a second reporter, enhanced green fluorescent protein (EGFP) (Fig. 1D). Only first-generation Cre transgenics were used because the transgene is prone to rearrangement. Thus, in subsequent generations, ectopic expression, even ubiquitous expression, can be seen (unpublished observations).

Construction of Recombination Cassette

The recombination cassette was constructed by cloning the IRES-Cre-frt-pgk/em7/Neo/bpA-frt expression cassette from p459 (a gift from Neal G. Copeland) with two flanking polymerase chain reaction (PCR)-amplified recombination fragments (A and B) into the pBC KS+ shuttle vector (Invitrogen, Carlsbad, CA, http://www.invitrogen.com). Fragments A (263 base pairs [bp]: 3,305–3,567; GenBank accession number nm_011210) and B (319 bp: 3,568–3,886; from nm_011210) were designed to flank the insertion site for the expression cassette upstream of the stop codon at the 3′ end of exon 33 of the *CD45* gene (Fig. 1A). The plasmid was introduced into *Escherichia coli* using heat shock, single ampicillin-resistant colonies were selected and propagated, and the plasmid was isolated by mini-prep and linearized for homologous recombination.

Homologous Recombination

BAC 131H7 (RPCI-23 mouse BAC library; Invitrogen) was used for these studies. This BAC is approximately 190,000 bp long. There are approximately 30,000 bp of DNA 5′ to the first exon of CD45 and 50,000 bp 3′ to the last exon. The recombination cassette was inserted to the BAC by homologous recombination [14] (Fig. 1A). Briefly, the BAC was electroporated into *E. coli* EL250, which hosts a temperature-inducible λ prophage that facilitates recombination. BAC-containing bacteria were incubated at 42°C for 15 minutes and transformed with the linearized recombination cassette by means of electroporation. Double-resistant (kanamycin-chloramphenicol) colonies were selected and propagated, and the recombinant BAC was isolated using a NucleoBond BAC Maxi Kit (BD Biosciences, San Diego, http://www.bdbiosciences.com). Homologous recombination was confirmed by enzymatic digestion, PCR, and DNA sequencing (Fig. 1A).

Production of Double-Transgenic Mice

Recombined BAC DNA was microinjected into *C57BL/6J* zygotes that were implanted into estrogen-primed foster mothers, and transgenic founders were selected by PCR using the following primers amplifying Cre: 5′-ccggtcgatgcaacgagtgatgagg-3′ and 5′-gcgttaatggctaatcgccatcttcc-3′. The resulting *CD45/Cre* mice were bred with *C57BL/6J* mice. Subsequently, *CD45/Cre* offspring were bred with heterozygous *Z/EG* double reporter mice (Jackson Laboratory) that express GFP upon Cre-mediated recombination, and their offspring were screened by PCR for Cre using the primers described above and for GFP (5′-gggcgatgccacctacggcaagctgaccct-3′ and 5′-ccgtcctccttgaagtcgatgcccttcagc-3′) (Fig. 1B). Double-transgenic (*CD45/Cre-Z/EG*) animals were selected and used for the studies reported. The majority of nucleated cells in the blood of the double-transgenic mice produced from all four founder lines were GFP+, and their progeny seemed GFP+ as well (Fig. 1C–1F). Thus, although we did not study this extensively, we observed no line-to-line variation, and we have no evidence that the site of integration of the recombinant BAC affected Cre expression.

Animal Procedures

Animal care and procedures were approved by the Animal Care and Use Committee of National Institute of Mental Health, NIH. Double-transgenic (*CD45/Cre-Z/EG*) animals were anesthetized, sacrificed by perfusion, and examined at different ages: 18-day-old embryos (n = 2), 3-day-old pups (n = 2), 6-week-old young adult (n = 1), 12-week-old adults (n = 2), 12-week-old pregnant animals

($n = 2$), and 20-week-old adult ($n = 1$). Tissues were fixed by transcardiac perfusion or immersion (used for fixing embryos) with Zamboni solution, harvested, and processed for immunostaining.

Immunohistochemistry

Perfused tissues were cryoprotected by immersion in 20% sucrose solution and frozen. Twelve-μm-thick sections were cut at −24°C in a Leica cryostat (Heerbrugg, Switzerland, http://www.leica.com), thaw-mounted, and stained using the following reagents: 1:1,000 anti-GFP antibody (A11122; Molecular Probes Inc., Eugene, OR, http://probes.invitrogen.com) followed by 1:1,000 Alexa-488 conjugated anti-rabbit antibody (A31565; Molecular Probes), 1:100 anti-CD45 antibody (ab3088-100; Abcam, Cambridge, MA, http://www.abcam.com) followed by 1:1,000 Alexa-594-conjugated anti-rat antibody (A11007; Molecular Probes), 1:20,000 4,6-diamidino-2-phenylindole (DAPI) (D1306; Molecular Probes), and 1:200 biotinylated *Lotus tetragonolobus* lectin (B-1325; Vector Laboratories, Burlingame, CA, http://www.vectorlabs.com) followed by 1:1,000 Alexa-594-conjugated streptavidin (S11227; Molecular Probes) or 1:1,000 horseradish-peroxidase-conjugated streptavidin and 1:10,000 Alexa-350-conjugated tyramide (T20937; Molecular Probes). As a second marker, we also used a wide-spectrum cytokeratin antibody (MU-131-UC; BioGenex, San Ramon, CA, http://www.biogenex.com) at a 1:200 dilution followed by an anti-mouse IgG conjugated to Alexa-594 (1:1,000) to confirm the characterization of epithelial cells. GFP immunostaining was confirmed by a second anti-GFP antibody (1:2,000; AB16901; Chemicon, Temecula, CA, http://www.chemicon.com) that detects a different epitope of GFP and showed results identical to those described before (data not shown). Control immunohistochemistry stainings were performed using secondary antibodies after omitting the primary antibodies. Detailed controls and variations of GFP stainings are described in Toth et al. [15]. Random areas of sections were photographed at low magnification, and epithelial cells (approximately 500–1,000 per animal) were counted by two independent investigators. The number of GFP-positive cells was expressed as a percentage of all epithelial nuclei based on DAPI and *Lotus* staining.

In Situ Hybridization Histochemistry

Radiographic in situ hybridization was performed on 12-μm fixed sections as described before (http://intramural.nimh.nih.gov/lcmr/snge/Protocol.html). The primers that included a T7 and a T3 polymerase site were constructed to generate a template complementary to the GFP mRNA between nucleotides 1,524 and 1,823 (accession no. AB234879). This template was then transcribed using the Ambion (Austin, TX, http://www.ambion.com) Maxiscript transcription kit (catalog number 1324) following the manufacturer's instructions. After hybridization, the slides were dipped into autoradiographic emulsion (Nuclear Track Emulsion B; Kodak, Rochester, NY, http://www.kodak.com) and developed 2 weeks later. A Giemsa background staining was applied, and the slides were dried and coverslipped. The sections were viewed with a Leica DMI6000 inverted microscope, and images were captured using Volocity software (PerkinElmer Life and Analytical Sciences, Boston, http://www.perkinelmer.com).

Fluorescence In Situ Hybridization in Combination with GFP Immunostaining

The STARFISH kit (catalog no. 1597-KD-50; Cambio, Cambridge, U.K., http://www.cambio.co.uk) was used to detect the X chromosome in 6-μm thin sections of uterine epithelium from fixed mouse sections. This allowed us to determine whether GFP+ cells were the products of cell-fusion events. Following microwave-induced antigen retrieval, GFP immunostaining was performed as described above. Then the sections were dehydrated and stained according to the Cambio protocol. A Cy3-labeled chromosomal paint probe was used for final visualization. Random areas of eight sections of uterine epithelium from one of the pregnant mice were chosen, and 865 cell nuclei were examined, focusing throughout the whole thickness of the section to count the number of X chromosomes per nuclei. Of these nuclei, 240 belonged to GFP-positive epithelium, and we found no evidence of fusion; that is, we did not see any nondividing nucleus with four X chromosomes. In fact, all the nuclei that were uncut in the sections exhibited two X chromosomes.

Flow Cytometry

After preincubation with anti-mouse CD16/32 (Caltag Laboratories, Burlingame, CA, http://www.caltag.com) to block the Fc receptor, peripheral blood mononuclear cells were stained with the anti-mouse CD45 R-phycoerythrin-conjugated antibody (catalog no. MCD4504; Caltag). Rat R-phycoerythrin-conjugated IgG2b (Caltag) was used as an isotype control. CD45 staining and EGFP direct fluorescence were analyzed using a fluorescence-activated cell sorting (FACS) flow cytometer (Becton, Dickinson and Company, San Jose, CA, http://www.bd.com).

RESULTS

Analysis of Blood Cells in the CD45/Cre/Z/EG Mice

As expected, in adult *CD45/Cre-Z/EG* mice, CD45+ cells, such as lymphocytes, (Fig. 1D–1F) and the derivatives of CD45+ cells, such as Kupfer cells and microglia (data not shown), were GFP-positive. Most, but not all, of the white cells in blood that could be stained with an anti-CD45 antibody were GFP+. In some cells, the fluorescent signal may have been too weak to detect, or excision of the floxed lacZ cassette may not have occurred because expression of the Cre recombinase was poor. FACS analysis of peripheral blood showed that the majority (65%–85% in several animals tested) of the CD45-positive white blood cells of double-transgenic mice expressed GFP (Fig. 1C).

Analysis of Uterine Histology in Long-Term Irradiated and GFP Bone Marrow-Transplanted Mice

Irradiated mice are known to keep on cycling, although the length of the cycles may be more variable [16]. Eight to 12 months after we transplanted GFP-tagged bone marrow cells (including hematopoietic, mesenchymal, and any other BM stem cell populations) into six irradiated female mice, green cells were detected in the uterine endometrial epithelium and stroma of five of six animals (Fig. 2A, 2C). These bone marrow-derived GFP+ epithelial cells bound *L. tetragonolobus* lectin, a marker with affinity for glycoprotein on the luminal surface of epithelial cells in the uterus [17]. The GFP+ epithelial (i.e., immunopositive for *L. tetragonolobus* [Fig. 2D, 2E]) cells did not express the common leukocyte antigen CD45, but numerous CD45+/GFP+ cells were detected in the uterine stroma (Fig. 2A), which is known to harbor CD45+ lymphoid cells [18]. Immunostaining using a pan-cytokeratin (cytokeratins [CKs] 8, 18, and 19) antibody also showed colocalization with GFP (Fig. 2B), further confirming the epithelial character of the GFP-positive cells.

Analysis of Uterine Histology in the Virgin and Pregnant CD45/Cre/Z/EG Mice

Resident macrophages and lymphocytes in the endometrial stroma are known to express CD45 [18], and indeed, we saw many CD45+/GFP+ cells in the stroma of the transplanted mice and of the *CD45/Cre-Z/EG* mice (Figs. 2A, 3B). We also found GFP+ cells in the epithelial layer of the endometrium (Figs. 2, 3A). Although these GFP+ cells could be stained with *L. tetragonolobus* lectin (Figs. 2D, 2E, 3C, 3D) and with anti-keratin-8, -18, and -19 antibody (Fig. 2B), another marker for epithelial cells, they could not be stained with anti-CD45 anti-

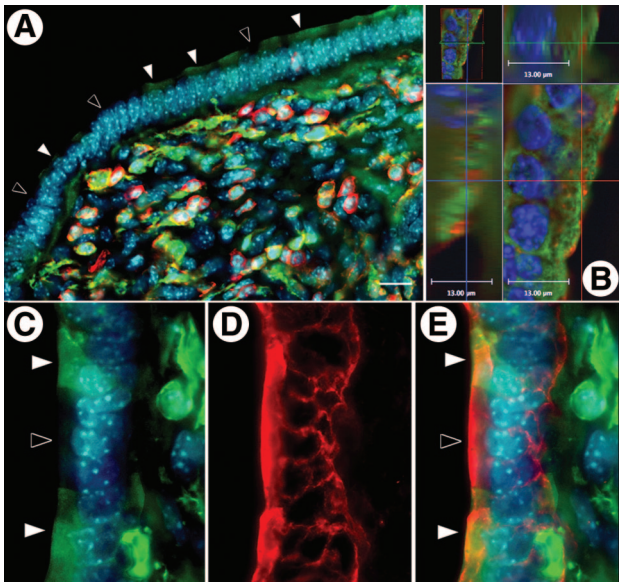

Figure 2. Endometrium of a mouse previously (10 months before) transplanted with enhanced green fluorescence protein bone marrow (BM) following irradiation. Green fluorescent protein (GFP) is shown in green, CD45 **(A)** and *L. tetragonolobus* **(C, D)** in red, and 4,6-diamidino-2-phenylindole (DAPI), the nuclear marker, in blue. **(A):** GFP+ and CD45− uterine epithelium in the recipient endometrium shows that BM cells can contribute to the regeneration of uterine epithelial cells. CD45+/GFP+ hematopoietic cells are present in the stromal layer. **(B):** Colocalization of a pan-cytokeratin immunostaining (in red) with GFP (in green) in epithelial cells. The image shows one level of a Z-stack in three-panel view. The stack was captured at 0.5-μm intervals, and iterative restoration was performed using Volocity 4.0 software (PerkinElmer) and a Leica DMI6000 inverted microscope. **(C–E):** GFP-positive nucleated (DAPI staining) cells appeared in the epithelial layer **(C)**, colocalized with *L. tetragonolobus*, a uterine epithelial marker **(D)**. **(E):** Overlay of **(C)** and **(D)**. Solid arrowheads indicate GFP+; open arrowheads indicate GFP− uterine epithelial cells. Scale bar in **(A)** = 20 μm **(A)** and 14 μm **(C–E)**.

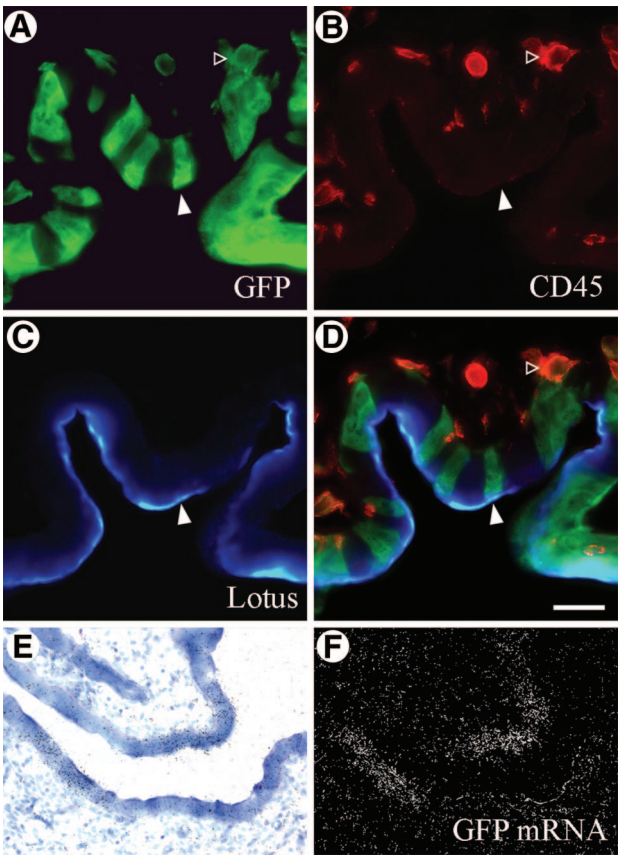

Figure 3. Green fluorescent protein (GFP)-expressing uterine epithelium of a double-transgenic (*CD45/Cre-Z/EG*) mouse. We observed GFP-positive (green) epithelial cells in the uterus **(A)** that did not express CD45 (red) **(B)** but bound the uterine epithelial marker *L. tetragonolobus* (blue) **(C). (D):** Overlay of the three stainings **(A–C)**. **(A–D):** Solid arrowheads point to GFP+/CD45− uterine epithelial cell; open arrowheads indicate GFP+/CD45+ stromal cell. **(E, F):** Uterine epithelium expressing GFP mRNA in bright-field **(E)** and dark-field **(F)** illumination. Scale bar = 20 μm **(A–D)** and 50 μm **(E–F)**. Abbreviation: GFP, green fluorescent protein.

body (Figs. 2A, 3B). Expression of GFP mRNA was further confirmed by in situ hybridization histochemistry (Fig. 3E, 3F). Thus, CD45+ cells appear to give rise to epithelial cells in the uterus of nonirradiated transgenic animals.

To determine the rate at which CD45+ cells contribute to the uterine epithelium and the extent of this contribution, we studied *CD45/Cre-Z/EG* animals at different ages. In mice, the estrous cycle is 5–6 days long [16, 19]. In contrast to humans, the epithelium does not shed, but it exhibits continuous degeneration and regeneration [20]. In the course of the cycle, epithelial cells undergo vacuolar degeneration and apoptosis and are replaced by newly generated cells [21]. The first cycle in mice occurs at 4–6 weeks of age. Consequently, a 1-week-old pup has not cycled yet, and 6-, 12-, and 20-week old animals have gone through approximately 2, 10, and 26 cycles, respectively. In the double-transgenic mice, we detected many CD45+/GFP+ cells in the uterine stroma (Fig. 4) at all ages examined (1, 6, 12, and 20 weeks). Although no GFP+ epithelial cells could be detected in the uterine epithelium in 1- and 6-week-old animals (Fig. 4A, 4B), 0.5% of the epithelial cells in 12-week-old mice and 6% in a 20-week-old animal were GFP+ (Fig. 4C–4F). The GFP+ epithelial cells were found in patches, suggesting that clonal expansion of individual progenitor cells gave rise to islands of epithelial cells. Thus, although we did not have enough animals at each time point to do a statistical analysis, we think that the number of uterine epithelial cells produced from CD45+ precursors increases with age and is related to the number of estrous cycles through which the animals have passed.

During pregnancy, the uterus undergoes marked proliferation. The endometrial surface of the pregnant mouse is approximately 25 times larger than that of a nonpregnant animal, and we wondered whether CD45+ cells might contribute to this increase. We were surprised to find that in one pregnant *CD45/Cre-Z/EG* mouse, the vast majority (82%) of uterine epithelial cells were also GFP+ (Fig. 4G, 4H). Our observations indicate that CD45+ progenitors could be the source of most of the new epithelial cells in the pregnant uterus. Based on double staining of GFP and the X chromosome, these cells seem unlikely to be the products of cell-fusion events, since they never contain more than two X chromosomes (Fig. 5).

Discussion

Eight to 12 months following the bone marrow transplantation using GFP-positive BM, the GFP-positive cells were detected in the endometrial epithelium and stroma of recipient animals. Bone marrow-derived GFP+ cells bound *L. tetragonolobus* lectin, which is an indicator of their epithelial nature. These GFP+ epithelial cells, however, did not express the common

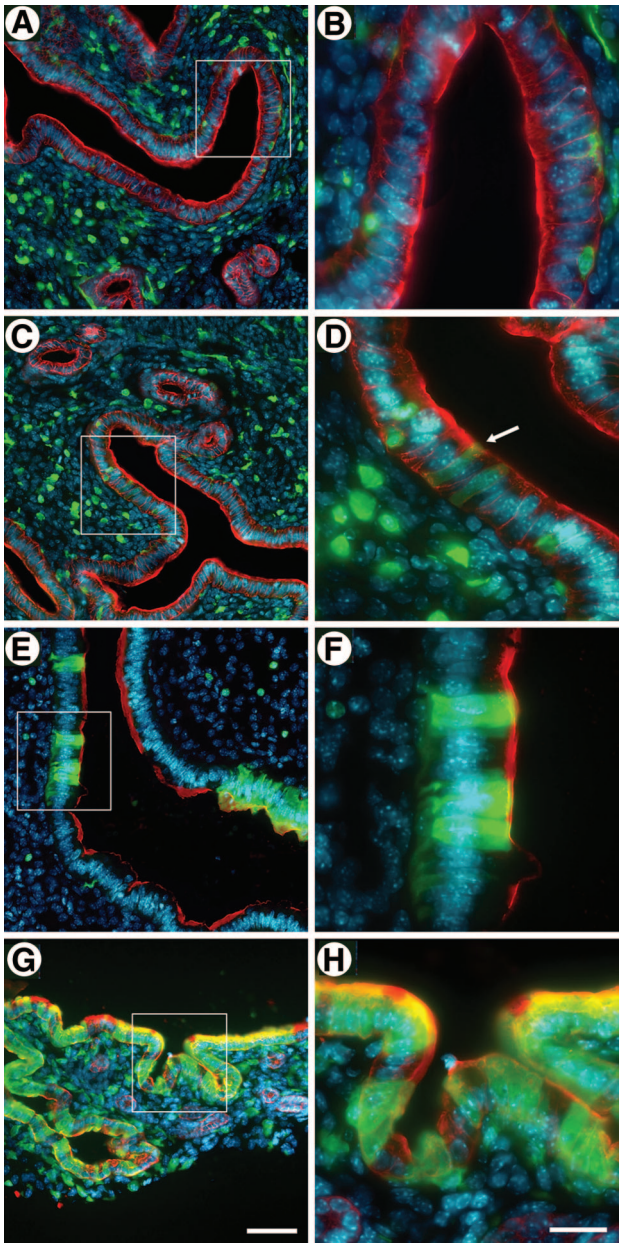

Figure 4. Green fluorescent protein (GFP)-expressing (green) uterine epithelial cells from double-transgenic animals of different ages and pregnant mice. All nuclei were stained in blue with 4,6-diamidino-2-phenylindole. **(A, B):** No GFP-positive (green) uterine epithelial (red staining represents *L. tetragonolobus*, the epithelial marker) cells were detected in 6-week-old animals. **(C, D):** Sporadic GFP-positive uterine epithelial cells were present at 12 weeks of age. Arrow indicates a GFP+ uterine epithelial cell. **(E, F):** At 20 weeks of age, 6% of uterine epithelial cells expressed GFP. **(G, H):** In 12-week-old pregnant mice, there was a robust increase in the number of GFP-expressing cells: 82% of the uterine epithelial cells were GFP+. Scale bars = 60 μm (left column) and 20 μm (right column).

leukocyte antigen CD45, whereas numerous CD45+/GFP+ cells were detected in the uterine stroma, which is known to harbor CD45+ lymphoid cells [18]. These findings clearly demonstrate that upon transplantation, BM cells enter the uterus and differentiate into epithelial cells there. The BM cells are unlikely to have fused with uterine cells after colonizing the organ because the GFP+ cells all appear to be diploid. BM cells are heterogeneous, however, and transplantation of tagged cells

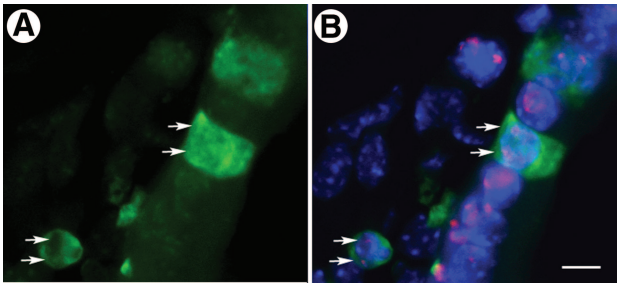

Figure 5. Arrows point to nuclei (4,6-diamidino-2-phenylindole, blue) of green fluorescent protein (GFP)-expressing (green) uterine epithelial cells **(A)** from double-transgenic animals that have two X chromosomes (red dots) **(B)**. GFP was visualized with a tyramide-fluorescein isothiocyanate conjugate, whereas the X chromosome was labeled by a Cy3-conjugated chromosomal paint probe. Scale bar = 10 μm.

did not not allow us to determine which sort of BM cell might give rise to the labeled epithelial cells in the recipient mice or whether irradiating the animals affected what we observed.

CD45 is expressed in hematopoietic cells and their derivatives [22] including muscle satellite cells [23]. As expected, in the *CD45/Cre-Z/EG* mice, CD45+ cells (such as lymphocytes [Fig. 2D–2F]) and the derivatives of CD45+ cells (such as tissue resident macrophages, Kupfer cells, and microglia [data not shown]) were GFP-positive. Most, but not all, white cells in the blood that could be stained with an anti-CD45 antibody were also GFP-positive.

To determine the rate at which CD45+ cells contribute to the uterine epithelium and the extent of this contribution, we studied female *CD45/Cre-Z/EG* animals at different ages. The number of uterine epithelial cells produced from CD45+ precursors seemed to increase with time and correlate with the number of estrous cycles through which the animals have passed.

During pregnancy, endometrial surface of the rodent uterus is approximately 25 times larger than that of a nonpregnant animal, and this change happens in a very short time. We wondered whether CD45+ cells might contribute to this increase and were surprised to find that in a pregnant *CD45/Cre-Z/EG* mouse, the vast majority (82%) of uterine epithelial cells were also GFP+ (Fig. 4G, 4H). Our observations indicate that CD45+ progenitors maybe the source of most of the new epithelial cells in the pregnant uterus.

Stem cells residing in the uterus were thought to be responsible for the expansion of epithelial cells that accompanies pregnancy [24]. The nature of these stem cells, whether they are replenished, and how replenishment might occur have been a matter of speculation, but a population of "label-retaining" putative stem cells (LRCs) has recently been observed in the uterus [25, 26]. Chan reported that these LRCs are frequently localized near vessels in the mouse endometrium [26]. Since our results show that CD45+ cells give rise to epithelial cells, we suggest that circulating CD45+ cells provide a renewable pool of epithelial precursors in the uterus. The fact that Chan et al. [24] did not detect CD45 in LRCs suggests that endometrial stem cells turn the marker off after they select their fates.

Circulating hematopoietic stem or progenitor cells might enter the stroma and, when they are needed, migrate toward the lumen, where they could serve to regenerate the epithelium. Alternatively, hematopoietic cells could colonize the stromal layer during fetal life and reside there from birth onwards, entering the epithelium on demand. CD45 was not thought to be produced by cells other than hematopoietic stem cells and their progeny [27], but recent work suggests that it may be made transiently by oligodendrocyte precursors during development

[28], and several groups have demonstrated that lung epithelial cells might derive from hematopoietic stem cells in injury models [29–31]. Uterine epithelial progenitors might also transiently express CD45 and then turn it off before they differentiate. Were this the case, their progeny would be GFP+ in the double-transgenic mice that we generated, but given the lack of GFP expression in the uterine epithelium during early postnatal development and during the first several estrous cycles, it seems unlikely that CD45 is activated in resident epithelial progenitors. Alternatively, if the BAC-based expression of Cre recombinase "leaks" briefly when the epithelial population expands, the cells could turn green. Since all of CD45's introns and long 5′ and 3′ flanking sequences are present in the BAC that we used (described in Materials and Methods), and since several founder animals gave similar results to those reported above, we feel that leakiness is unlikely to have been a problem. Instead, we prefer the hypothesis that circulating CD45+ BM cells are responsible for the phenomena that we observed. The fact that GFP-tagged bone marrow cells transplanted into adult *C57BL/6J* mice generate patches of GFP+ uterine epithelium supports this hypothesis.

We also observed GFP+ and GFP mRNA-positive uterine epithelial cells from animals studied 8–12 months after they underwent irradiation and transplantation with green bone marrow, suggesting that the colonization of the uterus by CD45-expressing cells and their conversion into uterine epithelium can take place after development is completed. Although whole-body irradiation prior to BM transplantation affects fertility and changes the length/number of estrus cycles in mice, uterine function seems to remain quite intact, and turnover of the epithelium does not stop [16]. This appears to be true in humans too; in fact, women who have received myeloablative doses of radiation can become pregnant and carry their fetus to term [32].

If BM progenitor cells do in fact contribute to the uterine epithelium, it is possible that alterations in these cells might result in clinical problems. For example, extramedullary hematopoiesis in the endometrium, although rare, is known to occur [33] and could be caused by CD45+ cells there. Furthermore, we agree with Gargett [8] that endometriosis might be caused by misplaced endometrial stem/progenitor cells, specifically CD45+ derivatives. Du and Taylor suggested in their recent work that bone marrow-derived cells contribute to the endometrium in a mouse model of endometriosis [10]. This chronic, painful condition results when endometrium-like tissue grows on the uterus, ovaries, fallopian tubes, uterine ligaments, abdominal lining, or lower part of the large intestine. In addition, such tissue has been seen in the axillary glands, lung, retina, sciatic nerve, skin, and even brain.

Like the endometrium, these ectopic growths respond to hormones; they grow, swell with blood, and degenerate in a cyclic manner. Since their breakdown products have no way to exit the body, however, they cause severe menstrual, abdominal, and lower back pain, and—in up to 40% of women suffering from it—scarring and infertility. Endometriosis is thought to have a genetic component; it is associated with autoimmune diseases, and it can be induced in rhesus monkeys by treatment with dioxin [34]. We feel that regardless of the abnormality (genetic, immunological, or hormonal) that drives the process, changes in CD45+ BM-derived cells could cause them to colonize sites other than the uterine lining and to differentiate and proliferate once they are there. If this is the case, one wonders whether the cells are conditioned in the endometrium and subsequently escape and take up residence in other, nearby tissues [35]. Alternatively, stem cells may occasionally make inappropriate fate choices in tissues (e.g., lung or brain) where they migrate via the blood. The fact that endometriosis has been reported in males might seem to lend support to the second of these suggestions; however, it appears that in some cases the growths may arise in the prostatic utricle, a uterine remnant found in men [36].

Clearly, it would be interesting to know whether CD45+ cells are important for regenerating tissues other than the endometrium and what cues are used to attract them into any given organ and to drive their differentiation. The *CD45/Cre-Z/EG* mouse strain may serve as a useful model for such studies.

Acknowledgments

This study was supported by the NIH intramural research program (National Institute of Dental and Craniofacial Research, National Institute of Mental Health, and National Institute of Neurological Disorders and Stroke). We thank Riccardo Dreyfuss for his help with photography. A.B. and M.J.B. contributed equally to this work.

Disclosure of Potential Conflicts of Interest

The authors indicate no potential conflicts of interest.

References

1 Coan PM, Ferguson-Smith AC, Burton GJ. Developmental dynamics of the definitive mouse placenta assessed by stereology. Biol Reprod 2004; 70:1806–1813.
2 Fuxe K, Nilsson O. The mouse uterine surface epithelium during the estrous cycle. Anat Rec 1963;145:541–548.
3 Tanaka M, Kyo S, Kanaya T et al. Evidence of the monoclonal composition of human endometrial epithelial glands and mosaic pattern of clonal distribution in luminal epithelium. Am J Pathol 2003; 163:295–301.
4 Harris RG, Herzog EL, Bruscia EM et al. Lack of a fusion requirement for development of bone marrow-derived epithelia. Science 2004;305: 90–93.
5 Krause DS, Theise ND, Collector MI et al. Multi-organ, multi-lineage engraftment by a single bone marrow-derived stem cell. Cell 2001;105: 369–377.
6 Mezey E, Chandross KJ, Harta G et al. Turning blood into brain: Cells bearing neuronal antigens generated in vivo from bone marrow. Science 2000;290:1779–1782.
7 Okamoto R, Yajima T, Yamazaki M et al. Damaged epithelia regenerated by bone marrow-derived cells in the human gastrointestinal tract. Nat Med 2002;8:1011–1017.
8 Gargett CE. Identification and characterisation of human endometrial stem/progenitor cells. Aust N Z J Obstet Gynaecol 2006;46:250–253.
9 Taylor HS. Endometrial cells derived from donor stem cells in bone marrow transplant recipients. JAMA 2004;292:81–85.
10 Du H, Taylor HS. Contribution of bone marrow derived stem cells to endometrium and endometriosis. STEM CELLS 2007;25:2082–2086.
11 Lynch L, Golden-Mason L, Eogan M et al. Cells with haematopoietic stem cell phenotype in adult human endometrium: Relevance to infertility? Hum Reprod 2007;22:919–926.
12 Okabe M, Ikawa M, Kominami K et al. 'Green mice' as a source of ubiquitous green cells. FEBS Lett 1997;407:313–319.
13 Novak A, Guo C, Yang W et al. Z/EG, a double reporter mouse line that expresses enhanced green fluorescent protein upon Cre-mediated excision. Genesis 2000;28:147–155.
14 Yu D, Ellis HM, Lee EC et al. An efficient recombination system for chromosome engineering in Escherichia coli. Proc Natl Acad Sci U S A 2000;97:5978–5983.
15 Toth ZE, Shahar T, Leker R et al. Sensitive detection of GFP utilizing tyramide signal amplification to overcome gene silencing. Exp Cell Res 2007;313:1943–1950.
16 Parkes AS. On the occurrence of the oestrus cycle after X-ray steriliza-

tion. Part I. Irradiation of mice at three weeks old. Proc R Soc Lond 1926;100:172–199.
17 Walter I, Klein M, Handler J et al. Lectin binding patterns of uterine glands in mares with chronic endometrial degeneration. Am J Vet Res 2001;62:840–845.
18 Tabibzadeh S. Proliferative activity of lymphoid cells in human endometrium throughout the menstrual cycle. J Clin Endocrinol Metab 1990; 70:437–443.
19 Allen E. The oestrous cycle in the mouse. Am J Anat 1922;30:297–371.
20 Evans GS, Gibson DF, Roberts SA et al. Proliferative changes in the genital tissue of female mice during the oestrous cycle. Cell Tissue Kinet 1990;23:619–635.
21 Dharma SJ, Kholkute SD, Nandedkar TD. Apoptosis in endometrium of mouse during estrous cycle. Indian J Exp Biol 2001;39:218–222.
22 Hermiston ML, Xu Z, Weiss A. CD45: A critical regulator of signaling thresholds in immune cells. Annu Rev Immunol 2003;21:107–137.
23 McKinney-Freeman SL, Jackson KA, Camargo FD et al. Muscle-derived hematopoietic stem cells are hematopoietic in origin. Proc Natl Acad Sci U S A 2002;99:1341–1346.
24 Chan RW, Schwab KE, Gargett CE. Clonogenicity of human endometrial epithelial and stromal cells. Biol Reprod 2004;70:1738–1750.
25 Cervello I, Martinez-Conejero JA, Horcajadas JA et al. Identification, characterization and co-localization of label-retaining cell population in mouse endometrium with typical undifferentiated markers. Hum Reprod 2007;22:45–51.
26 Chan RW, Gargett CE. Identification of label-retaining cells in mouse endometrium. STEM CELLS 2006;24:1529–1538.
27 Trowbridge IS, Thomas ML. CD45: An emerging role as a protein tyrosine phosphatase required for lymphocyte activation and development. Annu Rev Immunol 1994;12:85–116.
28 Nakahara J, Seiwa C, Tan-Takeuchi K et al. Involvement of CD45 in central nervous system myelination. Neurosci Lett 2005;379:116–121.
29 Aliotta JM, Keaney P, Passero M et al. Bone marrow production of lung cells: The impact of G-CSF, cardiotoxin, graded doses of irradiation, and subpopulation phenotype. Exp Hematol 2006;34:230–241.
30 Kotton DN, Ma BY, Cardoso WV et al. Bone marrow-derived cells as progenitors of lung alveolar epithelium. Development 2001;128: 5181–5188.
31 Theise ND, Henegariu O, Grove J et al. Radiation pneumonitis in mice: A severe injury model for pneumocyte engraftment from bone marrow. Exp Hematol 2002;30:1333–1338.
32 Moayeri SE, Westphal LM. Radiation and chemotherapy for cancer: Effects on the uterus. In: Alpin JD, Fazleabas A, Glasser S et al., eds. The Endometrium: Molecular, Cellular and Clinical Perspectives. London: Informa, 2007:42–93.
33 Valeri RM, Ibrahim N, Sheaff MT. Extramedullary hematopoiesis in the endometrium. Int J Gynecol Pathol 2002;21:178–181.
34 Rier SE, Martin DC, Bowman RE et al. Endometriosis in rhesus monkeys (Macaca mulatta) following chronic exposure to 2,3,7,8-tetrachlorodibenzo-p-dioxin. Fundam Appl Toxicol 1993;21:433–441.
35 Starzinski-Powitz A, Zeitvogel A, Schreiner A et al. [Endometriosis–a stem cell disease?]. Zentralbl Gynakol 2003;125:235–238.
36 Martin JD Jr, Hauck AE. Endometriosis in the male. Am Surg 1985;51: 426–430.

Differentiation of human bone marrow-derived cells into buccal epithelial cells in vivo: a molecular analytical study

Simon D Tran, Stanley R Pillemer, Amalia Dutra, A John Barrett, Michael J Brownstein, Sharon Key, Evgenia Pak, Rose Anne Leakan, Albert Kingman, Kenneth M Yamada, Bruce J Baum, Eva Mezey

Summary

Background Adult bone marrow-derived (BMD) cells could be used to repair damaged organs and tissues, but the intrinsic plasticity of these cells has been questioned by results of in-vitro studies suggesting that such cells might fuse with other cells giving the appearance of differentiation. We aimed to determine whether fusion events are important in vivo.

Methods To test whether BMD cells can colonise an epithelial tissue and differentiate there without fusion, we did in-situ hybridisation with Y and X chromosome probes labelled with 35-sulphur or digoxigenin, or labelled fluorescently. We did immunohistochemistry with anticytokeratin 13 along with fluorescence in-situ hybridisation to identify Y-chromosome positive buccal epithelial cells in cheek scrapings obtained from five females who had received either a bone-marrow transplant or an allogeneic mobilised peripheral-blood progenitor-cell transplant (enriched in CD34+ cells) from male donors.

Findings When examined 4–6 years after male-to-female marrow-cell transplantation, all female recipients had Y-chromosome-positive buccal cells (0·8–12·7%). In more than 9700 cells studied, we detected only one XXXY-positive cell (0·01%) and one XXY cell (0·01%), both of which could have arisen when an XY cell fused with an XX cell.

Interpretation Male BMD cells migrate into the cheek and differentiate into epithelial cells, an occurrence that does not depend on fusion of BMD cells to recipient cells. This finding might be an example of transdifferentiation of haemopoietic or stromal progenitor cells. Plasticity of BMD cells could be useful in regenerative medicine.

Lancet 2003; **361:** 1084–88

National Institute of Dental and Craniofacial Research, Gene Therapy and Therapeutics Branch (S D Tran DMD, S R Pillemer MD, R A Leakan RN, B J Baum DMD); **Craniofacial Developmental Biology and Regeneration Branch** (K M Yamada MD); **Biostatistics Core** (A Kingman PhD); **National Human Genome Research Institute, Cytogenetic Core** (A Dutra PhD, E Pak MD); **National Heart Lung and Blood Institute, Hematology Branch** (A J Barrett MD); **National Institute of Mental Health, Laboratory of Genetics** (M J Brownstein MD); **National Institute of Neurological Disorders and Stroke, Basic Neuroscience Programme** (S Key BS, E Mezey MD); **National Institutes of Health, Bethesda, MD, USA**

Correspondence to: Dr Simon Tran, National Institutes of Health/NIDCR, 10 Center Drive, Room 1N113, MSC 1190, Bethesda MD 20892-1190, USA (e-mail: stran@dir.nidcr.nih.gov)

Introduction

Evidence from studies in recipients of bone-marrow transplants shows that bone marrow-derived (BMD) cells can differentiate into cells other than blood. This occurrence is of importance because such cells could be used to regenerate organs after disease or trauma.[1–5] However, the plasticity of BMD cells has been questioned by results of studies suggesting that stem cells might fuse with other cells and give the appearance of differentiation.[6,7] Furthermore, caution is needed in interpretation of data purporting to show that non-haemopoietic cells are derived from donor BMD cells.[8–10] Tissues, especially when affected by graft-versus-host disease (GVHD), might contain infiltrating donor haemopoietic or lymphoid cells. In histological sections, non-haemopoietic tissue cells might be confounded with haemopoietic cells because of cell overlap (attributable to the thickness of the sections) or loss of haemopoietic lineage-specific markers.

We aimed to establish whether BMD cells differentiate into cells of another tissue lineage, and to assess whether this event is attributable to fusion. To avoid contamination of our samples by haemopoietic inflammatory cells, we did our studies on healthy transplant recipients without oral GVHD, several years after bone-marrow transplantation.

Methods

Patients

Bone-marrow stem-cell transplant recipients residing within the USA, who each had received an allogeneic transplant from a male sibling donor through protocols from the National Heart, Lung, and Blood Institute, were invited to participate in the study. All those who agreed to participate were well, in haematological remission, with full donor lymphohaemopoietic engraftment and no active oral GVHD. The transplants these patients had received consisted of at least 3×10^6 CD34+ cells/kg and a total of 1×10^7–3×10^8 CD3+ lymphocytes/kg given within 3 months of the stem cells. After the transplant, all patients received only irradiated blood products. We also recruited healthy volunteers as controls. This study was approved by the Institutional Review Board of the National Institute of Dental and Craniofacial Research (NIDCR), National Institutes of Health (NIH).

Procedures

We obtained cheek scrapings from all women to look for Y-chromosome-positive buccal epithelial cells. Study of buccal cells has the advantage of providing a non-invasively obtained, pure single-cell population of mature nucleated cells with a characteristic morphology and phenotype (anticytokeratin 13+). Cheek scrapings spread on glass slides were independently examined by two pathologists. We also gathered blood samples from these women.

	Recipient				
	1	2	3	4	5
Characteristic					
Age at transplant (years)	31	36	37	56	40
Reason for transplant	CML	MDS	AML	CML	CML
Type of transplant	BM	PBPC	PBPC	PBPC	BM
Chemotherapy/radiotherapy	Yes/Yes	Yes/Yes	Yes/Yes	Yes/No	Yes/Yes
Time from transplant to buccal samples (years)	5·2	4·5	4	4·2	6
History of pregnancy	Never	Never	1 daughter, 2 miscarriages	2 daughters, 1 son	2 daughters, 1 son, 1 miscarriage
History of blood transfusion	Never	Yes	Yes	Never	Never

AML=acute myelogenous leukaemia. BM=bone marrow transplant; CML=chronic myelogenous leukaemia; MDS=myelodysplastic syndrome; PBPC=peripheral-blood progenitor-cell allogeneic transplant (granulocyte-colony stimulating factor mobilised).

Table 1: **Characteristics of female transplant-recipients**

In situ hybridisation and immunohistochemistry

We did in-situ hybridisation as described,[3] with a digoxigenin-labelled riboprobe complementary to nucleotides 729–2053 of the Y-chromosomal marker DYZ1 (accession number X06228).[11] We prepared the template from human genomic DNA and produced a 1·3 kb riboprobe by T7 polymerase and either 35-sulphur-labelled or digoxigenin-labelled UTP. After hybridisation, the digoxigenin-labelled probe was visualised with a peroxidase-conjugated antidigoxigenin antibody (Roche, Indianapolis, IN, USA), followed by tyramide signal amplification with the FITC-tyramide plus reagent (TSA System, Perkin-Elmer, Boston, MA, USA). For autoradiographic detection of the Y chromosome, we used the method described elsewhere.[12] For double-labelling of cytokeratin and Y chromosome, buccal cells were fixed in a

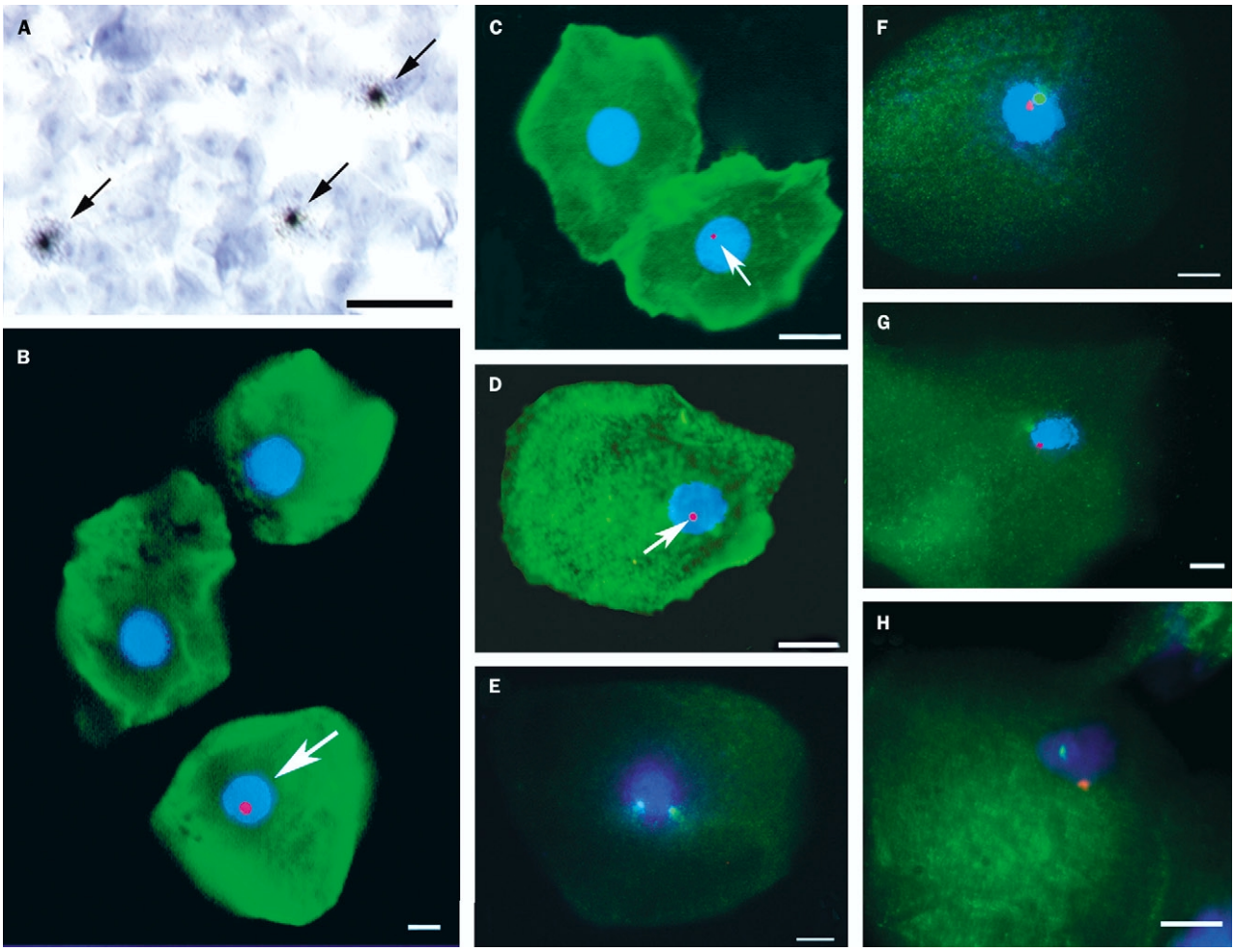

Figure 1: **In-situ hybridisation and immunohistochemistry in human buccal cells**

(A) Y-chromosome autoradiography on a smear of buccal cells from recipient 3 is shown in brightfield. The arrows point to the autoradiographic grains (black dots) above the nuclei of Y-chromosome containing cells. (B, C, D) Buccal cells from recipients 4, 2, and 3, respectively. The cells were first immunostained for cytokeratin 13 (green), then hybridised in situ with a human Y-chromosome riboprobe (red fluorescent dots shown by the arrows). The nuclei of the cells are stained blue with DAPI. (E, F, G, H) FISH with X-chromosome and Y-chromosome probes. Individual buccal cells are shown from a healthy female control (E), a healthy male control (F), recipient 3 (G), and recipient 1 (H). The green fluorescent dot in the nucleus represents the X probe and the red dot the Y probe hybridised to the appropriate regions of the sex chromosomes. The nuclei of the cells are stained blue with DAPI. The cytoplasm of cells in panels E–H are autofluorescent. The scale bar represents 10 μm in all panels, except 100 μm for panel A. An RGB version of this figure is available at http://image.thelancet.com/extras/02art10351webfigure.pdf.

	Recipient				
	1	2	3	4	5
S^{35}-radiolabelled Y probe					
Number of nuclei examined	3907	747	2658	966	1285
Number of Y-positive nuclei (%)	194 (5·0%)	13 (1·7%)	293 (11·0%)	13 (1·4%)	125 (9·7%)
FISH with X and Y probes					
Number of nuclei examined	1824	1779	1315	2853	1977
Number of Y-positive nuclei (%)	206 (11·3%)	42 (2·4%)	167 (12·7%)	23 (0·8%)	136 (6·9%)

Table 2: **Detection of Y-chromosome-positive cells in cheek scrapings from female transplant-recipients**

picric acid-aldehyde fixative for 15 min at room temperature, and we did immunocytochemistry first with a cytokeratin 13 antibody at a 1:1000 dilution (132M, BioGenex, San Ramon, CA, USA) followed by tyramide signal amplification (Perkin-Elmer). After immunostaining, we processed the slides for fluorescence in-situ hybridisation (FISH) and assessed them with a Leitz or Zeiss fluorescence microscope.[12]

FISH with X and Y chromosome probes

We placed buccal cells in Carnoy's fixative for 15 min at room temperature. A mixture of two centromeric probes—CEP X (alpha satellite DNA) labelled with spectrum green and CEP Y (satellite III DNA) labelled with spectrum orange (Vysis, Downers Grove, IL, USA)—was denatured at 74°C for 5 min and hybridised overnight at 37°C in a humidified chamber. We did post-hybridisation washes at 45°C in 50% formamide and 2×SSC for 15 min and 1×SSC for 15 min. We counterstained slides with 250 mg/L DAPI (4′,6-diamidino-2-phenylindole dihydrochloride) in mounting medium (Vectashield, Vector Laboratories, Burlingame, CA, USA).

Genotyping

DNA was extracted from the cheek cells and donor blood samples with PureGene reagents (Gentra, Minneapolis, MN, USA). We obtained markers from Research Genetics, amplified with TaqGold (Applied Biosystems, Foster City, CA, USA) in accordance with the manufacturer's protocol, and analysed them on an ABI 3100 capillary sequencer. Allele sizing was done with Genotyper software (version 2.5, Applied Biosystems).

Role of the funding source

The sponsor of the study had no role in study design, data collection, data analysis, data interpretation, or writing of the report.

Results

Five females, 4–6 years after receiving a transplant from an HLA-identical brother for leukaemia, agreed to participate (table 1). Recipients 1, 2, 3, and 5 underwent a myeloablative conditioning regimen consisting of 4 days of total body irradiation (13·6 Gy) and 2 days of cyclophosphamide 60 mg/kg. Recipient 4 received the same dose of cyclophosphamide plus fludarabine 125 mg/m^2 over 5 days. GVHD developed in four: acute grade 1 in recipient 1; chronic liver GVHD in recipient 3; extensive chronic GVHD in recipient 4; and acute grade 4 in recipient 5. Only recipient 3 had active GVHD at the time of testing.

Cheek scrapings from these five women consisted of discrete epithelial cells without contamination by mononuclear cells or macrophages. The S^{35}-radiolabelled Y-chromosome probe hybridised in situ with 97·7% of the 5354 buccal cells obtained from four healthy male volunteers and none of the buccal cells obtained from ten female volunteers (500–1000 buccal cells were counted per female volunteer). Therefore, the sensitivity of the S^{35}-radiolabelled Y-chromosomal probe was 97·7% (95% CI 96·9–98·5) and the specificity was 100% (99·8–100).

In the five transplant-recipients, frequency of Y-positive nuclei in buccal epithelial cells ranged between 1·4% and 11% (mean 5·76; 95% CI 0·24–11·28; figure 1 A, and table 2). Presence of male cells was confirmed in recipient 5 by DNA genotyping of the donor's blood, the patient's buccal epithelial cells, and her son's blood cells, with Y-chromosomal markers 289, 388, 390, and 391; none of these markers gave products when female control DNA was used as template (figure 2). On the other hand, patient 5's donor's blood and her own cheek samples always had the same genotypes. The alleles for the above markers were 148, 126, 211, and 287, respectively. However, patient 5's son had alleles 148, 126, 215, and 283. This finding shows that the patient's Y-chromosome-positive cheek cells could not have arisen by microchimerism,[13] and the fact that the genotypes of the patient's buccal cells and donor's blood cells are identical strongly suggests that the former arose from the graft. We detected no Y-positive amplicons in untransplanted female control samples, and no Y-positive buccal cells in ten healthy control women who have sons. Combined staining for the Y-chromosome by FISH and by histochemistry for anticytokeratin 13 confirmed the presence of male buccal epithelial cells (figure 1 B, C, and D). Cryopreserved bone-marrow samples, available from the donors of recipients 1 and 5, were negative for cytokeratin 13, indicating no epithelial cells were present in the bone-marrow transplant specimen.

We next used X and Y chromosomal FISH to search for cell fusion. As controls we analysed 3693 female and 1855 male buccal cells obtained from two female and two male healthy volunteers (figure 1 E and F). The sensitivity of detection of the Y-chromosome probe was 98·6% (95% CI 96·8–100) and the specificity was 100% (99·9–100). The X-chromosome probe hybridised to two X chromosomes in 99·0% of 3693 female control buccal cells (sensitivity 99·0%; 95% CI 97·8–100). We analysed between 1300 and 2800 cells per female transplant-recipient. The overall frequency of Y-positive nuclei in cheek scrapings of female transplant-recipients varied from 0·8 to 12·7% (mean 6·81; 95% CI 0·28–13·34; figure 1 G and H, and table 2). Of 9748 cells examined from the five transplant-recipients, one cell (0·01%) was XXXY and one was XXY (0·01%).

Discussion

These results indicate that cells derived from marrow or granulocyte-colony stimulating factor mobilised blood cells migrate into the cheek and differentiate into epithelial cells. These results might therefore represent transdifferentiation of haemopoietic or stromal stem cells, or transplantation of a hypothetical epithelial progenitor cell.

Four criteria have been proposed to show plasticity of adult stem cells.[14,15] The first criterion states that cells grafted should be clonal. Our study did not fulfil this requirement because small populations of blood-derived or

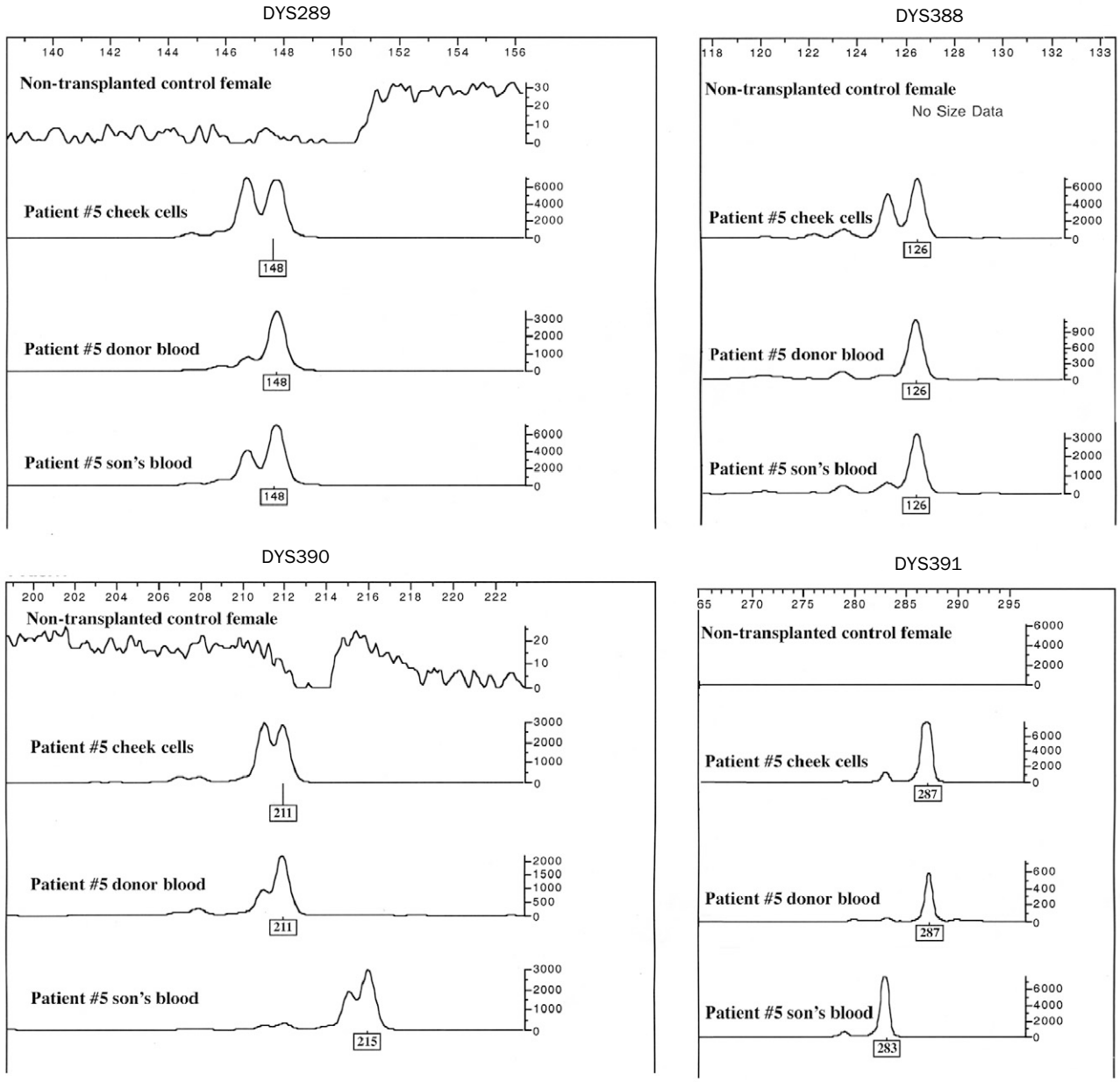

Figure 2: **DNA analysis**

Blood from a non-transplanted female control, buccal cells from recipient 5, her donor's blood, and her son's blood, were analysed with four sets of Y-chromosome markers. X axis shows product length in bases, and Y axis shows signal strength.

marrow-derived cells other than the CD34+ selected haemopoietic progenitors could have been transplanted. Therefore, the Y-chromosome positive buccal epithelial cells seen in our female transplant recipients could have originated from male donor haemopoietic stem cells, mesenchymal stem cells, or epithelial stem cells. Results of many reports suggest that both haemopoietic stem cells and mesenchymal stem cells can differentiate into epithelial cells.[5,16,17] However, results of some reports argue against the possibility that haemopoietic stem cells can differentiate into non-haemopoietic tissues.[18] Epithelial stem cells have not been described in the bone marrow, nor was cytokeratin 13 detected in the bone marrow of two male donors tested.

The second criterion for plasticity of adult stem cells requires that transplanted cells be prospectively isolated and transplanted without in-vitro culturing. Our study meets this criterion, since the sorted CD34+ fractions were transplanted without any in-vitro culturing.

The third criterion, which requires that the phenotype of the transdifferentiated cells be shown anatomically, molecularly, and functionally, is met: Y-chromosome positive buccal cells were morphologically distinguishable as buccal epithelial cells, and they expressed cytokeratin 13, a recognised epithelial marker located in the superficial buccal-cell layer of the cheek. Although the function of the differentiated cells could not be verified, the buccal mucosa of these individuals seemed unremarkable and intact.

The fourth criterion is to report the frequency of the transdifferentiation event. We noted that 0·8–12·7% of the nuclei studied were Y-chromosome positive. This high frequency of engraftment might be related to the rapid turnover rate (every 7–10 days) of the oral mucosa. Buccal epithelial cells obtained from cheek scrapings were dispersed on a glass slide. Thus, we could not establish whether the high frequency of transdifferentiation seen was attributable to clonal expansion of epithelial stem cells or

frequent transdifferentiation of individual graft-derived cells. To answer this question, one would need to obtain incisional biopsy specimens of the oral mucosa. Overall, this study meets three of the four proposed criteria for adult stem-cell plasticity.

A second important finding is that fusion between donor and recipient cells was a rare occurrence in vivo, just as it is in vitro.[6,7] With one or two exceptions, the greater than 9700 differentiated buccal cells seen in this study showed no evidence of fusion. Thus, differentiation was not attributable to host and donor cell fusion. Although the clinical implications of adult bone-marrow cell plasticity are still unclear, focusing on non-fusion mechanisms by which cell fate is ascertained in man is likely to benefit the areas of cell therapy and regenerative medicine.

Contributors

S D Tran, S R Pillemer, B J Baum, and E Mezey wrote the protocol for this clinical study. They were assisted in haematological consultation and management by A J Barrett, in cell biology consultation by K M Yamada, and in statistical consultation by A Kingman. A Dutra and E Pak provided the FISH X/Y results. E Mezey and S Key provided the in-situ hybridisation and immunohistochemistry results. M J Brownstein provided the DNA genotyping results. R A Leakan managed and coordinated the patients enrolled in this study. All authors were involved in the preparation of this report and agreed to its final version.

Conflict of interest statement

None declared.

Acknowledgments

We thank Marc R Kok, Antony Voutetakis, and Jonathan M Bryant (NIDCR), Ildiko Szalayova (NINDS), and Carol Markey (NIMH) for technical assistance; Robert S Redman (Veterans' Affairs Medical Center), Ana P Cotrim (NIDCR), Andrea Abatti and David Kleiner (NCI) for their expert advice in cytology; Peiman Hematti, Sheila Phang, and Adeira Greene (NHLBI) for patients' recruitment; Vidya Sankar (NIDCR) for her expertise in oral medicine; and James S Hodges (University of Minnesota) for statistical advice.

This research was supported solely by US government funding, through allocations of the Department of Health and Human Services to the National Institutes of Health Intramural Research Programmes for the following Institutes: National Institute of Dental and Craniofacial Research, National Human Genome Research Institute, National Heart Lung and Blood Institute, National Institute of Mental Health, and the National Institute of Neurological Disorders and Stroke. The views expressed in this manuscript are those of the authors, and are not to be construed as representing official viewpoints of the US government.

References

1 Horwitz EM, Gordon PL, Koo WK, et al. Isolated allogeneic bone marrow-derived mesenchymal cells engraft and stimulate growth in children with osteogenesis imperfecta: implications for cell therapy of bone. *Proc Natl Acad Sci USA* 2002; **99:** 8932–37.

2 Horwitz EM, Prockop DJ, Fitzpatrick LA, et al. Transplantability and therapeutic effects of bone marrow-derived mesenchymal cells in children with osteogenesis imperfecta. *Nat Med* 1999; **5:** 309–13.

3 Mezey E, Chandross KJ, Harta G, Maki RA, McKercher SR. Turning blood into brain: cells bearing neuronal antigens generated in vivo from bone marrow. *Science* 2000; **290:** 1779–82.

4 Orlic D, Kajstura J, Chimenti S, et al. Bone marrow cells regenerate infarcted myocardium. *Nature* 2001; **410:** 701–05.

5 Jiang Y, Jahagirdar BN, Reinhardt RL, et al. Pluripotency of mesenchymal stem cells derived from adult marrow. *Nature* 2002; **418:** 41–49.

6 Terada N, Hamazaki T, Oka M, et al. Bone marrow cells adopt the phenotype of other cells by spontaneous cell fusion. *Nature* 2002; **416:** 542–45.

7 Ying QL, Nichols J, Evans EP, Smith AG. Changing potency by spontaneous fusion. *Nature* 2002; **416:** 545–48.

8 Abkowitz JL. Can human hematopoietic stem cells become skin, gut, or liver cells? *N Engl J Med* 2002; **346:** 770–72.

9 Brouard M, Barrandon Y. Male cells in female recipients of hematopoietic-cell transplants. *N Engl J Med* 2002; **347:** 218–20.

10 Fogt F, Beyser KH, Poremba C, et al. Recipient-derived hepatocytes in liver transplants: a rare event in sex-mismatched transplants. *Hepatology* 2002; **36:** 173–76.

11 Nakahori Y, Mitani K, Yamada M, Nakagome Y. A human Y-chromosome specific repeated DNA family (DYZ1) consists of a tandem array of pentanucleotides. *Nucl Acids Res* 1986; **14:** 7569–80.

12 Laboratory of Cellular and Molecular Recognition, National Institute of Mental Health. Section on Neural Gene Expression. http://intramural.nimh.nih.gov/lcmr/snge/ (accessed Jan 24, 2003).

13 Nelson JL. Microchimerism: incidental byproduct of pregnancy or active participant in human health? *Trends Mol Med* 2002; **8:** 109–13.

14 Anderson DJ, Gage FH, Weissman IL. Can stem cells cross lineage boundaries? *Nat Med* 2001; **7:** 393–95.

15 Wells WA. Is transdifferentiation in trouble? *J Cell Biol* 2002; **157:** 15–18.

16 Clarke D, Frisen J. Differentiation potential of adult stem cells. *Curr Opin Genet Dev* 2001; **11:** 575–80.

17 Verfaillie CM. Adult stem cells: assessing the case for pluripotency. *Trends Cell Biol* 2002; **12:** 502–08.

18 Wagers AJ, Sherwood RI, Christensen JL, Weissman IL. Little evidence for developmental plasticity of adult hematopoietic stem cells. *Science* 2002; **297:** 2256–59.

ASBMT
American Society for Blood and Marrow Transplantation

Microchimerism in Salivary Glands after Blood- and Marrow-Derived Stem Cell Transplantation

Simon D. Tran,[1] Robert S. Redman,[2] A. John Barrett,[3] Steven Z. Pavletic,[4] Sharon Key,[5] Younan Liu,[1] Ashley Carpenter,[4] Hieu M. Nguyen,[1] Yoshinori Sumita,[1,6] Bruce J. Baum,[5] Stanley R. Pillemer,[7] Eva Mezey[5]

Blood- and marrow-derived stem cells (BMDSCs) provide disease-ameliorating effects for cardiovascular and autoimmune diseases. Microchimerism from donor BMDSCs has been reported in several recipient tissues. We hypothesized that this finding suggests a potential use of BMDSCs in the treatment of salivary dysfunctions. We investigated the presence of Y chromosome-positive cells in salivary gland biopsies of 5 females who had received a marrow or blood stem cell transplant from male donors. One to 16 years after transplantation, all recipients exhibited scattered Y chromosome-positive cells in the acini, ducts, and stroma of their salivary glands (mean of 1.01%). Potentially, these cells can be markers of transplantation tolerance, contribute to neoplastic epithelial tissues, or engraft at sites of injury. In addition, transplantation of BMDSCs could be used for treatment of Sjögren's syndrome and salivary glands damaged by therapeutic irradiation for cancers of the head and neck.

Biol Blood Marrow Transplant 17: 429-433 (2011) © 2011 American Society for Blood and Marrow Transplantation

KEY WORDS: Salivary glands, Microchimerism, Bone marrow stem cells, Blood stem cells, Transplantation

INTRODUCTION

Recent reviews suggest transplantation of blood- and marrow-derived stem cells (BMDSCs) provide disease-ameliorating effects for cardiovascular and autoimmune diseases [1,2]. Microchimerism arising from BMDSCs and organ transplantations has been reported in a variety of recipient tissues (heart, liver, kidney, gastrointestinal [GI] tract, lung, endometrium, buccal epithelium) [3-12]. We hypothesized that this phenomenon has implications for the potential use of BMDSCs in the treatment of salivary dysfunctions (eg, Sjögren's syndrome and salivary glands damaged by irradiation) for which no suitable conventional treatments are currently available. Here we report, for the first time, evidence of microchimerism resulting from BMDSCs in salivary glands of recipients.

METHODS

This study was approved by the institutional review boards at McGill University, National Institutes of Health, and Veterans Affairs Medical Center. Labial salivary gland tissue was collected from 5 female subjects who had previously received either an allogeneic bone marrow or peripheral blood stem cell transplant from their brothers (Table 1). This gender-mismatched strategy allowed us to detect donor Y chromosomes in cells of the female-recipient salivary tissue. At the time of salivary gland biopsy, all patients were well, in hematologic remission, with full donor lymphohematopoietic engraftment. We chose to biopsy minor labial salivary glands because they share abundant similarities with the major salivary glands (ie, parotid, submandibular, and sublingual glands), they are routinely used to obtain information about all salivary tissue in patients with Sjögren's syndrome and they can be obtained with little discomfort and morbidity compared to biopsies from the major glands [13]. We performed colocalization techniques to genetic and protein markers as we described previously [10]. Using fluorescence microscopy

From the [1]Faculty of Dentistry, McGill University, Montreal, Canada; [2]Oral Pathology Research Laboratory, Department of Veterans Affairs Medical Center, Washington, DC; [3]Stem Cell Allotransplantation Section, Hematology Branch, National Heart, Lung, and Blood Institute, NIH, Bethesda, Maryland; [4]Experimental Transplantation and Immunology Branch, Center for Cancer Research, National Cancer Institute, NIH, Bethesda, Maryland; [5]National Institute of Dental and Craniofacial Research, NIH, Bethesda, Maryland; [6]Department of Regenerative Oral Surgery, Nagasaki University, Japan; and [7]MacroGenics Inc., Rockville, Maryland.

Financial disclosure: See Acknowledgments on page 432.

Correspondence and reprint requests: Simon Tran, DMD, PhD, McGill University, Faculty of Dentistry, 3640 University Street, Room M-43, Montreal, Quebec H3A 2B2, Canada (e-mail: simon.tran@mcgill.ca).

Received August 13, 2010; accepted September 29, 2010

1083-8791/$36.00
doi:10.1016/j.bbmt.2010.09.021

dc_219_11

Table 1. Characteristics of the Female Transplant Recipients

	#1	#2	Recipient #3	#4	#5
Characteristic					
Age at transplant (years)	31	36	37	52	28
Reason for transplant	CML chronic phase	MDS (RAEB)	AML CR1	Aplastic anemia	CML chronic phase
Type of transplant	BM	PBSC	PBSC	PBSC	BM
Conditioning	Cy 120 TBI 13 Gy	Cy 120 TBI 12 Gy	Cy 120 TBI 12 Gy	Cy 120, Flu 125, ATG 120	Cy 120, AraC 500 TBI 5.5 Gy
Time from transplant to salivary gland biopsy	57 months	50 months	40 months	13 months	201 months
History of pregnancy	Never	Never	1 daughter 2 miscarriages	1 daughter 1 son	Never
History of blood transfusion	Never	Yes	Yes	Yes	Yes
GVHD	COP	None	Liver	Skin, oral	Skin, oral
Active at time of biopsy	no	—	no	yes	yes
% of positive male cells in salivary gland	1.09%	0.95%	0.65%	0.92%	1.44%
% of positive male cells in buccal mucosa	11.3%	2.4%	12.7%	n/a	n/a

AML CR1 indicates acute myelogenous leukemia in first complete remission; AraC, Cytarabine 500 mg/m^2; ATG, antithymocyte globulin 120 mg/kg; BM, bone marrow transplant; CML, chronic myelogenous leukemia; COP, cryptogenic organizing pneumonia; Cy, Cyclophosphamide 120 mg/kg; Flu, Fludarabine 125 mg/m^2; MDS (RAEB), myelodysplastic syndrome with excess of blasts; PBSC, peripheral blood stem cell transplant; TBI, total-body irradiation; GVHD, graft-versus-host disease.

on 10-μm-thick frozen salivary tissue sections: (1) cells from the male donors were identified using fluorescence in situ hybridization (FISH) using a human Y chromosome probe conjugated with digoxigenin and visualized with Tyramide-FITC, and in the same sections, (2) salivary epithelial cells were identified by the presence of epithelial markers (cytokeratins; CK) using fluorescence immunohistochemistry (FIHC). The CK antibodies (BioGenex, San Ramon, CA) stain the salivary gland parenchymal cells while leaving nonepithelial cells (such as endothelial cells, stromal cells, and blood cells) unstained. We further determined whether male donor BMDSCs had fused with female recipient cells using FISH with X and Y chromosomal probes (Vysis, Downers Grove, IL). The sensitivity and specificity of the Y and X chromosomal probes used was between 97% and 100% [10]. As negative and positive controls, the DNA probes and antibodies were tested on labial salivary glands of normal healthy male and female volunteers.

RESULTS AND DISCUSSION

One to 16 years after male-to-female BMDSC transplantation, all 5 female recipients had Y chromosome-positive salivary cells (mean of 1.01%, range: 0.65%-1.44%) in the gland parenchymal tissue (Table 1). Our Y chromosome probe used in FISH has a false-positive rate between 0% to 0.2%, and a false-negative rate between 1.5% to 3.1% (ie, we were using a Y chromosome probe that underestimated the true frequency of Y chromosome-positive cells, but was unlikely to overestimate it). These Y chromosome-positive cells expressed CK-8, -9, -13, -18 (markers for salivary cells) (Figure 1A-C). Many of these cells were identified in each of the parenchymal components of the glands, that is, acini and intercalated, striated, and excretory ducts. We also used the following markers to further characterize the phenotypes of the Y chromosome-positive cells (Figure 1D-F): Na^+-K^+-$2Cl^-$ cotransporter (NKCC1, a marker for acini; donated by R.J. Turner), claudin-1 (a tight junction protein in salivary ducts; Zymed, San Francisco, CA), and von Willebrand factor IV (a marker for endothelial cells; Novocastra, Newcastle, UK). Our salivary gland specimens had few foci of lymphocytic infiltration. However, in situations where these lymphocytic infiltrations were detected by H&E staining in proximity to salivary cells, we immunostained an additional slide combining a hematopoietic lineage (CD45) marker, an epithelial marker (NKCC1) and the Y chromosome probe. This modification of the technique described earlier [14] using different fluorescent colors, showed scattered Y^+/$CD45^+$ cells in the stroma, but these were exceedingly rare in the epithelial structures (Figure 1G). Therefore, we conclude that the vast majority of the Y chromosome-positive cells in the intercalated ducts and acini of our specimens were of epithelial phenotype. In more than 1000 cells examined per patient, we detected no XXXY-positive cells (no cell fusion events). We previously reported in our studies of buccal epithelial cells in a female recipient that DNA genotyping had excluded the possibility that all observed Y chromosome-positive cells were transferred in utero by her son during pregnancy (a process referred to as fetal microchimerism) [10].

Our results indicate that a small percentage (about 1%) of cells derived from marrow or granulocyte-colony stimulating factor (G-CSF) mobilized blood cells can migrate into the salivary glands. Higher rates of microchimerism seem to occur in tissues with high cell turnover rates and/or that are sites of frequent injuries, for example, buccal (oral) epithelial cells (~10%) [10], endometrial glands [12,15], skin (~20%) [16], and liver (25%; an organ exposed to

dc_219_11

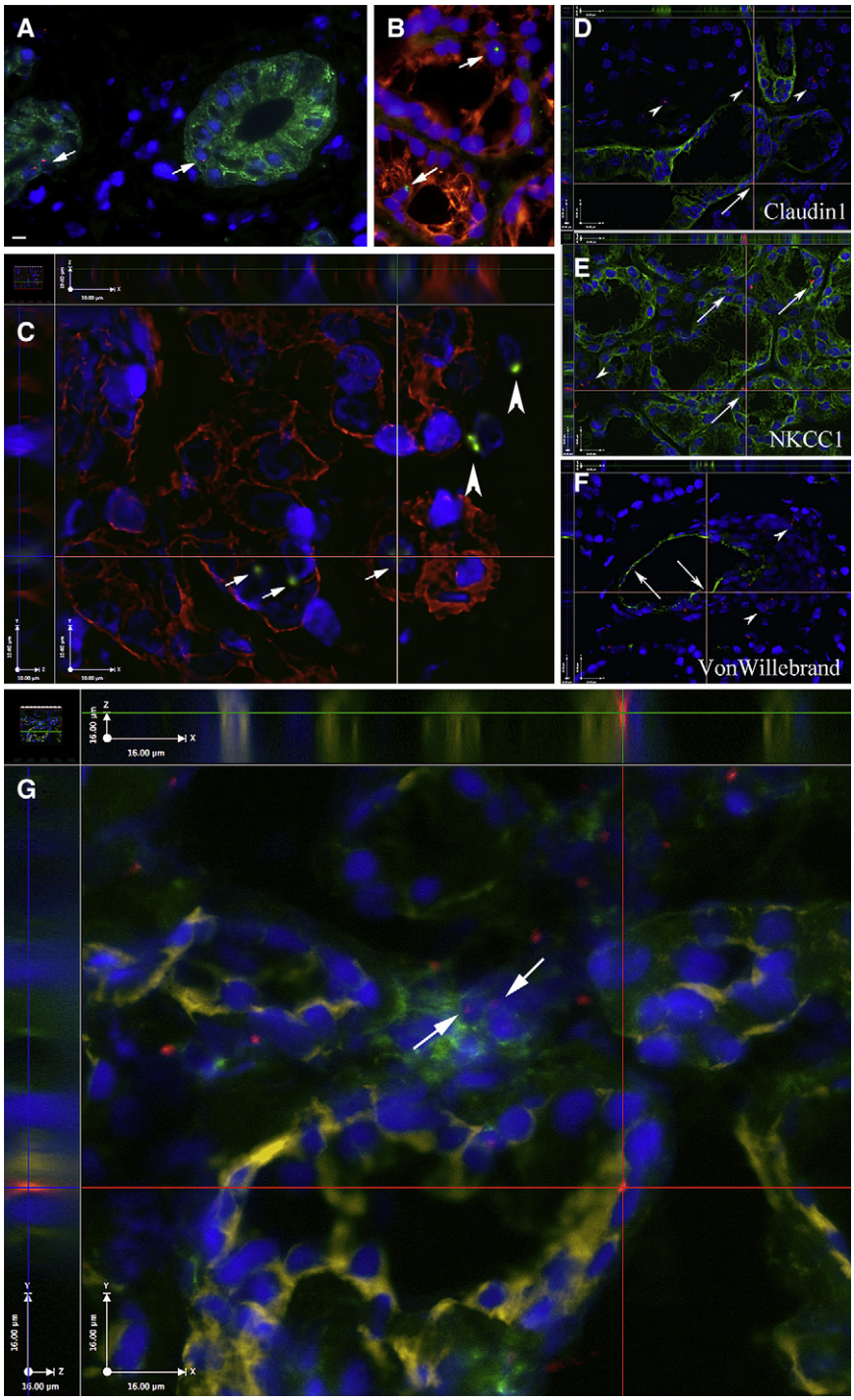

Figure 1. Labial salivary gland biopsies from female recipients of male BMDSCs. (A) Salivary cells are stained with the epithelial marker cytokeratin 13 (green). Y chromosome-positive cells (nuclei with red fluorescent dots, shown by the arrows) reside in an intercalated duct (left) and a striated duct (right). (B, C) Cytokeratins 8, 18, 19 are shown in red. Y-positive cells (green) reside in epithelial cells (arrows) and stromal cells (arrowheads). Panel C shows 3 planes restored from a Z-stack of sections taken at 0.5-μm intervals. The y and z dimensions are shown on the two sides of the x plane image and demonstrate the presence of the Y chromosome (green) in the same plane with the cytokeratins (red) and the nuclei (DAPI, blue). Further characterization of the phenotypes of Y chromosome-positive cells using additional cell markers (shown in green) such as: (D) claudin-1 (a tight junction protein in salivary ducts), (E) Na^+-K^+-$2Cl^-$ cotransporter (NKCC1; a marker for acini), and (F) von Willebrand factor IV (a marker for endothelial cells) indicate several epithelial and endothelial cells that are Y chromosome-positive (arrows); other Y-positive cells (arrowheads) in or near the wall of this blood vessel may be smooth muscle cells, fibroblasts, etc. (G) CD45 (a marker of the white blood cell lineage) in green (FITC); NKCC1 in yellow (CY5) and the Y chromosome in red (Alexa-594). All nuclei are blue (DAPI). The two arrows point to 2 CD45-positive cells in proximity to salivary cells. The intersection of the 2 red lines in this panel indicates a salivary epithelial cell (NKCC1, yellow) of male donor origin (Y chromosome, red dot). Panels D-G show 3 planes restored from a Z-stack of sections taken at 0.5-μm intervals. Scale bars equal 10 μm (A-C) and 16 μm in D-G.

dc_219_11

frequent chemical injuries) [7]. It is very interesting to compare our previous results on buccal cells to the results presented in this article in the partially overlapping patient population (3 out of the 5 patients were the same in both studies). The comparison clearly shows that tissues with high turnover rates (ie, the buccal epithelium) might need to replace stem cells more frequently during the life-span of the individual than tissues with slow turnover rates (ie, salivary glands). We found almost 10 times more differentiated epithelial cells of donor origin in the oral mucosa than in salivary glands of the same patients (Table 1).

The physiological significance of finding microchimerism in recipients' tissues after donor BMDSCs or organ transplantations is at present unclear. Ayala et al. [17] suggest using donor chimerism as a marker of transplantation tolerance that may help to tailor immunosuppressive treatment. Other groups have suggested that microchimerism might contribute to the development of neoplastic epithelial tissues [18,19]. However, this remains unresolved as there are also data arguing against the possibility that BMDSCs represent a direct source of carcinomas in the recipients [20]. There are reports of better BMDSC donor cell engraftment at sites with injury, such as lung after radiation [6], GI inflammation [21], and skin blistering [16]. Regarding the latter injury, Wagner et al. [16] showed histologic evidence of increased amounts of collagen type VII (C7) at the dermal-epidermal junction of children with recessive dystrophic epidermolysis bullosa, a genetic skin disorder caused by a mutation in the C7 gene. They hypothesized that donor BMDSCs mobilized to the skin secreted C7, which resulted in reduced blistering and increased clinical benefit for their patients. Of particular interest with the findings reported here are specific injuries that occur to the salivary glands, such as from therapeutic radiation for head and neck cancers and autoimmune insults in Sjögren's syndrome. These injuries (either radiation induced or immunologic) might increase donor cell engraftment/microchimerism. A more efficient delivery of BMDSCs into irradiation-damaged salivary glands might be achieved via infusion up the ductal tree [22]. For now, we demonstrate, as a proof-of-concept, that donor cell microchimerism can be identified in human salivary glands.

ACKNOWLEDGMENTS

Roseanne Leakan, Peiman Hematti, David Kleinman, Jane Atkinson, Amalia Dutra, Evgenia Pak, Vidya Sankar, Kathy Kalinyak, and for donating the Na^+-K^+-$2Cl^-$ cotransporter antibody, R. James Turner (NIDCR). This study was supported in part by research funding from the Intramural Research Programs of NCI, NIDCR, and NHLBI, the Canadian Institutes of Health Research, and the Department of Veterans Affairs.

Financial disclosure: The authors declare no competing financial interests.

AUTHORSHIP STATEMENT

S.D.T., A.J.B., S.Z.P., B.J.B., S.R.P., and E.M. designed research; S.D.T., R.S.R., A.J.B., S.Z.P., S.K., Y.L., H.M.N., A.C., Y.S., and E.M. performed or collected data; all the authors analyzed, interpreted data, contributed to the writing of the manuscript; all the authors approved the manuscript.

REFERENCES

1. Burt RK, Loh Y, Pearce W, et al. Clinical applications of blood-derived and marrow-derived stem cells for nonmalignant diseases. *JAMA*. 2008;299:925-936.
2. Tyndall A, Gratwohl A. Adult stem cell transplantation in autoimmune disease. *Curr Opin Hematol*. 2009;16:285-291.
3. Scandling JD, Busque S, Dejbakhsh-Jones S, et al. Tolerance and chimerism after renal and hematopoietic-cell transplantation. *N Engl J Med*. 2008;358:362-368.
4. Alexander SI, Smith N, Hu M, et al. Chimerism and tolerance in a recipient of a deceased-donor liver transplant. *N Engl J Med*. 2008;358:369-374.
5. de Weger RA, Verbrugge I, Bruggink AH, et al. Stem cell-derived cardiomyocytes after bone marrow and heart transplantation. *Bone Marrow Transplant*. 2008;41:563-569.
6. Krause DS. Bone marrow-derived lung epithelial cells. *Proc Am Thorac Soc*. 2008;5:699-702.
7. Gaia S, Cappia S, Smedile A, et al. Epithelial microchimerism: consistent finding in human liver transplants. *J Gastroenterol Hepatol*. 2006;21:1801-1806.
8. Matsumoto T, Okamoto R, Yajima T, et al. Increase of bone marrow-derived secretory lineage epithelial cells during regeneration in the human intestine. *Gastroenterology*. 2005;128:1851-1867.
9. Ishikawa F, Yasukawa M, Yoshida S, et al. Human cord blood- and bone marrow-derived CD34+ cells regenerate gastrointestinal epithelial cells. *FASEB J*. 2004;18:1958-1960.
10. Tran SD, Pillemer SR, Dutra A, et al. Differentiation of human bone marrow-derived cells into buccal epithelial cells in vivo: a molecular analytical study. *Lancet*. 2003;361:1084-1088.
11. Körbling M, Katz RL, Khanna A, et al. Hepatocytes and epithelial cells of donor origin in recipients of peripheral-blood stem cells. *N Engl J Med*. 2002;346:738-746.
12. Ikoma T, Kyo S, Maida Y, et al. Bone marrow-derived cells from male donors can compose endometrial glands in female transplant recipients. *Am J Obstet Gynecol*. 2009;201:608.e1-e8.
13. Fox PC. Simplified biopsy technique for labial minor salivary glands. *Plast Reconstr Surg*. 1985;75:592-593.
14. Tóth ZE, Mezey E. Simultaneous visualization of multiple antigens with tyramide signal amplification using antibodies from the same species. *J Histochem Cytochem*. 2007;55:545-554.
15. Bratincsak A, Brownstein MJ, Cassiani-Ingoni R, et al. CD45-positive blood cells give rise to uterine epithelial cells in mice. *Stem Cells*. 2007;25:2820-2826.
16. Wagner JE, Ishida-Yamamoto A, McGrath JA, et al. Bone marrow transplantation for recessive dystrophic epidermolysis bullosa. *N Engl J Med*. 2010;363:629-639.
17. Ayala R, Grande S, Albizua E, et al. Long-term follow-up of donor chimerism and tolerance after human liver transplantation. *Liver Transpl*. 2009;15:581-591.
18. Dubernard G, Oster M, Chareyre F, et al. Increased fetal cell microchimerism in high grade breast carcinomas occurring during pregnancy. *Int J Cancer*. 2009;124:1054-1059.

dc_219_11

19. Janin A, Murata H, Leboeuf C, et al. Donor-derived oral squamous cell carcinoma after allogeneic bone marrow transplantation. *Blood*. 2009;113:1834-1840.
20. Soldini D, Moreno E, Martin V, Gratwohl A, Marone C, Mazzucchelli L. BM-derived cells randomly contribute to neoplastic and non-neoplastic epithelial tissues at low rates. *Bone Marrow Transplant*. 2008;42:749-755.
21. Matsumoto T, Okamoto R, Yajima T, et al. Increase of bone marrow-derived secretory lineage epithelial cells during regeneration in the human intestine. *Gastroenterology*. 2005;128:1851-1867.
22. Redman RS, Ball WD, Mezey É, Key S. Dispersed donor salivary gland cells are widely distributed in the recipient gland when infused up the ductal tree. *Biotechnol. Histochem*. 2009;84: 253-260.

nature medicine

Bone marrow stromal cells attenuate sepsis via prostaglandin E_2–dependent reprogramming of host macrophages to increase their interleukin-10 production

Krisztián Németh[1,6], Asada Leelahavanichkul[2,6], Peter S T Yuen[2], Balázs Mayer[1], Alissa Parmelee[1], Kent Doi[2], Pamela G Robey[1], Kantima Leelahavanichkul[1], Beverly H Koller[4], Jared M Brown[5], Xuzhen Hu[2], Ivett Jelinek[3], Robert A Star[2,6] & Éva Mezey[1,6]

Sepsis causes over 200,000 deaths yearly in the US; better treatments are urgently needed. Administering bone marrow stromal cells (BMSCs—also known as mesenchymal stem cells) to mice before or shortly after inducing sepsis by cecal ligation and puncture reduced mortality and improved organ function. The beneficial effect of BMSCs was eliminated by macrophage depletion or pretreatment with antibodies specific for interleukin-10 (IL-10) or IL-10 receptor. Monocytes and/or macrophages from septic lungs made more IL-10 when prepared from mice treated with BMSCs versus untreated mice. Lipopolysaccharide (LPS)-stimulated macrophages produced more IL-10 when cultured with BMSCs, but this effect was eliminated if the BMSCs lacked the genes encoding Toll-like receptor 4, myeloid differentiation primary response gene-88, tumor necrosis factor (TNF) receptor-1a or cyclooxygenase-2. Our results suggest that BMSCs (activated by LPS or TNF-α) reprogram macrophages by releasing prostaglandin E_2 that acts on the macrophages through the prostaglandin EP2 and EP4 receptors. Because BMSCs have been successfully given to humans and can easily be cultured and might be used without human leukocyte antigen matching, we suggest that cultured, banked human BMSCs may be effective in treating sepsis in high-risk patient groups.

Sepsis, a serious medical condition that affects 18 million people per year worldwide, is characterized by a generalized inflammatory state caused by infection. Widespread activation of inflammation and coagulation pathways progresses to multiple organ dysfunction, collapse of the circulatory system (septic shock) and death. Because as many people die of sepsis annually as from acute myocardial infarction[1], a new treatment regimen is desperately needed. In the last few years, it has been discovered that BMSCs are potent modulators of immune responses[2–5]. We wondered whether such cells could bring the immune response back into balance, thus attenuating the underlying pathophysiology that eventually leads to severe sepsis, septic shock and death[6,7].

As a model of sepsis, we chose cecal ligation and puncture (CLP), a procedure that has been used for more than two decades[8]. This mouse model closely resembles the human disease: it has a focal origin (cecum), is caused by multiple intestinal organisms, and results in septicemia with release of bacterial toxins into the circulation. With no treatment, the majority of the mice die 24–48 h postoperatively.

RESULTS

BMSC treatment improves survival and organ function after CLP

First, we looked at survival rates after CLP in untreated and BMSC-treated mice. There was a statistically significant ($P < 0.01$) improvement in the survival of mice given 1 million BMSCs intravenously at the time of surgery; 50% of the mice survived until the end of day 4, when all were killed (**Fig. 1a**). The beneficial effect on survival was seen when the cells were injected 24 h before or 1 h after CLP (**Fig. 1a**). In contrast, intravenous injection of isolated skin fibroblasts, whole bone marrow or heat-killed BMSCs did not alter survival (**Fig. 1a**). BMSCs isolated from different strains of mice (C57/BL6, BALB/c or FVB/NJ) all rescued the C57/BL6 mice that we used in our studies (**Fig. 1a**).

Because the lethality in sepsis is associated with organ failure, we examined the pathology and function of major organs often injured in human subjects. Kidney function, as measured by serum creatinine and renal tubular injury scores, was markedly improved in the treated mice (**Fig. 1b**). BMSCs reduced organ damage when they were administered up to 24 h before CLP surgery (**Supplementary Fig. 1**

[1]National Institute of Dental and Craniofacial Research (NIDCR), Craniofacial and Skeletal Diseases Branch, [2]National Institute of Diabetes and Digestive Kidney Diseases (NIDDK), Renal Diagnostics and Therapeutics Unit, [3]National Cancer Institute (NCI), Experimental Immunology Branch, US National Institutes of Health (NIH), 9000 Rockville Pike, Bethesda, Maryland, 20892, USA. [4]Department of Genetics, University of North Carolina, 4341 Medical Biomolecular Research Building, Chapel Hill, North Carolina 27599, USA. [5]Department of Pharmacology and Toxicology, East Carolina University, Greenville, North Carolina 27858, USA. [6]These authors contributed equally to this work. Correspondence should be addressed to E.M. (mezeye@mail.nih.gov).

Received 13 August 2008; accepted 20 November 2008; published online 21 December 2008; corrected after print 6 April 2009; doi:10.1038/nm.1905

online). In the livers, improved glycogen storage was observed in treated mice versus control mice (**Fig. 1c**). Concentrations of liver enzymes (alanine aminotransferase and aspartate aminotransferase) that are released into the circulation upon injury and death of liver cells were significantly decreased in the serum after treatment (**Fig. 1d**), as were serum amylase values, which mirror pancreatic damage (**Fig. 1e**). Similarly, there was a significant decrease in the number of apoptotic (activated caspase-3–positive) and necrotic cells in the spleen (**Fig. 1f**). These results suggest that BMSCs protect infected mice from death and organ damage.

Effect of BMSCs on plasma cytokine concentrations

We hypothesized that BMSCs might alter the immune response to infection; therefore, we studied TNF-α and IL-6, proinflammatory cytokines that have a central role in sepsis[1]. Twenty-four hours after injection of BMSCs, there was a significant reduction in serum TNF-α and IL-6 concentrations in treated versus untreated mice (**Fig. 1g**). Serum concentrations of interferon-γ were unaltered by BMSCs (**Supplementary Fig. 2** online), but IL-10 abundance started to rise 3 h after the cells were given, almost doubled by the sixth hour and was still elevated 12 h afterward. (**Fig. 1h**).

To learn where injected BMSCs go and how long they remain detectable, we prelabeled the cells with carboxyfluorescein diacetate succinimidyl ester (CFDA-SE) fluorescent tracking dye and visualized them 1–24 h later. We found BMSCs in the blood up to 1 h after intravenous injections and saw many cells in the lung parenchyma, with some in the spleen and kidney. The labeled cells in the lung seemed to be surrounded by macrophages (**Fig. 2a–c**). What attracts these cells to each other remains to be determined. The number of cells in the lung gradually decreased over time; few were visible 24 h after they were administered (data not shown).

Alterations in vascular permeability are central to the pathogenesis of sepsis-induced organ injury, and the benefits of BMSC treatment in reducing vascular permeability have already been reported[9–12]. We studied this in the peritoneum, lung, liver and kidney by measuring Evans blue dye leakage 24 h after CLP. CLP surgery significantly increased peritoneal, liver and renal vascular permeability ($P < 0.01$, $P < 0.01$ and $P < 0.001$, respectively); all three were significantly ($P < 0.05$, $P < 0.05$ and $P < 0.05$, respectively) decreased in mice treated with BMSCs (**Supplementary Fig. 3** online).

Involvement of immune cell subtypes in the effect of BMSCs

The observations summarized above suggested that BMSCs might quickly act to reprogram a specific population of cells involved in mediating the immune response. To test this hypothesis, we examined the effects of BMSCs in mice that genetically lack mature T and B cells (*Rag2*$^{-/-}$)[13] or are depleted of natural killer (NK) cells with a rabbit ganglio-*N*-tetraosylceramide (asialo GM1)-specific antibody, resulting in nearly complete elimination of NK cell activity[14,15]. The effect of BMSC injections on the survival of the mice was still present in both of these models, suggesting that lymphocyte populations of T, B and NK cells do not mediate the effect of BMSCs in the CLP model (**Supplementary Fig. 4** online). Because BMSCs were found in close proximity to lung macrophages, we asked whether monocytes and/or macrophages are needed for the beneficial effects of the BMSCs. To deplete monocytes and macrophages, we administered clodronate-filled liposomes to the mice[16] before we performed the CLP procedure and then treated them with BMSCs. BMSCs were no longer effective in mice lacking monocytes and macrophages (**Fig. 2d**).

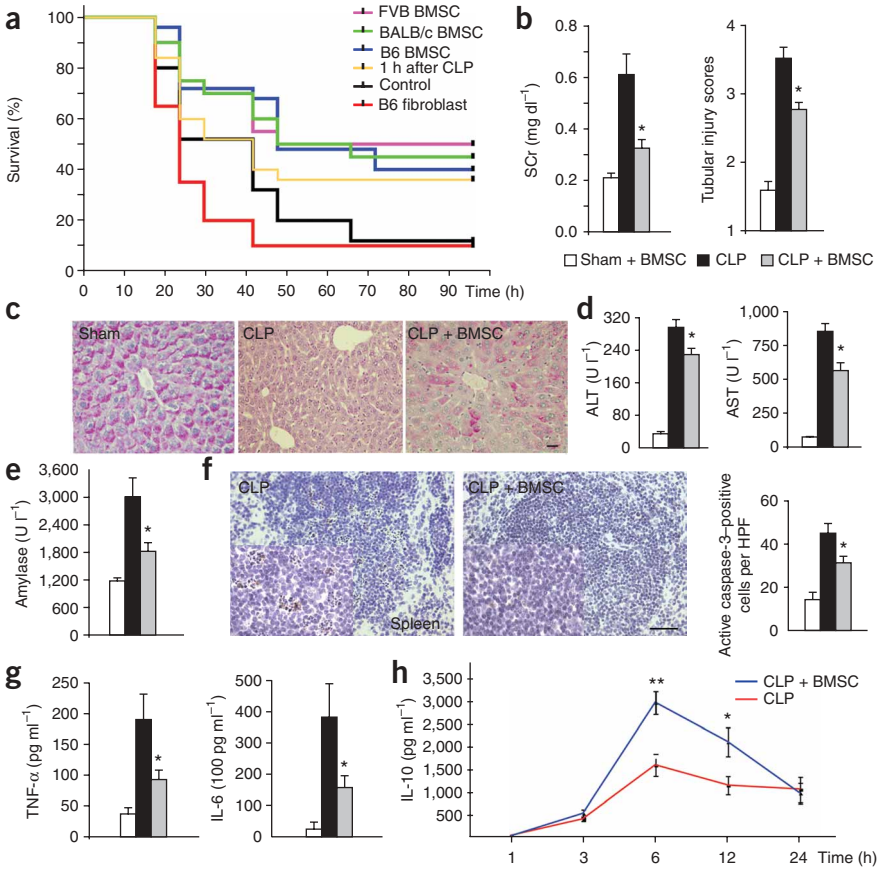

Figure 1 Effect of intravenous injection of BMSCs on the course of sepsis after CLP. (**a**) Survival curves of mice after CLP and a variety of treatments using BMSCs from C57/BL6, FVB/NJ and BALB/c mice, as well as C57/BL6-derived fibroblasts. (**b**) BMSC treatment effects on kidney function, as reflected by serum concentration of creatinine (SCr). The number of mice in all measurements is as follows: sham, $n = 5$; CLP, $n = 13$; CLP + BMSC, $n = 14$. Tubular injury scores are shown at right. (**c**) Intense PAS staining of hepatocytes is shown after sham operation and BMSC treatment. No staining can be seen in CLP. After treatment (CLP + BMSC), the red staining by PAS in hepatocytes indicates partial glycogen storage capacity. Scale bar, 20 μm. (**d**) Alanine aminotransferase (ALT) and aspartate aminotransferase (AST) concentrations in the liver after sham and BMSC, CLP or CLP and BMSC treatment. (**e**) Serum amylase concentrations after sham and BMSC, CLP or CLP and BMSC treatment. (**f**) DAB staining of caspase-3 cells in untreated spleen sections and BMSC-treated spleen sections. A quantitative comparison between the numbers of apoptotic splenic cells in treated versus untreated mice (right) shows a significant decrease with BMSC treatment. Scale bar, 100 μm. (**g**) Serum TNF-α and IL-6 concentrations after sham and BMSC, CLP or CLP and BMSC treatment. (**h**) Serum IL-10 concentrations at 3, 6 and 12 h after CLP. $n = 8$–11 at each time point. Error bars represent means ± s.e.m.; $^*P < 0.05$; $^{**}P < 0.01$.

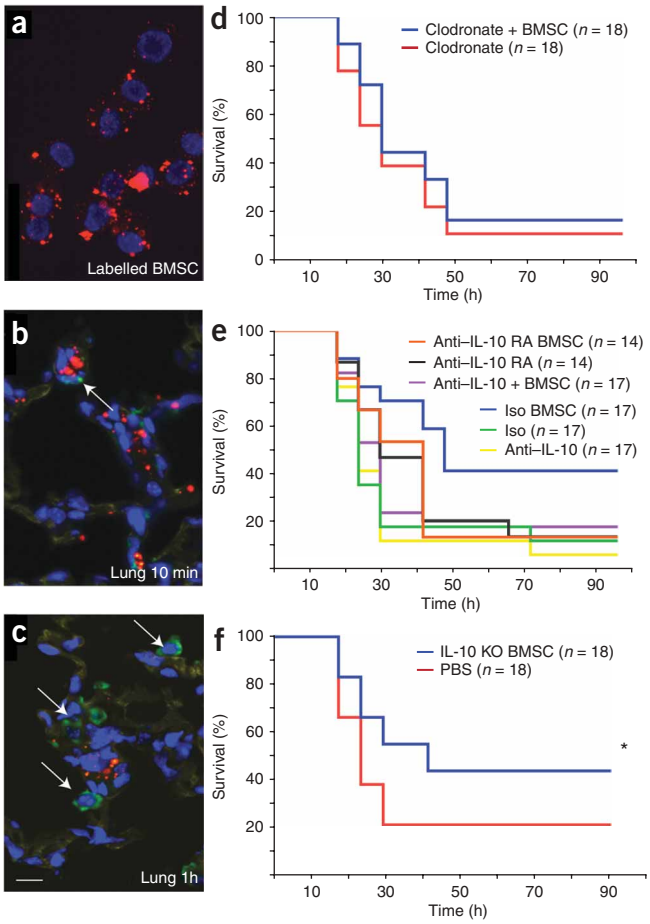

Figure 2 Fate of injected BMSCs and effect of BMSC treatment on survival of normal and immune cell–depleted mice. (**a**–**c**) Immunohistochemical staining showing that BMSCs prelabeled with Q-dot (red punctate staining; **a**) travel to the lung (**b**) and take up residence in close proximity to macrophages (**c**). The latter cells were immunostained with an antibody to Iba1 (ionized calcium-binding adaptor molecule-1, a specific marker of the macrophage lineage[47]) and visualized with Alexa-Fluor-488 conjugated to a secondary antibody (green). Scale bar, 10 μm. (**d**–**f**) Summary of the effectiveness of BMSC treatment of mice genetically lacking or depleted of certain subsets of immune cells or soluble mediators. Survival curves show survival percentage of macrophage-depleted mice with or without BMSC treatment (**d**), survival percentage of BMSC-treated CLP mice and untreated mice after neutralizing IL-10 or blocking the IL-10 receptor (**e**) and survival percentage of after treatment with BMSCs derived from *Il10*$^{-/-}$ septic mice (**f**). $^{*}P < 0.05$.

Macrophage-derived IL-10 is key for the effect of BMSCs

Because IL-10 serum levels were increased in CLP mice that were treated with BMSCs as compared to sham controls, we asked whether IL-10 might be important for the actions of BMSCs. To test this hypothesis, we treated mice with an antibody to IL-10 or an antibody to the IL-10 receptor before CLP. In both of these groups, the BMSC injections were ineffective (**Fig. 2e**), suggesting that IL-10 is a major mediator of the effect. To see whether the injected BMSCs might be producing an essential pool of IL-10, we used BMSCs isolated from *Il10*$^{-/-}$ mice. These BMSCs were still effective in improving the survival of mice after CLP (**Fig. 2f**), suggesting that the source of the IL-10 is an endogenous population of cells. Large amounts of IL-10 are known to be produced by subsets of T cells and monocytes and macrophages[17]. As mentioned earlier (**Fig. 2d**), monocyte and consequent macrophage depletion eliminated the beneficial effect of BMSCs; thus, we focused on monocytes and macrophages as the probable source of IL-10 required for survival after CLP. BMSC treatment resulted in a significant decrease in the number of circulating monocytes and an increase in the number of circulating neutrophils (**Fig. 3a**,**b**). Because tissue macrophages are derived from circulating monocytes, we speculated that the decrease in monocyte numbers might be due to their tissue invasion. We found a significant increase in the number of lung monocytes and macrophages in CLP versus unoperated mice by immunocytochemistry (data not shown). This increase was completely eliminated when circulating monocytes were depleted with clodronate-filled liposomes (**Fig. 3c**). To confirm the histological findings, we used FACS to determine the relative percentages of immune cells isolated from the lungs of four treated versus four untreated septic mice. There was an increase in monocytes but not lymphoid cells in the lung (**Fig. 4a**,**b**). Monocytes and macrophages (CD11b^{+}) were isolated from the lungs of BMSC-treated and untreated mice[18], placed in culture and restimulated with LPS. Three and five hours after LPS stimulation *ex vivo*, monocytes and macrophages from BMSC-treated septic mice produced and released significantly more IL-10 than did untreated mice (**Fig. 4c**). To determine whether the change in IL-10 production was due to direct interaction between BMSCs and monocytes and macrophages, we cultured the two cell populations together or placed them in a transwell system in which two cell populations were separated from one another by a permeable membrane. In addition, we put monocytes and macrophages in BMSC-conditioned medium. When the

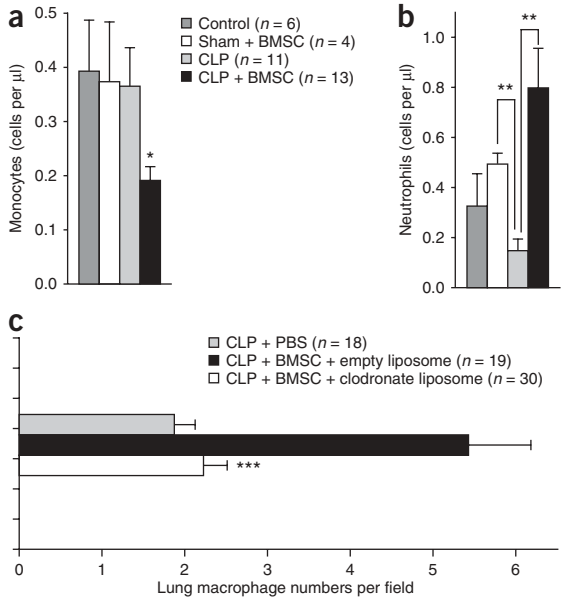

Figure 3 Effect of BMSC treatment on leukocyte trafficking. (**a**,**b**) The average number of circulating monocytes (**a**) and the number of circulating neutrophils (**b**) after BMSC treatment. The cell counts are the average of data from five mice per group, 24 h after the induction of CLP. (**c**) The average number of macrophages isolated from lungs of CLP mice with no treatment, with BMSC treatment and BMSC treatment after depletion of circulating monocytes using clodronate. The numbers of macrophages are per random microscope visual field. Five mice were studied in each group. The numbers in parentheses are the total number of fields in which cells were counted. Error bars represent means ± s.e.m. $^{**}P < 0.01$; $^{***}P < 0.001$.

macrophages were in direct contact with BMSCs (**Fig. 4d**), they produced significantly ($P < 0.001$) more IL-10 in response to LPS stimulation than when they were cultured in transwell plates without direct contact with the BMSCs or exposed to BMSC-conditioned medium. We also used intracellular cytokine staining by FACS to compare the number of IL-10–producing monocytes and macrophages isolated from treated versus untreated septic mice and found a significantly higher number of IL-10–producing monocytes and macrophages in the treated mice (**Fig. 4e**).

Because IL-10 has been reported to inhibit the rolling, adhesion[19] and transepithelial migration[20–22] of neutrophils, we examined the white cell counts in the circulation of treated and untreated CLP mice and found a significant increase in the number of circulating neutrophils in the treated mice (**Fig. 3a**). It is possible that the high circulating neutrophil counts in the BMSC-treated mice could help lower blood bacterial counts (**Fig. 4f**), but further studies are necessary to explore this hypothesis. Neutrophils are also known to migrate into the tissues in septic states, where they can cause oxidative organ damage[23–25], an unwanted side effect of myeloperoxidase, an enzyme that neutrophils use to eliminate bacteria[26]. To see whether a change in myeloperoxidase abundance could contribute to BMSC-related organ protection, we measured the amount of myeloperoxidase in the kidney and liver of septic mice with and without BMSC treatment. We found that the amount of myeloperoxidase was significantly decreased (**Fig. 4g**) in the mice that received BMSC injections, which would be consistent with the lack of neutrophil invasion and the lesser extent of organ damage. The above data suggest that the intravenously injected BMSCs are able to optimally balance circulating and tissue-bound immune cells to maximize bacterial killing in the circulation while minimizing organ damage due to leukocyte invasion.

Molecular basis of the BMSC-macrophage interaction

To understand the molecular basis of the interaction between BMSCs and macrophages, we performed a series of experiments *in vitro* and *in vivo*. Wild-type BMSCs showed NF-κB activation 30 min after LPS stimulation (**Fig. 5a**). In a number of cell types, NF-κB has been shown to induce prostaglandin production and release through a pathway involving cyclooxygenase-2 (COX2; refs. 26–29). BMSCs have been shown to produce prostaglandin E_2 and possibly affect other immune cells via EP1–EP4 receptors[30,31]. We found a significant increase in the expression and activity of COX2 (which produces the substrate for prostaglandin synthase enzymes) in BMSCs 3 h and 5 h after LPS stimulation (**Fig. 5b,c**), but when the BMSCs were treated with an antibody to TNF-α or collected from *Tlr4*$^{-/-}$ mice, the COX2 expression did not change (**Fig. 5d**). This suggested that prostaglandin E_2

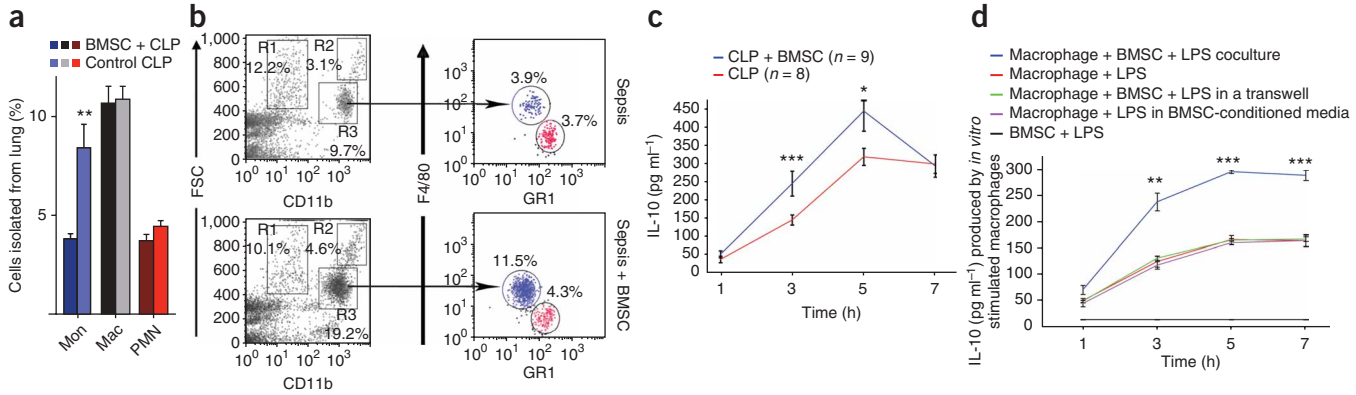

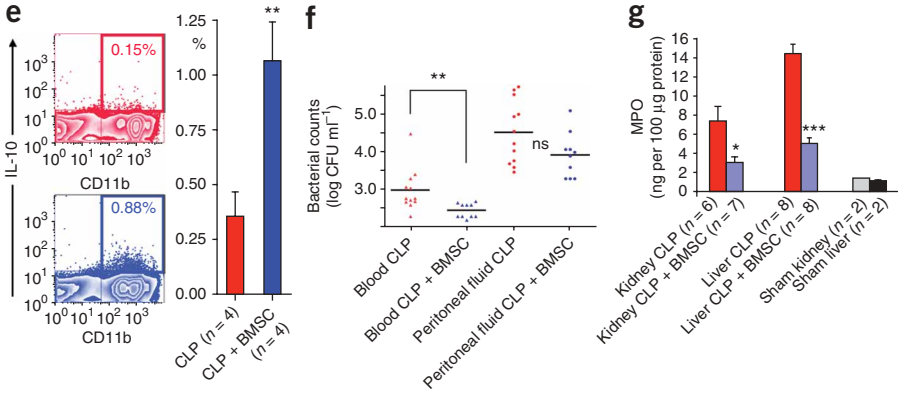

Figure 4 Characterization of control and stimulated mononuclear cells in CLP mice *in vivo* and *in vitro*. (**a**) The distribution of monocytes (Mon), macrophages (Mac) and polymorphonuclear cells (PMN) among cells isolated from septic lungs. Error bars represent means ± s.e.m. (**b**) FACS plots of lung mononuclear cells. The cells were first gated on forward scatter (FSC) and CD11b. The R1 group (high FSC, dim CD11b) represents resident macrophages. R2 (high FSC and bright CD11b) represents a group of myeloid cells. R3 (medium FSC and bright CD11b) is a mixed population of monocytes and PMN cells when it is further gated on a monocyte-lineage marker (F4/80) and a PMN marker (GR1). The FACS is a representative example of the four mice shown on the bar graph in **a**. Blue color indicates monocytes and red indicates polymorphonuclear cells in both **a** and **b** expressed as percentage of total number of cells analyzed. (**c**) Quantification of IL-10 secretion after *ex vivo* LPS treatment of lung macrophages. Six hours after the induction of CLP, lung macrophages were isolated from mice with or without BMSC treatment (four mice per group), cultured and treated *ex vivo* with LPS. IL-10 production of these isolated macrophages is shown 3 and 5 h after LPS stimulation. (**d**) To test whether the increased IL-10 production could be due to a BMSC-macrophage interaction, macrophages from bone marrow were cocultured *in vitro* with BMSCs and stimulated with LPS. IL-10 production of macrophages cocultured with BMSCs is shown compared to macrophages that had no contact with BMSCs at 1, 3, 5 and 7 h after LPS stimulation. (**e**) Lungs of four BMSC-treated and four untreated mice were used for a FACS experiment with CD11b and an intracellular marker for IL-10. The number of IL-10 producing monocytes and macrophages after the treatment is shown. (**f**) Bacterial counts in the peritoneal space and in the circulation in 12 untreated (red) and 10 BMSC treated (blue) mice. (**g**) Myeloperoxidase (MPO) abundance in the kidney and the liver after BMSC treatment. Error bars represent means ± s.e.m. $^*P < 0.05$, $^{**}P < 0.01$ and $^{***}P < 0.001$.

dc_219_11

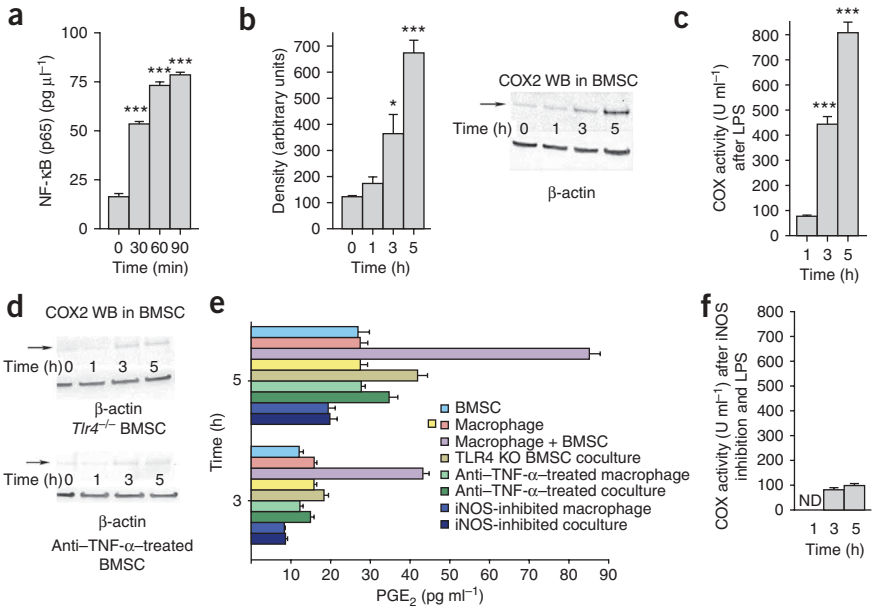

Figure 5 Studies of molecular alterations underlying the effect of BMSCs on macrophages. (**a**) NF-κB abundance in nuclei isolated from triplicate samples of BMSCs 30, 60 and 90 min after addition of LPS to the culture medium. (**b**) Western blot (WB) analysis of COX2 abundance in LPS-stimulated cocultures. Density measurements of three western blots are quantified in the bar graph. (**c**) The COX2 activity after LPS treatment of cocultures (triplicate samples). (**d**) Western blot analysis of COX2 abundance in *Tlr4*$^{-/-}$ (KO) BMSCs or in cultures treated with antibody to TNF-α (anti–TNFα). (**e**) Prostaglandin E_2 (PGE_2) abundance in macrophage cultures or coculture supernatants in a variety of conditions 3 and 5 h after LPS stimulation. Four samples were run for each condition. (**f**) COX2 enzyme activity after iNOS inhibition and 1, 3 and 5 h after LPS stimulation in triplicate samples. Error bars represent means ± s.e.m. $^{*}P < 0.05$, $^{***}P < .001$.

might indeed be responsible for reprogramming the macrophages. For this reason, we measured the amount of prostaglandin E_2 in the coculture medium and found a significant increase in its concentration after LPS stimulation (**Fig. 5e**). This increase was eliminated if the BMSCs lacked TLR4 or if they were incubated with antibody to TNF-α (**Fig. 5e**). Inducible nitric oxide synthase (iNOS) inhibition resulted in a significant reduction of COX2 enzyme activity 1 h, 3 h and 5 h after LPS stimulation (**Fig. 5f**). Although IL-10 concentrations in the medium were increased by LPS when BMSCs from *Ptgs1*$^{-/-}$ mice (lacking COX1) were used in the assay or when the cells were treated with a COX1 inhibitor (SC-560), the increased IL-10 release was not seen when *Ptgs2*$^{-/-}$ cells (lacking COX2) were used or a COX2 inhibitor (NS-398) was added (**Fig. 6a**).

To further examine the effect of BMSCs on macrophages, we cultured macrophages with BMSCs, added LPS and measured the IL-10 concentration in the culture medium. Because Toll-like receptor-4 (TLR4) is the receptor to which LPS binds and through which it acts[32], we were not surprised to see that BMSCs from *Tlr4*$^{-/-}$ mice could not increase IL-10 production and secretion in our assay (**Fig. 6a**). Myeloid differentiation primary response gene-88 (MyD88)

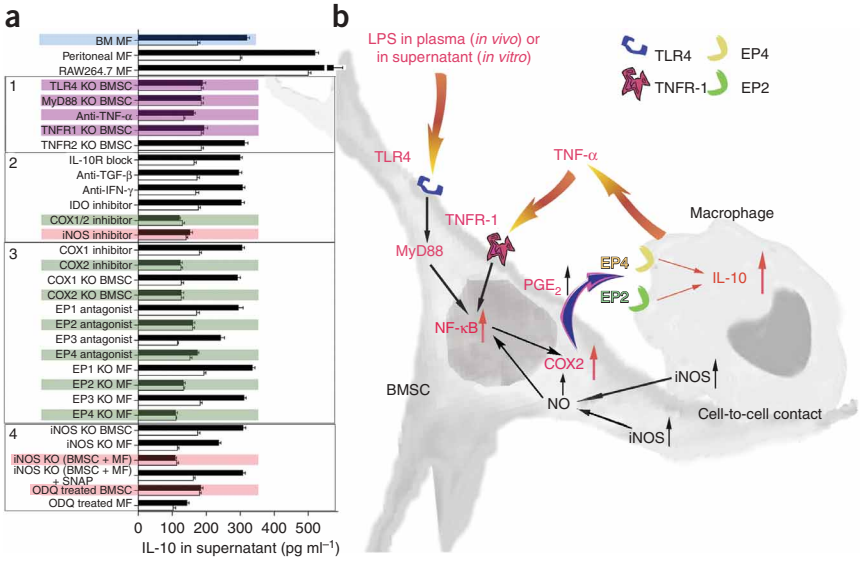

Figure 6 Summary of studies of the molecular pathways involved in the interaction between BMSC and macrophages. (**a**) IL-10 concentration changes in supernatants of cocultures in a variety of treatment conditions after LPS stimulation. Colored graphs (except for the blue color that labels the bone marrow macrophages as the source of all consecutive experiments) show treatments that eliminate the effect of BMSCs on macrophages. Black graphs show IL-10 levels after LPS stimulation, whereas open graphs show the control (nonstimulated) values. The experiments where the conditions eliminated the effect are colored. Purple color shows the effect of septic environment, green color shows agents and cellular compartments related to the PGE2 pathway and pink color shows agents related to the nitric oxide pathway. Three separate kinds of macrophages (bone marrow macrophages; peritoneal macrophages and the RAW264.7 cell line) were examined initially. Because they behaved identically in the assay, we used bone marrow derived macrophages (BM MF) for the rest of the experiments. In the box labeled 1, the effect of septic environment on the BMSCs is studied in BMSCs from TLR4-, MyD88-, TNFR1- and TNFR2- deficient mice, or antibody to TNF-α was used to neutralize the effect of TNF. The box labeled with 2 shows the cytokines and agents that have been implicated in the literature in immunomodulation of T cells by BMSCs, including COX1/2 and iNOS inhibitors. The box labeled 3 shows studies of the COX2 pathway, including the prostaglandin receptors EP1–EP4. Finally, in the box labeled with 4, we show studies related to nitric oxide. (**b**) A summary of our current hypothesis about the mechanisms that underlie the interactions between BMSCs and macrophages in the CLP sepsis model. Bacterial toxins (for example, LPS) and circulating TNF-α act on the TLR4 and TNFR-1 of the BMSCs, respectively. This results in the translocation of NF-κB into the nucleus. This activation process seems to be nitric oxide dependent. Activated NF-κB induces the production of COX2, resulting in increased production and release of PGE_2. PGE_2 binds to EP2 and EP4 receptors on the macrophage, increasing its IL-10 secretion and reducing inflammation.

is required for activation of nuclear factor-κB (NF-κB) by TLR4, and cells from *Myd88*$^{-/-}$ mice did not stimulate IL-10 secretion either (**Fig. 6a**). Because TNF-α has also been implicated in upregulating NF-κB in BMSCs, and both TNF receptor-1 (TNFR-1) and TNFR-2 have been reported to be present in BMSCs[33], we next tested whether these receptors are involved in the function. We used antibody to TNF-α and BMSCs from *Tnfrsf1a*$^{-/-}$ or *Tnfrsf1b*$^{-/-}$ mice and found that TNF-α and TNFR-1 are also necessary for the activation of BMSCs (**Fig. 6a**). In the absence of TNFR-2, BMSCs still increased IL-10 concentrations in the cocultures (**Fig. 6a**).

Because it seemed that prostaglandin E_2 might mediate the effect of BMSCs on macrophage cytokine production, we asked whether specific EP receptors could be involved in transducing the prostaglandin signal. To answer this question, we used prostaglandin receptor antagonists and macrophages from EP receptor–knockout mice. EP1 and EP3 receptor antagonists had no effect on LPS-induced IL-10 secretion, and neither did substituting *Ptger1*$^{-/-}$ macrophages (lacking the gene encoding prostaglandin E receptor-1) or *Ptger3*$^{-/-}$ macrophages (lacking the gene encoding prostaglandin E receptor-3) for wild-type cells in the assay (**Fig. 6a**). However, both EP2 and EP4 receptor antagonists prevented the increase in IL-10 secretion, as did using *Ptger2*$^{-/-}$ or *Ptger4*$^{-/-}$ macrophages instead of wild-type ones (**Fig. 6a**). TNFR-1 and TLR4 do not seem to be the only elements in the BMSCs required for COX2 induction. Nitric oxide produced in the BMSCs, the macrophages or both may be involved. Using BMSCs from *Nos2*$^{-/-}$ mice with WT macrophages or *Nos2*$^{-/-}$ mice macrophages with WT BMSCs did not eliminate the effect on IL-10 production (**Fig. 6a**). However, when BMSCs and macrophages were both derived from *Nos2*$^{-/-}$ mice (lacking iNOS-2), IL-10 was not induced (**Fig. 6a**). To show that this effect is specifically related to loss of iNOS activity and reduced production of nitric oxide, we added *S*-nitroso-*N*-acetylpenicillamine (SNAP), an external nitric oxide donor, to the system[34]. SNAP fully restored the ability of *Nos2*$^{-/-}$ cells to increase IL-10 production in response to LPS (**Fig. 6a**). To determine whether nitric oxide might act through guanylyl cyclase in the BMSCs, we pretreated these cells with 1*H*-[1,2,4]oxadiazolo[4,3-a]quinoxalin-1-one (ODQ), an irreversible inhibitor of soluble guanylyl cyclase[35] (**Fig. 6a**). The IL-10 increase was eliminated when the BMSCs, but not the macrophages, were treated with ODQ. This suggests that the BMSCs need nitric oxide to achieve the effect on IL-10. Apparently, the nitric oxide can either be produced by the BMSCs themselves or by the macrophages. Thus, on the basis of our *in vitro* studies, we concluded that BMSCs respond to the presence of infectious agents by increasing prostaglandin E_2 synthesis and secretion, and that subsequent activation of prostaglandin E_2 and E_4 receptors on the macrophages results in IL-10 induction. We tested this hypothesis *in vivo*, and, as predicted, BMSCs lacking TNFR1, MyD88 or COX2 all failed to rescue mice subjected to CLP (**Supplementary Fig. 5** online). Cells from *Tlr4*$^{-/-}$ mice had partial efficacy, reflecting the fact that their detection of pathogens is impaired but not absent (**Supplementary Fig. 5**), raising the possibility of the involvement of other TLRs *in vivo*.

DISCUSSION

Our results suggest that an intravenous injection of bone marrow stromal cells can beneficially modulate the response of the host immune system to sepsis and improve survival. BMSCs were first reported to have a potent immunosuppressive effect *in vivo* in humans in 2004, when a young individual with resistant graft-versus-host disease was successfully treated with transplanted haploidentical mesenchymal stem cells[2]. Subsequently, cases of hemorrhagic cystitis and peritonitis were treated with allogeneic mesenchymal stem cells[5]. Thus, in humans and in animals[3,36–39], bone marrow stromal cells seem to be potent immunomodulators, but their mechanism of action has been unclear. BMSCs are known to inhibit T cell proliferation[4] and to modulate B cell function[40]. In the present study, we show that BMSCs can be used to fight sepsis in mice. We suggest that the injected BMSCs interact with circulating and tissue (mostly lung) monocytes and macrophages and reprogram them. Treated monocytes and macrophages produce large amounts of IL-10, and the treatment decreases the amounts of circulating TNF-α and IL-6. This reduces harm caused by unbridled immune responses to the host tissues. The observation that the macrophages isolated from treated septic mice produce significantly higher amounts of IL-10 than those from nontreated mice suggest a temporary reprogramming of monocyte and macrophage function that persists for at least 12 h. The monocyte and macrophage–derived IL-10 seems to prevent neutrophils from migrating into tissues and causing oxidative damage, thus mitigating multiorgan damage. This inhibition of neutrophil migration into tissues also results in a buildup of neutrophils in the blood, allowing for more efficient bacterial clearance. The combination of our *in vitro* and *in vivo* experiments shows that the beneficial effect is likely to be due to an increased release of prostaglandin E_2 from the BMSCs acting on the EP2 and EP4 receptors of the macrophages and stimulating the production and release of IL-10, an anti-inflammatory cytokine (**Fig. 6b**). Simultaneous stimulation of EP2 and EP4 receptor subtypes by prostaglandin E_2 has been shown to promote monocyte-derived dendritic cell maturation[41]. In peritoneal macrophages, prostaglandin E_2 was shown to modulate inflammatory reactions via the EP2 and EP4 receptors[42], and EP2 and EP4 agonists were shown to cause upregulation of zymosan-induced IL-10 production[42]. Because both of these receptors work through cyclic AMP, one wonders why both are necessary for the effect to take place. Why eliminating either the EP2 or the EP4 receptor affects IL-10 induction remains to be determined. The two receptors could increase cyclic AMP levels more when they act in concert than they do alone, or they could have partially nonoverlapping actions that are essential for induction to occur[43]. It is also possible that the receptors form functional heterodimers in macrophages.

Our model is somewhat similar to peritonitis in humans. The mechanism of how BMSCs are beneficial might be universal in infectious diseases, or it might be unique to this model. It is possible that the mechanism described could be harmful in other models or that there are other beneficial mechanisms related to BMSCs in other infectious or noninfectious diseases. Owing to the effectiveness of BMSCs in the CLP model, and because BMSCs have been successfully given to humans[2,44] and can easily be cultured and used without human leukocyte antigen matching, we suggest that cultured, banked human BMSCs should be tested for their ability to prevent sepsis in very high-risk groups.

METHODS

Mice. Mouse care was in full compliance with the US NIH criteria for the care and use of laboratory animals in research and all studies were approved by the Animal Care and Use Committee of the NIDDK and NIDCR, NIH. Aged (42–44 weeks old) male C57BL/6 mice (NIH) had free access to water and chow before and after surgery. In addition, 8–12-week-old males with a variety of genetic manipulations were used as listed in the **Supplementary Methods** online. All reagents used are summarized in **Supplementary Table 1** online.

Polymicrobial cecal ligation and puncture sepsis. We performed CLP as previously described, with some modifications, in C57BL/6 mice[45,46]. We ligated the cecum by silk 4-0 and punctured it twice with a 21-gauge needle,

gently squeezed it to express a small amount of fecal material and then returned it to the central abdominal cavity. In sham-operated mice, we located the cecum but neither ligated nor punctured it. We closed the abdominal incision in two layers with 6-0 nylon sutures. After surgery, we gave 1 ml per 30 g body weight of pre-warmed normal saline. All mice received antibiotic and fluid therapy subcutaneously (a combination of imipenem and cilastatin; 14 mg per kg in 1.5 ml of normal saline at 6 h and 7 mg per kg in 1.5 ml of normal saline at 18 h after surgery). The details of the tissue harvest are described in the **Supplementary Methods**.

Treatment of cecal ligation and puncture mice with bone marrow stromal cells. We injected one million BMSCs in 0.3 ml sterile PBS via the tail vein. We gave untreated control mice 0.3 ml sterile PBS with no cells. There was no difference in organ injury, cytokine abundance, Evans blue dye level or pathology in the sham-operated mice with or without BMSC injection. Details of cell isolation and culture are provided in the **Supplementary Methods**.

Survival studies. We assessed survival after surgery every 6 h within the first 48 h and then every 8 h for 4 d. We began antibiotic injection and fluid resuscitation 6 h after CLP by subcutaneous injection and repeated it every 12 h for 4 d. We killed all mice at the end of the fourth day.

***Ex vivo* studies on isolated lung monocytes and macrophages.** We killed septic mice 6 h after CLP induction with or without intravenous injection of 1 million BMSCs. We removed the lungs, minced them into small pieces and incubated the pieces in RPMI 1640 medium with 1% penicillin-streptomycin and 1% glutamine for 30 min at 37 °C 5% CO_2 in the presence of collagenase type 1 (300 U ml^{-1}) and DNase I (50 U ml^{-1}) (Worthington Biochemicals). After the incubation, we filtered the cell suspension through a 70-μm cell strainer and then washed it with complete RPMI medium. We incubated the resulting cells for 15 min at 4 °C with CD11b magnetic beads and subsequently applied them to MS columns (Miltenyi) for the positive selection of CD11b cells. The cell purity of the $CD11b^+$ cells, as assessed by FACS analysis, was greater than 97%. After washing, we plated the isolated cells in 96-well plates at a concentration of 50,000 cells per well per 200 μl RPMI medium (with 10% FBS, 1% glutamine and 1% penicillin-streptomycin) containing 10 μg ml^{-1} LPS (from *Escherichia coli* O111:B4, Sigma). We incubated cells for 1, 3, 5 and 7 h after stimulation and collected supernatants sequentially from wells dedicated to each time point. For each time point, we used triplicate wells. We collected supernatants in microtubes, spun the tubes down at maximum speed for 10 min to get rid of cell debris, aliquoted the supernatants and froze them at –20 °C until use. We performed ELISA for IL-10 (R&D Systems) on the samples. We made measurements in duplicates from three independent experiments. To determine intracellular amounts of IL-10 produced in lung cells, we prepared single-cell suspensions as described above and plated cells in six-well plates containing 10 μg ml^{-1} LPS and 3 μg ml^{-1} brefeldin A, a Golgi-blocking agent frequently used to prepare samples for intracellular FACS analysis. After 5 h of LPS restimulation, we collected the cells, washed them and performed intracellular IL-10 staining combined with cell surface staining.

Macrophage–bone marrow stromal cells coculture experiments. First, we plated macrophages in 96-well plates at a concentration of 40,000 cells per 200 μl. After 1 h, we removed the supernatants and added either 40,000 BMSCs in fresh medium or fresh medium alone to the wells. As a control, we plated BMSCs without macrophages. After an overnight incubation, we added LPS to the cocultures to reach a final concentration of 1 μg ml^{-1}. We collected supernatants 1, 3, 5 and 7 h after the stimulation and performed ELISA (R&D Systems) on the samples to detect the released IL-10. For the transwell or conditioned medium experiments, we either added BMSCs on the insert membrane of the transwell system (HTS Transwell 0.4-μm pore size polycarbonate membrane, from Corning Incorporated) or added conditioned medium diluted 1:1 with fresh medium to the macrophages. For generation of BMSC-conditioned medium, we cultured BMSCs in complete medium. After 3 d, we collected supernatants, spun them down to remove possible cell contamination (500*g* for 10 min) and stored the resulting supernatants at –20 °C until further use. Further details on ELISA and western blotting are in the **Supplementary Methods**.

Blood chemistry, natural killer cell and macrophage depletion and IL-10 neutralization, microvascular permeability, bacterial counts, cell tracking, histology and flow cytometry. Detailed methodology is described in the **Supplementary Methods**.

Statistical analyses. We examined the differences between the groups for statistical significance by Student's *t*-test or analysis of variance with an appropriate correction. We compared survival curves with a log-rank test (Prism 4.0; Graphpad Software). A P value of <0.05 was accepted as statistically significant.

Note: Supplementary information is available on the Nature Medicine website.

ACKNOWLEDGMENTS
We would like to thank M.J. Brownstein for continuous advice and discussions; J. M. Weiss (NCI, NIH) for supplying the *Ifng*$^{-/-}$ mice; A. Keane-Myers (NIAID) for supplying the *Il10*$^{-/-}$ mice; Christophe Cataisson (NCI) for supplying the *Tnfrsf1a*$^{-/-}$ and *Tnfrsf1b*$^{-/-}$ mice; T. Merkel (US Food and Drug Administration) for supplying the *Tlr4*$^{-/-}$ and *Myd88*$^{-/-}$ mice; K. Holmbeck and L. Szabova (NIDCR) for the FVB/NJ mouse cells; and I. Szalayova and S. Key (NIDCR) for their superb technical help. The research was supported by the intramural programs of the NIDCR and the NIDDK, NIH.

AUTHOR CONTRIBUTIONS
K.N., A.L., P.S.T.Y., R.A.S. and E.M. formulated the basic hypotheses and experimental design; K.N., A.L., E.M., P.S.T.Y. and R.A.S. collected and evaluated data on survival and organ injury; K.N. and A.L. performed the *in vivo* experiments; A.L., P.S.T.Y., A.P., K.D., K.L. and X.H. assisted in the *in vivo* experiments and histology; P.G.R. consulted on BMSC biology; K.N. formulated the molecular mechanism hypothesis and designed and performed *in vitro* and *ex vivo* assays; B.H.K. helped to test the involvement of the prostaglandin receptors; J.M.B. and B.M. contributed to testing the involvement of COX2; B.M. performed the measurements for tissue peroxidase; I.J. performed FACS experiments; E.M. wrote the initial manuscript and prepared the figures; all of the authors edited the manuscript.

Published online at http://www.nature.com/naturemedicine/
Reprints and permissions information is available online at http://npg.nature.com/reprintsandpermissions/

1. Ulloa, L. & Tracey, K.J. The "cytokine profile": a code for sepsis. *Trends Mol. Med.* **11**, 56–63 (2005).
2. Le Blanc, K. *et al.* Treatment of severe acute graft-versus-host disease with third party haploidentical mesenchymal stem cells. *Lancet* **363**, 1439–1441 (2004).
3. Noel, D., Djouad, F., Bouffi, C., Mrugala, D. & Jorgensen, C. Multipotent mesenchymal stromal cells and immune tolerance. *Leuk. Lymphoma* **48**, 1283–1289 (2007).
4. Rasmusson, I. Immune modulation by mesenchymal stem cells. *Exp. Cell Res.* **312**, 2169–2179 (2006).
5. Ringden, O. *et al.* Tissue repair using allogeneic mesenchymal stem cells for hemorrhagic cystitis, pneumomediastinum and perforated colon. *Leukemia* **21**, 2271–2276 (2007).
6. Bochud, P.Y. & Calandra, T. Pathogenesis of sepsis: new concepts and implications for future treatment. *BMJ* **326**, 262–266 (2003).
7. Calandra, T. Pathogenesis of septic shock: implications for prevention and treatment. *J. Chemother.* **13** (Spec. No. 1), 173–180 (2001).
8. Hubbard, W.J. *et al.* Cecal ligation and puncture. *Shock* **24** Suppl 1, 52–57 (2005).
9. Togel, F. *et al.* Vasculotropic, paracrine actions of infused mesenchymal stem cells are important to the recovery from acute kidney injury. *Am. J. Physiol. Renal. Physiol.* **292**, F1626–F1635 (2007).
10. Togel, F. *et al.* Administered mesenchymal stem cells protect against ischemic acute renal failure through differentiation-independent mechanisms. *Am. J. Physiol. Renal Physiol.* **289**, F31–F42 (2005).
11. Semedo, P. *et al.* Mesenchymal stem cells ameliorate tissue damages triggered by renal ischemia and reperfusion injury. *Transplant. Proc.* **39**, 421–423 (2007).
12. Lange, C. *et al.* Administered mesenchymal stem cells enhance recovery from ischemia/reperfusion-induced acute renal failure in rats. *Kidney Int.* **68**, 1613–1617 (2005).
13. Shinkai, Y. *et al.* RAG-2–deficient mice lack mature lymphocytes owing to inability to initiate V(D)J rearrangement. *Cell* **68**, 855–867 (1992).
14. Habu, S. *et al.* *In vivo* effects of anti-asialo GM1. I. Reduction of NK activity and enhancement of transplanted tumor growth in nude mice. *J. Immunol.* **127**, 34–38 (1981).
15. Kasai, M. *et al.* *In vivo* effect of anti-asialo GM1 antibody on natural killer activity. *Nature* **291**, 334–335 (1981).
16. van Rooijen, N., Sanders, A. & van den Berg, T.K. Apoptosis of macrophages induced by liposome-mediated intracellular delivery of clodronate and propamidine. *J. Immunol. Methods* **193**, 93–99 (1996).

dc_219_11

17. Moore, K.W., O'Garra, A., de Waal Malefyt, R., Vieira, P. & Mosmann, T.R. Interleukin-10. *Annu. Rev. Immunol.* **11**, 165–190 (1993).
18. Wang, J., Wakeham, J., Harkness, R. & Xing, Z. Macrophages are a significant source of type 1 cytokines during mycobacterial infection. *J. Clin. Invest.* **103**, 1023–1029 (1999).
19. Bonder, C.S. *et al.* P-selectin can support both T_H1 and T_H2 lymphocyte rolling in the intestinal microvasculature. *Am. J. Pathol.* **167**, 1647–1660 (2005).
20. Perretti, M., Szabo, C. & Thiemermann, C. Effect of interleukin-4 and interleukin-10 on leucocyte migration and nitric oxide production in the mouse. *Br. J. Pharmacol.* **116**, 2251–2257 (1995).
21. Cassatella, M.A. The neutrophil: one of the cellular targets of interleukin-10. *Int. J. Clin. Lab. Res.* **28**, 148–161 (1998).
22. Ajuebor, M.N. *et al.* Role of resident peritoneal macrophages and mast cells in chemokine production and neutrophil migration in acute inflammation: evidence for an inhibitory loop involving endogenous IL-10. *J. Immunol.* **162**, 1685–1691 (1999).
23. Hernandez, L.A. *et al.* Role of neutrophils in ischemia-reperfusion–induced microvascular injury. *Am. J. Physiol.* **253**, H699–H703 (1987).
24. Jaeschke, H. & Smith, C.W. Mechanisms of neutrophil-induced parenchymal cell injury. *J. Leukoc. Biol.* **61**, 647–653 (1997).
25. Nussler, A.K., Wittel, U.A., Nussler, N.C. & Beger, H.G. Leukocytes, the Janus cells in inflammatory disease. *Langenbecks Arch. Surg.* **384**, 222–232 (1999).
26. Matthijsen, R.A. *et al.* Myeloperoxidase is critically involved in the induction of organ damage after renal ischemia reperfusion. *Am. J. Pathol.* **171**, 1743–1752 (2007).
27. Jung, Y.J., Isaacs, J.S., Lee, S., Trepel, J. & Neckers, L. IL-1beta-mediated up-regulation of HIF-1α via an NFkappaB/COX-2 pathway identifies HIF-1 as a critical link between inflammation and oncogenesis. *FASEB J.* **17**, 2115–2117 (2003).
28. Nakao, S. *et al.* Tumor necrosis factor α (TNF-α)-induced prostaglandin E_2 release is mediated by the activation of cyclooxygenase-2 (COX-2) transcription via NFκB in human gingival fibroblasts. *Mol. Cell. Biochem.* **238**, 11–18 (2002).
29. Ramsay, R.G., Ciznadija, D., Vanevski, M. & Mantamadiotis, T. Transcriptional regulation of cyclo-oxygenase expression: three pillars of control. *Int. J. Immunopathol. Pharmacol.* **16**, 59–67 (2003).
30. Aggarwal, S. & Pittenger, M.F. Human mesenchymal stem cells modulate allogeneic immune cell responses. *Blood* **105**, 1815–1822 (2005).
31. Sotiropoulou, P.A., Perez, S.A., Gritzapis, A.D., Baxevanis, C.N. & Papamichail, M. Interactions between human mesenchymal stem cells and natural killer cells. *Stem Cells* **24**, 74–85 (2006).
32. Pevsner-Fischer, M. *et al.* Toll-like receptors and their ligands control mesenchymal stem cell functions. *Blood* **109**, 1422–1432 (2007).
33. Crisostomo, P.R. *et al.* Gender differences in injury induced mesenchymal stem cell apoptosis and VEGF, TNF, IL-6 expression: role of the 55 kDa TNF receptor (TNFR1). *J. Mol. Cell. Cardiol.* **42**, 142–149 (2007).
34. Park, Y.K. *et al.* Nitric oxide donor, (+/−)-*S*-nitroso-*N*-acetylpenicillamine, stabilizes transactive hypoxia-inducible factor-1α by inhibiting von Hippel-Lindau recruitment and asparagine hydroxylation. *Mol. Pharmacol.* **74**, 236–245 (2008).
35. Bal-Price, A., Gartlon, J. & Brown, G.C. Nitric oxide stimulates PC12 cell proliferation via cGMP and inhibits at higher concentrations mainly via energy depletion. *Nitric Oxide* **14**, 238–246 (2006).
36. Bianco, P., Riminucci, M., Gronthos, S. & Robey, P.G. Bone marrow stromal stem cells: nature, biology, and potential applications. *Stem Cells* **19**, 180–192 (2001).
37. Chamberlain, G., Fox, J., Ashton, B. & Middleton, J. Concise review: mesenchymal stem cells: their phenotype, differentiation capacity, immunological features, and potential for homing. *Stem Cells* **25**, 2739–2749 (2007).
38. Mansilla, E. *et al.* Human mesenchymal stem cells are tolerized by mice and improve skin and spinal cord injuries. *Transplant. Proc.* **37**, 292–294 (2005).
39. van Laar, J.M. & Tyndall, A. Adult stem cells in the treatment of autoimmune diseases. *Rheumatology (Oxford)* **45**, 1187–1193 (2006).
40. Corcione, A. *et al.* Human mesenchymal stem cells modulate B-cell functions. *Blood* **107**, 367–372 (2006).
41. Kubo, S. *et al.* E-prostanoid (EP)2/EP4 receptor-dependent maturation of human monocyte-derived dendritic cells and induction of helper T2 polarization. *J. Pharmacol. Exp. Ther.* **309**, 1213–1220 (2004).
42. Shinomiya, S. *et al.* Regulation of TNFα and interleukin-10 production by prostaglandins I_2 and E_2: studies with prostaglandin receptor–deficient mice and prostaglandin E-receptor subtype-selective synthetic agonists. *Biochem. Pharmacol.* **61**, 1153–1160 (2001).
43. Hata, A.N. & Breyer, R.M. Pharmacology and signaling of prostaglandin receptors: multiple roles in inflammation and immune modulation. *Pharmacol. Ther.* **103**, 147–166 (2004).
44. Le Blanc, K. *et al.* Mesenchymal stem cells for treatment of steroid-resistant, severe, acute graft-versus-host disease: a phase II study. *Lancet* **371**, 1579–1586 (2008).
45. Miyaji, T. *et al.* Ethyl pyruvate decreases sepsis-induced acute renal failure and multiple organ damage in aged mice. *Kidney Int.* **64**, 1620–1631 (2003).
46. Yasuda, H., Yuen, P.S., Hu, X., Zhou, H. & Star, R.A. Simvastatin improves sepsis-induced mortality and acute kidney injury via renal vascular effects. *Kidney Int.* **69**, 1535–1542 (2006).
47. Imai, Y., Ibata, I., Ito, D., Ohsawa, K. & Kohsaka, S. A novel gene iba1 in the major histocompatibility complex class III region encoding an EF hand protein expressed in a monocytic lineage. *Biochem. Biophys. Res. Commun.* **224**, 855–862 (1996).

dc_219_11

Corrigendum: VEGF modulates erythropoiesis through regulation of adult hepatic erythropoietin synthesis

Betty YFY Tam, Kevin Wei, John S Rudge, Jana Hoffman, Joceyln Holash, Sang-ki Park, Jenny Yuan, Colleen Hefner, Cecile Chartier, Jeng-Shin Lee, Shelly Jiang, Nihar R Nayak, Frans A Kuypers, Lisa Ma, Uma Sundram, Grace Wu, Joseph A Garcia, Stanley L Schrier, Jacquelyn J Maher, Randall S Johnson, George D Yancopoulos, Richard C Mulligan & Calvin J Kuo
***Nat. Med.* 12, 793–800 (2006); published online 25 June 2006; corrected after print 6 April 2009**

In the version of this article initially published, the name of one of the authors, Nihar R. Nayak, was misspelled as Nihar R. Niyak. The error has been corrected in the HTML and PDF versions of the article.

Corrigendum: Bone marrow stromal cells attenuate sepsis via prostaglandin E_2–dependent reprogramming of host macrophages to increase their interleukin-10 production

Krisztián Németh, Asada Leelahavanichkul, Peter S T Yuen, Balázs Mayer, Alissa Parmelee, Kent Doi, Pamela G Robey, Kantima Leelahavanichkul, Beverly H Koller, Jared M Brown, Xuzhen Hu, Ivett Jelinek, Robert A Star & Éva Mezey
***Nat. Med.* 15, 42–49 (2009); published online 21 November 2008; corrected after print 6 April 2009**

In the version of this article initially published, the labeling in (Figure 4) was incorrect. In panel (b), the cells in the left two FACS plots are shown based on their size (FSC, *y* axis) and CD11b expression (*x* axis), and the cells in the right two FACS plots are shown based on their F4/80 expression (*y* axis) and GR1 expression (*x* axis). In panel (c), the curves should start at 1 h. In panel (d), the text labeling the *y* axis should read "*in vitro*," not "*in vivo*." The errors have been corrected in the HTML and PDF versions of this article.

Corrigendum: The cerebral cavernous malformation signaling pathway promotes vascular integrity via Rho GTPases

Kevin J Whitehead, Aubrey C Chan, Sutip Navankasattusas, Wonshill Koh, Nyall R London, Jing Ling, Anne H Mayo, Stavros G Drakos, Christopher A Jones, Weiquan Zhu, Douglas A Marchuk, George E Davis & Dean Y Li
***Nat. Med.* 15, 177–184 (2009); published online 18 January; corrected after print 6 April 2009**

In the version of this article initially published, Christopher A. Jones and Weiquan Zhu were not included in the list of authors. The error has been corrected in the HTML and PDF versions of the article.

Corrigendum: Effector memory T cell responses are associated with protection of rhesus monkeys from mucosal simian immunodeficiency virus challenge.

Scott G Hansen, Cassandra Vieville, Nathan Whizin, Lia Coyne-Johnson, Don C Siess, Derek D Drummond, Alfred W Legasse, Michael K Axthelm, Kelli Oswald, Charles M Trubey, Michael Piatak Jr, Jeffrey D Lifson, Jay A Nelson, Michael A Jarvis & Louis J Picker
***Nat. Med.* 15, 293–299 (2009); published online 15 February 2009; corrected after print 6 April 2009**

In the version of this article initially published, a "left" and "right" designation was switched in the legend for Figure 4d. The legend should read "FCICA of peripheral blood $CD8^+$ T cells from the four protected vaccinees, examining the response of these cells to SIV proteins that were (Rev-Tat-Nef) or were not (Pol and Vif) expressed by the administered RhCMV vectors before (left) and 133 d after (right) initiation of the SIVmac239 intrarectal challenge protocol." The error has been corrected in the HTML and PDF versions of the article.

Erratum: Straight talk with...Mac Cowell and Jason Bobe

Prashant Nair
***Nat. Med.* 15, 230–231 (2009); published online 5 March 2009; corrected after print 6 April 2009**

In the print version of this interview, the first response contained an unrelated excerpt from the previous month's Q & A. The text begins with "who could mobilize..." and ends with "…results and more results." The error did not appear online in the HTML and PDF versions of the article.

Bone marrow stromal cells use TGF-β to suppress allergic responses in a mouse model of ragweed-induced asthma

Krisztian Nemeth[a,b,1], Andrea Keane-Myers[c], Jared M. Brown[c], Dean D. Metcalfe[c], James D. Gorham[d], Virgilio G. Bundoc[c], Marcus G. Hodges[c], Ivett Jelinek[e], Satish Madala[c], Sarolta Karpati[b], and Eva Mezey[a,1]

[a]National Institute of Dental and Craniofacial Research, Craniofacial and Skeletal Diseases Branch, National Institutes of Health, Bethesda, MD 20892; [b]Department of Dermato-Venereology and Dermato-Oncology, Semmelweis University, H-1085 Budapest, Hungary; [c]Laboratory of Allergic Diseases, National Institute of Allergy and Infectious Diseases, National Institutes of Health, Bethesda, MD 20892; [d]Department of Pathology and of Microbiology and Immunology, Dartmouth Medical School, Lebanon, NH 03756; and [e]National Cancer Institute, Experimental Immunology Branch, National Institutes of Health, Bethesda, MD 20892

Edited* by Susan E. Leeman, Boston University School of Medicine, Boston, MA, and approved January 22, 2010 (received for review September 18, 2009)

Bone marrow stromal cells [BMSCs; also known as mesenchymal stem cells (MSCs)] effectively suppress inflammatory responses in acute graft-versus-host disease in humans and in a number of disease models in mice. Many of the studies concluded that BMSC-driven immunomodulation is mediated by the suppression of pro-inflammatory Th1 responses while rebalancing the Th1/Th2 ratio toward Th2. In this study, using a ragweed induced mouse asthma model, we studied if BMSCs could be beneficial in an allergic, Th2-dominant environment. When BMSCs were injected i.v. at the time of the antigen challenge, they protected the animals from the majority of asthma-specific pathological changes, including inhibition of eosinophil infiltration and excess mucus production in the lung, decreased levels of Th2 cytokines (IL-4, IL-5, and IL-13) in bronchial lavage, and lowered serum levels of Th2 immunoglobulins (IgG1 and IgE). To explore the mechanism of the effect we used BMSCs isolated from a variety of knockout mice, performed in vivo blocking of cytokines and studied the effect of asthmatic serum and bronchoalveolar lavage from ragweed challenged animals on the BMSCs in vitro. Our results suggest that IL-4 and/or IL-13 activate the STAT6 pathway in the BMSCs resulting in an increase of their TGF-β production, which seems to mediate the beneficial effect, either alone, or together with regulatory T cells, some of which might be recruited by the BMSCs. These data suggest that, in addition to focusing on graft-versus-host disease and autoimmune diseases, allergic conditions—specifically therapy resistant asthma—might also be a likely target of the recently discovered cellular therapy approach using BMSCs.

allergy | cellular therapy | immunomodulation | mesenchymal stem cell

Asthma is a chronic inflammatory airway disease affecting 16 million people in the United States alone and more than 300 million worldwide (1). It can range from a mild, intermittent disease to one that is severe, persistent, and difficult to treat (i.e., therapy-resistant) (2). Asthma-related deaths are uncommon, but they appear to be increasing; currently there are approximately 5,000 deaths per year in the United States and 100,000 throughout the world (3). New treatments are needed for therapy-resistant, severe cases.

Bone marrow stromal cells (BMSCs) have recently been shown to suppress harmful immune responses in patients with acute graft-versus-host disease (4, 5) and in several animal models of allogeneic rejection (6–8), a variety of autoimmune diseases (9–11), and lung injury (12–15). The authors of many of these studies concluded that BMSC-driven immunosuppression results from a shift in Th1/Th2 balance (8, 16, 17). During BMSC treatment, Th1 responses appear to be decreasing while Th2 responses begin to dominate. In animals with established allergies, Th2 responses are already dominant, and we wondered how BMSCs would react to such an environment. In this study we thus examined the effect of BMSCs on Th2-driven allergic reactions in a mouse model of asthma (18, 19).

Results

Lung Pathology. Following ragweed (RW) challenge (for timing of the events see Fig. 1), microscopic examination of the lungs showed minimal or no inflammation in mice sensitized with PBS solution and alum but no RW (Fig. 2*A*). Conversely, RW-sensitized mice showed extensive inflammation with eosinophil and lymphocyte invasion and severe perivascular and peribronchial cuffing (Fig. 2*B*). Mice that were challenged with RW but treated with i.v. injections of BMSCs had significantly less lung pathology: few inflammatory cell infiltrates were observed (Fig. 2*C*). Although no abnormal mucus-filled cells were observed in controls as defined by histological staining using PAS (Fig. 2*D*), the amount of stainable mucus in the airways was visibly increased following RW challenge (Fig. 2*E*). BMSC treatment reduced the amount of mucus to near control levels (Fig. 2*F*). In addition to improved lung scores (Fig. 3*A*), we also observed a significant decrease in both total inflammatory cell numbers and eosinophils in the bronchoalveolar lavage (BAL) fluid (Fig. 3 *B* and *C*).

Cytokine Response. RW-challenged mice showed increased levels of IL-4, IL-13, and IL-5 in BAL, all characteristic Th2 cytokines that highlight allergic inflammation. IL-4 and IL-13 levels were significantly reduced when the animals were treated with i.v. BMSCs (Fig. 3 *D–F*).

Ig Response. RW sensitization and subsequent antigen challenge is known to affect Th2-specific Ig concentrations in blood (19). Indeed, we found that both IgG1 and IgE serum levels were significantly increased following RW application, whereas IgG2a did not change. BMSC treatment resulted in a significant decrease of RW induced elevation of IgG1 and IgE concentrations (Fig. 3 *G–I*).

Use of Allogeneic BMSCs or Skin Fibroblasts Instead of Syngeneic BMSCs. In a few groups of mice, we determined whether there was a difference in effect when we use allogeneic BMSCs prepared from Balb/C mice or syngeneic C57BL/6J dermal fibroblasts instead of syngeneic (C57/BL6) BMSCs. We measured total cell numbers and the number of eosinophils (Fig. 4 *A* and *B*) as well as IL-4 and IL-13 levels (Fig. 4 *C* and *D*) from BAL and immunoglobulins from serum (Fig. 4 *E–G*). We found that there was no significant dif-

Author contributions: K.N., A.K.-M., D.D.M., and E.M. designed research; K.N., A.K.-M., J.M.B., V.G.B., S.M., and M.G.H. performed research; D.D.M., J.D.G., and I.J. contributed new reagents/analytic tools; K.N., A.K.-M., J.M.B., I.J., S.K., and E.M. analyzed data; and K.N. and E.M. wrote the paper.

The authors declare no conflict of interest.

*This Direct Submission article had a prearranged editor.

[1]To whom correspondence may be addressed. E-mail: mezeye@mail.nih.gov or nemethk@mail.nih.gov.

This article contains supporting information online at www.pnas.org/cgi/content/full/0910720107/DCSupplemental.

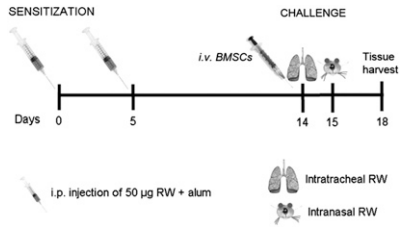

Fig. 1. Timeline of the experiments showing the days of the interventions.

ference between syngeneic versus allogeneic BMSCs (i.e., both were equally effective), and skin fibroblasts had only partial effect. Although the number of total cells in BAL was reduced following fibroblast treatment, the number of eosinophils was not different from the untreated group. Fibroblasts behaved similarly to BMSCs in regulating cytokine levels, but they had no effect on serum IgE concentrations. Interestingly, IgG2a levels were highly increased following fibroblast administration—an effect that we never observed using BMSCs.

Searching for Mechanism of Action. One hour after i.v. injection of BMSCs on d 14, the cells were found exclusively in the lung whereas virtually no cells were seen in other organs as demonstrated by bioluminescence measurements using luciferase expressing stromal cells (Fig. 5*A*). To determine if the inflammatory environment seen in asthma could influence homing to and/or survival of BMSCs in the lung, we injected luciferase-expressing cells into animals on d 14, immediately after intra-airway application of PBS solution or RW. Comparing emitted luminescence at different time points we assessed the number of stromal cells still present in the lungs. At 1, 12, and 24 h, the number of BMSCs in control and asthmatic animals were comparable, whereas at 36 h—and more evidently after 48 h—we detected considerably more BMSCs in the asthmatic lungs (Fig. 5*A*). To follow up on this observation, we injected Q-dot–labeled BMSCs into control and RW-challenged animals and isolated

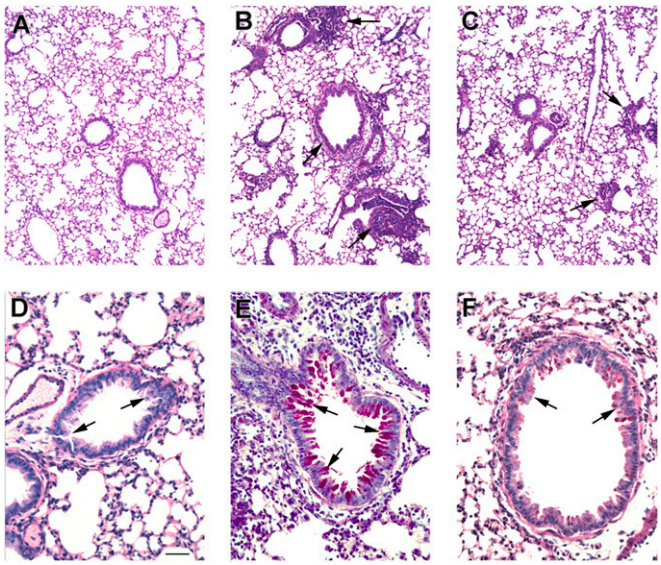

Fig. 2. Histological images of airways stained with PAS to show the mucin-producing goblet cells (dark red in the lumen). Low-magnification images depict a control lung (*A*), a lung following RW challenge with no treatment (*B*), and a lung with BMSC treatment (*C*). Note the significant increase in lymphocytic infiltrates (arrows) in *B* and their decrease in *C*. The high magnification images of the airways show a normal bronchus in *D*, a bronchus from RW-challenged mouse with mucus buildup (arrows) in the luminal surface (*E*), and a treated mouse with less mucus in *F*. (Scale bar, 250 µm in *A*–*C* and 50 µm in *D*–*F*.)

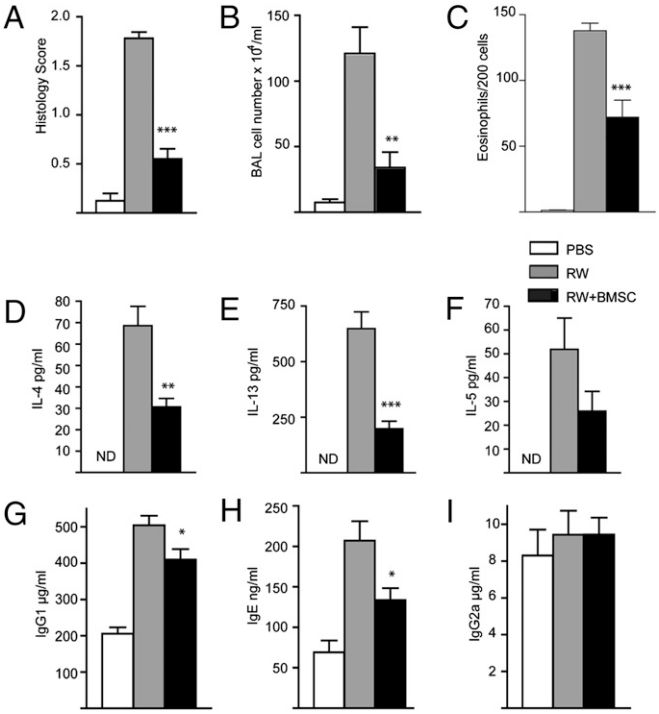

Fig. 3. Evaluation of the effect of BMSC treatment on the different parameters of RW-induced asthma. Mice treated with BMSCs showed a significant reduction in lung histology scores (*A*), total number of BAL cells (*B*), relative ratio of BAL eosinophils (*C*), and levels of allergy-specific Th2 cytokines IL-4 (*D*), IL-13 (*E*), and IL5 (*F*) in BAL. From the sera of challenged mice we measured Ig concentrations, and in the BMSC-treated group we found a significant decrease in the level of Th2-specific Ig concentrations IgG1 (*G*) and IgE (*H*), whereas there was no change in the level of IgG2a (*I*). There were four to eight mice per group. $*P < 0.05$, $**P < 0.01$, and $***P < 0.001$ in all graphs.

the Q-dot–positive BMSCs from the protease-digested lung cell suspensions using FACS. At 6, 12, and 24 h after injection, the number of Q-dot–positive cells did not differ between the two groups. After 36 h, however, we detected a significant increase in the number of BMSCs retained in the asthmatic lungs, and this difference remained detectable at 48, 72, and 96 h after BMSC injection (Fig. 5 *B* and *C*). These observations suggest that the developing allergic environment is capable to attract and retain more BMSCs than unaffected lungs, indicating that asthmatic lungs are likely to secrete factors that affect BMSC homing and survival. We next continued to explore the nature of such factors.

Among the number of cytokines known to suppress allergic responses the antiinflammatory actions of IL-10, TGFβ, and IFN-γ are especially well established. To determine whether any of these factors contributes to the beneficial effect of BMSCs, we first examined their levels in BAL fluid. There was a significant increase in the level of TGF-β in BAL fluid collected from BMSC-treated versus untreated mice, but no change in IFN-γ or IL-10 levels (Fig. 6 *A*–*C*). As TGF-β was increased in BAL fluid, and BMSCs are reported to be able to secrete TGF-β (20), we next asked whether serum or BAL fluid from RW-challenged mice could affect TGF-β production by BMSCs in vitro. TGF-β increased in the medium when BMSCs were cultured in the presence of RW-challenged serum or BAL, suggesting that allergy-specific microenvironment (i.e., serum or BAL) is capable of modulating immunoregulatory functions of BMSCs. It has been reported that stimulation of certain immune cells through the IL-4R pathway results in up-regulated TGF-β expression (32). To find out if enhanced TGF-β production by BMSCs in the presence of allergic

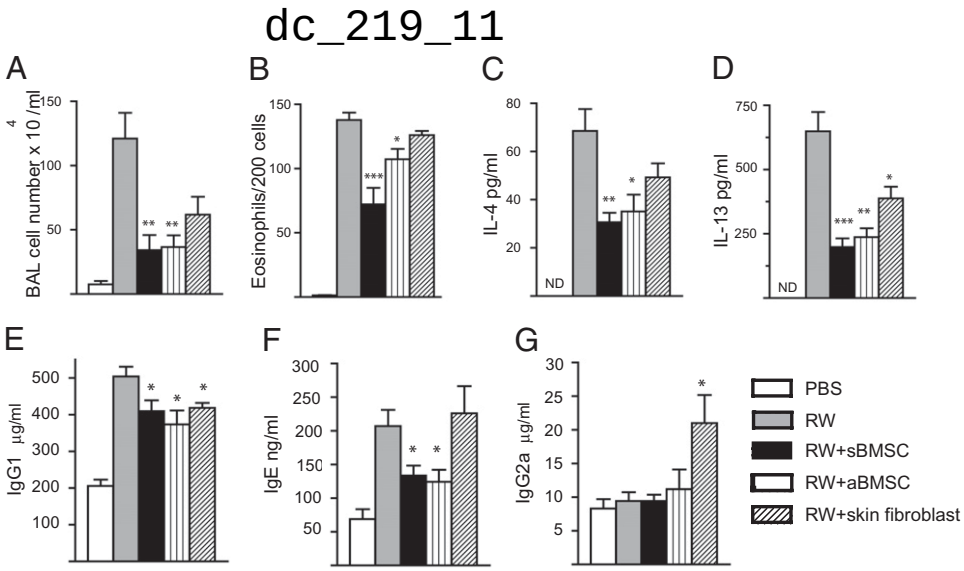

Fig. 4. Assessing the effect of allogeneic BMSCs or syngeneic skin fibroblasts on RW-induced asthma. Allogeneic BMSCs exhibit a similar inhibitory effect as syngeneic BMSCs on the total number of BAL cells (*A*), relative ratio of eosinophils (*B*), BAL inflammatory cytokines IL-4 (*C*) and IL-13 (*D*), and serum immunoglobulins IgG1 (*E*), IgE (*F*), and IgG2a (*G*). There were four to eight mice per group. Skin fibroblasts had a partial effect on the aforementioned parameters (see same graphs).

serum or BAL could be triggered by activation through the IL-4R, we repeated the aforementioned experiments using IL-4R–deficient BMSCs. We found that RW-challenged serum or BAL could not enhance TGF-β production in IL-4R–KO BMSCs, suggesting an important role for IL-4 (Fig. 6*D*).

As both IL-4 and IL-13 are able to bind to IL-4R, in another series of experiments we examined the effect of blocking (using specific antibodies) IL-4, IL-13, or both on the TGF-β production by BMSCs when they came in contact with RW-sensitized serum or BAL (Fig. 6 *E* and *F*). When serum from RW challenged mice was added to the media, IL4 neutralization alone eliminated the increased TGF-β production but blocking IL-13 did not have this effect (Fig. 6*E*). Interestingly, when BAL from RW challenged mice was added, the BMSCs increased their TGF-β production even when either IL-4 or IL-13 was blocked; however, blocking both cytokines simultaneously eliminated the effect (Fig. 6*F*). On the other hand, neither recombinant IL-4 or IL-13 alone or in combination increased TGF-β production (Fig. S1), suggesting a possible role for other factors.

When treating mice with TGF-β– and IL-10–specific neutralizing antibodies before BMSC injection, we observed that blocking TGF-β—but not IL-10—eliminated the beneficial effect of BMSCs demonstrated by the lack of reduction in BAL total cell numbers and eosinophil counts (Fig. 7 *A* and *B*). Furthermore, in mice injected with TGF-β1–KO BMSCs, the beneficial effect was no longer seen: treated animals showed no reduction in BAL cell numbers, asthma-specific BAL cytokines, or serum Th2 immunoglobulins. Importantly TGF-β1–KO cells were unable to elicit increase in BAL TGF-β concentrations, suggesting that BMSC-derived TGF-β1 is responsible for the effect (Fig. 7*C*).

The IL-4 receptor is known to activate the STAT6 signaling pathway (21). To see if the IL4Ra/STAT6 pathway is indeed necessary for the BMSCs to act beneficially in an allergic environment—as suggested by the in vitro studies just described—we injected STAT6-deficient BMSCs instead of WT cells and observed no TGF-β elevation in the BAL samples (Fig. 7*C*). In accordance with this result the elimination of STAT6 also reversed

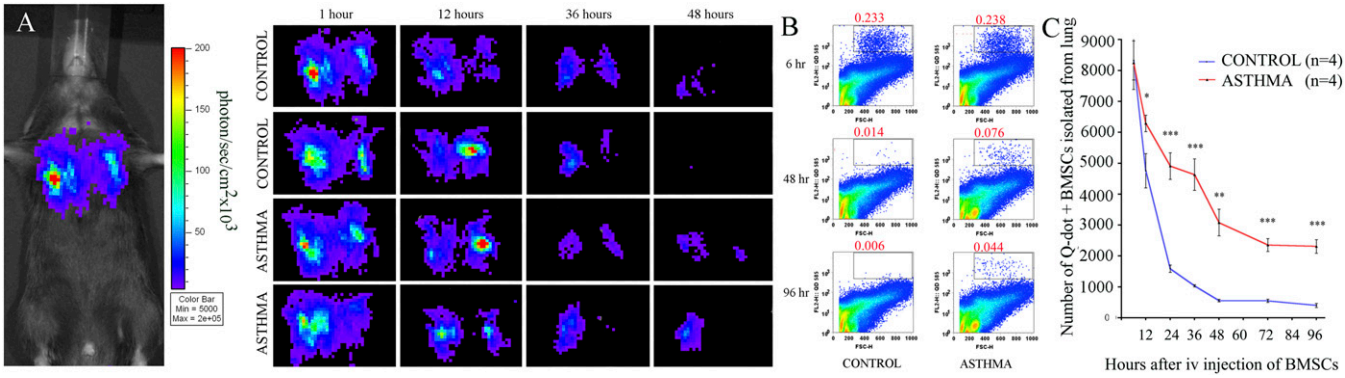

Fig. 5. After i.v. delivery of BMSCs at the time of the first challenge, stromal cells are concentrated in the lung. Asthmatic lungs seem to retain more BMSCs than control unchallenged lungs at 48 h after administration, demonstrated by bioluminescence detection of luciferase-expressing stromal cells. Two representative mice of three used are shown (*A*). To confirm this observation, Q-dot–labeled BMSCs were injected at the time of the first challenge, and lung cell suspensions were analyzed using FACS at several time points after injection. After 6 h, the number of Q-dot–positive cells (BMSCs) are still comparable in the two groups (each had four mice), but starting at 12 h there are significantly more BMSCs retained in the asthmatic lungs compared with the controls at all time points examined (*B* and *C*).

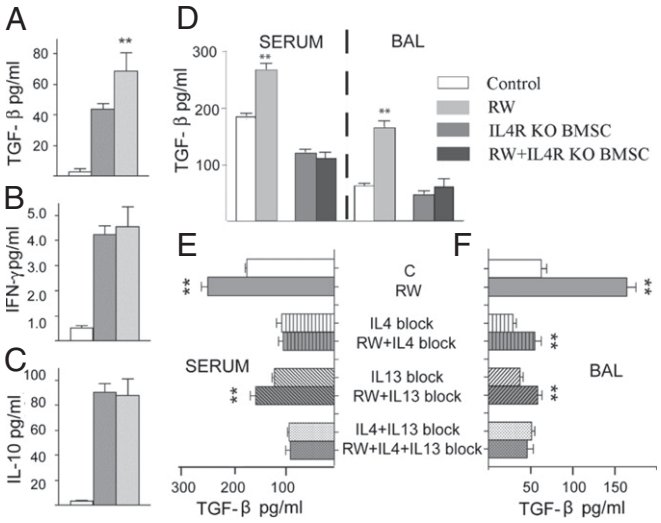

Fig. 6. Studying the mechanism of BMSC effect. In BAL BMSC treatment resulted in elevated TGF-β levels (*A*). IFN-γ (*B*) and IL-10 (*C*) did not change. Serum or BAL from RW challenged mice induced BMSCs to producemore TGF-β in vitro, but this effect was eliminated when BMSCs lacked IL-4Ra (*D*). Using neutralizing antibodies for IL-4 or IL-13 suggested both cytokines are involved in stimulating BMSC's TGF-β production when cocultured with serum (*E*) or BAL (*F*) from RW challenged mice.

the BMSC-derived attenuation of RW-induced asthma, pointing to the importance of the IL4R/STAT6 pathway (Fig. 7 *D–J*).

As regulatory T cells (T-regs) are known to play a role in alleviating asthma symptoms and TGF-β has been suggested to

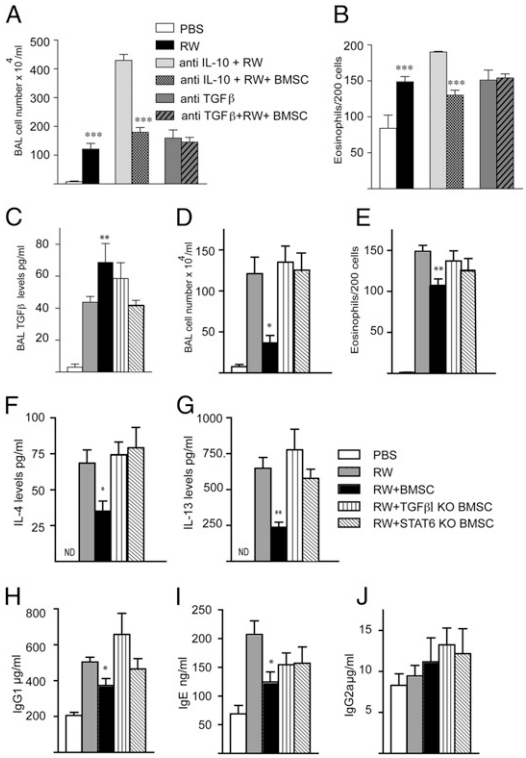

Fig. 7. In vivo demonstration of mechanism of action. The beneficial effect of BMSCs on inflammatory changes is eliminated in the presence of TGF-β neutralizing antibodies, but spared when animals are treated with anti-IL-10 antibodies (*A* and *B*). BMSCs from TGF-β or STAT6 deficient animals did not induce TGF-β production (*C*) or decrease BAL total cell numbers (*D*), eosinophil numbers (*E*), cytokine levels (*F* and *G*), or serum immunoglobulin concentrations (*H–J*).

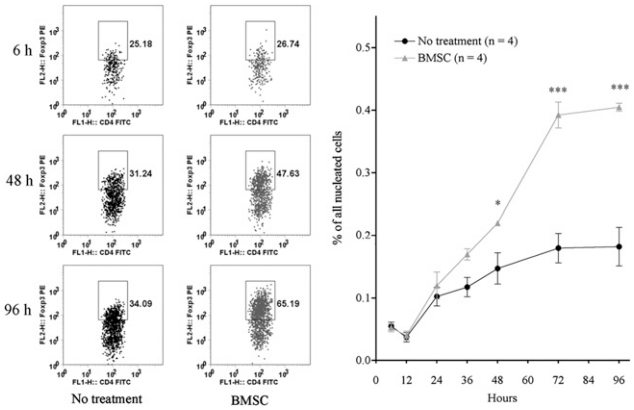

Fig. 8. Quantification of regulatory T cells in asthmatic lungs. With time there is a gradual increase in the number of regulatory T cells in lungs challenged with RW. BMSC-treated asthmatic lungs show a greater influx of T-regs starting at 36 h after challenge and further increasing up to 96 h.

play a role in T-reg differentiation, we wondered if the number of T-regs in the lung tissue could also be affected by the BMSC treatment in our model. Analyzing lung single cell suspensions using FACS, we detected a steady increase in the number of T-regs in challenged animals over time. Importantly, as early as after 48 h, as well as after 72 and 96 h after challenge, we found significantly more T-regs in the BMSC-treated lungs than the ones collected from challenged but untreated animals (Fig. 8).

Discussion

Asthma is an inflammatory disease of the airways. In asthma, the lungs are invaded by a variety of inflammatory cells, including eosinophils and lymphocytes. These cells, in addition to resident mast cells, secrete cytokines and chemokines that trigger constriction of the bronchi and secretion of mucus.

The current working hypothesis is that asthma is caused by an abnormal shift in the Th1/Th2 balance in favor of Th2 cells and the production of IL-4, IL-5, and IL-13. Through these mediators, Th2 lymphocytes are thought to recruit additional effector cells to the lungs, and the cells recruited promote allergic inflammatory events (22). BMSCs have been shown to have useful effects in a number of diseases and disease models. In the majority of these disorders, however, the T cell balance is shifted toward Th1 dominance. As BMSCs seem to "normalize" immune responses and reestablish the physiological balance in a variety of autoimmune and infectious diseases (23–27), we wondered whether these cells might also be able to tip the balance back to normal in an allergic environment with already-established Th2 dominance. The rebalancing act would require that the cells detect an imbalance and then take appropriate measures to correct it.

Our initial experiments showed that injecting BMSCs on d 14, when first challenging the sensitized animals significantly improved lung pathology, such as total cell number in BAL; number of eosinophils in BAL and lung scores. Using luciferase-expressing or Q-dot–labeled BMSCs, we demonstrated that lungs are the primary site of BMSC accumulation following i.v. injection, confirming the known phenomenon of cell trapping in the pulmonary microvasculature that is partially related to cell size (28, 29). However, using Q-dot–labeled BMSCs we found significantly more BMSCs retained in the lungs when RW-induced allergic inflammation was present compared with the unchallenged state—a tendency also suggested by the bioluminescent measurements. As in our model, the primary site of pathologic processes is the lung itself, and the enhanced presence of BMSCs could deliver a concentrated effort to modulate pathological immune responses.

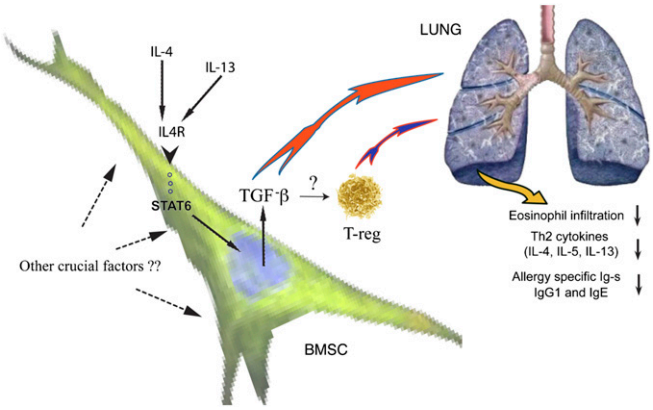

Fig. 9. Schematic drawing shows the mechanism of effect based on data of the present study. BMSCs "sense" the allergic environment, and as a result of the increased levels of IL-4/IL-13, they respond by producing higher amounts of TGF-β that, either alone or by recruiting regulatory T cells, will ultimately lead to a decrease of lung eosinophil infiltration, as well as allergy-specific cytokine and Ig production.

IL-10 and TGF-β, two well characterized antiinflammatory cytokines, and IFN-γ, a key Th1 cytokine capable of down-regulating Th2-mediated pathological responses, are all thought to be capable of suppressing asthma (22, 30). As IL-10 has been shown to play a significant role in the beneficial effect of BMSCs in sepsis (27), we first measured cytokines in serum and BAL in the treated versus untreated RW-challenged mice. We found no change in IL-10 or IFN-γ levels, but there was a significant increase in the level of TGF-β, suggesting a different mechanism of action than what was found in a septic environment. We then demonstrated the importance of TGF-β in vivo by treating the mice with TGF-β–specific neutralizing antibodies before BMSC injection. Blocking TGF-β—but not IL-10—eliminated the beneficial effect of BMSC treatment. Next we looked for a possible source of TGF-β. BMSCs themselves are capable of secreting TGF-β (31), which has been implicated as one of the possible mediators of the BMSCs' immunosuppressive effect. We thus repeated the experiment injecting BMSCs derived from TGF-β1–KO mice and found no beneficial effect, suggesting that the BMSC-derived TGF-β is critical in suppressing the allergic responses. As TGF-β synthesis can be enhanced through IL-4R in some immune cells (32), we wondered if it is the IL-4 and IL-13 that "turns on" the BMSCs to make TGF-β. We first used BMSCs from mice lacking the IL-4R (which is used by both IL-4 and IL-13) and found that RW-challenged serum or BAL could no longer elicit increased TGF-β production in these cells in vitro. In another set of experiments using neutralizing antibodies against IL-4 or IL-13, we could further demonstrate the importance of the IL4R. As the IL-4R is known to activate the STAT6 pathway (21), we wanted to confirm our results by using BMSCs that genetically lacked STAT6. As expected, STAT6-KO BMSCs were ineffective in alleviating asthma pathology and could not trigger TGF-β elevation in the BAL fluids either. Based on these data, we suggest that IL-4 and/or IL-13 bind to IL-4R receptors on BMSCs activating the STAT6 pathway. This, in turn, drives the cells to produce increased amounts of TGF-β. When this TGF-β is released from the BMSCs in the allergic (i.e., Th2-dominant) environment, TGF-β receptor activation on immune cells could result in a decrease in IL-4 production (33) and ultimately leads to a shift back toward immunological equilibrium (Fig. 9). Surprisingly, neither recombinant IL-4 nor IL-13 alone or in combination was able to elicit the elevation of TGF-β by BMSCs seen with RW-conditioned BAL fluid or blood serum in vitro. This indicates that activation of the IL-4R/STAT6 pathway is necessary but not sufficient to cause TGF-β up-regulation in BMSCs. In addition to IL-4 or IL-13, there must be other important factors in vivo (present in BAL fluid or serum) that contribute to the production and subsequent release of TGF-β by BMSCs.

We also demonstrated that BMSC-treated asthmatic animals recruit significantly more regulatory T cells to the lungs than untreated mice. In animal models of allergic airways disease, T-regs can suppress established airway inflammation and airway hyperresponsiveness (34). Regulatory T cells are thought to suppress infection/inflammation by secreting antiinflammatory molecules (e.g., IL-10, TGF-β) (35, 36). It is possible that BMSCs work together with regulatory T cells to suppress harmful allergic responses in our model. BMSCs could initiate the suppressive process by secreting TGF-β to block the proinflammatory Th2 responses and at the same time induce the differentiation and help the survival of regulatory T cells (30) that will then continue to improve asthma pathology after the BMSCs disappear.

It is worth mentioning that dermal fibroblasts—cells frequently used as control cells in studies of BMSCs—had beneficial effects in the model that we used when injected intravenously. The effect of the fibroblasts was not as strong as that of BMSCs. This suggests, however, that fibroblast-like cells, whether derived from the bone marrow or other organs (including skin dermis), may also have some immunomodulatory properties (37).

In the present study we demonstrated that i.v. injected BMSCs are capable of suppressing Th2-driven allergic responses. It appears that IL-4 and/or IL-13 induce production and secretion of TGF-β by the BMSCs, which in turn effectively suppresses allergy specific pathological changes in the asthma model we studied. These data provide another example of the ability of BMSCs to "sense" their immunological environment and respond accordingly. It is hard to imagine a drug or combination of drugs that could act this way, and further work should be done to determine whether the cells could be used to treat patients with therapy-resistant asthma.

Methods

Mice. C57BL/6J or Balb/C mice (6 to 8 weeks old) were obtained from Taconic Farms. IL-4Rα–KO and STAT6-KO animals were purchased from Jackson Laboratories. TGF-β1–KO mice have previously been produced and characterized (38). The animals were housed and maintained in the National Institute of Allergy and Infectious Diseases or National Institute of Dental and Craniofacial Research animal facilities. All studies conformed to the principles for laboratory animal research outlined by the Animal Welfare Act, and were approved by the National Institute of Dental and Craniofacial Research and/or National Institute of Allergy and Infectious Diseases Animal Care and Use Committee. The groups for in vivo studies contained four to 10 mice, and each experiment was repeated two to three times.

Antigen Challenge. To elicit a bronchial allergic response, RW sensitization and challenge were used (18, 19). C57BL/6J mice were sensitized on d 0 and 5 with 200 μL i.p. injections of 50 μg RW extract (Greer Laboratories), emulsified in an equal volume (100 μL/antigen injection) of alum (Pierce) as described earlier (39). Control animals were injected i.p. with the same amount of alum mixed with PBS solution. Subsequently, as shown in Fig. 1, the mice were challenged on d 14 and 15 with 50 μg RW extract in PBS solution by intratracheal and intranasal inoculation (30 μL), respectively. Control mice received an equal volume of PBS solution administered via the same routes. In all cases, mice were killed by anesthetizing them with ketamine (Fort Dodge Animal Health) and xylazine (Phoenix Pharmaceuticals) 100 mg/kg and 10 mg/kg, respectively, followed by exsanguination.

Histology. To assess pulmonary inflammation, BAL was performed 72 h after the final allergen challenge (as described later). Lungs were then immediately placed in 10% neutral buffered formalin and sent to Histoserv (Germantown, MD), where they were embedded in paraffin and stained. H&E was used to evaluate cellular inflammation and periodic acid–Schiff (PAS) stain was used to visualize mucus-containing goblet cells. Slides were coded and read "blind"; a minimum of four lungs per group were given scores ranging from 0 to 2 based on the level of peribronchial cuffing, perivascular cuffing, goblet cell hyperplasia, and interstitial inflammation (40).

BAL. Immediately after the mice were exsanguinated, the lungs were cannulated with a 20-gauge i.v. catheter and gently washed once with 500 μL 1% FBS (HyClone) in PBS solution (for cytokine analysis) or twice with 750 μL 1% FBS in PBS solution (for analysis of cellular infiltration). Samples for cytokine analysis were stored at −80°C. Samples for cellular analysis were spun onto glass slides in a cytospin instrument (Thermo-Shandon) and stained with Kwik-Diff for differential cell analysis (Thermo-Shandon). A fraction was used to determine total cell counts.

In Vivo Neutralization of Cytokines. IL-10– or TGF-β–neutralizing antibodies (Clone 2A5 from Pierce Endogen or Clone 1D11 from R&D Systems, respectively) were injected intraperitoneally (10 μg/g body weight in 200 μL PBS) on two consecutive days at the approximate time of BMSC injection (d 14 and 15).

Measurement of Serum Antibody Isotypes. Antibody isotypes (IgG1, IgG2a, and IgE) were assayed in sera collected 72 h after last RW challenge using ELISA kits according to the manufacturer's instructions (Immunology Consultants Laboratory). All samples, including standards, were assayed in duplicate.

Preparation of Lung Cell Suspension. Lungs were removed, minced into small pieces, and incubated in RPMI medium 1640 with 1% penicillin–streptomycin and 1% glutamine for 30 min at 37 °C 5% CO_2 in the presence of collagenase type 1 (300 U mL^{-1}) and DNase I (50 U mL^{-1}; Worthington Biochemicals). After the incubation, the cell suspension was filtered through a 70-μm cell strainer and then washed with complete RPMI medium.

Data Analysis. Data are summarized as mean ± SE. Student *t* test or two-way ANOVA were performed using GraphPad Prism version 4.00 for Macintosh (GraphPad Software). The statistical significance value was set at $P < 0.05$.

ACKNOWLEDGMENTS. We thank Dr. William Paul for his continuing support and suggestions during the preparation of the study. We also thank Dr. Natasha Chairman for her help with the differentiation assays, Dr. Silvio Gutkind for providing the luciferase expressing lentiviral vectors, and Dr. Daniel Martin for his help with the bioluminescence measurements. This research was supported by the Division of Intramural Research Program of the National Institute of Dental and Craniofacial Research and National Institute of Allergy and Infectious Diseases.

1. Urbano FL (2008) Review of the NAEPP 2007 Expert Panel Report (EPR-3) on asthma diagnosis and treatment guidelines. *J Manag Care Pharm* 14:41–49.
2. Chung KF, et al., European Respiratory Society (1999) Difficult/therapy-resistant asthma: the need for an integrated approach to define clinical phenotypes, evaluate risk factors, understand pathophysiology and find novel therapies. ERS Task Force on Difficult/Therapy-Resistant Asthma. *Eur Respir J* 13:1198–1208.
3. Papiris S, Kotanidou A, Malagari K, Roussos C (2002) Clinical review: severe asthma. *Crit Care* 6:30–44.
4. Le Blanc K, et al. (2004) Treatment of severe acute graft-versus-host disease with third party haploidentical mesenchymal stem cells. *Lancet* 363:1439–1441.
5. Le Blanc K, Ringdén O (2005) Use of mesenchymal stem cells for the prevention of immune complications of hematopoietic stem cell transplantation. *Haematologica* 90:438.
6. Aggarwal S, Pittenger MF (2005) Human mesenchymal stem cells modulate allogeneic immune cell responses. *Blood* 105:1815–1822.
7. Kuo YR, et al. (2009) Mesenchymal stem cells prolong composite tissue allotransplant survival in a swine model. *Transplantation* 87:1769–1777.
8. Zhou HP, et al. (2006) Administration of donor-derived mesenchymal stem cells can prolong the survival of rat cardiac allograft. *Transplant Proc* 38:3046–3051.
9. Rafei M, Birman E, Forner K, Galipeau J (2009) Allogeneic mesenchymal stem cells for treatment of experimental autoimmune encephalomyelitis. *Mol Ther* 17:1799–1803.
10. Rafei M, et al. (2009) Mesenchymal stromal cells ameliorate experimental autoimmune encephalomyelitis by inhibiting CD4 Th17 T cells in a CC chemokine ligand 2-dependent manner. *J Immunol* 182:5994–6002.
11. Zappia E, et al. (2005) Mesenchymal stem cells ameliorate experimental autoimmune encephalomyelitis inducing T-cell anergy. *Blood* 106:1755–1761.
12. Gupta N, et al. (2007) Intrapulmonary delivery of bone marrow-derived mesenchymal stem cells improves survival and attenuates endotoxin-induced acute lung injury in mice. *J Immunol* 179:1855–1863.
13. Kumamoto M, Nishiwaki T, Matsuo N, Kimura H, Matsushima K (2009) Minimally-cultured bone marrow mesenchymal stem cells ameliorate fibrotic lung injury. *Eur Respir J* 34:740–748.
14. Mei SH, et al. (2007) Prevention of LPS-induced acute lung injury in mice by mesenchymal stem cells overexpressing angiopoietin 1. *PLoS Med* 4:e269.
15. Ortiz LA, et al. (2007) Interleukin 1 receptor antagonist mediates the antiinflammatory and antifibrotic effect of mesenchymal stem cells during lung injury. *Proc Natl Acad Sci USA* 104:11002–11007.
16. Bai L, et al. (2009) Human bone marrow-derived mesenchymal stem cells induce Th2-polarized immune response and promote endogenous repair in animal models of multiple sclerosis. *Glia* 57:1192–1203.
17. Wang Q, et al. (2008) Murine bone marrow mesenchymal stem cells cause mature dendritic cells to promote T-cell tolerance. *Scand J Immunol* 68:607–615.
18. McConchie BW, et al. (2006) Ascaris suum-derived products suppress mucosal allergic inflammation in an interleukin-10-independent manner via interference with dendritic cell function. *Infect Immun* 74:6632–6641.
19. Norris HH, et al. (2007) Inhibitory receptor gp49B regulates eosinophil infiltration during allergic inflammation. *J Leukoc Biol* 82:1531–1541.
20. Nasef A, et al. (2007) Identification of IL-10 and TGF-beta transcripts involved in the inhibition of T-lymphocyte proliferation during cell contact with human mesenchymal stem cells. *Gene Expr* 13:217–226.
21. Takeda K, et al. (1996) Essential role of Stat6 in IL-4 signalling. *Nature* 380:627–630.
22. Hamid Q, Tulic M (2009) Immunobiology of asthma. *Annu Rev Physiol* 71:489–507.
23. Rasmusson I (2006) Immune modulation by mesenchymal stem cells. *Exp Cell Res* 312: 2169–2179.
24. Tyndall A, et al. (2007) Immunomodulatory properties of mesenchymal stem cells: a review based on an interdisciplinary meeting held at the Kennedy Institute of Rheumatology Division, London, UK, 31 October 2005. *Arthritis Res Ther* 9:301.
25. Uccelli A, Moretta L, Pistoia V (2006) Immunoregulatory function of mesenchymal stem cells. *Eur J Immunol* 36:2566–2573.
26. Uccelli A, Moretta L, Pistoia V (2008) Mesenchymal stem cells in health and disease. *Nat Rev Immunol* 8:726–736.
27. Németh K, et al. (2009) Bone marrow stromal cells attenuate sepsis via prostaglandin E(2)-dependent reprogramming of host macrophages to increase their interleukin-10 production. *Nat Med* 15:42–49.
28. Harting MT, et al. (2009) Intravenous mesenchymal stem cell therapy for traumatic brain injury. *J Neurosurg* 110:1189–1197.
29. Schrepfer S, et al. (2007) Stem cell transplantation: the lung barrier. *Transplant Proc* 39:573–576.
30. Qian BF, Wahl SM (2009) TGF-beta can leave you breathless. *Curr Opin Pharmacol* 9: 454–461.
31. Di Nicola M, et al. (2002) Human bone marrow stromal cells suppress T-lymphocyte proliferation induced by cellular or nonspecific mitogenic stimuli. *Blood* 99:3838–3843.
32. Elovic AE, et al. (1998) IL-4-dependent regulation of TGF-alpha and TGF-beta1 expression in human eosinophils. *J Immunol* 160:6121–6127.
33. Holter W, et al. (1994) Transforming growth factor-beta inhibits IL-4 and IFN-gamma production by stimulated human T cells. *Int Immunol* 6:469–475.
34. Robinson DS (2009) Regulatory T cells and asthma. *Clin Exp Allergy* 39:1314–1323.
35. Corthay A (2009) How do regulatory T cells work? *Scand J Immunol* 70:326–336.
36. Sakaguchi S, Wing K, Onishi Y, Prieto-Martin P, Yamaguchi T (2009) Regulatory T cells: how do they suppress immune responses? *Int Immunol* 21:1105–1111.
37. Jones S, Horwood N, Cope A, Dazzi F (2007) The antiproliferative effect of mesenchymal stem cells is a fundamental property shared by all stromal cells. *J Immunol* 179:2824–2831.
38. Gorham JD, Lin JT, Sung JL, Rudner LA, French MA (2001) Genetic regulation of autoimmune disease: BALB/c background TGF-beta 1-deficient mice develop necroinflammatory IFN-gamma-dependent hepatitis. *J Immunol* 166:6413–6422.
39. Miyazaki D, et al. (2005) Macrophage inflammatory protein-1alpha as a costimulatory signal for mast cell-mediated immediate hypersensitivity reactions. *J Clin Invest* 115:434–442.
40. Al-Shami A, Spolski R, Kelly J, Keane-Myers A, Leonard WJ (2005) A role for TSLP in the development of inflammation in an asthma model. *J Exp Med* 202:829–839.

Corrections

PHYSIOLOGY

Correction for "Bone marrow stromal cells use TGF-β to suppress allergic responses in a mouse model of ragweed-induced asthma," by Krisztian Nemeth, Andrea Keane-Myers, Jared M. Brown, Dean D. Metcalfe, Jared D. Gorham, Victor G. Bundoc, Marcus G. Hodges, Ivett Jelinek, Satish Madala, Sarolta Karpati, and Eva Mezey, which appeared in issue 12, March 23, 2010, of *Proc Natl Acad Sci USA* (107:5652–5657; first published March 15, 2010; 10.1073/pnas.0910720107).

The authors note that the author name Jared D. Gorham should have appeared as James D. Gorham. Additionally, the author name Victor G. Bundoc should have appeared as Virgilio G. Bundoc. The corrected author line appears below. The online version has been corrected.

Krisztian Nemeth[a,b,1], Andrea Keane-Myers[c], Jared M. Brown[c], Dean D. Metcalfe[c], James D. Gorham[d], Virgilio G. Bundoc[c], Marcus G. Hodges[c], Ivett Jelinek[e], Satish Madala[c], Sarolta Karpati[b], and Eva Mezey[a,1]

www.pnas.org/cgi/doi/10.1073/pnas.1003664107

GENETICS

Correction for "BG1 has a major role in MHC-linked resistance to malignant lymphoma in the chicken," by Ronald M. Goto, Yujun Wang, Robert L. Taylor, Jr., Patricia S. Wakenell, Kazuyoshi Hosomichi, Takashi Shiina, Craig S. Blackmore, W. Elwood Briles, and Marcia M. Miller, which appeared in issue 39, September 29, 2009, of *Proc Natl Acad Sci USA* (106:16740–16745; first published September 11, 2009; 10.1073/pnas.0906776106).

The authors note the following statement should be added to the Acknowledgments: "This material is based on work supported in part by National Science Foundation Grant MCB-0524167."

www.pnas.org/cgi/doi/10.1073/pnas.1003235107

BIOCHEMISTRY

Correction for "Pathway of ATP utilization and duplex rRNA unwinding by the DEAD-box helicase, DbpA," by Arnon Henn, Wenxiang Cao, Nicholas Licciardello, Sara E. Heitkamp, David D. Hackney, and Enrique M. De La Cruz, which appeared in issue 9, March 2, 2010, of *Proc Natl Acad Sci USA* (107:4046–4050; first published February 16, 2010; 10.1073/pnas.0913081107).

The authors note that due to a printer's error, several of the Supporting Figures were referenced incorrectly in the main text. All references to Supporting Figure 3 should have instead referred to Supporting Figure 5, and all references to Supporting Figure 5 should have instead referred to Supporting Figure 3. All references to Supporting Figure 4 should have instead referred to Supporting Figure 6, and all references to Supporting Figure 6 should have instead referred to Supporting Figure 4. The online version has been corrected.

www.pnas.org/cgi/doi/10.1073/pnas.1003450107

BIOCHEMISTRY

Correction for "Remosomes: RSC generated non-mobilized particles with approximately 180 bp DNA loosely associated with the histone octamer," by Manu Shubhdarshan Shukla, Sajad Hussain Syed, Fabien Montel, Cendrine Faivre-Moskalenko, Jan Bednar, Andrew Travers, Dimitar Angelov, and Stefan Dimitrov, which appeared in issue 5, February 2, 2010, of *Proc Natl Acad Sci USA* (107:1936–1941; first published January 13, 2010; 10.1073/pnas.0904497107).

The authors note the following statement should be added to the Acknowledgments: "J.B. also acknowledges the support of Czech Grants LC535, MSM0021620806, and AV0Z50110509."

www.pnas.org/cgi/doi/10.1073/pnas.1003712107

dc_219_11
doi: 10.1111/j.1365-2222.2010.03685.x
Clinical & Experimental Allergy, 41, 526–534

ORIGINAL ARTICLE Basic Mechanisms in Allergic Disease

Bone marrow stromal cells inhibit mast cell function via a COX2-dependent mechanism

J. M. Brown[1,*,†], K. Nemeth[2,*], N. M. Kushnir-Sukhov[1], D. D. Metcalfe[1] and E. Mezey[2]
[1]*Laboratory of Allergic Diseases, NIAID, NIH, Bethesda, MD, USA and* [2]*CSDB, NIDCR, NIH, Bethesda, MD, USA*

Clinical & Experimental Allergy

Summary

Background Mast cells (MCs) have a central role in the induction of allergic inflammation, such as seen in asthma, and contribute to the severity of certain autoimmune diseases, such as rheumatoid arthritis. The MC thus represents an important inflammatory cell, and one which has resisted therapeutic attempts to alter its role in disease.

Objective Because bone marrow-derived stromal cells (BMSC, also known as mesenchymal stem cells or MSCs) have been reported to alter allergic inflammation *in vivo*, we chose to study the interaction between mouse BMSC and mouse bone marrow-derived MCs.

Methods MC degranulation, cytokine production and chemotaxis were evaluated *in vitro* following co-culture with BMSCs either in cell contact or a transwell. In addition, MC degranulation was assessed *in vivo* following administration of BMSCs in a model of passive cutaneous anaphylaxis and a peritoneal degranulation assay. Mechanisms of MC suppression by BMSCs were determined through use of inhibitors or antibodies to COX1, COX2, nitric oxide, indoleamine 2, 3-dioxygenase, EP1–4 receptors, TGF-β and IL-10. Lastly, we utilized either BMSCs or MCs deficient in COX1, COX2 or EP1-4 receptors to confirm the mechanisms of inhibition of MC function by BMSCs.

Results We discovered that BMSCs will effectively suppress specific MC functions *in vitro* as well as *in vivo*. When MCs are cocultured with BMSCs to allow cell-to-cell contact, BMSCs suppressed MC degranulation, pro-inflammatory cytokine production, chemokinesis and chemotaxis. Similarly, MC degranulation within mouse skin or the peritoneal cavity was suppressed following *in vivo* administration of BMSCs. Further, we found that these inhibitory effects were dependent on up-regulation of COX2 in BMSCs; and were facilitated through the activation of EP4 receptors on MCs.

Conclusion and Clinical Relevance These observations support the concept that BMSCs have the ability to suppress MC activation and therefore could be the basis for a novel cell based therapeutic approach in the treatment of MC driven inflammatory diseases.

Keywords allergy, COX2, EP4 receptor, mesenchymal stem cell, stromal cell
Submitted 15 April 2010; revised 6 December 2010; accepted 7 December 2010

Correspondence:
Jared M. Brown, Laboratory of Allergic Diseases, NIAID, NIH, Building 10, Rm 11C207, Bethesda, MD, USA.
E-mail: brownja@ecu.edu
Cite this as: J. M. Brown, K. Nemeth, N. M. Kushnir-Sukhov, D. D. Metcalfe and E. Mezey, *Clinical & Experimental Allergy*, 2011 (41) 526–534.

Introduction

Bone marrow-derived stromal cells (BMSCs, also known as mesenchymal stem cells or MSCs) are multipotent progenitor cells which may be isolated from the bone marrow by adherence and culture expansion. These cells have the natural ability to differentiate into bone, fat or cartilage. Recently, there is a renewed interest in BMSCs due to their immunomodulatory properties *in vitro* as well as *in vivo*. Intravenously injected BMSCs have been shown to have a beneficial effect in a variety of animal models of disease with an inflammatory component; and to prevent graft vs. host disease in humans [1–5]. We have successfully utilized BMSCs to therapeutically treat Th2-mediated allergic responses in a mouse model of asthma [6]. While clinical trials using BMSCs as cellular therapy are currently ongoing for treatment of Th1 inflammatory diseases, such as Crohn's disease [7], our data suggests that also targeting Th2-dominant allergic diseases with

*Contributed equally.
†Current address: Jared M. Brown, Department of Pharmacology & Toxicology, Brody School of Medicine East Carolina University Greenville, NC 27834, USA.

BMSC treatment has the potential to restore immune balance and therefore may provide a novel therapeutic approach for diseases with a Th2 bias.

The interactions between BMSCs and T cells [8–11] and B cells [9, 12] have been well established. There is also emerging data suggesting that BMSCs have the ability to modulate cells of the macrophage/monocyte/dendritic cell lineage, including their differentiation, maturation and activation [11, 13–17]. Mast cells (MCs) represent an important component of the immune system that are involved many allergic and Th2-mediated inflammatory diseases. MCs are derived from hematopoietic progenitor cells and influence both innate and adaptive immunity. They are well documented to be a critical effector cell in acute allergic reactions and to release histamine as well as cytokines and chemokines that influence innate and acquired immune responses [18]. Since MCs are critical effector cells in allergic inflammation, they represent an important cell type to therapeutically target using the immunomodulatory properties of BMSCs. Further, there are currently no data in the literature regarding the possible interactions between MCs and BMSCs; and how these interactions might influence MC activation. We therefore initiated *in vitro* and *in vivo* experiments to study the immunomodulatory effects BMSCs on MC function.

Materials and methods

Mice

C57BL/6, B6.Cg-Kit^{W-sh}, COX1$^{-/-}$ and COX2$^{-/-}$ mice were obtained from Jackson Laboratories at 4–6 weeks of age (Bar Harbor, ME, USA). Bone marrow from EP1–4$^{-/-}$ mice were a generous gift of Dr Beverly H. Koller. Mice were allowed food and water *ad libitum*; and were used experimentally between 6 and 8 weeks of age. All animal use procedures were in accordance with an institutional Animal Care and Use Committee.

Cell culture

Bone marrow-derived MCs. Mouse bone marrow-derived MCs (MC) were derived and cultured from femoral marrow cells of C57Bl/6 mice (Jackson Laboratories). Cells were cultured in RPMI-1640 medium supplemented with 10% FBS, 100 U/mL penicillin, 100 μg/mL streptomycin, 25 mM HEPES, 1.0 mM sodium pyruvate, non-essential amino acids (BioSource International, Camarillo, CA, USA), 0.0035% 2-ME and 300 ng/mL recombinant mouse IL-3 (PeproTech, Rocky Hill, NJ, USA). MCs were used following 4–6 weeks of culture at 37 °C and 5% CO_2.

Bone marrow stromal cells

Mouse BMSCs were collected from femora and tibiae of mice under aseptic conditions. Cells were cultured in α-MEM with 20% FBS, 1% glutamine and 1% penicillin/streptomycin. Macrophages were depleted from cultures using magnetic cell sorting with CD11b/CD45 beads (Miltenyi Biotec, Auburn, CA, USA). All BMSCs were shown to lack the hematopoietic lineage markers CD45, CD11b and Gr-1 (BD Biosciences) by FACS analysis. BMSCs were also shown to be able to differentiate into osteogenic and adipogenic lineages *in vitro*.

Mast cell degranulation and cytokine production

IgE-mediated MC degranulation was determined by measuring release of intracellular pre-formed β-hexosaminidase (β-hex) 30 min following challenge with antigen. For these experiments, MCs were seeded at 5×10^4 cells/well in 96-well flat-bottom plates; and were sensitized with 100 ng/mL mouse IgE anti-dinitrophenyl (DNP) antibody (Sigma-Aldrich, St Louis, MO, USA) for 24 h for degranulation experiments. MC degranulation was induced by the addition of 100 ng/mL dinitrophenylated human serum albumin (DNP-HSA) (Sigma-Aldrich). Thirty minutes (at 37 °C) after addition of DNP, we measured β-hex release as described [19], using *p*-nitrophenyl-*N*-acetyl-β-D-glucopyranoside (8 mM; Sigma-Aldrich) as a substrate for β-hex. For experiments where MCs and BMSCs were co-cultured, we added BMSCs at a ratio of 100 : 1, 10 : 1 or 1 : 1 24 h before stimulation of MC degranulation. The reaction between β-hex and *p*-nitrophenyl-*N*-acetyl-β-D-glucopyranoside was stopped after 90 min with 0.2 M glycine. Optical density (OD) was measured at 405 nm using a GENios ELISA plate reader (ReTirSoft Inc. Toronto, ON, Canada). β-Hex release was expressed as the percentage of total cell content after subtracting background release from unstimulated cells. Cell content of β-hex from unstimulated and antigen challenged cells was determined by lysing cells with 0.1% Triton X-100.

For cytokine measurements, the cells were plated as above, but the cytokines were measured in cell culture supernatants 12 h following addition of 100 ng/mL DNP-HSA; MCs alone were used as a positive control. Additionally, cytokines were measured in supernatants of BMSCs exposed to IgE and DNP-HSA to account for any cytokine production from the BMSC population in the co-cultures. Ninety-six well transwell plates (Corning, Lowell, MA, USA) were utilized in cytokine measurement experiments to determine the contribution of a contact-dependent mechanism, and the contribution of soluble mediators in the genesis of BMSC-mediated immunosuppression. For these experiments, BMSC were coated onto the bottom chamber of the transwell system, while MCs were added to the upper chamber. IgE sensitized MCs were then stimulated by the addition of DNP-HSA followed by collection of supernatants from the upper chamber 12 h later. In addition, conditioned medium from BMSC cultures was added to standard BMMC cultures followed by

IgE sensitization and challenge 24 h following addition of the conditioned medium in the MC cultures. For all cytokine measurements, we used mouse TNF-α/TNFSF1A Quantikine ELISA kits (R&D Systems, Minneapolis, MN, USA). In addition to the co-culture experiments described above, we utilized the following inhibitors and antibodies within the co-cultures system to determine a mechanism by which BMSCs suppress TNF-α production by MCs: 5 μM indomethacin (Cayman Chemicals, Ann Arbor, MI, USA), 1 μM NS-398 (Sigma, Ann Arbor, MI, USA), 1 μM SC560 (Sigma), 1 mM L-NAME (Sigma), 1 mM methyl-D-tryptophane (Sigma), 10 μg/mL IL-10 neutralizing Ab (Pierce, Ann Arbor, MI, USA), and 10 μg/mL TGF-β neutralizing Ab (R&D Systems).

Passive cutaneous anaphylaxis and peritoneal degranulation assay

The immunomodulatory effects of murine BMSCs on *in vivo* MC degranulation were determined by monitoring both the passive cutaneous anaphylaxis (PCA) reaction and peritoneal degranulation. The PCA reaction measures changes in vascular permeability, as determined by local tissue extravasation of intravenously administered Evans blue dye that is induced by release of vasodilatory mediators following MC degranulation. For the PCA experiments, C57BL/6 mice (6–8 weeks of age) ($n = 6$ mice per group) received intradermal injections of 1 μg mouse monoclonal IgE anti-DNP (Sigma-Aldrich) in 25 μL phosphate-buffered saline (PBS) in the right ear to sensitize tissue MCs, followed by intradermal injection of 0.5×10^6 BMSC in 25 μL PBS in the same ear 24 h later. The left ear served as a negative control and received an intradermal injection of PBS. Positive control mice received only an injection of IgE anti-DNP in the right ear and PBS in the left ear. Thirty minutes after BMSC injection, mice were challenged with antigen by intravenous injection into the tail vein with 0.5 mg/mL DNP-HSA which was resuspended in 1% Evan's blue in 100 μL saline. The mice were euthanized by CO_2 asphyxiation 30 min after injection of antigen and Evan's blue, and the ears were excised and incubated in 200 μL formamide at 55 °C for 24 h to extract the Evan's blue dye from the tissue. The total content of Evan's blue that was extracted from each ear was quantitated by spectrophotometric analysis at 620 nm. The net Evan's blue was determined by subtraction of the amount of Evan's blue in the IgE positive ear or BMSC-treated ear minus the PBS-treated ear. Comparison was made between IgE/antigen positive control mice and mice that received IgE/antigen and a local administration of BMSCs.

A second method was used to measure MC degranulation within the peritoneal cavity of mice. For the peritoneal degranulation assay (PDA) experiments, the resident peritoneal MCs in C57BL/6 mice ($n = 6$ mice/group) were sensitized intraperitoneal (i.p.) with 1 μg monoclonal IgE anti-DNP (Sigma) followed 24 h later by i.p. challenge with DNP-HSA. To determine the degree of MC degranulation following challenge, the peritoneal cavity was irrigated with PBS and the irrigation fluid collected to measure β-hex release as described above. The reaction between β-hex in the peritoneal fluid and *p*-nitrophenyl-*N*-acetyl-β-D-glucopyranoside was stopped after 90 min with 0.2 M glycine. OD was measured at 405 nm using a GENios ELISA plate reader (ReTirSoft Inc.). For PDA experiments, β-hex release is expressed as OD values. To determine the effects of BMSCs on peritoneal MC degranulation, an additional set of mice received 1×10^6 BMSCs 1 h before challenge with DNP-HSA. We used B6.Cg-Kit^{W-sh} (MC-deficient) mice in these experiments to establish that the observed response is MC specific; and that the β-hex measured in the peritoneal cavity is a result of MC degranulation.

To study EP receptor function *in vivo*, we used specific receptor antagonists (Cayman Chemicals) at different doses (EP1 antagonist SC-51322, 3 mg/kg; EP2 antagonist AH 6809, 1 mg/kg; EP4 antagonist GW627368X, 1 mg/kg). All antagonists were administered as a single injection in 200 μL PBS at the time of BMSC injection.

Quantitative polymerase chain reaction

MCs were co-cultured with BMSC at a ratio of 100 : 1, 10 : 1 or 1 : 1. Following 24 h co-culture, MCs were stimulated by aggregation of FcεRI with antigen as described above. The non-adherent MC population was washed off (between 2% and 13% of MC were adherent and not washed off as assessed by morphology), and thus separated from the BMSC population. Total RNA from MCs was collected using a Qiagen Rneasy Mini Kit (Qiagen, Valencia, CA, USA) following the manufacturer's instructions. RNA was reverse-transcribed using the Quantitect reverse transcription kit (Qiagen). Quantitative real-time PCR was performed using a Quantitech SYBR Green PCR Kit (Qiagen) and the ABI PRISM 7500 Detection system (Applied Biosystems, Foster City, CA, USA) to obtain cycle threshold (C_t) values for target and internal reference cDNA levels. Gene specific primers for TNF-α were obtained from Qiagen. Target cDNA levels were normalized to GAPDH, an internal reference using the equation $2^{-[\Delta C_t]}$, where ΔC_t is defined as $C_{t_{target}} - C_{t_{internalreference}}$. Values shown were derived from the average of three independent experiments.

Chemokinesis and chemotaxis

We cultured MCs in the presence of BMSCs for 24 h, after which we placed only the MCs in a 96-well microchemotaxis plate with 8 μm pore size (Neuroprobes, Gaithersburg, MD, USA) as described [20]. The lower chamber either contained only PBS (assay for spontaneous

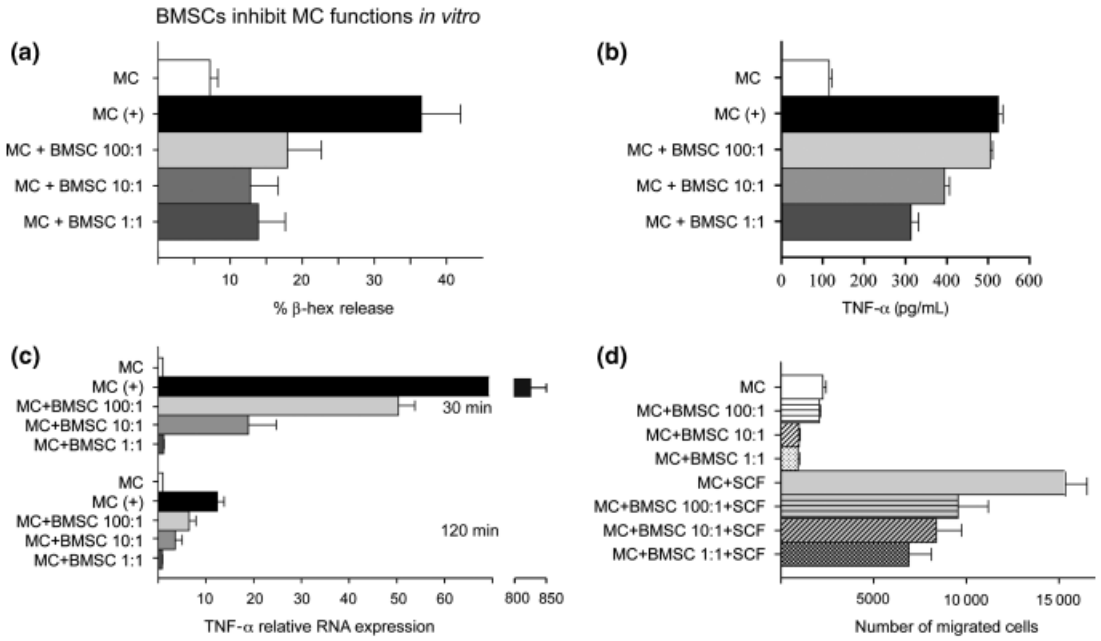

Fig. 1. *In vitro* studies of the interactions between MCs and bone marrow-derived stromal cells (BMSCs). (a) Different ratios (1 : 1; 1 : 10 and 1 : 100) of IgE sensitized MCs and BMSCs were cultured together for 24 h before IgE specific antigen challenge. β-hexosaminidase (β-hex) release was used as a marker of MC degranulation. BMSCs attenuate MC degranulation in all ratios tested. (b) Different ratios (1 : 1; 1 : 10 and 1 : 100) of IgE sensitized MCs and BMSCs were cultured together for 24 h before IgE specific antigen challenge for 12 h. TNF-α release was measured by ELISA. The BMSCs decreased the amount of released TNF-α in a ratio-dependent manner. (c) The experiment in (b) was repeated to measure TNF-α mRNA levels at two time-points (30 and 120 min) following antigen challenge. Similar to the levels of TNF-α protein, mRNA synthesis also decreased in response to the presence of BMSCs at both time-points in a ratio-dependent manner. (d) The migration of MCs was affected by the presence of BMSCs in the culture with increasing numbers of BMSCs within the co-culture, the spontaneous (upper four columns) as well as stem cell factor (SCF)-induced migration (chemokinesis and chemotaxis, respectively) of MCs were significantly reduced. $^{*}P<0.05$; $^{**}P<0.01$ and $^{***}P<0.001$

migration or chemokinesis) or contained stem cell factor (SCF) as an attractant (chemotaxis). Cells from the lower well were collected and counted by flow cytometry. Chemotaxis of MC to SCF was examined either alone or in the presence of BMSC. MC chemotaxis was measured following a 24 h co-culture with BMSC. MCs were plated on the chemotaxis filters at 30 000 cells/well and allowed to settle for 10 min. The filter was assembled with the lower plate filled with PBS/0.1% bovine serum albumin (BSA), with or without 100 ng/mL SCF and placed at 37 °C for 60 min. The lower well content (30 μL of PBS/0.1% BSA with transmigrated cells) was collected, and the total number of migrated cells was determined by counting the total events of unlabeled MCs by allowing the total volume of cells to flow through the flow cytometer (FACS Caliber, Becton Dickinson, Franklin Lakes, NJ, USA). Each condition was performed in triplicate and two experiments were averaged.

Statistics

Data are summarized as mean±SEM. Student's *t*-test or two-way ANOVA were performed using GraphPad Prism version 4.00 for Macintosh (GraphPad Software, San Diego, CA, USA). The statistical significance value was set at $P<0.05$.

Results

Bone marrow-derived stromal cells suppress mast cell degranulation and cytokine production

To determine if BMSCs could alter MC function, we first co-cultured MCs with BMSCs at ratios from 1 : 1 to 1 : 100. We found that BMSCs significantly decreased degranulation of MCs as measured by release of β-hex, even at culture ratios of 100 MCs to 1 BMSC (Fig. 1a). Similarly, co-culture of MCs with BMSCs for 24 h significantly reduced MC-derived TNF-α 12 h following challenge with antigen in a dose-dependent manner (Fig. 1b). Since we established a decrease in the protein level of TNF-α in the medium of co-cultured MCs and BMSCs, we next verified that this observation was associated with a concomitant decrease in TNF-α mRNA synthesis within the MCs co-cultured with BMSCs. Our data revealed that MCs transcribed significantly less TNF-α mRNA when they were in contact with BMSCs at both 30 and 120 min following challenge with antigen. Lastly, we measured TNF-α expression by BMSCs co-cultured with MCs in a transwell

system to exclude the possibility that BMSCs are not indirectly activated by MC mediators; however, we did not observe any TNF-α production by BMSCs (data not shown). Thus, BMSCs do have the capacity to down-regulate certain MC responses.

Bone marrow-derived stromal cells significantly reduce mast cell chemotaxis

Once we observed that BMSCs affect the degranulation and cytokine synthesis of MCs, we determined if BMSCs might also influence the ability of MCs to migrate towards a stimulus. Cells collected from the lower well of a microchemotaxis plate were counted by flow cytometry. When the lower chamber in the chemotaxis plate contained only PBS, there was significantly less migration of MCs (Fig. 1d). Similarly, when the lower chamber contained SCF as an attractant, the number of MCs that migrated was significantly decreased when the MCs had been co-cultured with BMSCs, as compared to MCs that had not been co-cultured with BMSCs (Fig. 1d). Thus, MCs cultured in the presence of BMSCs for 24 h were significantly impaired in their ability to migrate.

Mast cell activation in vivo *is impaired following administration of bone marrow-derived stromal cells*

We next wanted to examine whether MC behaviour could be altered by BMSCs *in vivo*. To assess this possibility, we used two separate *in vivo* assays of MCs responsiveness. Using a PCA model, when antigen-specific IgE was injected intradermally into the ear followed by systemic antigen challenge 24 h later, we found that the increased vascular permeability resulting from MC activation was significantly reduced when BMSCs were administered (Fig. 2a). In the PDA assay, where MCs in the peritoneal cavity are sensitized with antigen-specific IgE and then challenged with antigen, we found a significant decrease in the amount of β-hex in the peritoneal fluid when BMSCs were present (Fig. 2b). To confirm that the change in β-hex levels was due to MC degranulation, we repeated the experiment using B6.Cg-Kit^{W-sh} MC-deficient mice. In these experiments, we did not observe any increase in β-hex release within the peritoneal cavity following challenge with antigen, consistent with the conclusion that the β-hex measured in the C57BL/6 mice is indeed derived from MCs (Fig. 2b).

Up-regulation of cyclooxygenase-2 by bone marrow-derived stromal cells mediates the suppression of mast cell activation via the EP4 receptor

Next we set out to identify a mechanism of action with regard to the ability of BMSCs to suppress MC function. For these experiments, we used MC-derived TNF-α production as an end-point. Following the addition of a variety of pharmacological inhibitors (COX1/2 inhibitors, IDO inhibitor, NO inhibitor), blocking antibodies (anti-TGF-β and anti-IL-10) to our co-cultures or use of BMSC conditioned media or a transwell system, we measured TNF-α release by MCs. We found that BMSCs were still effective at suppressing MC derived TNF-α production in transwell system or in the presence of COX1 inhibitor, NO inhibitor, IDO inhibitor and blocking antibodies to IL-10 and TGF-β. Further, the BMSC conditioned media did not have an effect on MC TNF-α production suggesting that presence of MCs either in contact with BMSCs or in a transwell system are required to elicit the suppressive effect of BMSCs. When we added indomethacin (a COX1/COX2 non-selective inhibitor) or a specific COX2 inhibitor (NS-398), the suppressive effect mediated by BMSCs was eliminated (Fig. 3a). To determine which cell population was targeted by the COX2 inhibitors for suppression of TNF-α release by MCs, we repeated the *in vitro* co-cultures using either BMSCs or MCs that were deficient in COX2. The suppressive effect was eliminated when COX2-deficient BMSCs were used, but persisted when COX2-deficient MCs were used in the co-culture system (Fig. 3b).

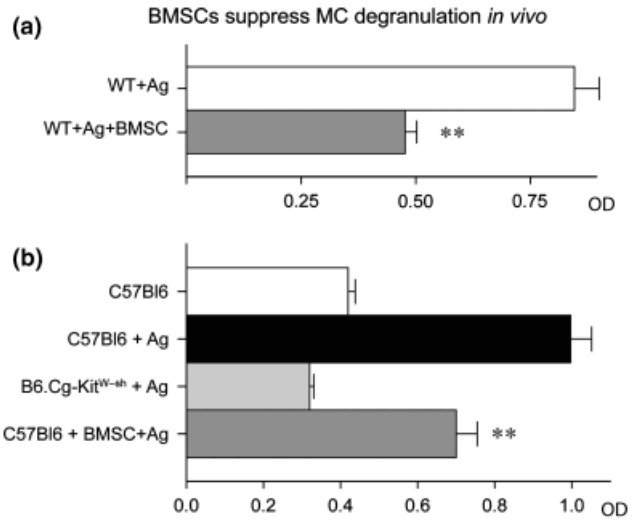

Fig. 2. Suppression of mast cell (MC) degranulation by bone marrow-derived stromal cells (BMSCs) *in vivo*. (a) Passive cutaneous anaphylaxis (PCA) was performed using systemically administered Evans blue as a marker of tissue permeability within the mouse ear. Administration of BMSCs to the IgE sensitized mouse ear before challenge with IgE-specific antigen significantly decreased the amount of Evans blue leakage into the tissues as quantified by optical density. (b) *In vivo* MC degranulation was also examined by challenging IgE sensitized peritoneal MCs with antigen (PDA) following intraperitoneal (i.p.) administration of either PBS or BMSCs. MC degranulation was quantified by measuring an increase in peritonealβ-hexosaminidase (β-hex) release following challenge as shown in the top two bars. In the bottom two bars, an increase in β-hex release was not observed in MC-deficient mice, whereas i.p. administration of BMSCs significantly decreased the amount of β-hex release in C57Bl/6 mice which the MCs were sensitized and challenged with antigen.

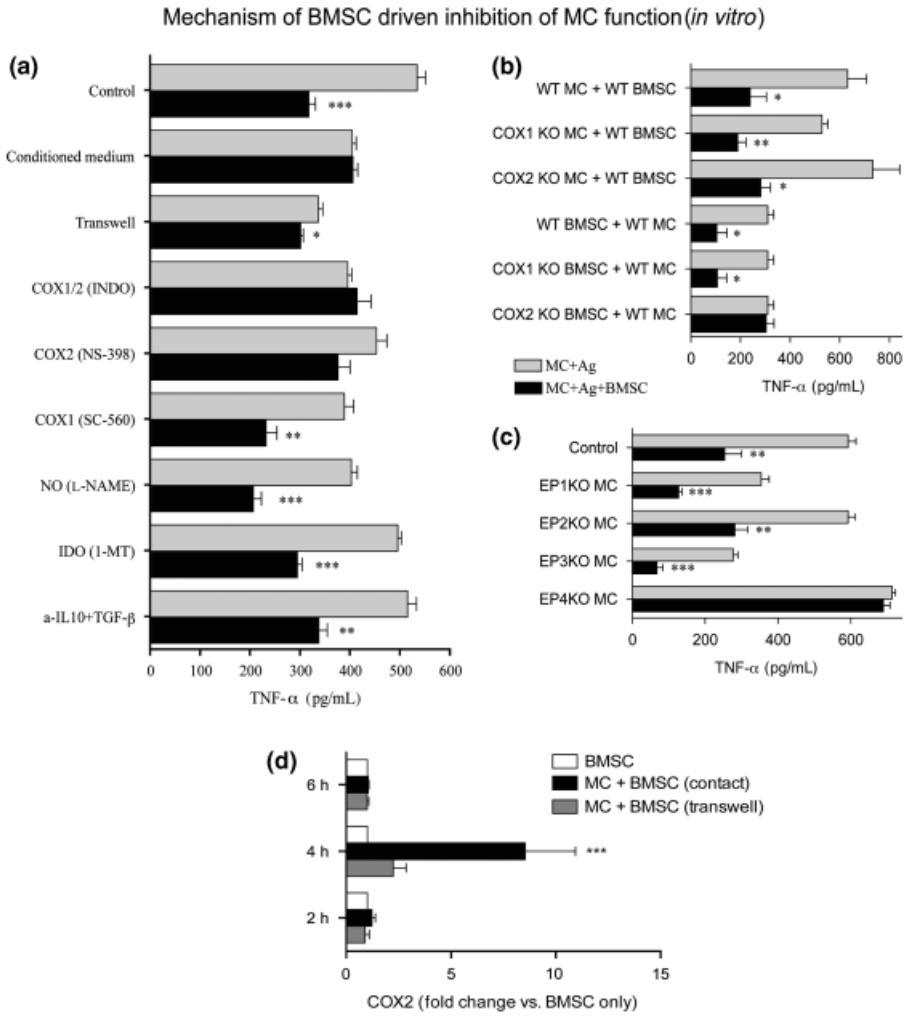

Fig. 3. Identifying a mechanism of mast cell (MC) suppression. (a) In the co-culture system, a variety of inhibitor and blocking antibodies were used to test if they prevent the immunosuppressive effect of bone marrow-derived stromal cells (BMSCs) on MCs TNF-α production. The suppressive effect of BMSCs was not altered when a COX1 inhibitor, IDO inhibitor, NO inhibitor or antibodies to TGF-β and IL-10 were applied to the co-culture. However, when indomethacin (a COX1 and COX2 inhibitor) or a specific COX2 inhibitor (NS-398) were used the immuno-suppressive effect of the BMSCs was eliminated. (b) Identifying the cellular source of COX2 in the system. Using COX1- and COX2-deficient cells (either MCs or BMSCs) in the co-culture system, TNF-α production was measured following antigen stimulation of MCs. Exclusively, the use of COX2 knock-out (KO) BMSC in the co-culture eliminated the effect suggesting that BMSC up-regulate COX2 synthesis. (c) Screening for the responsible receptor in the MC. MCs lacking the individual EP receptors (EP1–4) was used to determine their effect on TNF-α production in the co-culture system with BMSCs. BMSCs were still able to suppress MC derived TNF-α production when the EP13 receptors were absent. When EP4 KO MCs were used in the culture system, the immunosuppressive effect of BMSCs was eliminated. (d) Up-regulation of COX2 in BMSC following co-culture with MCs. COX2 mRNA levels were measured by quantitative PCR at 2, 4 and 6 h following co-culture with MCs in either contact-dependent or a transwell system. COX2 mRNA was significantly up-regulated in BMSCs 4 h following co-culture with MCs. While BMSC COX2 mRNA expression was increased in the transwell system, we observed a greater increase in COX2 expression when the cells were in contact.

Since COX2 will induce prostaglandin (PGE_2) production, which exerts its effects through binding to the EP1–4 receptors, we next examined the involvement of each of these individual receptors in the MC population. Once again, we used TNF-α production as a marker of MC response. Data revealed that when MCs were derived from EP1-, EP2- or EP3-deficient mice, they remained responsive to the suppressive effects of the BMSCs. However, when EP4-deficient MCs were used in the co-culture, the BMSCs were unable to suppress TNF-α production by MCs (Fig. 3c). Lastly, we confirmed that COX2 mRNA is up-regulated upon co-culture of BMSCs and MCs. As shown in Fig. 3d, we observed a significant up-regulation of COX2 mRNA in BMSCs 4 h following co-culture. This up-regulation was observed in both the contact and transwell co-cultures; however, the expression of COX2 was much greater when the cells were co-cultured in contact. Finally, to test the mechanism of suppressive effect *in vivo*, we repeated the PDA experiments and found that BMSCs derived from $COX2^{-/-}$ mice were unable to suppress

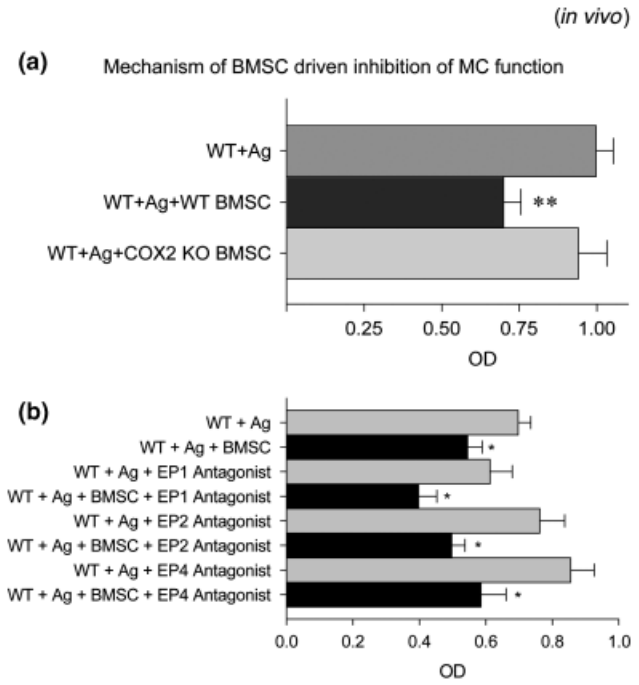

Fig. 4. *In vivo* confirmation of COX2 mediated mechanism. (a) The peritoneal assay depicted in Fig. 2 was repeated using COX2 knock-out (KO) bone marrow-derived stromal cells (BMSCs) followed by challenging the sensitized resident MCs with antigen. In contrast to wild-type BMSCs, COX2-deficient BMSCs failed to suppress β-hexosaminidase (β-hex) release by peritoneal MCs. (b) The peritoneal assay depicted in Fig. 2 was repeated using EP1–4 receptor antagonists delivered to the peritoneal cavity at the same time as injection of BMSCs which was followed 24 h later by challenging the sensitized resident MCs with antigen and measuring β-hex release. In contrast to injection of COX2-deficient BMSCs as shown in Fig. 4a, addition of EP receptor antagonists did not abrograte the suppressive effect of BMSCs. $N = 4$ mice/group and was repeated two times.

β-hex release by MCs *in vivo* (Fig. 4a). Surprisingly we could not confirm the importance of EP4 receptor *in vivo* using EP receptor antagonists (Fig. 4b). Pre-treating the mice with different EP receptor antagonists before BMSC injection and antigen challenge could not eliminate the suppressive effect observed *in vivo*.

Discussion

There are now a number of studies which report that BMSCs are capable of suppressing T and B cells, dendritic cells and NK cells *in vitro*, and ameliorating inflammatory responses *in vivo* [3–5, 21, 22]. The majority of these studies explored how BMSCs could be used to treat graft vs. host disease (GVHD) or inflammatory diseases mediated by autoimmune pathology. More recent studies have explored if BMSCs could influence innate immune functions; and if these interactions could provide any benefit in host defense [21, 23]. Indeed, we have demonstrated that BMSCs provide protection against the development of sepsis and more recently have reported that BMSCs can modulate disease pathology in an allergic model of ragweed-induced asthma [6, 24].

MCs have long been recognized for their role in the genesis of allergic inflammation [18], thereby providing an ideal cell target in which the immunomodulatory effects of BMSCs may be beneficial. Despite the central effector role of MCs in allergic inflammation, no studies are yet available to address if BMSCs interact with MCs and could thereby influence allergic inflammation.

In this study we address this question, and provide evidence that mouse BMSCs co-cultured with MCs *in vitro* effectively suppress MC activation, including FcεRI-mediated degranulation, TNF-α production and SCF-induced migration. Using a classic PCA model and a model of peritoneal MC degranulation, we found that in accordance with our *in vitro* data, BMSCs also attenuate MC activation *in vivo*. As such, these *in vivo* models demonstrate the potential of BMSCs to reduce the severity of MC-initiated allergic diseases.

The suppression of MC activation by BMSCs is greatest when the cells are in contact as compared to when the cells are co-cultured in a transwell system (Fig. 3a). Further, BMSC conditioned media does not have the ability to suppress MC activation. The lack of an effect with conditioned media suggests that there is cross-talk required between the MC and BMSC to initiate the suppressive effect elicited by the BMSC. These findings are similar to what is reported with the attenuation of MC degranulation by bronchial epithelial cells [25]. Yang et al. [25] demonstrated that after 16 h of co-culture with bronchial epithelial cells, human lung MCs have significantly attenuated response to IgE-mediated activation. Similar to our data, the effect of bronchial epithelial cells was contact dependent. In contrast, it has been reported that several other cell types may promote MC survival and proliferation. Hollins et al. [26] have shown that airway smooth muscle promotes lung MC survival, proliferation and activation primarily through a physical interaction between membrane-bound SCF and its receptor on MCs. In addition, it has been recently demonstrated that generation of cord blood-derived MCs can be enhance when co-cultured with a bone marrow stomal cell line [27]. It remains to be determined what effects BMSCs may have on MC proliferation and maturation.

To identify the molecular pathways involved in such a suppressive effect by BMSCs, we employed specific inhibitors as well as cells isolated from specific knock-out mice. Based on our initial screening experiments using inhibitors, we identified COX2 as a crucial intermediate in the BMSC driven suppression of MCs. As both BMSCs and MCs up-regulate COX2 in response to stimuli, we repeated our experiments using co-culture systems where either MCs or BMSCs lacked the COX2 gene. Based on these studies, we identified that the up-regulation of COX2 is

occurring within the BMSC population; and is critical regulator of their suppressive action on MCs. Further, MC derived COX2 did not prove essential.

Our next question was whether COX2 up-regulation mediates the suppression of MCs by BMSC derived PGE_2 by acting through EP receptors expressed on MCs. To explore this hypothesis, we used MCs deficient for one of the four known receptors for PGE_2: EP1, EP2, EP3 or EP4. Through the use of EP-deficient MCs, we demonstrate that lack of EP4 in MCs abrogated the suppressive effect elicited by BMSCs *in vitro* while the presence of EP1, EP2, or EP3 was not critical. To determine whether EP4 is critical to BMSC directed suppression of MC activation *in vivo*, we used antagonists specific to EP1, EP2, EP3 and EP4 receptors. However, when we probed the importance of EP receptors *in vivo* using these receptor antagonists we could not confirm our *in vitro* data. EP4 receptor antagonists did not prevent BMSCs from inhibiting MC degranulation. In fact neither of the receptor antagonists could hinder the BMSC suppressive phenotype. These seemingly contradicting data between *in vitro* and *in vivo* findings could be explained in several ways. First, *in vitro* we utilized MCs deficient for EP receptors while *in vivo* we pretreated wild-type mice with specific EP receptor antagonists. It is possible that pharmacologic inhibition of MC EP receptors is not as efficient as complete deletion of the genes using transgenic technology. It is also possible that *in vivo*, and in particular within the peritoneal cavity, there are other cell types (macrophages, neutrophils, etc.) that influence either direct interactions between BMSCs and MCs or influence the pharmacological intervention used to study the importance of EP receptors considering these cell types also express EP receptors. In fact, we have shown that PGE_2 released from BMSCs acting through EP2 and EP4 receptors modulates macrophage phenotype in a mouse model of sepsis [24] which in turn could influence MC activation and pharmacological intervention. Lastly, the fact that EP4 antagonists did not prevent the suppression of MC degranulation *in vivo* further highlights that ability of these cells to adjust to their environment and lead to suppression of immune responses.

The effect of PGE_2 on MCs varies with the model system employed. Several studies suggest that the presence of PGE_2 is inhibitory to MC activation [28–32]. Other data reported that addition of PGE_2 potentiates activation of MCs stimulated with IgE and antigen [33–37]. In our experiments, we examined the cellular interactions between MCs and BMSCs and our results are consistent with the conclusion that PGE_2 derived from a cellular source (e.g. BMSCs) inhibits MC activation. In this regard they are most consistent with published data showing that PGE_2 inhibits lung MC degranulation and the resultant inflammation and Th2 cytokine production [29, 31, 32].

When BMSCs are administered into the circulation they will eventually end up in the microvascular bed of different organs. Since MCs are primarily located in the perivascular space of vessels BMSCs will inevitably interact with them when leaving the vascular space during the process of homing. It is also well described that BMSCs preferentially home to sites of active inflammation, responding to a wide variety of inflammatory signals. In an anaphylactic setting MCs predominate such an inflammatory environment hence there is an increased chance for them to communicate with and to be suppressed by injected BMSCs. Based on our data, we suggest that BMSC infusion (either systematic or local) could effectively suppress immunologic responses mediated by MCs in the setting of anaphylaxis. There is also an increasing amount of data emphasizing the importance of MCs in the coordination of autoimmune diseases [38]. In many cases, the presence of MCs is critical to orchestrate autoimmune inflammation as shown in animal models of multiple sclerosis, rheumatoid arthritis or bullous pemphigoid [38]. Since BMSCs are known to be able to attenuate autoimmune inflammation [39], we hypothesize that BMSC/MC interactions could – at least in part – explain this suppressive phenotype and guide us in a better understanding of BMSC immune biology.

In summary, we have shown that BMSCs have the ability to influence the biology of MCs by limiting their activation and migration. Our data additionally document that these effects are mediated through prostaglandin pathways. These observations support the conclusion that BMSCs should be explored as a cell-based therapy in the treatment of MC-directed allergic inflammation.

Acknowledgements

The authors would like to thank Dr Beverly H. Koller for supplying the EP1-4 KO mice.

This research was supported by the Division of Intramural Research programs of NIDCR and NIAID.

References

1 Chen X, Armstrong MA, Li G. Mesenchymal stem cells in immunoregulation. *Immunol Cell Biol* 2006; **84**: 413–21.

2 Le Blanc K, Ringden O. Immunobiology of human mesenchymal stem cells and future use in hematopoietic stem cell transplantation. *Biol Blood Marrow Transplant* 2005; **11**:321–34.

3 Nasef A, Ashammakhi N, Fouillard L. Immunomodulatory effect of mesenchymal stromal cells: possible mechanisms. *Regen Med* 2008; **3**: 531–46.

dc_219_11

4 Nauta AJ, Fibbe WE. Immunomodulatory properties of mesenchymal stromal cells. *Blood* 2007; **110**:3499–506.

5 Sotiropoulou PA, Papamichail M. Immune properties of mesenchymal stem cells. *Methods Mol Biol* 2007; **407**:225–43.

6 Nemeth K, Keane-Myers A, Brown JM *et al*. Bone marrow stromal cells use TGF-beta to suppress allergic responses in a mouse model of ragweed-induced asthma. *Proc Natl Acad Sci USA* 2010; **107**:5652–7.

7 Dryden GW Jr Overview of biologic therapy for Crohn's disease. *Expert Opin Biol Ther* 2009; **9**:967–74.

8 Di Nicola M, Carlo-Stella C, Magni M *et al*. Human bone marrow stromal cells suppress T-lymphocyte proliferation induced by cellular or nonspecific mitogenic stimuli. *Blood* 2002; **99**:3838–43.

9 Glennie S, Soeiro I, Dyson PJ, Lam EW, Dazzi F. Bone marrow mesenchymal stem cells induce division arrest anergy of activated T cells. *Blood* 2005; **105**:2821–7.

10 Krampera M, Glennie S, Dyson J *et al*. Bone marrow mesenchymal stem cells inhibit the response of naive and memory antigen-specific T cells to their cognate peptide. *Blood* 2003; **101**:3722–9.

11 Maccario R, Moretta A, Cometa A *et al*. Human mesenchymal stem cells and cyclosporin a exert a synergistic suppressive effect on in vitro activation of alloantigen-specific cytotoxic lymphocytes. *Biol Blood Marrow Transplant* 2005; **11**:1031–2.

12 Augello A, Tasso R, Negrini SM *et al*. Bone marrow mesenchymal progenitor cells inhibit lymphocyte proliferation by activation of the programmed death 1 pathway. *Eur J Immunol* 2005; **35**:1482–90.

13 Chen L, Zhang W, Yue H *et al*. Effects of human mesenchymal stem cells on the differentiation of dendritic cells from $CD34^+$ cells. *Stem Cells Dev* 2007; **16**:719–31.

14 Jiang XX, Zhang Y, Liu B *et al*. Human mesenchymal stem cells inhibit differentiation and function of monocyte-derived dendritic cells. *Blood* 2005; **105**:4120–6.

15 Li H, Guo Z, Jiang X, Zhu H, Li X, Mao N. Mesenchymal stem cells alter migratory property of T and dendritic cells to delay the development of murine lethal acute graft-versus-host disease. *Stem Cells* 2008; **26**:2531–41.

16 Zhang W, Ge W, Li C *et al*. Effects of mesenchymal stem cells on differentiation, maturation, and function of human monocyte-derived dendritic cells. *Stem Cells Dev* 2004; **13**:263–71.

17 Aggarwal S, Pittenger MF. Human mesenchymal stem cells modulate allogeneic immune cell responses. *Blood* 2005; **105**:1815–22.

18 Brown JM, Wilson TM, Metcalfe DD. The mast cell and allergic diseases: role in pathogenesis and implications for therapy. *Clin Exp Allergy* 2008; **38**:4–18.

19 Dastych J, Walczak-Drzewiecka A, Wyczolkowska J, Metcalfe DD. Murine mast cells exposed to mercuric chloride release granule-associated N-acetyl-beta-D-hexosaminidase and secrete IL-4 and TNF-alpha. *J Allergy Clin Immunol* 1999; **103**:1108–14.

20 Kushnir-Sukhov NM, Gilfillan AM, Coleman JW *et al*. 5-hydroxytryptamine induces mast cell adhesion and migration. *J Immunol* 2006; **177**:6422–32.

21 Uccelli A, Moretta L, Pistoia V. Mesenchymal stem cells in health and disease. *Nat Rev Immunol* 2008; **8**:726–36.

22 Rasmusson I. Immune modulation by mesenchymal stem cells. *Exp Cell Res* 2006; **312**:2169–79.

23 Spaggiari GM, Abdelrazik H, Becchetti F, Moretta L. MSCs inhibit monocyte-derived DC maturation and function by selectively interfering with the generation of immature DCs: central role of MSC-derived prostaglandin E2. *Blood* 2009; **113**:6576–83.

24 Nemeth K, Leelahavanichkul A, Yuen PS *et al*. Bone marrow stromal cells attenuate sepsis via prostaglandin E(2)-dependent reprogramming of host macrophages to increase their interleukin-10 production. *Nat Med* 2009; **15**:42–9.

25 Yang W, Wardlaw AJ, Bradding P. Attenuation of human lung mast cell degranulation by bronchial epithelium. *Allergy* 2006; **61**:569–75.

26 Hollins F, Kaur D, Yang W *et al*. Human airway smooth muscle promotes human lung mast cell survival, proliferation, and constitutive activation: cooperative roles for CADM1, stem cell factor, and IL-6. *J Immunol* 2008; **181**:2772–80.

27 Yamaguchi M, Azuma H, Fujihara M, Hamada H, Ikeda H. Generation of a considerable number of functional mast cells with a high basal level of FcepsilonRI expression from cord blood $CD34^+$ cells by co-culturing them with bone marrow stromal cell line under serum-free conditions. *Scand J Immunol* 2007; **65**:581–8.

28 Chan CL, Jones RL, Lau HY. Characterization of prostanoid receptors mediating inhibition of histamine release from anti-IgE-activated rat peritoneal mast cells. *Br J Pharmacol* 2000; **129**:589–97.

29 Herrerias A, Torres R, Serra M *et al*. Subcutaneous prostaglandin E(2) restrains airway mast cell activity in vivo and reduces lung eosinophilia and Th(2) cytokine overproduction in house dust mite-sensitive mice. *Int Arch Allergy Immunol* 2009; **149**:323–32.

30 Hogaboam CM, Bissonnette EY, Chin BC, Befus AD, Wallace JL. Prostaglandins inhibit inflammatory mediator release from rat mast cells. *Gastroenterology* 1993; **104**:122–9.

31 Kay LJ, Yeo WW, Peachell PT. Prostaglandin E2 activates EP2 receptors to inhibit human lung mast cell degranulation. *Br J Pharmacol* 2006; **147**:707–13.

32 Wang XS, Wu AY, Leung PS, Lau HY. PGE suppresses excessive anti-IgE induced cysteinyl leucotrienes production in mast cells of patients with aspirin exacerbated respiratory disease. *Allergy* 2007; **62**:620–7.

33 Abdel-Majid RM, Marshall JS. Prostaglandin E2 induces degranulation-independent production of vascular endothelial growth factor by human mast cells. *J Immunol* 2004; **172**:1227–36.

34 Gomi K, Zhu FG, Marshall JS. Prostaglandin E2 selectively enhances the IgE-mediated production of IL-6 and granulocyte-macrophage colony-stimulating factor by mast cells through an EP1/EP3-dependent mechanism. *J Immunol* 2000; **165**:6545–52.

35 Leal-Berumen I, O'Byrne P, Gupta A, Richards CD, Marshall JS. Prostanoid enhancement of interleukin-6 production by rat peritoneal mast cells. *J Immunol* 1995; **154**:4759–67.

36 Nakayama T, Mutsuga N, Yao L, Tosato G. Prostaglandin E2 promotes degranulation-independent release of MCP-1 from mast cells. *J Leukoc Biol* 2006; **79**:95–104.

37 Nguyen M, Solle M, Audoly LP *et al*. Receptors and signaling mechanisms required for prostaglandin E2-mediated regulation of mast cell degranulation and IL-6 production. *J Immunol* 2002; **169**:4586–93.

38 Benoist C, Mathis D. Mast cells in autoimmune disease. *Nature* 2002; **420**:875–8.

39 Pistoia V, Raffaghello L. Potential of mesenchymal stem cells for the therapy of autoimmune diseases. *Expert Rev Clin Immunol* 2010; **6**:211–8.